# ADVANCEMENTS IN FLAVOR AND NEUTRINO PHYSICS

A Dissertation

Presented to the Faculty of the Graduate School

of Cornell University

in Partial Fulfillment of the Requirements for the Degree of

Doctor of Philosophy

by

Mitrajyoti Ghosh

August 2023

ADVANCEMENTS IN FLAVOR AND NEUTRINO PHYSICS

Mitrajyoti Ghosh, Ph.D.

Cornell University 2023

The flavor structure of the Standard Model (SM), as dictated by the Cabbibo-Kobayashi-Maskawa (CKM) matrix, is far from generic. Probing the elements of the CKM matrix is thus important, not only as tests of the SM but also as probes of new physics beyond it. In part of my work, I look at various phenomena in the realm of flavor physics towards this goal. I focus on the study of the decay of neutral kaons to a dimuon pair. Due to long-distance effects, the decay of the short-lived neutral kaon, $K_S$, to two muons was initially thought to be theoretically unclean. I show that time-dependence measurements of the decay rate are theoretically very clean and can still provide meaningful checks of the Standard Model and look for new physics.

The rest of my work is dedicated to the study of neutrinos. Neutrinos are the lightest particles in the Standard Model and they interact very weakly with ordinary matter, making their detection difficult. In my work, I study how an exchange of two neutrinos between two objects can mediate a long ranged force between them, thereby potentially allowing us to probe their properties indirectly. This two-neutrino exchange force, which is a quantum effect, can be treated in the non-relativistic limit as a classical addition to the Coulomb potential. Although this force is weak and below experimental sensitivity levels today, I study how in certain situations it can be enhanced and potentially observed.

## BIOGRAPHICAL SKETCH

Mitrajyoti Ghosh (born October 23, 1994) obtained his Bachelor's degree in Physics from St. Stephen's College, University of Delhi, New Delhi, India in the year 2016. He thereafter earned his Master of Advanced Study (MASt) in Physics from St. Edmund's College, Cambridge University, UK in the year 2017. Since 2017, he has been pursuing his doctoral degree at Cornell University in theoretical high energy physics, advised by Prof. Yuval Grossman. He was the John David Boochever fellow in theoretical physics at Cornell University during the spring semester of the year 2022. While not at work doing physics, his free time is spent painting and looking out for interesting culinary experiences. He loves movies, video games and savoring creative opportunities in the kitchen!

This work is dedicated to the loving memory of my grandfather, who left an indelible mark on everyone who knew him, and who taught me what it truly means to learn, and teach.

## ACKNOWLEDGEMENTS

As a child, I had the impression that good science is a result of some serendipitous stroke of genius. It is true that popular culture feeds the world a very different image of what a being scientist feels like, and how a scientist does what they do. In reality, "Eureka" moments do not happen over a split second – there is no being struck by genius, but simply that things happen to gradually fall in place when you are fortunate enough. I would call my career thus far as merely one that has "fallen in place" for the most part, and my role in it feels most like a curious spectator.

Thus I now begin the very difficult task of giving credit where it is rightly due: My parents and my brother, for vicariously bearing the challenges of a PhD program, channelized and amplified through me. My grandmother and my aunt for always being optimistic about my abilities. It was indeed difficult to be physically separated from them over six years, during both the good times and the bad. I would truly not be here if it was not for all the help I had - Arnab and Mridu for truly being home away from home, and for being my adopted family in Ithaca; Anna for our many walks over the pandemic at Stewart Park – those evening hours were essential to my mental health and I cannot thank you enough! My housemates of four years, Samriddha, Sayak, Ritwik, Rohan and Indrayudh, for many important life lessons, many conversations, both serious and otherwise, that made these six years feel much shorter than they actually were, and for maintaining my sanity during the rough COVID-stricken years of 2020 and 2021.

Within the walls of the physics department, Namitha for listening to a lot of

my irrational complaints without ever a sign of annoyance. Fernanda for the unwavering company and support through both good and horrible times, you are the kindest and most empathetic person I have ever met. Andrew and Eric for some very stimulating conversations about the world both within and without physics, I will remember the year we shared an office forever. Steven, for making the department a much lighter and colorful place, how you can juggle so many things at once I can never fathom. The wonderful Margarita and Ameen for always pushing me to work harder, and for being a constant source of positivity on the fourth floor, which is indeed something we all need more of. And Gowri, for being my go-to therapist while she was around, you are sorely missed! And how can I forget, my deepest gratitude to the lovely Katerina for all the help with bureaucracy – without you, the department would truly have gone extinct!

I thank my professors Maxim and Csaba for keeping an eye out for me at all times, from behind the shadows. I have much left to learn from the both of them, and having them as my role models is a distinct honor. I thank all my collaborators for teaching me about everything I know about physics - Walter, Stefan and Avital, my deepest appreciation for bearing with me on all fronts. It was a joy working with all of you.

I leave the last paragraph for the person who undoubtedly played the biggest role in making all of this happen in the first place – my advisor Yuval. It is impossible to quantify how much I have learned from him both in academic contexts and beyond. But if there is one lesson I value the most, it is that there are many ways to be a physicist, but none worth changing who you are for. Yuval was more

than an advisor, he was a friend, a philosopher and a guide in the truest sense of the terms. He had my back in difficult times, without ever making me feel that I was responsible for them. I would always have felt like an impostor on the fourth floor, had it not been for Yuval . He made me feel like an important member of the department, and this little paragraph can do but little to sum up my deep respect and gratitude to him.

It takes an entire village to raise a child. And indeed, the people I have named here are way too few compared to all those I had in mind to thank. I apologize for anyone I may have missed, and I sincerely hope that this temporary lapse of my memory can be forgiven!

– *Mitrajyoti Ghosh*
Ithaca, July 2023

## TABLE OF CONTENTS

CHAPTER 1

# INTRODUCTION

The Standard Model (SM) of particle physics is hailed as one of the crowning jewels of human endeavor. And yet, it is no mystery that the Standard Model is inadequate. Many phenomena, such as neutrino masses and their nature (Dirac or Majorana?), the issue of dark matter, several anomalies in flavor physics in which lepton universality may be broken (to name a few), are without satisfactory explanation. And on top of it all, attempts to complete the SM bring forth new issues to be resolved. This is truly an exciting time for the particle physicist, because the particle theory community today faces the challenge of not only proposing solutions to these problems, but also taking care that the theories are in line with constraints from experiment, and are in themselves, well behaved.

Although it is a common notion that most experiments in particle physics happen inside the collider, it does not necessarily have to be so. The cost and scale of collider projects make experimentation a very expensive affair. However, new physics can affect many low energy observables, and this opens the avenues of studying signatures of new physics in more modest systems, ie., in atomic and condensed matter systems. Cosmological processes can also act as effective colliders in space which can teach us more about physics beyond the SM. My work in graduate school aims primarily at studying these signatures of physics, both SM and beyond, through non-collider probes.

Non-collider probes of new physics are exciting, and very interdisciplinary. Whether it be the use of superconductors to detect dark matter, the use of atomic and molecular transitions to detect neutrinos or light new bosons or using measuring energy loss from classical systems by the emission of new particles, there are exciting prospects of finding new physics amidst old phenomena. New physics corrections to well studied physical systems can sometimes lead to surprising effects when some symmetry is broken, such as in atomic parity violation, or in kaon physics, as I discuss in this thesis. Thus the work phenomenologist is indeed very exciting – to look for tiny ways new physics can affect the mundane world around us, in hopes that experiments will soon become sensitive enough to probe these effects as well.

My work is largely divided into three sections, as below:

## 1.1 Neutrino physics

It is well known that exchange of a boson between two species gives rise to a force between them. In the non-relativistic limit, scattering of two particles by boson exchange can be described using a static potential, such as the Coulomb potential when the boson exchanged is a photon. However, the exchange of two fermions can also lead to a static potential description, as if two fermions behave like an effective boson. These forces are called "quantum forces", and the range of these forces is inversely proportional to the mass of the fermions being exchanged. As a

way to probe these forces, consider the issue of parity violation. In the SM, parity is violated by the weak interaction, and parity violation mediated by the weak interaction has been observed in nuclear beta decay. The weak bosons are thought to be too massive to have any significant effect in parity violation in low energy systems, since the forces between two atomic constituents is very short ranged. However the force mediated by exchange of two neutrinos is in principle, long ranged, since neutrinos are very light. At leading order, it has been well studied and in the limit of massless neutrinos, the force goes as $G_F^2/r^5$, where $G_F$ is Fermi's constant and $r$ is the distance between the two particles interacting via an exchange potential. However, if we go beyond leading order and explore the spin-dependent structure of these forces, we find that the 2-neutrino exchange force is parity violating, and in fact, the longest ranged parity violating interaction in the SM. In an attempt to learn more about neutrino masses, we computed the effects of the parity violating 2-neutrino force between the electron and the proton in the hydrogen atom, incorporating neutrino-flavor mixing and masslessness. Due to parity violation, the electromagnetic transitions between hydrogen atom states that are forbidden by the well-known selection rules are now possible, and their rates depend on neutrino mass. Atomic transitions are therefore low energy observables that can in principle be used to learn more about fundamental particles. And what is more, although the tree level forces mediated by the weak bosons are stronger than the neutrino force, they are shorter ranged and so for hydrogen states with higher angular momentum, the tree level forces are insignificant. We find the rate of these transitions being largely below experimental sensitivity, for

the hydrogen atom, but all hope is not lost yet.

For one, the hydrogen atom is not the perfect playground for such parity-violating effects to shine - larger atoms with more nuclear content enhance the effects of the weak force, and hence also the neutrino force. The atomic transition rates in such systems are also more challenging to compute, but such computations have been performed by the atomic/molecular physics community using Hartree-Fock methods. It will require enthusiastic collaboration from both particle physics and atomic physics communities to bring such projects to fruition, which makes it an avenue for excitement. Secondly, the parity violating effects may be strongly enhanced by forces mediated by new physics mediators such as dark matter. So far a parity violating dark sector has rarely been discussed, but as of yet, nothing rules these classes of models out entirely. Thirdly, the forces mediated by a fermion pair can be enhanced greatly in the presence of backgrounds. In a recent work, we show that in the presence of a background of neutrinos, the neutrino potential at distances $r \gg E_\nu^{-1}$ goes as $V_{\rm bkg}(r) \sim 1/r$ in the massless limit, as opposed to $1/r^5$. This is a huge enhancement over the case of neutrino forces in vacuum, roughly due to the fact that the external background puts one of the fermions being exchanged on shell. In fact, this potential is only about $10^{14}$ times weaker than the gravitational potential between the two bodies. Since the radial dependence of this force is the same as the behavior of the gravitational potential, i.e $1/r$, this force causes a violation of the equivalence principle. Thus experiments (such as the former Eot-Wash experiment) that look for violations of the equivalence principle may be good probes of the neutrino force in a background.

The Eot-Wash experiment, for instance, could detect violations in the equivalence principle with a precision of about 1 in $10^{13}$, Since we find that the neutrino force is only about $10^{14}$ times smaller than gravity, it is possible that the experiment may achieve sensitivity to the neutrino force in the future. The inability to detect a significant effect might say something about the neutrino masses as well. Forces in other new physics backgrounds such as those from dark matter, also deserve to be studied, and I leave those to be studied in future work. A lot of potential exists in the study of quantum forces, and more can be done in this area, particularly since most of the existing study of the 2-fermion exchange forces are done in the ambit of four-Fermi theory by integrating out heavy bosons. This gives non-renormalizable potentials that are challenging to apply to atomic systems since matrix elements involving such potentials tend to blow up for atomic states with low angular momentum.

In [1], we compute the power loss formula (analogous to the Larmor formula in electromagnetism) for fermion-antifermion radiation from a classical system. We apply our formula to power loss due to neutrino emission from a binary star system containing muons, for two models - one where the neutrinos are radiated via a gauge boson of a new $U(1)'$ symmetry $L_\mu - L_\tau$, and another where the neutrinos are emitted via a scalar mediator.

## 1.2 Kaon physics

Moving on from quantum forces, I focus now on another area of my research, namely flavor physics. The majority of my work in flavor, however, has been in the subject of kaons. The flavor structure of the SM is encoded in the Cabbibo-Kobayashi-Maskawa (CKM) matrix, which governs the weak interactions of the up-type quark $(u, c, t)$ mass eigenstates and the down-type $(d, s, b)$ mass eigenstates, and is the source of Charge-Parity (CP) violation in the SM. Historically, determination of the CKM matrix has been largely done through decays of $B$ mesons. Kaon decays are not placed in spotlight largely due to the presence of non-perturbative "long-distance" effects of QCD that make most of them "theoretically unclean" and uninformative of SM parameters. The study of the SM with a different flavor system such as kaons is therefore, crucial as an independent test of the SM, and may also lead the way to signatures of BSM physics. The few theoretically clean kaon decays such as $K_L \to \pi^0 \nu\bar{\nu}$ and $K^+ \to \pi^+ \nu\bar{\nu}$ are thus considered "golden modes" in kaon physics since these decays have little hadronic uncertainty. In my research, I propose a **third** golden mode: $K \to \mu^+\mu^-$.

In [2], we showed that under the well-motivated assumption that the decay of $K_S$ to the $s$-wave dimuon pair is purely CP violating, $K_S \to (\mu^+\mu^-)_{\ell=0}$ is rendered theoretically clean. This allows us extract SM information from $K_S \to (\mu^+\mu^-)_{\ell=0}$ using time-evolution measurements of the oscillating $K^0 - \bar{K}^0$ two state system. This provides a unique way to test the SM, in particular, to extract the CKM matrix element combination $|V_{ts}V_{td}\sin(\beta + \beta_s)|$.

The SM prediction for $K_S \to (\mu^+\mu^-)$ is about 3 orders of magnitude below the current bounds on the $K_S \to \mu^+\mu^-$ decay rate, implying ample opportunity for NP searches in this mode. In [3], we show that NP models involving leptoquarks, or $Z'$ particles can actually saturate the bounds on the rate of $K_S \to \mu^+\mu^-$. This is strong motivation to design an experiment that can measure the time evolution of the neutral kaon wavefunction.

In [4], we find that the phase appearing in the unitarity relation between $\mathcal{B}(K_L \to \mu^+\mu^-)$ and $\mathcal{B}(K_L \to \gamma\gamma)$ is equal to the phase shift in the interference term of time-dependent $K \to \mu^+\mu^-$ decays. A probe of this relation at future kaon facilities constitutes a Standard Model test with a theory precision of $\sim 1\%$.

## 1.3 B physics

$SU(3)$-flavor is an approximate symmetry of the SM between the constituents of the light quark triplet $(uds)$. In the quark model of hadrons, this symmetry allows us to derive linear relationships between various hadronic decay amplitudes, which are known as "sum rules". In [5] we studied the various $SU(3)_F$ sum-rules of $b \to c\bar{c}s(d)$ decays of the beauty baryons $(\Lambda_b, \Xi_b^0, \Xi_b^-)$ to one of $\Sigma^{0,-}$, $\Xi^{0,-}$, $\Lambda$, $n$ baryons and a singlet. Under several reasonable assumptions we found $|\mathcal{A}(\Xi_b^0 \to \Lambda S)/\mathcal{A}(\Xi_b^0 \to \Xi_0 S)| \approx 1/\sqrt{6}|Vcs^*V_{cd}/(V_{cb}^*V_{cs})|$ and $|\mathcal{A}(\Lambda_b \to \Sigma^0 S)/\mathcal{A}(\Lambda_b \to \Lambda S)| \sim 0.02$. These two relations have been recently probed by LHCb for the case of $S = J/\psi$. The former agrees with the measurement, while for

the latter our prediction lies close to the upper bound set by LHCb.

CHAPTER 2

# PROBING THE TWO-NEUTRINO EXCHANGE FORCE USING ATOMIC PARITY VIOLATION

## 2.1 Introduction

The fact that a pair of massless neutrinos mediate a long-range force via one-loop diagrams, as shown in Fig. 2.1, has been known for a long time [6, 7, 8, 9]. At leading order, this diagram gives rise to a force of the form

$$V(r) = \frac{G_F^2}{4\pi^3 r^5}, \tag{2.1}$$

where $G_F$ is the Fermi constant. The force is very weak. At distances larger than about a nanometer its magnitude is smaller that the gravitational force between two protons. At this scale, the electromagnetic Van der Waals force overpowers both. Thus, it has not been observed yet and furthermore, there is no realistic proposal to build an experiment that could see it. It is, therefore, an interesting question to ask if there is any way to probe this force that has not been explored yet.

In many cases in the past, to observe a very small effect, one looked for symmetries that are broken by it. For example, the weak interaction was observed, even though it is much weaker than the strong and electromagnetic interactions, because it violates the flavor symmetries of these stronger forces. Thus, one way

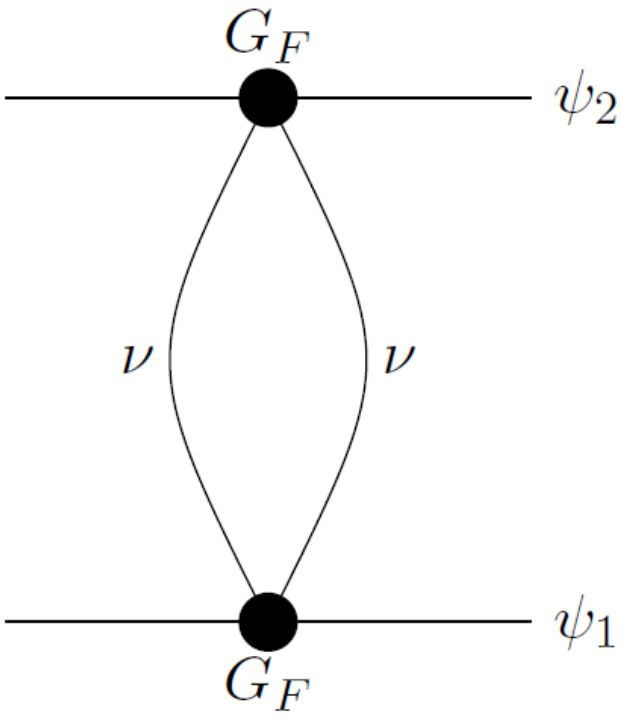


The four-Fermi effective diagram for two-neutrino exchange forces between two fermions, labeled $\psi_1$ and $\psi_2$.

to try to achieve sensitivity to the two-neutrino force is to look for symmetries that it violates.

In this chapter, we point out that the two-neutrino force is the largest long-range parity-violating interaction in the Standard Model (SM). This is in contrast to the parity violation mediated by the $W$ and the $Z$ bosons, which is a short-distance effect. The reason is that in the case of the two-neutrino force the mediator is massless (or close to massless), while in the case of the $W$ and the $Z$ the mediators are massive.

In recent years atomic and molecular systems have attracted considerable interest as probes of physics within and beyond the SM. For instance, the work of Fichet [10] explores molecular spectroscopy as a probe of dark matter. Another example is Ref. [11], where Stadnik shows how the long-range neutrino force can be probed using atomic and nuclear spectroscopy. Given that parity violation in atoms has also been suggested as a probe of new physics, for example, in [12], a natural question to ask is whether it is possible to see effects of the neutrino force in parity-violation experiments done on atomic systems. In this chapter, we explore this idea in some depth.

We find that the effect of the parity non-conserving force on atomic systems is tiny, much smaller than what one can hope to achieve in the near future. Yet, our approach in this chapter can be used in other setups and, while we do not have a concrete idea where it can be practical, the hope is that a system where long-range parity violation can be large enough to probe experimentally will be found.

The arrangement of the chapter is as follows: In Sec. 2.2, we briefly review the literature regarding the two-neutrino force. Sec. 2.3 aims to provide some background on atomic parity violation. We discuss parity violating forces in atomic systems in Sec. 2.4. Thereafter, we shift our focus to the hydrogen atom and compute the parity-violating two-neutrino force between the proton and the electron in the hydrogen atom in Sec. 2.5. The effects of this force on hydrogen eigenstates are discussed in Sec. 2.6, while a sample calculation to illustrate the idea has been performed in Sec. 2.7. Finally, we present our concluding remarks in Sec. 7.6. More

details about the calculations in Sec. 2.5 and Sec. 2.7 are given in the Appendix.

## 2.2 A review of the two-neutrino force

A classical force is mediated by a boson. The two-neutrino exchange gives rise to a long-range force since two fermions, to some extent, can be treated as a boson. This force is also called "a quantum force" as it arises at the loop level. In this section, we provide a brief review of the literature on the long-range force generated by the exchange of a pair of neutrinos.

Although the idea of a two-neutrino mediated force was conceived by Feynman [13], the first calculation of the force dates back to Ref. [6], where Feinberg and Sucher computed the leading form of the two-neutrino force to obtain Eq. (2.1). They worked in the four-Fermi approximation, that is, neglecting terms of order $E/m_W$, $E$ being the energy of the interaction, and $m_W$ the mass of the $W$ boson. The same authors repeated the calculation in Ref. [7] to incorporate the previously ignored neutral current interaction. In both calculations, the velocity-dependent terms of the potential were ignored under the assumption that the velocity of the fermions was much smaller than the speed of light. Later, Sikivie and Hsu performed a similar calculation in Ref. [8], employing a different technique and keeping terms to first order in $v$ in the non-relativistic limit. All these calculations assumed that the neutrino is massless and that there is only one flavor of neutrinos.

Despite being a very small effect, in Ref. [9], Fischbach claimed that if neutrinos were massless, the two-neutrino force between neutrons in a neutron star could raise the self energy of the system to a value that is much higher than the mass of the star itself. Without any other mechanism to stop this, Fischbach proposed that the neutrino is, in fact, massive. A massive mediator would shorten the range of the two-neutrino force and solve the problem. However, Smirnov and Vissani [14] posited that low-energy neutrinos created and subsequently captured in the star (the phenomenon is described in [15]) fill a degenerate Fermi sea that blocks the free propagation of the neutrinos that are responsible for the neutrino force. In response, Fischbach in Ref. [16] stated that more work needs to be done to understand the capturing process and that, for low energies, the two-neutrino force can be repulsive leading to the neutron star actually repelling neutrinos instead of filling up the Fermi sea. Then, Kiers and Tytgat in Ref. [17] argued that the neutrino self-energy does not destabilize the neutron star. Yet in a recent paper by Fischbach [18], he does not agree with that conclusion. In our work, we do not investigate this issue, and do not put any bound on the neutrino mass from neutron star considerations. Our focus is on aspects of the neutrino force that are relevant to atomic physics.

Following Fischbach's calculation of the potential due to massive Dirac neutrinos, Grifols et al. [19] calculated the same potential for massive Majorana neutrinos, which differ from Dirac neutrinos in the non-relativistic limit because of the different spinor structure of Majorana fermions. Their approach is the same as that in [6]. For future reference, the parity-conserving form of the two-neutrino

potential to leading order in $v$ for the case of a single flavor of neutrinos with mass $m_\nu$ is given by

$$V_{\nu\nu}^{\text{Dirac}}(r) = \frac{G_F^2 m_\nu^3}{4\pi^3} \frac{K_3(2m_\nu r)}{r^2}, \qquad V_{\nu\nu}^{\text{Majorana}}(r) = \frac{G_F^2 m_\nu^2}{2\pi^3} \frac{K_2(2m_\nu r)}{r^3}, \tag{2.2}$$

where $K_n(x)$ is the $n$th order modified Bessel functions of the second kind.

An additional effect in neutrino physics, due to the non-zero masses, is flavor mixing (for a review, see, for example, Ref. [20]). This phenomenon was incorporated into the computation of the two-neutrino force in Ref. [21], although a closed form for the neutrino force was not attained. One can also look in [22] for a treatment of the spin-independent part of the neutrino force with flavor mixing. Lastly, thermal corrections to the neutrino force, in both the Dirac and Majorana cases, were computed in [23].

All the calculations mentioned above compute terms in the potential that are parity conserving, i.e. parity-violating terms have been ignored. In this work, we go beyond the leading-order results in $v$ and compute terms in the potential that are spin and momentum dependent and also parity violating. Our key results are described in section 2.4, and their implications are described in Sec. 2.6. We keep terms to first order in $v$ in our non-relativistic calculation.

## 2.3 Observing Atomic Parity Violation – a review

In this section, we review the concepts of Atomic Parity Violation (APV) that are relevant to the present work. We look at atomic parity violation from the perspective of transitions in atoms, more specifically, stimulated emission processes, wherein an emission is caused by shining light on a sample of atoms. For a more detailed review of APV from both theoretical and experimental perspectives, see Refs. [24, 25, 26, 27].

The key idea behind looking for APV is to exploit the fact that in the presence of a parity violating term in the atomic Hamiltonian, the energy eigenstates have no definite parity. As per the well-known selection rules, electric dipole ($E1$) transitions happen between states of opposite parity while magnetic dipole ($M1$) transitions take place only between states of same parity. If the energy eigenstates, however, have no definite parity, then both $E1$ and $M1$ transitions are allowed between them. Since the parity violating interactions are usually very weak compared to the parity conserving ones, we treat them as perturbations to a parity conserving Hamiltonian. Eigenstates of the full Hamiltonian, therefore, are superpositions of a predominant state of definite parity with small opposite parity corrections.

A direct consequence of the presence of parity-violating interactions is that left-polarized light has a different refractive index from right-polarized light in a sample of atomic vapors, which leads to optical rotation of light in the sample.

This is the property that has been exploited to probe APV so far. An intuitive physical interpretation of this effect is due to Khriplovich [26]: Mixing opposite parity states in the hydrogen atom, for instance, results in the creation of a state wherein the electron effectively has a position-dependent spin orientation that assumes a helical shape. Recall that helical shapes of molecules lead to rotation of the plane of polarization of incident light on a sample. Classically speaking, this is because the electric field of light moving perpendicular to the helical axis causes electrons to produce an electric field along the helical axis, which induces a changing magnetic field perpendicular to the electric field. The combined effect of this is to rotate the plane of polarization of the incident electromagnetic wave.

A stimulated emission transition is basically an electron-photon scattering process, represented by the diagram in Fig. 2.3. If both photons have the same polarization, and the photon is incident on a sample with electron density $N_e$, the scattering process can be translated into an index of refraction [28]. The refractive index $n_P$ depends on the polarization of the photon, labeled by the subscript $P = L, R$, and it is given by

$$n_P^2(k) = 1 + \frac{4\pi N_e}{k^2} f_P(0). \tag{2.3}$$

Here, $f_P(0)$ is the forward scattering amplitude for a photon with polarization $P$, and $k$ is the magnitude of the momentum of the photon.

When the electron is bound in the electromagnetic field of a proton, as in hydrogen, the stimulated emission process, in the presence of Coulombic binding, is represented by the diagram in Fig. 2.3. We treat the proton as an elementary par-

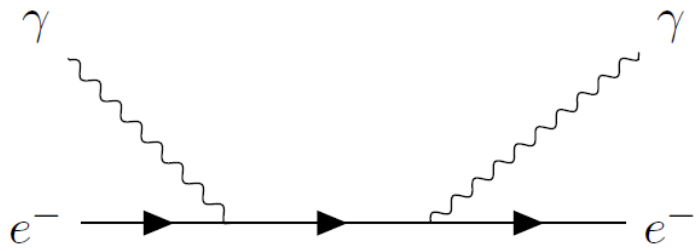


Stimulated emission as electron photon scattering

ticle, since we work at energy scales small enough that the internal substructure of the proton can be ignored. In Fig. 2.3, the proton can be seen as a correction to the electron propagator. Therefore, instead of calculating the transition amplitude using the matrix element from Feynman rules, we can alternatively first compute the static potential that mimics the scattering of the electron off the proton (in this case, the binding). This gives us, at lowest order, the Coulomb force. Thereafter, the external photons effectively become electromagnetic perturbations to the Coulomb field. We can now use time-dependent perturbation theory to calculate the transition amplitude. This is a simple quantum mechanical picture [29] as opposed to a field theoretic perspective. In this picture, we usually talk about electric and magnetic dipole transitions whereas from the perspective of field theory, both transitions are just electron-photon scattering processes.

For incoming and outgoing photons with equal polarization, we can compute the refractive index in hydrogen gas using Eq. (2.3). Note that parity is a good symmetry of QED, and hence $f_R(0) = f_L(0)$ for the process in Fig. 2.3. This implies that the refractive index is the same for left-handed and right-handed polarized

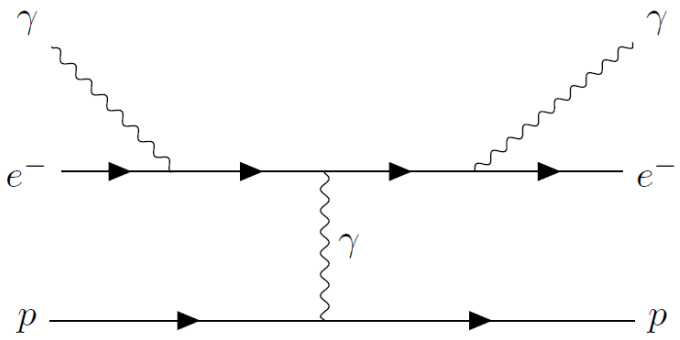


Stimulated emission in hydrogen atom. The electron is shown to be bound to the proton by the mediation of a photon. This is the lowest order diagram at tree level.

photons. When parity is violated, the amplitudes for an incoming right circularly polarized photon and a left circularly polarized photon are different, that is $f_R(0) \neq f_L(0)$, hence $n_R(k) \neq n_L(k)$, causing optical rotation. In the SM the leading-order effect that violates parity is due to $Z$ exchange, and it arises from a diagram similar to the one in Fig. 2.3 with the photon propagator replaced by a $Z$ propagator. We discuss this process in the next section.

The refractive index, which we denote here by $n(\omega)$, of any material in general, and a gas of atoms in particular, has both real and imaginary components, corresponding to the dispersive and absorptive powers of the gas, respectively. The imaginary component is negligible for most values of the frequency, but it is large near bound-state resonances (i.e, when the energy of the incident photon equals the energy difference between two energy eigenstates), which is when the material becomes strongly absorbent. The real part is the well-known index of

refraction. The Kramers-Kronig equations (see Ref. [30]) relate the two quantities as shown below:

$$\mathcal{R}e[n(\omega)] = 1 + \frac{2}{\pi}\int_0^\infty \mathrm{d}\omega' \, \frac{\omega' \, \mathcal{I}m[n(\omega')]}{\omega'^2 - \omega^2}. \tag{2.4}$$

Eq. (2.4) implies that the real part of the refractive index has a maximum near the resonance frequency and thus the local maxima of the real and imaginary parts are close in frequency, see Fig. 2.3.

In a sample, the rotation of the plane of polarization of incident light is proportional to the real part of the refractive index [31]:

$$\Phi = \frac{\pi L}{\lambda}\mathcal{R}e(n_R(\lambda) - n_L(\lambda)) \tag{2.5}$$

where $\Phi$ is the angle of rotation of the plane of polarization of incident light, $L$ is the length of the path of light through the sample and $\lambda$ is the wavelength of incident light. Therefore, near a resonance, there is an enhancement of optical rotation in a material or a gas.

In time-dependent perturbation theory, one can compute the left-right asymmetry between the dipole-transition amplitudes (both electric and magnetic) for right-polarized and left-polarized light [26, 29]. This asymmetry is related to the difference in the real part of the refractive indices for the two respective polarizations. Subsequent analysis yields $\Phi$, for states with the same predominant parity [29] in terms of electric/magnetic dipole transition amplitudes. In the case that

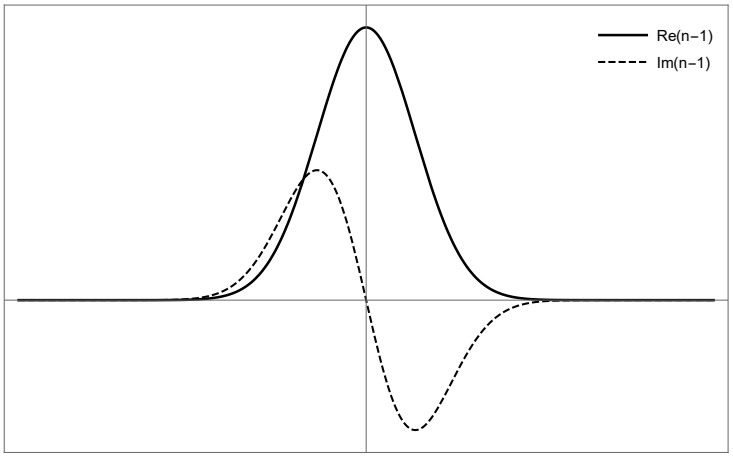


The real and imaginary parts of the refractive index $n$ near a resonance. Absorption follows the imaginary part, while dispersion, and hence, optical rotation follows the real part.

the wavelength is close to the difference in energy between two states of predominantly the same parity, the rotation is given by

$$\Phi = \frac{4\pi L}{\lambda}\mathcal{R}e(n(\lambda) - 1)R, \qquad R = \mathcal{I}m\left(\frac{E1_{PV}}{M1}\right), \tag{2.6}$$

where $n(\lambda) = \frac{1}{2}(n_R(\lambda) + n_L(\lambda))$ is the average refractive index of the sample, $E1_{PV}$ is the forbidden electric-dipole transition element, and $M1$ is the magnetic-dipole transition element between two states of the system with the same predominant parity.

A few points are in order regarding Eq. (2.6):

1. Note that if parity is conserved, the $E1_{PV}$ amplitude is zero and hence the angle of rotation is zero.

2. One could also consider a situation where the two states are of opposite parity. In this case $M1 = 0$ and the effect is proportional to $M1_{PV}$ and we get a formula similar to that of Eq. (2.6). Magnetic-dipole amplitudes, however, are much smaller than electric dipole amplitudes, so probing parity violating effects by observing parity-forbidden magnetic transitions is generally harder.

3. To obtain the largest angle of rotation, the wavelength $\lambda$ must be close to the energy spacing between the states that we are interested in, but far away enough to avoid resonance, as it is clear from Fig. 2.3. In other words, if $\omega_r$ is the frequency at which a resonance occurs, and $\omega$ is the frequency of the incident light, then for a large enough effect, we need to have $|\omega - \omega_r| \sim \Gamma$, where $\Gamma$ is the width of the resonance.

In summary, an important consequence of APV is that, near a resonance, the emitted light has a rotated plane of polarization relative to the incident light. Experimentally, therefore, a measurement of this rotation is a measure of APV. From our theoretical perspective, the important quantity that encodes the effects of APV is $R$, defined in Eq. (2.6).

## 2.4 Parity violating forces in atomic systems

### 2.4.1 Generic effects

The general expression for a non-relativistic potential between two fermions contains only a handful of terms – the only difference between the potentials mediated by different mechanisms is in the numerical coefficients coming with each term and the form of the radial function [32].

Consider a generic atom with a nucleon of mass $m_N$. We are looking for the parity violating potential due to some Feynman diagram. To that end, we make two simplifying assumptions:

1. We consider a static nucleus, that is, we neglect effects that scale like $m_e/m_N$.
2. We treat the electron velocity, $v_e$, as a small parameter and keep only terms linear in $v_e$.

Under these assumptions, the most general form of the parity-violating potential from [32] reduces to the following:

$$V_{PNC}(r) = H_1 F(r)\vec{\sigma}_e \cdot \vec{v}_e + H_2 F(r)\vec{\sigma}_N \cdot \vec{v}_e + C(\vec{\sigma}_e \times \vec{\sigma}_N) \cdot \vec{\nabla}\left[F(r)\right], \tag{2.7}$$

where $\vec{\sigma}_e/2$ is the spin of the electron, $\vec{\sigma}_N/2$ is the net nuclear spin, $H_1$, $H_2$ (for "helicity", since the corresponding terms look like helicity) and $C$ (for cross-product)

are real constants, and $F(r)$ is a radial real function.

The values of the $H_1$, $H_2$, $C$, and $F(r)$ depend on the specific diagram. In case there are several diagrams, each diagram contributes linearly to the total potential, so we can write

$$V_{PNC}(r) = \sum_i V^i_{PNC}(r) \tag{2.8}$$

and we add a sub-index $i$ to $H_1$, $H_2$, $C$, and $F(r)$.

In the following sections, we shall consider the special case of the hydrogen atom. While experiments are not done with it, it simplifies the theoretical investigation. When we consider hydrogen, we replace the sub-index $N$ with $p$.

### 2.4.2 The tree-level process

We begin by briefly revisiting the effective parity-violating potential due to the interaction between an electron and a nucleus at tree level via $Z$ exchange in the SM as depicted in Fig. 2.4.2. In the SM, the coupling of the $Z$ boson to a pair of identical fermions is given by

$$\mathcal{L}_{Z\bar{\psi}\psi} = \frac{1}{2}\frac{g}{\cos\theta_W}\bar{\psi}\left[(g_V^{\psi} - g_A^{\psi}\gamma^5)\not{Z}\psi\right], \tag{2.9}$$

where $\theta_W$ is the Weak angle. $g_V^{\psi}$ and $g_A^{\psi}$ are the vectorial and axial couplings of the fermion $\psi$ to the $Z$ boson. As an example, the coupling constants for the electron and the proton (which can be treated as an elementary particle at energy scales

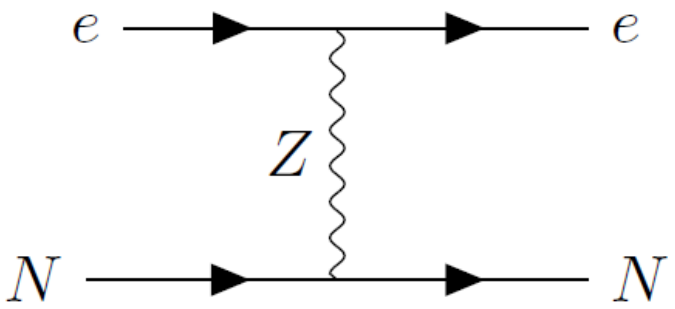


Tree-level interaction between the electron and a nucleus.

relevant to atomic physics) are given by:

$$g_V^e = \left(-\frac{1}{2} + 2\sin^2\theta_W\right), \quad g_A^e = -\frac{1}{2}, \quad g_V^p = \left(\frac{1}{2} - 2\sin^2\theta_W\right), \quad g_A^p = \frac{G_A}{2}, \tag{2.10}$$

where $G_A \approx 1.25$ [33] is the axial form factor of the proton.

The resulting parity-violating potential is given by Eq. (2.7) with the constants and the radial function given by:

$$H_1 = H_1^{\text{tree}} = \frac{g^2}{2\cos^2\theta_W} g_A^e g_V^p, \tag{2.11}$$

$$H_2 = H_2^{\text{tree}} = \frac{g^2}{2\cos^2\theta_W} g_V^e g_A^p, \tag{2.12}$$

$$C = C^{\text{tree}} = \frac{g^2}{2\cos^2\theta_W} \frac{g_V^e g_A^p}{2m_e}, \tag{2.13}$$

$$F(r) = F^{\text{tree}}(r) = \frac{e^{-m_Z r}}{4\pi r}. \tag{2.14}$$

In the APV literature, most notably in [34], the terms that depend on nuclear

spin (that is, terms that come with $H_2$ and $C$) are ignored. This is because, in most heavy atoms used in APV experiments, the nuclei have paired nucleons with opposite spins, and a net nuclear spin of zero. Thus, terms in the potential containing the nuclear spin vanish. This is not true for the case of hydrogen, where the nucleus consists of just one spin-half proton.

### 2.4.3 Loop level processes: The effective four-Fermi operator with neutrinos

Now that we have discussed the tree level diagram that violates parity, we move on to loop level effects. The diagrams that contribute to atomic parity violation at one loop are given in Fig. 2.4.3. At atomic energy scales, the use of the four-Fermi approximation is well justified and so in this section, we will derive expressions for the four-Fermi vertices with two fermions of the same type $\psi$ and two neutrinos.

In the SM, the four-Fermi interactions between two neutrinos and two fermions are obtained by integrating out the $Z$ and $W$ bosons in the diagrams shown in Fig. 2.4.3. However, since we consider massive neutrinos, we need to incorporate flavor mixing. The $Z$-boson case is simple because the interactions of neutrinos with the $Z$ boson is universal and thus diagonal in any basis:

$$\mathcal{L}_Z = -\frac{g}{2c_W}\delta_{ij}\bar{\nu}_i \not{Z} \nu_j, \tag{2.15}$$

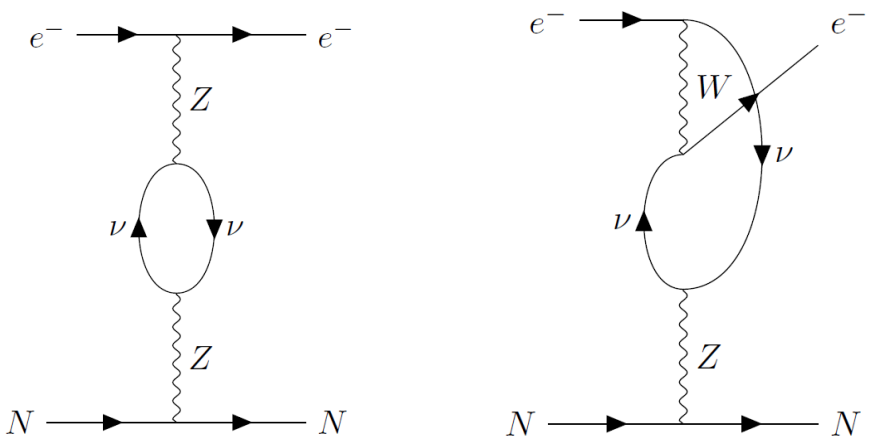


(a) (b)

The loop level diagrams that contribute to the binding of the electron to the nucleus in an atomic system.

with $c_W \equiv \cos\theta_W$. The corresponding four-Fermi operator for a vertex involving two fermions $\psi$, and two neutrino mass eigenstates, $\nu_i$ and $\nu_j$, due to $Z$ exchange is therefore

$$(O_Z)_{ij} = -\frac{g^2}{8m_Z^2 c_W^2}[\bar{\psi}\gamma^\mu(g_V^\psi - g_A^\psi\gamma^5)\psi]\delta_{ij}[\bar{\nu}_j\gamma_\mu(1-\gamma^5)\nu_i], \tag{2.16}$$

where $g_A^\psi$ and $g_V^\psi$ are defined above Eq. (2.10).

The case of the $W$ exchange is more complicated as we need to take into account the non-diagonal nature of the flavor mixing. The $W$ interaction Lagrangian in the mass basis for the neutrinos is given by:

$$\mathcal{L}_W = -\frac{g}{\sqrt{2}}U_{\alpha i}\bar{\ell}_{L\alpha}\not{W}\nu_i, \tag{2.17}$$

where the fields $\ell$ represent leptons and $i$ ($\alpha$) represents mass (flavor) indices, and $U_{\alpha i}$ are the elements of the Pontecorvo-Maki-Nakagawa-Sakata (PMNS) matrix.

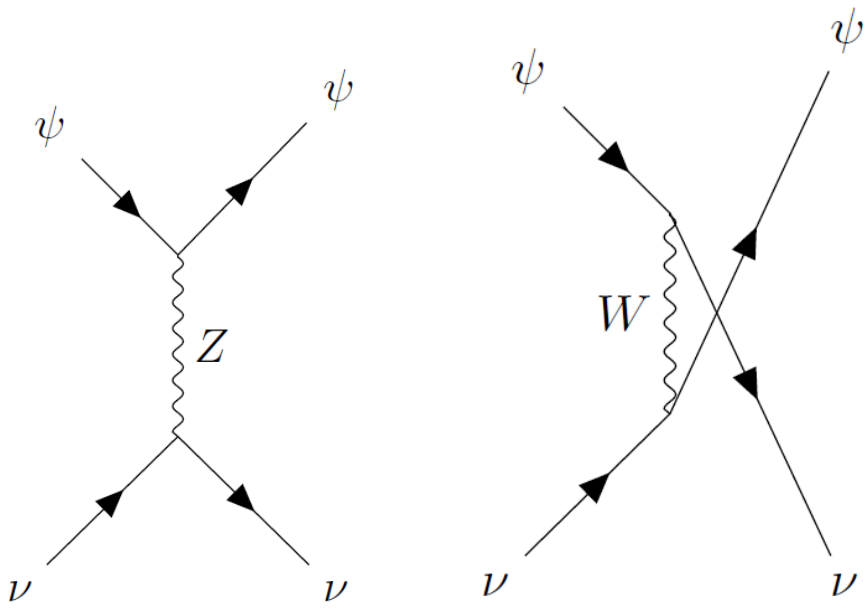


(a) (b)

The two diagrams that contribute to the effective four-Fermi vertex for two neutrinos and two fermions $\psi$. The $Z$-diagram on the left corresponds to the effective operator $O_Z$. The $W$ diagram on the right corresponds to the effective operator $O_W$.

The operator for the case of two external $\psi$ leptons of flavor $\alpha$ and two neutrino mass eigenstates $i$ and $j$ is then given by

$$\begin{aligned}(O_W)_{ij} &= -\frac{g^2}{8m_W^2}U_{\alpha j}U_{\alpha i}^*[\bar{\nu}_j\gamma^\mu(1-\gamma^5)\psi][\bar{\psi}\gamma_\mu(1-\gamma^5)\nu_i], \\ &= -\frac{g^2}{8m_W^2}U_{\alpha j}U_{\alpha i}^*[\bar{\psi}\gamma^\mu(1-\gamma^5)\psi][\bar{\nu}_j\gamma_\mu(1-\gamma^5)\nu_i], \end{aligned} \tag{2.18}$$

where we used the Fierz transformations to obtain the second line.

The sum of the operators in Eqs. (2.16) and (2.18) yields the four-fermion vertex

between two neutrino mass eigenstates and two $\psi$ leptons. Using $G_F = g^2/4\sqrt{2}m_W^2$, we obtain

$$\begin{aligned} O_{ij} &= (O_Z)_{ij} + (O_W)_{ij} \\ &= -\frac{G_F}{\sqrt{2}}\left[\bar{\psi}\gamma^\mu\{\delta_{ij}(g_V^\psi - g_A^\psi\gamma^5) + U_{\alpha j}U_{\alpha i}^*(1-\gamma^5)\}\psi\right]\left[\bar{\nu}_j\gamma_\mu(1-\gamma^5)\nu_i\right], \\ &= -\frac{G_F}{\sqrt{2}}\left[\bar{\psi}\gamma^\mu(a_{ij}^\psi - b_{ij}^\psi\gamma^5)\psi\right]\left[\bar{\nu}_j\gamma_\mu(1-\gamma^5)\nu_i\right]. \end{aligned} \tag{2.19}$$

We emphasize that there is no sum over $i$, $j$ or $\alpha$ here. In Eq. (2.20), we introduced the effective vectorial and axial couplings, $a_{ij}$ and $b_{ij}$ respectively, in terms of the couplings to the $Z$. If $\psi$ is a lepton and therefore has a flavor index $\alpha$, we have:

$$a_{ij}^\psi = \delta_{ij}g_V^\psi + U_{\alpha j}U_{\alpha i}^*, \quad b_{ij}^\psi = \delta_{ij}g_A^\psi + U_{\alpha j}U_{\alpha i}^*. \tag{2.20}$$

If $\psi$ were not a lepton, it would not couple to neutrinos through the $W$, and therefore the PMNS matrix would not be involved. Then we would have:

$$a_{ij}^\psi = \delta_{ij}g_V^\psi, \quad b_{ij}^\psi = \delta_{ij}g_A^\psi, \tag{2.21}$$

In order to compute the neutrino force between two fermionic species $\psi_1$ and $\psi_2$, we need to insert the operator $O_{ij}$ twice in order to obtain the diagram in Fig. 2.1. If both $\psi_1$ and $\psi_2$ are leptons, we have nine diagrams from assigning three neutrino mass eigenstates into the two propagators. Each diagram is labeled by two indices $i$ and $j$, and we sum over them. If $\psi_1$ or $\psi_2$ is a non-lepton, then the only possible four-Fermi vertices are the ones with both neutrinos in the same mass eigenstate. Thus, there are three diagrams over which to sum over. We only need one label $i = 1, 2, 3$ to denote a diagram since the effective couplings $a$

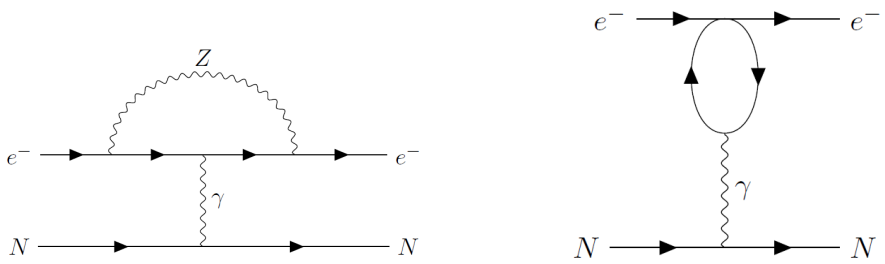


(a) (b)

The photon penguin is shown on the left, and again on the right after integrating out the $Z$ boson.

and $b$ are diagonal. We shall make use of precisely this fact to explore APV in the simplest atomic system, i.e, the hydrogen atom, in Sec. 2.5.

### 2.4.4 The photon penguin

In this subsection, we digress to talk about another possible parity violating diagram in our atomic system, the photon penguin, shown in Fig. 2.4.4. This diagram is also parity violating since it has two weak interaction vertices. However, it does not give rise to a long ranged parity violating potential, as we discuss below.

Assuming that the momentum transfer is much smaller than the $Z$ boson mass, we can integrate out the $Z$ resulting in an effective photon penguin diagram as shown in Fig. 2.4.4. Using the same approach as in Ref. [7], the parity-violating potential is found to be in accordance with Eq. (2.7), with the quantities $H_1$, $H_2$, $C$,

and $F(r)$ given by:

$$H_1 = H_1^{\text{penguin}} = (g_V^e)(g_A^e)G_F\ \alpha\ m_e, \tag{2.22}$$

$$H_2 = H_2^{\text{penguin}} = 0, \tag{2.23}$$

$$C = C^{\text{penguin}} = 0, \tag{2.24}$$

$$F(r) = F^{\text{penguin}}(r) \tag{2.25}$$

where the explicit calculation gives

$$F^{\text{penguin}}(r) = 2e^{-2m_e r}\int_0^\infty dx\ e^{-rx}\frac{\sqrt{x^2+4xm_e}}{(x+2m_e)^2}\left(x^2+4xm_e+6m_e^2\right). \tag{2.26}$$

We were unable to find a closed form of $F^{\text{penguin}}(r)$. However, for our purpose, all we care about is the $r \gg m_e$ limit. In that limit, we obtain the asymptotic form of $F^{\text{penguin}}(r)$ to be:

$$F^{\text{penguin}}(r) \sim 12\Gamma\left(\frac{3}{2}\right)\sqrt{m_e}\frac{e^{-2m_e r}}{r^{5/2}}. \tag{2.27}$$

The main conclusion from Eq. (2.27) is that the potential due to the photon penguin far away from the nucleus is suppressed by an exponential term that has a range given by $(2m_e)^{-1}$. The factor of 2 is because the penguin diagram consists effectively of two exchanged electrons, just like in the neutrino case where we exchanged two neutrinos. The potential is sensitive to the mass of the electron because there is a branch cut in the scattering amplitude for the diagram in the complex$-t$ plane starting at $t = 4m_e^2$.

Some important differences between this potential and the potential with two internal neutrinos are as follows:

1. The potential due to the photon penguin has only one factor of $G_F$, as opposed to the neutrino case which is suppressed by two factors of $G_F$. Yet, given the short range nature of the photon penguin for atomic physics, which is what our concern in this work, this force is not relevant.

2. The other possible photon penguin has a $Z$ boson joining the proton legs. But as it is clear from this calculation, the diagram analogous to Fig. 2.4.4 for this process has a proton in the loop, and thus the radial function will have its range governed by the proton mass. This makes the parity violating force shorter ranged than the force obtained from the photon penguin with the electron loop, and thus negligible.

To conclude, the key takeaway is that the photon penguin does not contribute to long rage parity violation at atomic scales. We can safely ignore its effects for the systems that we care about in this work.

## 2.5 The neutrino force in the hydrogen atom

We now apply the results obtained above to the hydrogen atom. In the hydrogen atom, the proton does not couple to the neutrinos through the $W$ boson, and so the only diagrams that contribute are the three diagrams with the same neutrino mass eigenstate on both propagators in the loop. Using Eqs. (2.20) and (2.21), we find that in this case, the corresponding couplings are diagonal and are given by

(superscripts refer to the electron and the proton respectively)

$$\begin{aligned} a_{ii}^{e} &= \left(-\frac{1}{2}+2s_W^2+|U_{ei}|^2\right), \quad a_{ii}^{p}=\left(\frac{1}{2}-2s_W^2\right) \\ b_{ii}^{e} &= \left(-\frac{1}{2}+|U_{ei}|^2\right), \quad b_{ii}^{p}=\frac{G_A}{2}\approx 0.625, \end{aligned} \tag{2.28}$$

where $G_A$ is the axial form factor, as defined below Eq. (2.10), and $s_W = \sin\theta_W$. Since both propagators have the same mass eigenstate, the non-diagonal entries in $a_{ij}$ and $b_{ij}$ are zero. For the same reason, we only keep one index $i$ from now on.

Using the couplings from Eq. (2.28), we calculate the parity-violating potential from the neutrino loop, which results in a form given by Eq. (2.8) (see appendix A.1 for details of the calculation). with the constants and the radial function given by (no sum over $i$ in any of the expressions):

$$H_{1i} = H_{1i}^{\text{loop}} = -2\frac{a_i^p b_i^e}{m_e}, \tag{2.29}$$

$$H_{2i} = H_{2i}^{\text{loop}} = 2\frac{a_i^e b_i^p}{m_e}, \tag{2.30}$$

$$C_i = C_i^{\text{loop}} = \left(\frac{a_i^e b_i^p}{m_e}+\frac{a_i^p b_i^e}{m_p}\right), \tag{2.31}$$

$$F_i = F_i^{\text{loop}}(r) = V_{\nu_i\nu_i}(r), \tag{2.32}$$

where $V_{\nu_i\nu_i}(r)$ can be found in Eq. (2.2).

Using the fact that $s_W^2 \approx 0.23$, so that $a_i^p$ is very small and that $m_e \ll m_p$, we note that $H_{1i}$ is negligible. The parity-violating potential then simplifies to:

$$V_{PNC}^{\text{loop}} \approx \sum_i \frac{G_A}{m_e}\left(-\frac{1}{4}+s_W^2+\frac{1}{2}|U_{ei}|^2\right)\left[(2\vec{\sigma}_p\cdot\vec{p_e})V_{\nu_i\nu_i}(r)+(\vec{\sigma_e}\times\vec{\sigma_p})\cdot\vec{\nabla}V_{\nu_i\nu_i}(r)\right]. \tag{2.33}$$

Eqs. (2.29)-(2.33) are the key results in our work. The parity-violating terms obtained here have the same spin structure as in the case of the tree-level potential, but the radial behavior is different. Investigation of these terms in the neutrino potential has not been carried out before.

## 2.6 Effects of the neutrino force on hydrogen eigenstates and transitions

In this section, we treat the neutrino potential in Eq. (2.33) as a perturbation to the hydrogen atom Hamiltonian. We work in the limit $m_p \to \infty$, so that the proton is essentially static. We assume that the neutrino is of Dirac nature subsequently in this work, but one could also treat them as Majorana fermions and perform an analogous computation.

The neutrino force is much smaller than the fine or hyperfine interactions and therefore, we need to include the fine-structure and the hyperfine splittings as well in our calculations. As always, we should look for an operator that commutes with the neutrino potential, and use the eigenbasis of this operator as the basis of choice in first-order degenerate perturbation theory. Since the neutrino potential is a scalar, we know that an operator that commutes with it is $\hat{F}^2$, where

$$\vec{F} \equiv \vec{L}_e + \vec{S}_e + \vec{S}_p$$

is the total angular momentum of the entire system. We also define $\vec{J} \equiv \vec{L}_e + \vec{S}_e$ as

the total angular momenta of the electron alone.

The unperturbed eigenstates $|n, f, m_f, j, \ell, s_p, s_e\rangle$ with which we work are simultaneous eigenstates of $\hat{H}_0, \hat{F}^2, \hat{F}_z, \hat{J}^2, \hat{L}_e^2, \hat{S}_p^2$ and $\hat{S}_e^2$, where $\hat{H}_0 = \vec{p}^2/2m_e - e^2/r$ is the unperturbed hydrogen atom with only the Coulombic interaction. The eigenvalues of $\hat{F}^2, \hat{F}_z, \hat{J}^2, \hat{L}_e^2, \hat{S}_p^2$ and $\hat{S}_e^2$ are $f(f+1), m_f, j(j+1), \ell(\ell+1), s_p(s_p+1)$ and $s_e(s_e+1)$ respectively. Every state is thus described by 7 quantum numbers. But $s_e = s_p = 1/2$ are fixed numbers, and so we really need just 5 numbers to label a state. This is indeed what we expect since the hydrogen atom has a total of 8 degrees of freedom (dof): there are 3 position dof and 1 spin dof each for the electron and the proton. However, we do not care about the three dof of the center of mass, leaving us with 5 dof to describe the internal dynamics of our system.

The angular momentum states can be constructed using the standard procedure of angular momentum addition using Clebsch-Gordon coefficients, as done in Ref. [35], for instance. The orbital angular momentum of the electron $\ell$ takes values $0, 1, 2, \ldots$ Depending on $\ell$, the result of the angular-momentum addition of one orbital angular momentum and two spin-1/2 systems (the electron and the proton are both spin-1/2) can be summarized in the following notation:

$$\ell \otimes \frac{1}{2} \otimes \frac{1}{2} = \underbrace{(\ell+1) \oplus \ell}_{j=(2\ell+1)/2} \oplus \underbrace{\ell \oplus (\ell-1)}_{j=(2\ell-1)/2}. \tag{2.34}$$

These vector spaces contain eigenstates of the hydrogen atom written in the basis of $\hat{F}^2$ for a given principal quantum number $n$. The first two vector spaces in the direct sum consist of states with a well-defined value of $j = (2\ell + 1)/2$, while the latter two vector spaces have well-defined $j = (2\ell - 1)/2$.

In the unperturbed hydrogen atom, all these states would be degenerate. But with the perturbations, such as the fine structure corrections and the hyperfine splitting interactions included, the degeneracy is lifted, and only the degeneracy in $m_f$ is left. The energy of an eigenstate with quantum numbers $f, j, \ell, s_e = s_p = \frac{1}{2}$, for the case where $\ell > 0$, is given by (see Ref. [36])

$$E_{nfj\ell} = (E_0)_n + (E_{\text{fine}})_{nj} + (E_{\text{hyperfine}})_{nfj\ell} \tag{2.35}$$

where:

$$(E_0)_n = -\frac{\alpha^2 m_e}{2n^2}, \tag{2.36}$$

$$(E_{\text{fine}})_{nj} = -\frac{\alpha^4 m_e}{2n^4}\left(\frac{n}{j+\frac{1}{2}} - \frac{3}{4}\right), \tag{2.37}$$

$$(E_{\text{hyperfine}})_{nfj\ell} = \frac{\alpha^4 g_p}{m_p} a_0^3 \frac{\ell(\ell+1) m_e^2 \left(f(f+1) - j(j+1) - \frac{3}{4}\right)}{4j(j+1)} \left\langle \frac{1}{r^3} \right\rangle_{n\ell} \tag{2.38}$$

are the energies contributed by the Coulombic potential, fine structure and hyperfine interactions respectively, $r$ is the radial coordinate of the electron, $a_0 = (m_e\alpha)^{-1}$ is the Bohr radius, and $g_p \approx 5.56$ is the $g$-factor of the proton [37].

As a reminder, in first-order perturbation theory, in the presence of a perturbation $V$, the corrected states are given by

$$|\psi_q^1\rangle = |\psi_q^0\rangle + \sum_{p \neq q} \frac{\langle \psi_p^0 | V | \psi_q^0 \rangle}{E_q^0 - E_p^0} |\psi_p^0\rangle \tag{2.39}$$

Here, $|\psi_p^0\rangle$ are the states in our chosen eigenbasis. Note that in this basis our perturbation is diagonal in each degenerate subspace. Under the perturbation, we say that the states in this basis "mix" among themselves to give the true eigenstates of the system.

The energy difference between states of different $n$ is much larger than that for those states with the same principal quantum number. Since the corrections to the eigenstates in perturbation theory go as $(\Delta E)^{-1}$, we keep corrections contributed by states with the same $n$ as our unperturbed states when calculating opposite-parity corrections to eigenstates in first-order perturbation theory.

Note that states mix among themselves under a scalar perturbation only when they have the same value of $f$. But, for any eigenstate of $\hat{F}^2$, the correcting states have a different value of $\ell$ if the perturbation violates parity. Therefore, under the effect of a parity-violating perturbation, a state attains an opposite parity admixture as expected. As discussed in Sec. 2.3, both $E1$ and $M1$ transitions are therefore allowed between the actual eigenstates and we can expect to see an interference of $E1$ and $M1$ amplitudes that leads to optical rotation in a sample of atomic hydrogen. In Sec. 2.7, we shall compute this effect for certain states in hydrogen.

Parity violation in hydrogen is also manifest from the tree-level $Z$-potential. Intuitively, for states with $\ell = 0$ , this tree-level process should completely overpower the neutrino loop diagram because these states have strong presence at the origin, which is also where the $Z$-potential has strong support. Thus, isolating an observable effect from the loop is unfeasible for such states. Higher-$\ell$ states do not have strong support at the origin and it would appear that the $Z$-potential does not have much effect on them. However, special care is needed, as we discuss in the next paragraph.

The neutrino-loop potential is highly singular. Therefore, at very short dis-

tances, the four-Fermi theory breaks down and we cannot trust our calculations all the way to $r = 0$. (In order to still use our theory at short distances, we need to follow the methodology described in [38]. See also [39] for a discussion of singular potentials in the Schrödinger equation. Alternatively, we could simply compute the diagrams in Fig. 2.4.3 explicitly without integrating out the heavy bosons, as in the paper by Asaka et.al. [40]) However, if the momentum transfer is much smaller than the mass of the $Z$ boson or, in other words, the length scales are larger than $m_Z^{-1}$, then our calculations can still be trusted. Thus, we are interested in those high-enough values of $\ell$ for which the effects of the loop potential dominate over the $Z$-potential, while being far enough from the origin such that the four-Fermi theory is valid. In the next two subsections, we select those eigenstates of hydrogen that are suitable for the task and show that, for states with orbital angular momentum $\ell \geq 2$, our conditions are met. A full computation of the loop diagrams as done in [40] would give us finite results for $\ell = 0, 1$, but is not necessary here since for $\ell < 2$, the effects of the tree level $Z$-diagram dominates over the neutrino mediated diagrams that we are interested in. We ultimately deal with eigenstates of $\hat{F}^2$, which do not have definite $\ell$, so we need to make sure that the eigenstate of $\hat{F}^2$ is a superposition of eigenstates of $\hat{L}^2$ with $\ell \geq 2$.

### 2.6.1 Matrix elements of the tree-level potential

In order to extract some features of the tree-level parity violating potential, we write out the potential here as given in Eqs. (2.11)-(2.14), but we suppress most of

the dimensionless constants for the sake of clarity:

$$V_{PNC}^{\text{tree}} \sim \frac{g^2}{m_e}\left[\frac{e^{-m_Z r}}{r}\vec{\sigma}_e \cdot \vec{p} + \frac{e^{-m_Z r}}{r}\vec{\sigma}_p \cdot \vec{p} + (\vec{\sigma}_e \times \vec{\sigma}_p)\cdot\vec{\nabla}\left(\frac{e^{-m_Z r}}{r}\right)\right]. \tag{2.40}$$

We are interested in computing the matrix elements of this potential in the space of hydrogen eigenfunctions. In this section, we simply consider the radial integrals in the matrix elements since the angular integrals simply give some $O(1)$ number upon evaluation. We define $\eta \equiv r/a_0$, where $r$ is the radial coordinate. The radial part of the wavefunction, close to the origin, behaves as $u(\eta) \sim \eta^\ell$. Given this, we can write the matrix element as an integral:

$$\langle n\ell m|V_{PNC}^{\text{tree}}|n'\ell' m'\rangle \sim \int_0^\infty \mathrm{d}\eta\, \eta^2\, \eta^{\ell'} V_{PNC}^{\text{tree}}(\eta)\eta^\ell, \tag{2.41}$$

Note that, although the above dependence of the wavefunction is only correct near the origin, we integrate all the way to $\eta \to \infty$ because the potential drops very rapidly in magnitude and so the contribution far away from zero from the wavefunction is negligible anyway.

Terms in the potential of Eq. (2.40) that have angular dependence make the integral vanish unless $\ell' = \ell \pm 1$ (from the properties of the spherical harmonics). Without loss of generality, we take the smaller of the two to be $\ell$, and the larger to be $\ell + 1$. Then the matrix element goes as (notice that the momentum operator introduces a factor of $1/\eta$, as does a gradient)

$$\begin{aligned}\langle n\ell m|V_{PNC}^{\text{tree}}|n', \ell \pm 1, m'\rangle \;&\sim\; \frac{\alpha}{m_e a_0^2}\int_0^\infty \mathrm{d}\eta\, \eta^{\ell+1}\exp\left(-m_Z a_0 \eta\right)\eta^\ell, \\ &\sim \frac{\alpha^{2\ell+5} m_e^{2\ell+3}}{m_Z^{2\ell+2}} = m_e \alpha^{2\ell+5}\left(\frac{m_e}{m_Z}\right)^{2\ell+2}.\end{aligned} \tag{2.42}$$

### 2.6.2 Matrix elements of the neutrino loop potential

There are two terms in the loop potential (2.33): the "helicity" term and the spin-cross term. Once again, we consider only the radial integrals since the angular integrals give some $O(1)$ number. The radial dependence of the integrands in the matrix elements is roughly the same, since the momentum operator and the gradient operator have the same radial structure.

The leading-order dependence of the parity non-conserving loop terms goes like $G_F^2/m_e r^6$. Matrix elements for this operator go as

$$\begin{aligned}\langle n\ell m|V_{PNC}^{\text{loop}}|n'\ell' m'\rangle &\sim \tfrac{G_F^2}{m_e a_0^6}\int \mathrm{d}\eta\, \eta^2\eta^{\ell'}\left(\tfrac{1}{\eta^6}\right)\eta^{\ell}\exp\left[-\eta\left(\tfrac{1}{n}+\tfrac{1}{n'}\right)\right]\\ &\sim \tfrac{\alpha^2}{m_e m_Z^4 a_0^6}\int \mathrm{d}\eta\, \eta^2\eta^{\ell'}\left(\tfrac{1}{\eta^6}\right)\eta^{\ell}\exp\left[-\eta\left(\tfrac{1}{n}+\tfrac{1}{n'}\right)\right].\end{aligned} \tag{2.43}$$

In the expression above, $\left(\frac{1}{n}+\frac{1}{n'}\right) \sim O(1)$ number, which yields some exponential suppression. Let us denote this number by $n_{sup}$. The angular integrals vanish unless $\ell' = \ell \pm 1$ and, like before, we can estimate a naive dependence of the wave function on $\alpha$, $m_e$, etc. We write

$$\begin{aligned}\langle n'(\ell+1)m'|V_{PNC}^{\text{loop}}|n\ell m\rangle &\sim \tfrac{\alpha^2}{m_e m_Z^4 a_0^6}\int \mathrm{d}\eta\, \eta^2\eta^{\ell+1}\left(\tfrac{1}{r^6}\right)\eta^{\ell}\exp(-n_{sup}\eta)\\ &\sim \tfrac{\alpha^2}{m_e m_Z^4 a_0^6}\int \mathrm{d}\eta\, \eta^{2\ell-3}\exp(-n_{sup}\eta).\end{aligned} \tag{2.44}$$

Now, we have the following sub-cases:

1. For $\ell = 0$ and $\ell = 1$: The radial integral does not converge, indicating the failure of four-Fermi theory as we discussed previously.

| $\ell$ | From $V_{PNC}^{\text{tree}}$ | $V_{PNC}^{\text{loop}}$ |
|---|---|---|
| $\ell = 0$ | $\sim \alpha^5 \left(\frac{m_e}{m_Z}\right)^2$ | does not converge |
| $\ell = 1$ | $\sim \alpha^7 \left(\frac{m_e}{m_Z}\right)^4$ | does not converge |
| $\ell \geq 2$ | $\sim \alpha^{2l+5} \left(\frac{m_e}{m_Z}\right)^{2\ell+2}$ | $\sim \alpha^8 \left(\frac{m_e}{m_Z}\right)^4$ |

Tree-level and loop-level matrix elements for different values of $\ell$

2. $\ell \geq 2$: In this case, the integral in Eq. (2.44) does converge and four-Fermi theory is suitable for such states. The result is

$$\frac{\alpha^2}{m_e m_Z^4 a_0^6} \int_0^\infty \mathrm{d}\eta \, \eta^{2\ell-3} \exp(-n_{sup}\eta) \sim m_e \alpha^8 \left(\frac{m_e}{m_Z}\right)^4, \tag{2.45}$$

where we have ignored some $O(1)$ constants that depend on $\ell$.

In Table 2.6.2,we compare the tree-level and loop-level matrix elements for different values of $\ell$. For $\ell = 2$, the tree-level matrix element behaves as $\alpha^9 (m_e/m_Z)^6$, while the loop matrix element goes as $\alpha^8 (m_e/m_Z)^4$. Thus, naively, for $\ell = 2$,

$$\frac{\mathcal{M}_{\text{tree}}}{\mathcal{M}_{\text{loop}}} \sim \alpha \left(\frac{m_e}{m_Z}\right)^2 \approx 10^{-13}. \tag{2.46}$$

In other words, the effect of the tree-level potential is much smaller than the effect of the loop-level potential for $\ell \geq 2$. If we only care about powers of $\alpha$ and $m_e/m_Z$, then our calculations suggest that the effect of the loop remains the same as $\ell \geq 2$, i.e, $\sim \alpha^8 (m_e/m_Z)^4$, but the powers in $\alpha$ and $m_e/m_Z$ in the tree-level effect increase with $\ell$, rendering it much smaller. Thus, to isolate the effects of the loop, we need to consider states for which $\ell \geq 2$.

## 2.7 A sample calculation

Note that while calculating matrix elements of the potential between two states of definite orbital angular momenta, we took the lesser of the two to be $\ell$ and the higher to be $\ell'$. In order for the matrix element to converge in the four-Fermi approximation, we need $\ell \geq 2$. In other words, the lowest angular momentum state that we can work with in a matrix element calculation is $\ell = 2$. Based on this, we explore parity-violating corrections to some of the $\ell = 3$ states of the hydrogen atom. Because of a parity non-conserving potential, $\ell = 3$ states can only mix with $\ell = 2$ and $\ell = 4$ states, which both satisfy the convergence criterion. At the same time, the wave function of these states falls to zero at the origin faster than the $s$ or the $p$ states, and so one could hope that, in states with $\ell = 3$, some parity-violation effect can be brought about predominantly by the neutrino loop instead of by the $Z$-interaction. We emphasize here that we could not have chosen $\ell = 2$ states for this task, because these states mix with $\ell = 1$ states when there is parity violation, which do not satisfy the convergence criterion that $\ell \geq 2$.

As discussed in Sec. 2.1, parity violation in atoms is measured in optical rotation experiments, wherein the degree of rotation of the plane of polarization of light is proportional to $R$ defined in Eq. (2.6). In this section, we study a particular interference process between two eigenstates of hydrogen and its effect on the plane of polarization of linearly-polarized incident light on a hydrogen sample.

Note that $M1$ transitions between states of different principal quantum number

$n$ do not occur in hydrogen because of the orthogonality of states with different $n$. To observe this effect, we therefore need to look for two states with the same parity and the same principal quantum number. To this end, we consider the following states of definite $n, f, m_f, j, \ell$ in the notation $|n, f, m_f, j, \ell\rangle$:

$$|A\rangle = |4, 3, 3, 5/2, 3\rangle \equiv 4F_{5/2,F=3}, \tag{2.47}$$

$$|B\rangle = |4, 3, 3, 7/2, 3\rangle \equiv 4F_{7/2,F=3}, \tag{2.48}$$

$$|\Delta\rangle = |4, 3, 3, 5/2, 2\rangle \equiv 4D_{5/2,F=3} \tag{2.49}$$

$|A\rangle$ and $|B\rangle$ are eigenstates of $\hat{F}^2$ which, in the presence of the neutrino potential, mix with all other states with $f = 3$ and $m_f = 3$ to form a true energy eigenstate of hydrogen. Before adding the neutrino potential, these states have the same $\ell$ and hence there can be an $M1$ transition between them, but no $E1$ transition. However, once these states are corrected by the neutrino potential, the resulting eigenstates can have both $E1$ and $M1$ transitions between them because of the small parity violating correction, from which we can calculate $R$, as in Eq. (2.6).

Consider now the state $|\Delta\rangle$. This state has different parity than the two base states $|A\rangle$ and $|B\rangle$ while having the same $f$ and $m_f$ quantum numbers and, hence, can mix with them. Before we proceed, we note that other states with the same values of $f$ and $m_f$, such as $|5, 3, 3, 7/2, 4\rangle$ for instance, mix very weakly with our base states because the quantum number $n$ puts these states much farther away in energy than $|\Delta\rangle$. We therefore ignore the contribution of these states in the perturbation expansion. Lastly, we must keep in mind that the matrix element of a parity-violating operator between states with the same parity is zero. Therefore,

the base states do not get any corrections from each other since they have the same $\ell = 3$.

Our aim is to compute

$$\frac{\langle A'|\text{Electric Dipole}|B'\rangle}{\langle A'|\text{Magnetic Dipole}|B'\rangle} \approx \frac{\langle A'|\text{Electric Dipole}|B'\rangle}{\langle A|\text{Magnetic Dipole}|B\rangle} \tag{2.50}$$

where $|A'\rangle$ and $|B'\rangle$ are the true eigenstates of hydrogen, obtained from $|A\rangle$ and $|B\rangle$ using the perturbation expansion as in Eq. (2.39). For details of the calculation, see appendix C. The approximation in Eq. (2.50) holds because the selection rules permit magnetic transitions to occur between states of the same parity, so perturbative corrections, which are much smaller than the unperturbed transition amplitude, can be ignored.

Using the electric and magnetic dipole moment operators (details in the appendix), we compute the inner products by performing the integrals involving the hydrogen atom wavefunctions. We define a small parameter $\nu_i$ by:

$$\nu_i \equiv \frac{1}{\alpha}\frac{m_{\nu_i}}{m_e} \tag{2.51}$$

The final result, up to leading order in $\nu_i$ is

$$\begin{aligned} R \;=\; & \frac{-7\alpha m_e^3 m_p G_A G_F^2 \left(-\frac{1}{4} + s_W^2 + \frac{1}{2}|U_{ei}|^2\right)}{302778777600\pi^3 g_p (29 g_p m_e - 21609000 m_p)} \\ & \times \left[(24335 g_p m_e - 17503290000 m_p) + \nu_i^2 (3858 g_p m_e + 84015792000 m_p)\right] + O(\nu_i^4), \end{aligned} \tag{2.52}$$

where there is an implicit sum over the neutrino flavor $i$. Using the standard values of the quantities above, we find

$$R = \mathcal{I}m\left(\frac{E1_{PV}}{M1}\right) \approx \left(-\frac{1}{4} + s_W^2 + \frac{1}{2}|U_{ei}|^2\right)\left(-7.7 \times 10^{-33} + 3.7 \times 10^{-32}\nu_i^2\right). \tag{2.53}$$

The result above shows that the leading-order contribution to $R$ is a number of order $O(10^{-32})$. The next-to-leading-order term depends on the neutrino mass through the parameter $\nu_i$. Using current experimental bounds on the neutrino mass ($m_\nu < 0.12$ eV), we see that the next-to-leading-order term has a magnitude of $O(10^{-41})$ radians.

Upon completing the calculation of the specific rotation here, let us provide some perspective on the result. We first compare the value of $R$ obtained from a neutrino loop diagram to the typical values obtained from a $Z$ diagram. To this end, we choose the states $|2,1,1,\frac{1}{2},1\rangle$ and $|2,1,1,\frac{3}{2},1\rangle$. Both of these states have $f = 1$, and $\ell = 1$ and both are corrected by the state $|2,1,1,\frac{1}{2},0\rangle$. Note that we have picked low $\ell$ states since we show in Sec. 2.6 that the $Z$ diagram dominates for such states. The precise choice of states is not completely without motivation: We have picked $p$-wave states with $n = 2$ because these states experience relatively large corrections from the $s$-wave states with the same principal quantum number. Had we picked $s$-wave states with $n = 1$, the corrections would be rather small. This is because they would come from $\ell = 1$ states which are much farther separated in energy, since the $n = 1$ shell does not possess any $\ell = 1$ states.

We repeat the process outlined in this section with only the first term in Eq. (2.40) for these two states, and obtained

$$R = \mathcal{I}m\left(\frac{E1_{PV}}{M1}\right) = \frac{27g^2 m_p[g_p m_e(4323\eta_Z + 1730) - 162m_p(2\eta_Z + 1)]}{6904\pi\cos^2\theta_W \alpha^3 g_p m_e(\eta_Z + 1)^3(865g_p m_e - 81m_p)}, \tag{2.54}$$

where $\eta_Z = m_Z(m_e\alpha)^{-1} \gg 1$. After plugging in the standard numerical values, we

have

$$R = \mathcal{I}m\left(\frac{E1_{PV}}{M1}\right) \sim 10^{-10}. \tag{2.55}$$

It turns out, therefore, that the $Z$-diagram gives an optical rotation for $\ell = 1$ states that is about $10^{22}$ times larger than the optical rotation obtained from the neutrino loops for the higher $\ell = 3$ states.

## 2.8 Final remarks

From the results in Sec. 2.7, it is clear that the measurement of optical rotation due to the neutrino loop is extremely challenging given the resolutions we can achieve today. In that regard, there is another obstacle in the path to measuring this effect – that of statistical suppression. Since we are looking at high-$\ell$ states, they necessarily occur at high $n$, which means that these are high-energy states and are thermally suppressed. We saw earlier that, for the lower energy states, the parity-violating interaction via the Z exchange dominates over the neutrino process. Hence, at low temperatures, the chances of isolating the neutrino-mediated transition are pretty low.

Nonetheless, this calculation, performed for other systems, could lead to somewhat larger quantities and the next step would most likely be an application of this idea to many-electron atoms, beyond the simple hydrogen case. Multi-electron atoms are important to explore particularly because the matrix elements in these

atoms are amplified by an additional $Z^3$ factor [34], $Z$ being the atomic number of the heavy atom in question. The $Z^3$ amplification is only present when one considers low-$\ell$ states of heavy atoms - one factor of $Z$ comes in through the weak nuclear charge and the other two factors appear out of the relativistic behavior of low-$\ell$ electrons near the nucleus. It might be worthwhile to try to explore the long-range parity violation in heavier atoms, but it is still very unlikely that we may be able to isolate the effect of the neutrino loop since the $Z^3$ amplification factor acts on both the tree level and loop level effects.

To conclude, we highlight the merits and demerits of the calculation: Although the effects of the neutrino force on the hydrogen atom are extremely small to measure in an experiment, the neutrino force is the largest long-range parity-violating force there is.

CHAPTER 3

# NEUTRINO FORCES IN NEUTRINO BACKGROUNDS

## 3.1 Introduction

It is well known that classical forces, like the Coulomb potential, can be derived from a $t$-channel mediator-exchange diagram in quantum field theory. The same treatment can be applied to the exchange of massive gauge bosons and scalars, resulting in a Yukawa potential. To obtain a classical force, the mediator of the force must be a boson. However, a pair of fermions behaves as an effective scalar and can mediate long-range forces. Such forces are sometimes called "quantum forces." Quantum forces have been studied extensively in the literature, for example, see [8, 41, 10, 42], in an attempt to both test the Standard Model (SM) and to probe new physics beyond.

In the SM, the force between fermions due to neutrino pair exchange is also well studied. Since neutrinos are very light, the force mediated by them is long range, without any significant exponential suppression with distance. Neutrino forces are generated by the exchange of a neutrino-antineutrino pair between two particles, as shown in the left panel of Fig. 3.1. The original idea of the neutrino-mediated force can be traced back to Feynman, who tried to explain the $1/r$ gravity as an emergent phenomenon due to the exchange of two neutrinos when taking into account multi-body effects [43]. Previous calculations of such forces in vac-

uum were first carried out in Refs. [6, 7, 8] using the dispersion technique for massless neutrinos. Later, the effects of neutrino masses [19] and flavor mixing [21, 44, 45] were included, which in principle can be used to determine the nature of neutrinos [46, 45], namely, whether neutrinos are Dirac or Majorana particles. The study of neutrino forces in the framework of effective field theories was carried out in Ref. [47].

Neutrino forces have important cosmological and astrophysical effects, such as the stability of neutron stars [9, 14, 48, 49, 17, 50, 51] and the impact on dark matter in the early universe [52, 53]. Recently, the calculation of neutrino forces went beyond the four-fermion contact interaction and a general formula describing the short-range behavior of neutrino forces was derived [54].

While theoretically we know that the force should be there, it has never been confirmed experimentally. The reason is that the force is very weak. The fact that it is second order in the weak interaction makes it proportional to $G_F^2$. In the limit of massless neutrinos, it is explicitly

$$V(r) \sim \frac{G_F^2}{r^5} \,, \tag{3.1}$$

where $G_F = 1.166 \times 10^{-5}\text{GeV}^{-2}$ is the Fermi constant and $r$ is the distance between the two particles. Thus, already at distances longer than about a nanometer, the neutrino force is smaller than the gravitational force between elementary particles.

Confirming the neutrino force experimentally would be interesting for several reasons. First, it would establish an exciting prediction of quantum field theory

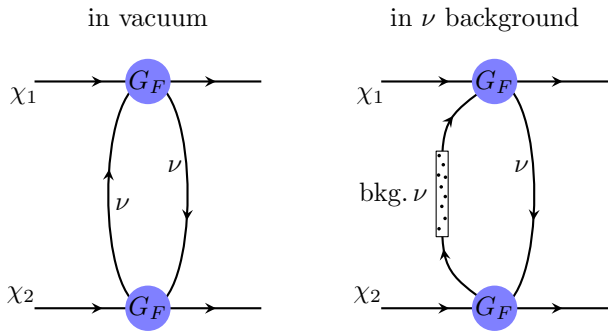


A diagrammatic explanation of neutrino forces in the vacuum (left) and in a neutrino background (right). The background effect can be taken into account by replacing one of the neutrino propagators with a background-modified propagator (bkg. $\nu$), which can be computed in finite temperature field theory. The effect can be physically interpreted as absorbing a neutrino from the background and then returning it back to the background.

that remains untested. Second, it would enable us to probe the neutrino sector of the SM since the neutrino force is sensitive to the absolute masses of the neutrinos. Also, it provides a test of the electroweak interaction and may serve as a probe of new physics beyond the SM. Lastly, it would enable us to look for other quantum forces that may be present due to yet undiscovered light particles [55, 56, 10, 41, 42, 57].

Given that the neutrino force is so feeble, we need to look for novel ways to probe it. One such idea was put forward in [58], which pointed out that the neutrino force provides the leading long-range parity-violation effect in the SM. Thus, it is natural to look for such effects. Yet even this seems too small to be probed experimentally.

In this chapter, we explore a different path: the neutrino force in the presence of an intense neutrino background, as shown in the right panel of Fig. 3.1. The presence of the background can significantly increase the strength of the interaction. In fact, the effect of a neutrino background was studied before, for the cosmic neutrino background (C$\nu$B), in Refs. [59, 23, 60]. However, the effect in this case is small because the number density of the cosmic neutrinos is very small today.

In this work, we focus on scenarios where the background is much more dense; in particular, for solar and reactor neutrinos. On the theoretical level, this differs from the case of C$\nu$B in that the background is not spherically symmetric. This results in a preferred direction, providing a fundamentally different signal than that of the vacuum and C$\nu$B cases.

Numerically, we find that the effect of reactor and solar neutrinos is remarkably significant and can enhance the signal by more than 20 orders of magnitude. In particular, the encouraging result is that the effect is close to the available sensitivity of fifth-force experimental searches. Thus, we hope that using the effect of background neutrinos will enable us to probe the neutrino force.

The chapter is organized as follows. In Sec. 3.2, we set up the general formalism to calculate the neutrino force in an arbitrary neutrino background. After applying this formalism to the case of C$\nu$B in Sec. 3.3, we calculate the neutrino force in a directional neutrino flux background in Sec. 3.4. In Sec. 3.5, we discuss the detection of neutrino forces in neutrino backgrounds and compare our theoretical results with the experimental sensitivities. Our main conclusions are

summarized in Sec. 3.6. The technical details are expanded in the appendices.

## 3.2 Formalism

In this section, we introduce the general formalism to compute neutrino forces between two fermions in a general neutrino background. Consider a four-fermion interaction with two Dirac neutrinos (for the case of Majorana neutrinos, see Sec. 3.3.3) and two fermions:

$$\mathcal{L}_{\text{int}} = -\frac{G_F}{\sqrt{2}} \left[\bar{\nu}\gamma^\mu (1-\gamma_5)\,\nu\right] \left[\bar{\chi}\gamma_\mu \left(g_V^\chi + g_A^\chi \gamma_5\right)\chi\right] \ , \tag{3.2}$$

where $G_F$ is the Fermi constant, $\nu$ denotes a Dirac neutrino with mass $m_\nu$, $\chi$ is a generic fermion in or beyond the SM with mass $m_\chi$, $g_V^\chi$ and $g_A^\chi$ are effective vector and axial couplings of $\chi$ to the neutrinos, obtained from integrating out heavy weak bosons.

Before we start, we note the following:

1. We work in the non-relativistic (NR) limit, i.e, the velocity of the interacting fermions $v \ll 1$ . The description of particle scattering via a potential $V(\mathbf{r})$ is accurate only in this limit.
2. Throughout our work, we only consider the spin-independent part of the potential. The reason is that the spin-dependent parts are usually averaged out when neutrino forces are added at macroscopic scales. The spin-independent part of the potential only depends on the vector coupling $g_V^\chi$.

| neutrino flavor | $\chi = e$ | $\chi = u$ | $\chi = d$ | $\chi$ =proton | $\chi$ =neutron |
|---|---|---|---|---|---|
| $\nu_e$ | $\frac{1}{2} + 2s_W^2$ | $\frac{1}{2} - \frac{4}{3}s_W^2$ | $-\frac{1}{2} + \frac{2}{3}s_W^2$ | $\frac{1}{2} - 2s_W^2$ | $-\frac{1}{2}$ |
| $\nu_\mu, \nu_\tau$ | $-\frac{1}{2} + 2s_W^2$ | $\frac{1}{2} - \frac{4}{3}s_W^2$ | $-\frac{1}{2} + \frac{2}{3}s_W^2$ | $\frac{1}{2} - 2s_W^2$ | $-\frac{1}{2}$ |

Values of the vector coupling $g_V$ in Eq. (3.2) in the SM. Here $s_W \equiv \sin\theta_W$ is the sine of the Weinberg angle.

In Table 3.2, we collect the values of $g_V^\chi$ in the SM [61]. When $\chi$ is the proton or the neutron, $g_V^\chi$ can be obtained by simply summing over the vector couplings to the quarks.

In vacuum, the diagram in the left panel of Fig. 3.1 leads to a long-range force that we can describe by an effective potential proportional to $r^{-5}$ in the massless-neutrino limit, $r$ being the distance of the two external particles. More explicitly, the spin-independent part of the neutrino potential between two fermions $\chi_1$ and $\chi_2$ in that limit reads

$$V_0(r) = \frac{G_F^2 g_V^1 g_V^2}{4\pi^3}\frac{1}{r^5} \qquad (m_{\chi_{1,2}}^{-1} \ll r \ll m_\nu^{-1}) \ . \tag{3.3}$$

Here, we use $g_V^1 \equiv g_V^{\chi_1}$ and $g_V^2 \equiv g_V^{\chi_2}$ to simplify the notation. Note that, for $r \gg 1/m_\nu$, the potential is exponentially suppressed by $e^{-2m_\nu r}$ [19], while the NR approximation of $\chi$ becomes invalid as $r$ approaches $m_{\chi_{1,2}}^{-1}$. The short-range behavior of neutrino forces was first investigated in Ref. [54].

In a neutrino background with finite neutrino number density or temperature, the neutrino propagator should be modified, as shown on the right panel of Fig. 3.1. The modified propagator is often derived in the real-time formalism in finite temperature field theory (for a detailed review, see Refs. [62, 63, 64, 65, 66].

Also, see Appendix B.1 for a simple and pedagogical re-derivation of the modified propagator.) We then have:

$$S_\nu(k) = (\not{k} + m_\nu)\left\{\frac{i}{k^2 - m_\nu^2 + i\epsilon} - 2\pi\delta\left(k^2 - m_\nu^2\right)\left[\Theta\left(k^0\right)n_+(\mathbf{k}) + \Theta\left(-k^0\right)n_-(\mathbf{k})\right]\right\}, \quad (3.4)$$

where $\epsilon \to 0^+$, $\Theta$ is the Heaviside theta function, and $n_\pm(\mathbf{k})$ denote the momentum distributions of the neutrinos and anti-neutrinos respectively, such that the integrals $\int n_\pm(\mathbf{k})\, d^3\mathbf{k}/(2\pi)^3$ correspond to their respective number densities. The first part is the usual fermion propagator in vacuum while the second part accounts for the background effect. The second part might seem counter-intuitive in the sense that the Dirac delta function requires the neutrino to be on-shell while, in Fig. 3.1, this on-shell neutrino is used to connect two spatially separated particles. To understand this effect, one should keep in mind that when $k$ in Eq. (3.4) is fixed, the uncertainty principle dictates that the neutrino cannot be localized and is spread out over space. So theoretically, the propagator's second (background) term, just like the vacuum part, can mediate momentum over a large distance.

According to the Born approximation, the effective potential is the Fourier transform of the low-energy elastic scattering amplitude of $\chi_1$ with $\chi_2$,

$$V(\mathbf{r}) = -\int \frac{d^3\mathbf{q}}{(2\pi)^3} e^{i\mathbf{q}\cdot\mathbf{r}}\mathcal{A}(\mathbf{q})\,. \quad (3.5)$$

Here, $\mathcal{A}(\mathbf{q})$ is the scattering amplitude in the NR limit, which should be computed by integrating the neutrino loop in Fig. 3.1 using the modified neutrino propagator in Eq. (3.4):

$$i\mathcal{A}(q) = \frac{G_F^2 g_V^1 g_V^2}{2}\int \frac{d^4k}{(2\pi)^4}\mathrm{Tr}\left[\gamma^0(1-\gamma_5)S_\nu(k)\gamma^0(1-\gamma_5)S_\nu(k+q)\right]. \quad (3.6)$$

Using the NR approximation we have $q \approx (0, \mathbf{q})$, thus the amplitude $\mathcal{A}$ only depends on the three-momentum $\mathbf{q}$. Substituting Eq. (3.4) into Eq. (3.6), one can see that when both neutrino propagators in Eq. (3.6) take the first term in the curly bracket of Eq. (3.4), it leads to the vacuum potential $V_0(r)$. When both propagators take the second term, the result vanishes, as we show in Appendix B.2. The background effect comes from cross terms, being proportional to $n_\pm$. We denote the background contribution to $\mathcal{A}(\mathbf{q})$ by $\mathcal{A}_{\rm bkg}(\mathbf{q})$ and, correspondingly, the contribution to $V(\mathbf{r})$ by $V_{\rm bkg}(\mathbf{r})$:

$$\mathcal{A}(\mathbf{q}) = \mathcal{A}_0(\mathbf{q}) + \mathcal{A}_{\rm bkg}(\mathbf{q})\,, \qquad V(\mathbf{r}) = V_0(\mathbf{r}) + V_{\rm bkg}(\mathbf{r})\,. \tag{3.7}$$

Notice that there is no interference between the vacuum and the background amplitudes in our calculation because, unlike computing cross sections, here we do not need to square the total amplitude. The background contribution $\mathcal{A}_{\rm bkg}(\mathbf{q})$, after some calculations in Appendix B.2, reduces to

$$\mathcal{A}_{\rm bkg}(\mathbf{q}) = 4G_F^2 g_V^1 g_V^2 \int \frac{d^3\mathbf{k}}{(2\pi)^3} \frac{n_+(\mathbf{k}) + n_-(\mathbf{k})}{2E_k} \left[ \frac{2|\mathbf{k}|^2 + m_\nu^2 + \mathbf{k}\cdot\mathbf{q}}{2\mathbf{k}\cdot\mathbf{q} + |\mathbf{q}|^2} + (\mathbf{k} \to -\mathbf{k}) \right]. \tag{3.8}$$

For isotropic distributions (e.g. cosmic neutrino background, diffuse supernova neutrino background), $n_\pm$ are independent of the direction of the momentum, i.e., $n_\pm(\mathbf{k}) = n_\pm(\kappa)$ with $\kappa \equiv |\mathbf{k}|$, leading to an isotropic $\mathcal{A}_{\rm bkg}$ and hence an isotropic $V_{\rm bkg}$. In this case, the angular part of the above integral can be integrated out analytically, resulting in the following expression for $V_{\rm bkg}$:

$$V_{\rm bkg}(r) = -\frac{G_F^2 g_V^1 g_V^2}{4\pi^3 r^4} \int_0^\infty d\kappa\, \kappa \frac{n_+(\kappa) + n_-(\kappa)}{\sqrt{\kappa^2 + m_\nu^2}} \left[ \left(1 + m_\nu^2 r^2\right) \sin(2\kappa r) - 2\kappa r \cos(2\kappa r) \right]. \tag{3.9}$$

Up to now, we have not used any specific neutrino distributions. In what follows, we apply the above formulae to specific forms of $n_\pm$ and compute the corresponding potentials.

## 3.3 Neutrino forces with isotropic neutrino background

We now discuss the case where the neutrino background is isotropic and focus on a thermal-like distribution. In particular, this applies to the cosmic neutrino background (C$\nu$B), which motivates this section.

The existence of isotropic C$\nu$B today, with a temperature around 1.9 K and number density about 56/cm$^3$ per flavor, is one of the most solid predictions from big bang cosmology [67]. The temperature correction to neutrino forces in the C$\nu$B was first calculated in Ref. [59] with the neutrino momentum distribution to be

$$n_\pm(\mathbf{k}, T) = \exp\left[(\pm\mu - \kappa)/T\right] \quad \text{with} \quad \kappa \equiv |\mathbf{k}| \ , \tag{3.10}$$

where $\mu$ and $T$ are the chemical potential and temperature of the C$\nu$B.

Ref. [59] studied the case of Dirac neutrinos in the massless ($m_\nu = 0$) and NR ($m_\nu \gg T$) limit. Later, the background effects of the C$\nu$B on neutrino forces were further studied in Ref. [23, 60]. In Ref. [23] the neutrino distribution was taken to be a standard Boltzmann distribution,

$$n_\pm(\mathbf{k}, T) = \exp\left[(\pm\mu - E_k)/T\right] \quad \text{with} \quad E_k = \sqrt{|\mathbf{k}|^2 + m_\nu^2} \ , \tag{3.11}$$

and the complete expressions of the background potential $V_{\rm bkg}(r)$ were given for both Dirac and Majorana neutrinos. The massless limit of the result in Ref. [23] matches that in Ref. [59]. However, the results of the massive case are very different. In particular, the expression of $V_{\rm bkg}(r)$ in Ref. [23] is exponentially suppressed at large distances, $V_{\rm bkg}(r) \sim e^{-2m_\nu r}$ (for $r \gg 1/m_\nu$), while that in Ref. [59] is not, $V_{\rm bkg}(r) \sim m_\nu/(Tr^5)$ (for $r \gg 1/T \gg 1/m_\nu$). This discrepancy on the long-range behavior of $V_{\rm bkg}(r)$ is due to the difference between the distributions in Eqs. (3.10) and (3.11): The former corresponds to the number density of relic neutrinos proportional to $T^3$, while the latter distribution corresponds to the number density that would be exponentially suppressed by $e^{-m_\nu/T}$ for NR neutrinos. In addition, in Ref. [60], $V_{\rm bkg}(r)$ was calculated for the standard Fermi-Dirac distribution

$$n_\pm(\mathbf{k}, T) = \frac{1}{e^{(E_k \mp \mu)/T} + 1} \,, \tag{3.12}$$

for arbitrary chemical potential, but the mass of neutrinos was neglected therein.

However, in the framework of standard cosmology, neutrinos decoupled at $T \sim$ MeV, after which they were no longer in thermal equilibrium with the cosmic plasma. Instead, they propagated freely until today, maintaining their own distribution:

$$n_\pm(\mathbf{k}, T) = \frac{1}{e^{(\kappa \mp \mu)/T} + 1} \,. \tag{3.13}$$

The reason why cosmic neutrinos obey the distribution function in Eq. (3.13), instead of Eq. (3.12), is that $\kappa$, rather than $E_k$, scales as inversely proportional to the scale factor $a$, i.e., $\kappa \propto 1/a$ [67]. In the relativistic limit, there is no difference

between Eqs. (3.12) and (3.13). However, we know that the temperature of C$\nu$B today is around $10^{-4}$ eV and neutrino oscillation experiments [68] tell us that at least two of the three active neutrinos are NR in the C$\nu$B today. Therefore, the results in Refs. [23, 60] using Eqs. (3.11) and (3.12) only hold for relativistic neutrino background and are *invalid* for the C$\nu$B today, while the computation in Ref. [59] using Eq. (3.10) is an approximate result.

We emphasize that a strict computation of the background effects on neutrino forces from the C$\nu$B today using Eq. (3.13) is still lacking, and this is what we do in this section.

### 3.3.1 Maxwell-Boltzmann distribution

As a warm-up, we first take the distribution function in Eq. (3.10), whose massless and NR limits have already been given in Ref. [59]. Substituting

$$n_+ (\mathbf{k}, T) + n_- (\mathbf{k}, T) = 2 \cosh\left(\frac{\mu}{T}\right) \exp\left(-\frac{\kappa}{T}\right) , \tag{3.14}$$

into Eq. (3.9), we obtain

$$V_{\rm bkg}(r) = -\frac{G_F^2 g_V^1 g_V^2}{2\pi^3} \cosh\left(\frac{\mu}{T}\right) \frac{T}{r^4} \left[\left(1 + b^2 x^2\right) \mathcal{I}_{\rm MB}\,(x, b) - b \frac{\partial}{\partial b} \mathcal{I}_{\rm MB}\,(x, b)\right] , \tag{3.15}$$

where we have defined the dimensionless quantities

$$x \equiv \frac{m_\nu}{T}, \qquad b \equiv rT, \qquad y \equiv \frac{\kappa}{T} , \tag{3.16}$$

and the dimensionless integral

$$\mathcal{I}_{\rm MB}(x,b) = \int_0^\infty dy \frac{y}{\sqrt{y^2+x^2}} e^{-y} \sin(2by) \ . \tag{3.17}$$

Eq. (3.17) cannot be integrated analytically but can be computed numerically for arbitrary values of $m_\nu$, $T$ and $r$. We are mainly interested in two special scenarios: $x = 0$ (the lightest active neutrino can still be massless) and $x \gg 1$ (according to the neutrino oscillation experiments, the heaviest active neutrino is at least 0.05 eV, which corresponds to $x \gtrsim 500$ if we consider the temperature of C$\nu$B).

For $x = 0$, we have

$$\mathcal{I}_{\rm MB}(0,b) = \frac{2b}{1+4b^2} = \frac{2rT}{1+4r^2T^2} \ , \tag{3.18}$$

and

$$V_{\rm bkg}(r) = -\frac{8G_F^2 g_V^1 g_V^2}{\pi^3} \cosh\left(\frac{\mu}{T}\right) \frac{T^4}{r\left(1+4r^2T^2\right)^2} \qquad (m_\nu = 0) \ , \tag{3.19}$$

which is consistent with the result in Refs. [59, 23]. In particular, for high temperatures, $r \gg 1/T$, we notice that $V_T(r) \sim 1/r^5$, which is almost independent of the temperature. For low temperature, $r \ll 1/T$, we find that $V_T(r) \sim T^4/r$.

For $x \gg 1$, since the integral in Eq. (3.17) with $y > 1$ is exponentially suppressed, the dominant contribution to the integral comes from the region $0 < y \ll x$, thus we have

$$\mathcal{I}_{\rm MB}(x,b) \simeq \frac{1}{x}\int_0^\infty dy y e^{-y} \sin(2by) = \frac{1}{x}\frac{4b}{\left(1+4b^2\right)^2} = \frac{4rT^2}{m\left(1+4r^2T^2\right)^2} \ , \tag{3.20}$$

and

$$V_{\rm bkg}(r) = -\frac{2G_F^2 g_V^1 g_V^2}{\pi^3} \cosh\left(\frac{\mu}{T}\right) \frac{m_\nu T^3}{r\left(1+4r^2T^2\right)^2} \qquad (m_\nu \gg T) \ , \tag{3.21}$$

which is consistent with the result in Ref. [59]. Note that, in contrast to the result in Ref. [23], there is no exponential suppression in Eq. (3.21). In particular, for $r \ll 1/T$, we obtain

$$V_{\rm bkg}(r) = -\frac{2G_F^2 g_V^1 g_V^2}{\pi^3} \cosh\left(\frac{\mu}{T}\right) \frac{m_\nu T^3}{r} \qquad (m_\nu \gg T, \quad r \ll T^{-1}) \,, \tag{3.22}$$

while, for $r \gg 1/T$,

$$V_{\rm bkg}(r) = -\frac{G_F^2 g_V^1 g_V^2}{8\pi^3} \cosh\left(\frac{\mu}{T}\right) \frac{m_\nu}{T} \frac{1}{r^5} \qquad \left(m_\nu \gg T, \quad r \gg T^{-1}\right) \,, \tag{3.23}$$

which is enhanced by a factor of $m_\nu/T$ compared with the vacuum result in Eq. (3.3) for NR background neutrinos.

### 3.3.2 Fermi-Dirac distribution

We now turn to the realistic distribution of background neutrinos in Eq. (3.13). The first thing to notice is that the neutrino degeneracy parameter $\zeta \equiv \mu/T$, which characterizes the neutrino–antineutrino asymmetry, is actually very small from constraints of big bang nucleosynthesis: $\zeta \lesssim O\left(10^{-2}\right)$ [69, 70]. Therefore, we can expand the neutrino distribution function into a series of $\zeta$,

$$n_+(\kappa, T) + n_-(\kappa, T) = \frac{2}{e^{\kappa/T} + 1} + O\left(\zeta^2\right) \,, \tag{3.24}$$

and only take the leading-order term, which is independent of $\zeta$. Then the background potential turns out to be

$$V_{\rm bkg}(r) = -\frac{G_F^2 g_V^1 g_V^2}{2\pi^3} \frac{T}{r^4} \left[\left(1 + b^2 x^2\right) \mathcal{I}_{\rm FD}(x, b) - b \frac{\partial}{\partial b} \mathcal{I}_{\rm FD}(x, b)\right] \,, \tag{3.25}$$

where $x$, $b$, and $y$ are defined in Eq. (3.16) and

$$\mathcal{I}_{\rm FD}\left(x,b\right) = \int_0^\infty dy \frac{y}{\sqrt{y^2+x^2}} \frac{1}{e^y+1} \sin\left(2b\,y\right) \ . \tag{3.26}$$

The integral in Eq. (3.26) can be numerically calculated for arbitrary values of $m_\nu$, $T$, and $r$. In the massless limit ($x = 0$) and NR limit ($x \gg 1$), $\mathcal{I}_{\rm FD}\left(x,b\right)$ can be carried out analytically.

For $x = 0$, we have

$$\mathcal{I}_{\rm FD}\left(x,b\right) = \frac{1}{4}\left[\frac{1}{b} - 2\pi\,{\rm csch}\left(2\pi b\right)\right] \ , \tag{3.27}$$

and the background potential

$$V_{\rm bkg}(r) = -\frac{G_F^2 g_V^1 g_V^2}{4\pi^3}\frac{1}{r^5}\left\{1 - \pi r T\,{\rm csch}\left(2\pi r T\right)\left[1 + 2\pi r T\coth\left(2\pi r T\right)\right]\right\} \quad (m_\nu = 0) \ , \tag{3.28}$$

which is consistent with the result obtained in Ref. [60], where the neutrino distribution Eq. (3.12) was taken but the neutrino mass was neglected. An interesting observation is that, in the long-range limit,

$$V_{\rm bkg}(r) = -\frac{G_F^2 g_V^1 g_V^2}{4\pi^3}\frac{1}{r^5} \qquad (m_\nu = 0, \quad r \gg T^{-1}) \ , \tag{3.29}$$

which happens to be the opposite of Eq. (3.3). This means that, for massless neutrinos in the limit $\zeta \to 0$, the vacuum potential is completely screened off by the C$\nu$B.

Let us now take a look at the NR limit of Eq. (3.26). As with the case of Boltzmann distribution, for $x \gg 1$, one obtains

$$\begin{aligned}
\mathcal{I}_{\rm FD}\left(x,b\right) &\simeq \frac{1}{x}\int_0^\infty dy \frac{y}{e^y+1}\sin\left(2by\right) \\
&= \frac{i}{8x}\left[\psi^{(1)}\left(\frac{1}{2}+ib\right) - \psi^{(1)}\left(\frac{1}{2}-ib\right) + \psi^{(1)}\left(1-ib\right) - \psi^{(1)}\left(1+ib\right)\right],
\end{aligned} \tag{3.30}$$

| $\nu$BDF | $m_\nu = 0,\ r \ll T^{-1}$ | $m_\nu = 0,\ r \gg T^{-1}$ | $m_\nu \gg T,\ r \ll T^{-1}$ | $m_\nu \gg T,\ r \gg T^{-1}$ |
|---|---|---|---|---|
| MB | $-\frac{8}{\pi^3} G_F^2 g_V^1 g_V^2 \frac{T^4}{r}$ | $-\frac{1}{2\pi^3} G_F^2 g_V^1 g_V^2 \frac{1}{r^5}$ | $-\frac{2}{\pi^3} G_F^2 g_V^1 g_V^2 \frac{m_\nu T^3}{r}$ | $-\frac{1}{8\pi^3} G_F^2 g_V^1 g_V^2 \frac{m_\nu}{T} \frac{1}{r^5}$ |
| FD | $-\frac{7\pi}{90} G_F^2 g_V^1 g_V^2 \frac{T^4}{r}$ | $-\frac{1}{4\pi^3} G_F^2 g_V^1 g_V^2 \frac{1}{r^5}$ | $-\frac{14.4}{8\pi^3} G_F^2 g_V^1 g_V^2 \frac{m_\nu T^3}{r}$ | $-\frac{1}{32\pi^3} G_F^2 g_V^1 g_V^2 \frac{m_\nu}{T} \frac{1}{r^5}$ |

Comparison of the short- and long-range behaviors of the background potential $V_{\rm bkg}(r)$ in the massless and non-relativistic limits with the neutrino Background Distribution Function ($\nu$BDF) taking the Maxwell-Boltzmann (MB) distribution in Eq. (3.10) and Fermi-Dirac (FD) distribution in Eq. (3.13). We have neglected the chemical potential in both distribution functions.

where the $n$-th ordered polygamma function is defined as

$$\psi^{(n)}(z) = \frac{d}{dz}\psi^{(n-1)}(z) = \frac{d^{n+1}}{dz^{n+1}} \log\Gamma(z) \,, \tag{3.31}$$

with $\Gamma(z)$ being the gamma function. Therefore, the background potential of NR cosmic neutrinos turns out to be

$$\begin{aligned} V_{\rm bkg}(r) &= -i\frac{G_F^2 g_V^1 g_V^2}{16\pi^3}\frac{T^2}{mr^4}\left\{\left[\psi^{(1)}\left(\frac{1}{2}+ib\right) - \psi^{(1)}\left(\frac{1}{2}-ib\right) + \psi^{(1)}(1-ib) - \psi^{(1)}(1+ib)\right]\right. \\ &\times \left.\left(1+b^2x^2\right) - ib\left[\psi^{(2)}\left(\frac{1}{2}+ib\right) + \psi^{(2)}\left(\frac{1}{2}-ib\right) - \psi^{(2)}(1-ib) - \psi^{(2)}(1+ib)\right]\right\}, \\ &\qquad\qquad\qquad\qquad\qquad\qquad\qquad\qquad\qquad\qquad\qquad\qquad (m_\nu \gg T) \end{aligned} \tag{3.32}$$

In particular, for $r \ll 1/T$, i.e., $b \ll 1$, we have

$$\begin{aligned} V_{\rm bkg}(r) &= -\left[\psi^{(2)}(1) - \psi^{(2)}\left(\frac{1}{2}\right)\right]\frac{G_F^2 g_V^1 g_V^2}{8\pi^3}\frac{m_\nu T^3}{r} \\ &= -14.4 \times \frac{G_F^2 g_V^1 g_V^2}{8\pi^3}\frac{m_\nu T^3}{r} \qquad \left(m_\nu \gg T,\ \ r \ll T^{-1}\right), \end{aligned} \tag{3.33}$$

while, for the long-range limit $b \gg 1$, one obtains

$$V_{\rm bkg}(r) = -\frac{G_F^2 g_V^1 g_V^2}{32\pi^3}\frac{m_\nu}{T}\frac{1}{r^5} \qquad \left(m_\nu \gg T,\ \ r \gg T^{-1}\right), \tag{3.34}$$

which is, as in the case of the Boltzmann distribution, enhanced by a factor of $m_\nu/T$ compared with the vacuum potential in Eq. (3.3).

To sum up, we have provided in Eq. (3.25) the general background potential valid for any temperatures and distances and discussed the special scenarios in the massless and NR neutrinos limits, which have simple analytical expressions. Compared to the results of Maxwell-Boltzmann distribution in last subsection, we conclude that both distributions lead to similar short-range and long-range behaviors of the background potential in the massless limit ($m_\nu = 0$) and NR limit ($m_\nu \gg T$), up to some numerical factors (cf. Table 3.3.2).

### 3.3.3 The case of Majorana neutrinos

The above calculations for Dirac neutrinos can be generalized to the scenario of Majorana neutrinos. If $\nu$ is a Majorana neutrino with mass $m_\nu$, then its general four-fermion interaction is given by

$$\mathcal{L}_{\text{int}} = \frac{G_F}{\sqrt{2}} \left[\bar{\nu}\gamma^\mu\gamma_5\nu\right] \left[\bar{\chi}\gamma_\mu \left(g_V^\chi + g_A^\chi\gamma_5\right)\chi\right] \,, \tag{3.35}$$

where we have used the identity $\bar{\nu}\gamma^\mu\nu = 0$ for Majorana fermions comparing with Eq. (3.2). Taking into account the modified neutrino propagator due to the background, Eq. (3.4), the scattering amplitude reads

$$i\mathcal{A}(q) = \frac{G_F^2 g_V^1 g_V^2}{2} \int \frac{d^4k}{(2\pi)^4} \text{Tr}\left[\gamma^0\gamma_5 S_\nu(k)\gamma^0\gamma_5 S_\nu(k+q)\right] \times 2 \,, \tag{3.36}$$

where the factor of 2 is due to the exchange of two neutrino propagators in the loop. As with the Dirac case, the background effect comes from the crossed terms. After some algebra, one obtains

$$\mathcal{A}_{\rm bkg}(\mathbf{q}) = 4G_F^2 g_V^1 g_V^2 \int \frac{d^3\mathbf{k}}{(2\pi)^3} \frac{n_+(\mathbf{k}) + n_-(\mathbf{k})}{2E_k} \left[ \frac{2|\mathbf{k}|^2 + \mathbf{k}\cdot\mathbf{q}}{2\mathbf{k}\cdot\mathbf{q} + |\mathbf{q}|^2} + (\mathbf{k} \to -\mathbf{k}) \right]. \tag{3.37}$$

For isotropic distributions $n_\pm(\mathbf{k}) = n_\pm(\kappa)$, Eq. (3.37) can be reduced to

$$V_{\rm bkg}(r) = -\frac{G_F^2 g_V^1 g_V^2}{4\pi^3 r^4} \int_0^\infty d\kappa\, \kappa \frac{n_+(\kappa) + n_-(\kappa)}{\sqrt{\kappa^2 + m_\nu^2}} \left[\sin(2\kappa r) - 2\kappa r \cos(2\kappa r)\right] , \tag{3.38}$$

which, as expected, matches the result for Dirac neutrinos in Eq. (3.9) in the massless limit.

We then take the Fermi-Dirac distribution in Eq. (3.13) to calculate $V_{\rm bkg}(r)$ in the C$\nu$B. Note that for Majorana neutrinos, the chemical potential vanishes, so that

$$n_+(\kappa) = n_-(\kappa) = \frac{1}{e^{\kappa/T} + 1} . \tag{3.39}$$

Therefore, the background potential turns out to be

$$V_{\rm bkg}(r) = -\frac{G_F^2 g_V^1 g_V^2}{2\pi^3} \frac{T}{r^4} \left[ \mathcal{I}_{\rm FD}(x,b) - b\frac{\partial}{\partial b} \mathcal{I}_{\rm FD}(x,b) \right] , \tag{3.40}$$

where $x$, $b$, and the integral $\mathcal{I}_{\rm FD}(x,b)$ is defined in Eqs. (3.16) and (3.26).

In the massless limit ($x = 0$), it is obvious that $V_{\rm bkg}(r)$ is the same as we have for the Dirac neutrino case in Eq. (3.28).

In the NR limit ($x \gg 1$), $\mathcal{I}_{\rm FD}(x,b)$ can be integrated analytically and is given by

| nature of neutrino | general expression | $r \ll T^{-1}$ | $r \gg T^{-1}$ |
|---|---|---|---|
| Dirac | Eq. (3.32) | $-\frac{14.4}{8\pi^3} G_F^2 g_V^1 g_V^2 \frac{m_\nu T^3}{r}$ | $-\frac{1}{32\pi^3} G_F^2 g_V^1 g_V^2 \frac{m_\nu}{T} \frac{1}{r^5}$ |
| Majorana | Eq. (3.41) | $-\frac{248.9}{8\pi^3} G_F^2 g_V^1 g_V^2 \frac{T^5}{m_\nu r}$ | $-\frac{1}{8\pi^3} G_F^2 g_V^1 g_V^2 \frac{1}{m_\nu T} \frac{1}{r^7}$ |

Comparison of the short- and long-range behavior of the background potential $V_{\rm bkg}(r)$ in non-relativistic C$\nu$B ($m_\nu \gg T$) with $n_\pm$ taking the Fermi-Dirac distribution in Eq. (3.13) for Dirac and Majorana background neutrinos.

Eq. (3.30). Therefore the background potential turns out to be

$$\begin{aligned} V_{\rm bkg}(r) &= -i\frac{G_F^2 g_V^1 g_V^2}{16\pi^3}\frac{T^2}{mr^4}\left\{\left[\psi^{(1)}\left(\frac{1}{2}+ib\right)-\psi^{(1)}\left(\frac{1}{2}-ib\right)+\psi^{(1)}(1-ib)-\psi^{(1)}(1+ib)\right]\right. \\ &\quad \left.-ib\left[\psi^{(2)}\left(\frac{1}{2}+ib\right)+\psi^{(2)}\left(\frac{1}{2}-ib\right)-\psi^{(2)}(1-ib)-\psi^{(2)}(1+ib)\right]\right\} . \end{aligned} \tag{3.41}$$

In particular, for the short-range limit ($b \ll 1$) one obtains

$$\begin{aligned} V_{\rm bkg}(r) &= -\left[\psi^{(4)}(1)-\psi^{(4)}\left(\frac{1}{2}\right)\right]\frac{G_F^2 g_V^1 g_V^2}{24\pi^3}\frac{T^5}{m_\nu r} \\ &= -248.9\times\frac{G_F^2 g_V^1 g_V^2}{8\pi^3}\frac{T^5}{m_\nu r} \qquad \left(m_\nu \gg T,\ \ r \ll T^{-1}\right) , \end{aligned} \tag{3.42}$$

while for the long-range limit ($b \gg 1$), we have

$$V_{\rm bkg}(r) = -\frac{G_F^2 g_V^1 g_V^2}{8\pi^3}\frac{1}{m_\nu T r^7} \qquad \left(m_\nu \gg T,\ \ r \gg T^{-1}\right) . \tag{3.43}$$

In Table 3.3.3, we have compared the short- and long-range behaviors of the background potential $V_{\rm bkg}(r)$ due to Dirac and Majorana neutrinos in the NR regime. Notice that, at short distances ($r \ll T^{-1}$ and $m_\nu^{-1} \ll T^{-1}$), the background potential of Majorana neutrinos differs from that of Dirac neutrinos by a factor of $m_\nu^2/T^2 \gg 1$. Whereas, at long distances ($r \gg T^{-1} \gg m_\nu^{-1}$), the relative factor

is $m_\nu^2 r^2 \gg 1$. This difference can be understood by the fact that the mass term in the neutrino propagator dominates in the NR limit, and there should be two mass insertions in the Dirac-neutrino propagator compared to just one mass insertion in the Majorana-neutrino propagator. Therefore, we conclude that for NR background neutrinos, the background potential of Dirac neutrinos is much larger than that of Majorana neutrinos at both long and short distances.

### 3.3.4 Discussion

We close this section by briefly summarizing the main results of the thermal corrections to neutrino forces from cosmic background neutrinos.

Neutrinos in the C$\nu$B are NR today (although the lightest neutrino can still be massless) and obey the Fermi-Dirac distribution in Eq. (3.13) with negligible chemical potential. The general expressions of the finite-temperature corrections, valid for arbitrary neutrino masses and distances, are given by Eqs. (3.25) and (3.40) for Dirac and Majorana neutrinos, respectively. In the massless limit, the background potential $V_{\rm bkg}(r)$ is the same for Dirac and Majorana neutrinos. However, for NR background neutrinos, $V_{\rm bkg}(r)$ is much larger for Dirac neutrinos. This distinction can, at least in principle, be used to determine the nature of neutrinos.

The most remarkable feature of the background potential from C$\nu$B is that, at large distances ($r \gg 1/m_\nu$), it is *not* exponentially suppressed, whereas the vacuum potential is suppressed by $e^{-2m_\nu r}$ [19]. This is because the number density of back-

ground neutrinos in the C$\nu$B is always proportional to $T^3$, no matter whether they are relativistic or not. Since the total potential is given by adding the vacuum part and the background part, neutrino forces between two objects will be dominated by the corrections of C$\nu$B in the long-range limit for massive mediated neutrinos. However, neutrino forces including thermal corrections of C$\nu$B are still too small to reach the experimental sensitivities today (cf. Sec. 3.5). Below we will discuss neutrino forces in other higher-energy neutrino backgrounds, which might offer prospects of experimental detection in the near future.

Finally, we comment on the controversial topic of many-body neutrino forces in neutron stars. In Ref. [9], a catastrophically large many-body neutrino force was obtained using the vacuum neutrino propagator. Matter effects due to the neutrons have been computed in Ref. [63]. It was claimed in [14, 48, 49, 17, 50, 51] that this changes the result of Ref. [9]. Our result is irrelevant to this issue as we only consider the neutrino background, and we do not elaborate any further.

## 3.4 Neutrino forces with directional neutrino backgrounds

In this section, we move to discuss anisotropic backgrounds. In particular, we consider one with a specific direction. Reactor, solar, and supernova neutrinos are example for such cases.

### 3.4.1 Calculations

Reactor, solar, and supernova neutrinos are anisotropic and much more energetic than cosmic relic neutrinos. Solar neutrinos arrive at the Earth with an almost certain direction. Reactor neutrinos can also be assumed to travel in a fixed direction if the sizes of the reactor core and the detector are much smaller than the distance between them. In addition, we also consider a galactic (10 kpc) supernova neutrino burst. Although such an event is rare ($2 \sim 3$ times per century), its neutrino flux is orders of magnitude higher than solar neutrinos with an extremely small angular spread, providing a unique opportunity for future experiments to search for such forces.

In order to compute the effect of these backgrounds on the neutrino force, we make two well-motivated assumptions:

1. We assume that the neutrino flux has a directional distribution with all neutrinos moving in the same direction. For solar and supernova neutrinos, this is a good approximation, whereas for reactor neutrinos it requires that the size of the reactor core and detector are much smaller than the distance between them.
2. We assume that the neutrino flux is monochromatic, i.e., all neutrinos in flux have the same energy. Although this is not exactly true, it is worth mentioning that among the four well-measured solar neutrino spectra ($^8$B, $^7$Be, *pep*, *pp*), two of them ($^7$Be, *pep*) are indeed monochromatic.

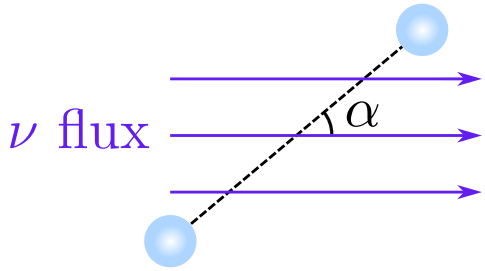


An illustration of neutrino forces between two objects in a directional neutrino flux background.

With these assumptions of directionality and monochromaticity, we consider the following distribution:

$$n_{\pm}(\mathbf{k}) = (2\pi)^3 \delta^3(\mathbf{k} - \mathbf{k}_0)\,\Phi_0\,, \tag{3.44}$$

where $\Phi_0 = \int n_{\pm}(\mathbf{k})\, d^3\mathbf{k}/(2\pi)^3$ is the flux of neutrinos. Although actual reactor and solar neutrino spectra are not monochromatic, our result derived below based on Eq. (3.44) can be applied to a generic spectrum by further integrating over $\mathbf{k}_0$, weighted by the corresponding $\Phi_0$, since any spectrum can be expressed as a superposition of delta functions. For the treatment of a directional spectrum with a finite energy spread, see Appendix B.3.

The anisotropic background leads to an anisotropic scattering amplitude, and hence an anisotropic potential that depends not only on $r$ but also on the angle between $\mathbf{k}_0$ and $\mathbf{r}$, denoted by $\alpha$ (cf. Fig. 3.4.1). Without loss of generality, we assume $\mathbf{k}_0$ is aligned with the $z$-axis and $\mathbf{r}$ lies in the $x$-$z$ plane:

$$\mathbf{k}_0 = E_\nu\,(0, 0, 1)\,, \quad \mathbf{r} = r\,(s_\alpha, 0, c_\alpha)\,, \tag{3.45}$$

where $(c_\alpha,\ s_\alpha) \equiv (\cos\alpha,\ \sin\alpha)$.

Substituting the distribution (3.44) into Eq. (3.8), we obtain

$$\begin{aligned}\mathcal{A}_{\rm bkg}\left(\mathbf{q}\right) &= 2G_F^2 g_V^1 g_V^2 \frac{\Phi_0}{E_\nu}\left[\frac{2E_\nu^2+\mathbf{k}_0\cdot\mathbf{q}}{\rho^2+2\mathbf{k}_0\cdot\mathbf{q}}+\frac{2E_\nu^2-\mathbf{k}_0\cdot\mathbf{q}}{\rho^2-2\mathbf{k}_0\cdot\mathbf{q}}\right]\\ &= 8G_F^2 g_V^1 g_V^2 \Phi_0 E_\nu \frac{1-\xi^2}{\rho^2-4E_\nu^2\xi^2},\end{aligned} \tag{3.46}$$

where $\rho \equiv |\mathbf{q}|$ and

$$\xi \equiv \frac{\mathbf{k}_0\cdot\mathbf{q}}{|\mathbf{k}_0||\mathbf{q}|}\,. \tag{3.47}$$

Note that the typical energy of reactor and solar neutrinos is $O$(MeV), so we can safely neglect the neutrino mass in Eq. (3.8). Thus, the background-induced potential is given by

$$V_{\rm bkg}(\mathbf{r}) = -\int \frac{d^3\mathbf{q}}{(2\pi)^3} e^{i\mathbf{q}\cdot\mathbf{r}} \mathcal{A}_{\rm bkg}(\mathbf{q}) = -\frac{g_V^1 g_V^2}{\pi^3} G_F^2 \Phi_0 E_\nu^2 \times \mathcal{I}\ , \tag{3.48}$$

where $\mathcal{I}$ is a dimensionless integral. We further define

$$\ell \equiv r E_\nu \tag{3.49}$$

and note that $\mathcal{I}$ is depends only on $\ell$ and $\alpha$:

$$\mathcal{I}(\ell,\alpha) \equiv \frac{1}{E_\nu}\int d^3\mathbf{q} e^{i\mathbf{q}\cdot\mathbf{r}} \frac{1-\xi^2}{\rho^2-4E_\nu^2\xi^2}\,. \tag{3.50}$$

In Appendix B.2, we show that, for generic $\alpha$ and $\ell$, the integral can be reduced to

$$\mathcal{I}\left(\ell,\alpha\right) = \frac{\pi^2}{2\ell}\left(3+\cos 2\alpha\right) - 2\pi\int_{-1}^{1} d\xi\,\xi\left(1-\xi^2\right)\int_0^\pi d\varphi\ \sin\left(2\ell\xi\left|c_\alpha\xi + s_\alpha\sqrt{1-\xi^2}\cos\varphi\right|\right). \tag{3.51}$$

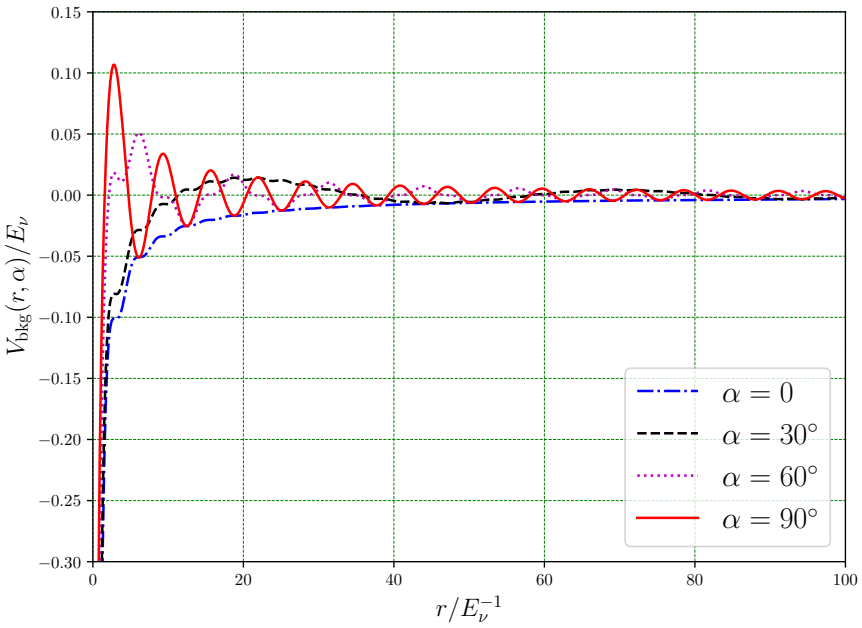


Evolution of the directional background potential with the distance for $\alpha = 0$, $30°$, $60°$ and $90°$. Notice that the distance $r$ is in the unit of $E_\nu^{-1}$ while the background potential $V_{\rm bkg}(r,\alpha)$ is in the unit of $E_\nu$. In addition, an overall dimensionless factor, $G_F^2 g_V^1 g_V^2 \Phi_0 E_\nu$, has been omitted for the background potential.

For the special cases of $\alpha = 0$ and $\alpha = \pi/2$, we find

$$\mathcal{I}\left(\ell, \alpha = 0\right) = \frac{\pi^2}{\ell}\left[1 + \frac{\sin 2\ell}{2\ell}\right], \tag{3.52}$$

$$\mathcal{I}\left(\ell, \alpha = \frac{\pi}{2}\right) = \frac{\pi^2}{\ell}\left[1 - 4\ell\int_0^1 d\xi\xi\left(1-\xi^2\right)H_0\left(2\ell\xi\sqrt{1-\xi^2}\right)\right], \tag{3.53}$$

where $H_0$ is the zeroth-order Struve H function.[1] For generic values of $\alpha$, though

[1]We note that `Mathematica` contains some unidentified bug leading to incorrect results of integrals involving the Struve H function, e.g. $\int_0^1 H_0(\sqrt{1-z^2}z)\,dz$ should be nonzero while

we cannot carry out the integration analytically, Eq. (3.51) can be readily used to compute $\mathcal{I}(\ell, \alpha)$ numerically. We have numerically verified that $\int \mathcal{I}(\ell, \alpha)\, dc_\alpha$ can reproduce the $r^{-4}$ dependence in Eq. (3.9), which is expected when Eq. (3.9) is applied to an isotropic and monochromatic flux. For illustration, in Fig. 3.4.1 we show the evolution of the directional background potential $V_{\rm bkg}$ with the distance $r$ for $\alpha = 0, \pi/6, \pi/3$ and $\pi/2$.

At long distances ($\ell \gg 1$), the numerical evaluation of the double integral in Eq. (3.51) is computationally expensive. We find that $\mathcal{I}(\ell, \alpha)$ has a simple analytical expression for $\ell \gg 1$:

$$\mathcal{I}(\ell \gg 1, \alpha) = \frac{\pi^2}{\ell} \cos^2\left(\frac{\alpha}{2}\right) \cos\left[(1 - \cos\alpha)\,\ell\right] + \frac{\pi^2}{\ell} \sin^2\left(\frac{\alpha}{2}\right) \cos\left[(1 + \cos\alpha)\,\ell\right] \ . \quad (3.54)$$

The analytical formula in Eq. (3.54) is very efficient to compute the background potential at a long distance. In Fig. 3.4.1 we compare the numerical results computed from Eq. (3.51) with the analytical results from Eq. (3.54). It can been seen that they match extremely well for $\ell \gg 1$. Recalling $\ell = rE_\nu$ the background potential at a long distance is given by

$$\begin{aligned} V_{\rm bkg}\left(r \gg E_\nu^{-1}, \alpha\right) \ &= \ -\frac{g_V^1 g_V^2}{\pi} G_F^2 \Phi_0 E_\nu \frac{1}{r} \left\{ \cos^2\left(\frac{\alpha}{2}\right) \cos\left[(1 - \cos\alpha)\, E_\nu r\right] \right. \\ &\left. + \sin^2\left(\frac{\alpha}{2}\right) \cos\left[(1 + \cos\alpha)\, E_\nu r\right] \right\} \ . \end{aligned} \quad (3.55)$$

We further consider the small $\alpha$ limit ($\alpha \ll 1$ while $E_\nu r \alpha^2$ can be arbitrarily large) and find

$$V_{\rm bkg}\left(r \gg E_\nu^{-1}, \alpha \ll 1\right) = -\frac{g_V^1 g_V^2}{\pi} G_F^2 \times \Phi_0 E_\nu \times \frac{1}{r} \times \cos\left(\frac{\alpha^2 E_\nu r}{2}\right). \quad (3.56)$$

`Integrate` in `Mathematica` only produces a vanishing result. The bug has been confirmed by the developers of `Mathematica`.

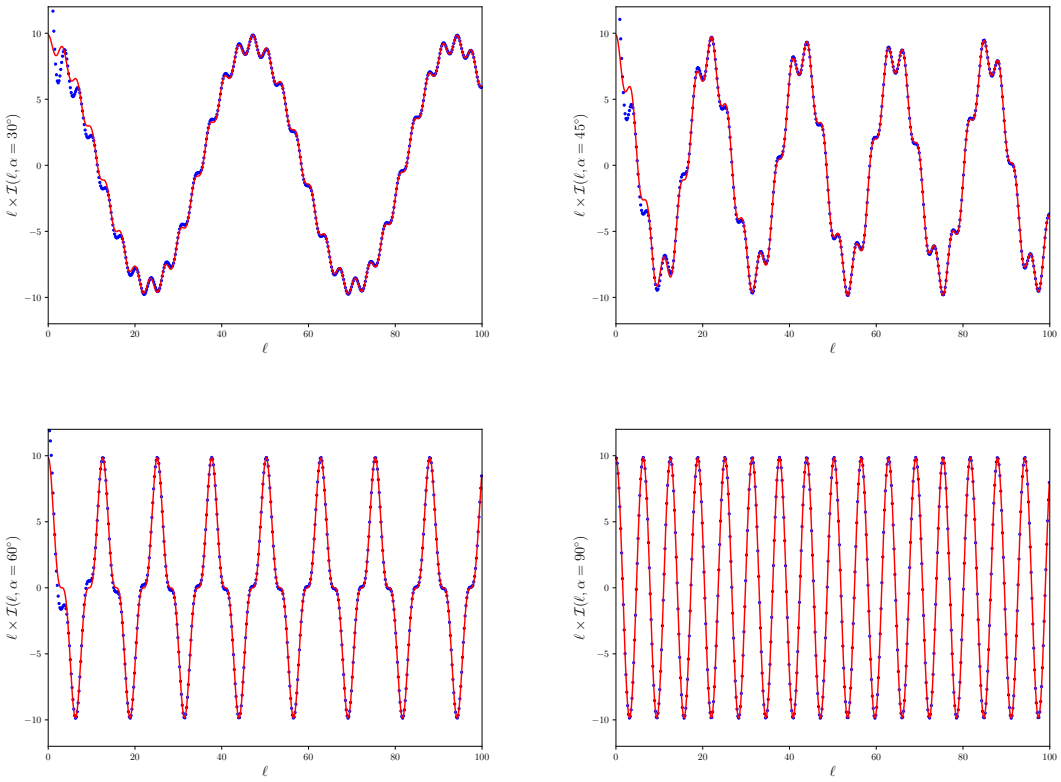


Comparison between the numerical results of $\ell \times \mathcal{I}(\ell, \alpha)$ computed from Eq. (3.51) (blue dotted points) and the analytical results computed from Eq. (3.54) (red solid line) for $\alpha = 30°$, $\alpha = 45°$, $\alpha = 60°$ and $\alpha = 90°$. They match excellently at large distances (i.e., $r \gg E_\nu^{-1}$).

A few remarks are in order:

- The first term depends on the couplings of the fermions to the neutrinos.
- The second term is the energy density of the background neutrinos.
- The third term is the leading $r$ dependence. We learn that we have a $1/r$

potential.

- The last term encodes the angular dependency. We discuss it in more detail below.
- To leading order, this effect has no mass dependence. This is because the mass of the neutrino is negligible compared to the energies of the background neutrinos.

We next move to discuss the forces between macroscopic objects. In that case, we need to integrate over the energy of the background neutrinos as well as over the distribution of the masses. This integration can result in a smearing of the force, leading to the oscillatory behavior averaging out as we span the size of the macroscopic objects.

In order to get an effective $1/r$ potential, the smearing should not be very strong. The $\alpha$-suppressed oscillation mode starts to rapidly oscillate when $\alpha^2 \Delta(E_\nu r) \sim \pi$, where $\Delta(E_\nu r)$ is the spread of the energy $E_\nu$ and the location of the test masses. So the $1/r$ dependence approximately holds if

$$\alpha^2 \lesssim \frac{\pi}{\Delta(E_\nu r)} \,. \tag{3.57}$$

### 3.4.2 Discussion

The neutrino-force effect is most significant when the background has a direction. There are several significant differences when comparing it to the vacuum case:

1. $r$ **dependence.** While in vacuum the force scales as $1/r^5$, the leading term for a directional background scales as $1/r$. This implies that, at large distances, the background effects always overcome the vacuum contribution. Moreover, it implies that this force scales like gravity and the Coulomb force.

2. **Oscillation.** The force exhibits oscillatory behavior. The oscillation length depends on the energy of the background neutrinos and the angle spanned by the background's direction and the direction of the induced force. Only at $\alpha = 0$ there is no oscillation.

We provide some intuition for these two effects below. (Some of the discussions below are based on ref. [71]). The point is that, in the presence of background neutrinos, one of the virtual neutrinos in the loop is effectively replaced by a real neutrino, as imposed by the delta function $\delta(k^2 - m^2)$ in the background propagator. Then, roughly speaking, the potential is related to the forward scattering amplitude of the real neutrinos between the two objects that are subject to the force. Usually, in the absence of a background, the mass suppression is a result of the "off-shellness" from the momentum transfer $q^2$. But in the presence of the high energy directional background, the departure from "off-shellness" is not so straightforward. The situation in vacuum is Lorentz invariant so the departure from $q^2$ is simply $m^2$. In the presence of the directional background, Lorentz-noninvariant quantities can be present in the propagator, which is what happens in this case.

Thus, in the vacuum case for a one-particle exchange potential, the potential

is the Fourier transform of $(\mathbf{q}^2 + m^2)^{-1}$, yielding $e^{-mr}/r$. In the background the propagator $\Pi(|\mathbf{q}|^2)$ is given by (as in Eq. (3.46)):

$$\Pi(|\mathbf{q}|^2) \sim \frac{1}{\mathbf{q}^2 - 4E_\nu^2 \cos^2\theta_{\mathbf{k}_0,\mathbf{q}}} = \frac{1}{\mathbf{q}^2 + (2iE_\nu \cos\theta_{\mathbf{k}_0,\mathbf{q}})^2}, \tag{3.58}$$

where $\theta_{\mathbf{k}_0,\mathbf{q}}$ is the angle between vectors $\mathbf{k}_0$ and $\mathbf{q}$ ($\xi \equiv \cos\theta_{\mathbf{k}_0,\mathbf{q}}$ in Eq. (3.47)). The propagator has no leading order dependence on $m_\nu$ since $E_\nu \gg m_\nu$. Note that the "off-shellness", which is real (i.e, $m^2$) in the vacuum case, is now imaginary in the presence of the background.

We naively therefore obtain a Fourier transform,

$$V(r) \sim \frac{e^{-2iE_\nu r f(\alpha)}}{r} \sim \frac{1}{r}\cos(2E_\nu r f(\alpha)), \tag{3.59}$$

where $f(\alpha)$ is some function of the angle $\alpha$, which we cannot predict without performing the integral explicitly. This rough form allows us to intuit the features of the potential:

1. The $1/r$ dependence is the geometrical factor for an exchange of a massless intermediate particle. The background neutrinos practically make the potential from a two body exchange into a one body exchange, as evident from Eq. (3.46). One of the neutrinos is not virtual.
2. The oscillation behavior arises from the fact that the background neutrinos modify the propagator to carry an imaginary "mass term". This makes the exchanged neutrino "real" as opposed to virtual, giving an oscillatory behavior. Another way this can be understood is as an interference effect between two amplitudes. One amplitude is the incoming background wave

and the other one that scatters off one of the two interacting objects. At large $r$, for $\alpha = 0$, the interference is pure constructive and the potential behaves as $1/r$, corresponding to $f(0) = 0$ in Eq. (3.59) above. While at $\alpha = \pi/2$, there is destructive interference and oscillatory behavior persists.

## 3.5 Experimental sensitivities and detection of neutrino forces

### 3.5.1 Current status of the experiments

There have been decades of experimental efforts to search for new long-range forces (also referred to as the fifth force) – see Refs. [72, 73, 74] for reviews. Searches that typically employ torsion balance devices are closely related to precision tests of gravity, more specifically, to tests of the gravitational inverse-square law (ISL) [75, 76, 77] and tests of the weak equivalence principle (WEP) [78, 79]. We summarize the experimental sensitivities in Table 3.5.1 and compare them with our theoretical expectations of neutrino forces including background corrections in Fig. 3.5.2. The details are explained in what follows.

Experiments testing the WEP look for possible differences between the accelerations of different test bodies in the same gravitational field. For example, the gravitational acceleration on the Earth, $a_\oplus \approx 9.8$ m/s$^2$, should be universal for all test bodies at the same location, independent of the material of the test body. In the presence of a new long-range force whose couplings to electrons and nucleons

| Experiment | $\delta V/V_{\text{gravity}}$ | $\langle r \rangle$ | Refs |
|---|---|---|---|
| Washington2007 | $3.2 \times 10^{-16}$ | $\sim$ 6400 km | [78] |
| Washington1999 | $3.0 \times 10^{-9}$ | $\sim$ 0.3 m | [79] |
| Irvine1985 | $0.7 \times 10^{-4}$ | 2 – 5 cm | [75] |
| Irvine1985 | $2.7 \times 10^{-4}$ | 5 – 105 cm | [75] |
| Wuhan2012 | $10^{-3}$ | $\sim$ 2 mm | [80] |
| Wuhan2020 | $3 \times 10^{-2}$ | $\sim$ 0.1 mm | [77] |
| Washington2020 | $\sim 1$ | 52 $\mu$m | [76] |
| Future levitated optomechanics | $\sim 10^4$ | 1 $\mu$m | [81] |

Sensitivities of long-range force search experiments.

are disproportional to their masses, the actual observed acceleration may violate the universality.

Using Be and Ti as test masses and measuring the difference between their gravitational accelerations, the Washington experiment group reported the following result in 2007 [78]:

$$a_{\text{Be}} - a_{\text{Ti}} = (0.6 \pm 3.1) \times 10^{-15} \text{ m/s}^2 \quad \text{(Earth attractor)} \,. \tag{3.60}$$

Here, the Earth serves as the gravitational attractor. The average distance between particles in the test body and in the attractor in this case is roughly the radius of the Earth, $\langle r \rangle \sim 6400$ km. Dividing the experimental uncertainty in Eq. (3.60) by $a_\oplus \approx 9.8$ m/s$^2$, we obtain $\delta V/V_{\text{gravity}} = 3.2 \times 10^{-16}$ where $V_{\text{gravity}}$ is the gravitational

potential and $\delta V$ denotes potential variations due to new forces. This experimental setup is referred to as Washington2007 in Table 3.5.1.

Instead of making use of the Earth's gravity, one can also employ laboratory attractors. An earlier experiment conducted by the same group using a 3-ton $^{238}$U attractor and test bodies of Cu and Pb reported [79]:

$$a_{\mathrm{Cu}} - a_{\mathrm{Pb}} = (1.0 \pm 2.8) \times 10^{-15}\ \mathrm{m/s^2} \quad (\text{3-ton } ^{238}\text{U attractor})\,. \tag{3.61}$$

Note that the uncertainty is close to the one in Eq. (3.60) but the result should be compared with the gravitational acceleration caused by the $^{238}$U attractor, which is $9.2 \times 10^{-7}$ m/s$^2$. The $^{238}$U attractor has an annular shape with inner and outer radii of 10.2 cm and 44.6 cm while the torsion balance is located in its center. Hence the average distance between particles in the test body and in the attractor in this case is roughly $\langle r \rangle \sim 0.3$ m. This experimental setup is referred to as Washington1999 in Table 3.5.1.

Experiments testing ISL measures the variation of the gravitational attraction between two test bodies when their distance varies. The Irvine experiment conducted in the 1980s was already able to probe ISL over a distance range from 2 cm to 105 cm at the precision of $10^{-4}$[75], ruling out a previously claimed deviation of ISL by $(0.37 \pm 0.07)\%$ in the 4.5 to 30 cm range [82]. In recent years, the precision of ISL testing experiments in the centimeter to meter range has not been improved significantly. The main progress that has been made so far is the successful measurement of gravitational forces at much smaller distance scales [76, 77]. So far, the smallest distance scale at which gravity has been probed in labora-

tory is 52 $\mu$m [76]. Above this scale, gravitational forces have been measured to certain precision (see results of Wuhan2012 [80], Wuhan2020 [77], and Washington2020 [76] in Table 3.5.1) and the measurements are fully consistent with ISL.

### 3.5.2 Detection of neutrino forces

When applying the above experimental sensitivities to neutrino forces, one should note that $\delta V$ caused by reactor and solar neutrinos are both direction-dependent. For solar neutrinos, the angle $\alpha$ varies with a period of 24 hours due to Earth's rotation. For reactor neutrinos, the angle $\alpha$ varies in experiments with moving attractors, as is the case of the Washington1999 experiment [79]. Since the reactor neutrino flux is only intense within a short distance from a reactor, the Washington2007 experiment does not provide strong probing power to the reactor neutrino force.

In order to compare the deviation of ISL gravitational potential from the background potentials to the experimental sensitivities, we need to compute $V_{\rm bkg}$ between two objects numerically and compare it to the gravity. As a bench mark point, we fix $\alpha = 0$.

This assumption is not valid in all of the examples that we study below. All of the current experiments are done between extended objects and the averaging over their shape is important, making the use of the $\alpha = 0$ result unjustified. Yet, we do use the $\alpha = 0$ as the most optimistic scenario just to get an idea how far the

effects are from current sensitivities.

Since in the cases we are considering, the vacuum potential is negligible the neutrino force between two particles in the directional neutrino background is simply given by

$$V_{\nu-\text{force}}(r) = -\frac{g_V^1 g_V^2}{\pi} G_F^2 \Phi E_\nu \frac{1}{r} \qquad \left(r \gg E_\nu^{-1},\ \alpha = 0\right) , \tag{3.62}$$

which is proportional to $1/r$, same as the gravitational potential. Notice that the typical energy of reactor and solar neutrino flux is $E_\nu \sim \text{MeV} \sim \left(10^{-11}\text{cm}\right)^{-1}$, while the average distance between two particles in the test body and in the attractor is larger than $\mu$m (cf. Table 3.5.1). Hence, we only need to consider the long-range behavior of the background potential, namely, $r \gg E_\nu^{-1}$. We use Eq. (3.62) below to compute the background potentials.

In Fig. 3.5.2, we plot the reactor neutrino force curves calculated from Eq. (3.62) using the standard reactor neutrino flux at 1 meter and 10 meters from the reactor core. For a reactor with 2.9 GW thermal power, the neutrino flux is $\Phi = 5 \times 10^{13}\ \text{cm}^{-2}\text{s}^{-1}$ at 10 meters away [83]. We take $E_\nu$ in Eq. (3.62) to be 2 MeV when computing the background potential from reactor neutrinos. The curves stop at $r = 0.5$ m and $r = 5$ m because experiments with much larger $r$ (such as Washington2007) are impossible to have test bodies and attractors all fitted in the limited space within 1 or 10 meters from the reactor.

For solar neutrinos, this is not a concern. So far, all experiments have $r$ much smaller than the distance to the Sun. However, one should note that the angle

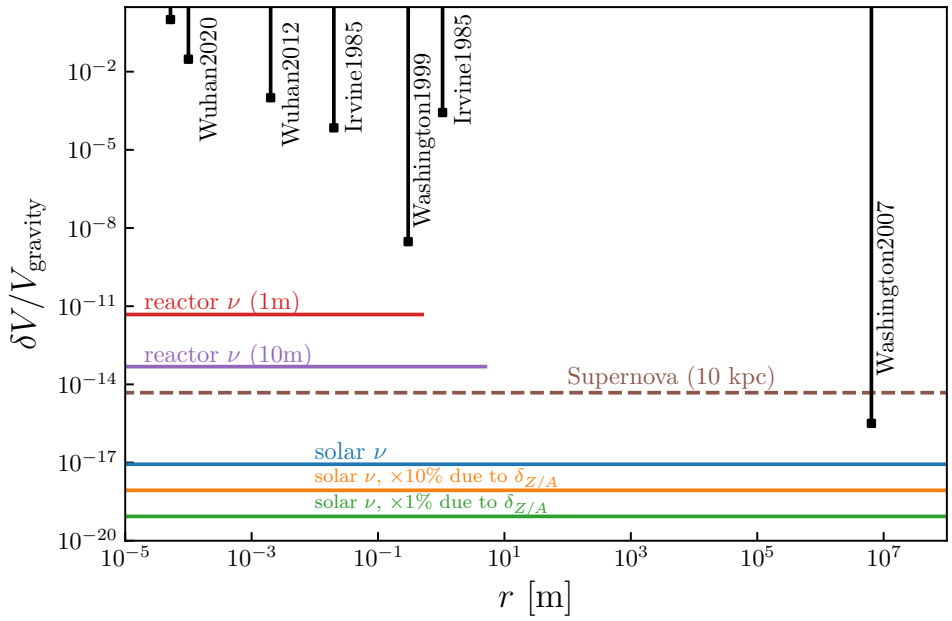


Neutrino forces in comparison with experimental sensitivities. Here all neutrino sources are assumed to be ideally point-like and the angular spread is assumed to be sufficiently small to meet Eq. (3.57). In reality, a sizable angular spread needs to be taken into account thus the above should be considered as an upper bound of the effect.

$\alpha$ varies with a period of 24 hours while a large number of noises are also 24-hour periodic. Hence the $\alpha$ dependence could be easily submerged in such noises. Nevertheless, we plot the solar neutrino line in Fig. 3.5.2 assuming that it could be resolved among various noises in future experiments.

The solar neutrino line in Fig. 3.5.2 is calculated from Eq. (3.62) by considering $pp$ neutrinos with the flux $\Phi = 5.99 \times 10^{10}\text{cm}^{-2}\text{s}^{-1}$ and the highest energy $E_{\rm max} = 0.42\,\text{MeV}$ [84]. In the computation we take $E_\nu = 0.3\,\text{MeV}$ since the $pp$ neu-

trino spectrum is not monochromatic. We have also calculated the background potential of the $^7$Be solar neutrinos whose flux is $\Phi = 4.84 \times 10^9\,\mathrm{cm^{-2}s^{-1}}$ with two monochromatic energies being $E_\nu = 0.862\,\mathrm{MeV}$ and $E_\nu = 0.384\,\mathrm{MeV}$ [84]. But the result is the same order of magnitude as that of $pp$ neutrinos.

It might be more feasible to make use of the material dependence feature of neutrino forces. Since the effective neutrino-proton vector coupling is suppressed by a factor of $1-4\sin^2\theta_W \approx 0.05$ with respect to the effective neutrino-neutron vector coupling, we can assume that neutrino forces mainly depend on the neutron number $N = A - Z$ ($A$: atomic mass number, $Z$: proton number) of the material used in test bodies. The contribution of electrons is more complicated since the charged-current interaction may or may not contribute (if not, the $1 - 4\sin^2\theta_W$ suppression also applies to electrons), depending on the neutrino flavor. For simplicity, here we neglect the electron contribution (see Appendix B.4 for a more strict treatment). Therefore, for neutrino forces on different materials, the difference is roughly

$$\frac{\delta V_{\nu-\mathrm{force}}}{V_{\nu-\mathrm{force}}} \sim \delta_{Z/A},\ \delta_{Z/A} = \begin{cases} 1.6\% & \text{for Be vs Ti} \\ 4.9\% & \text{for Cu vs Pb} \\ 8.2\% & \text{for Al vs Pt} \end{cases} . \tag{3.63}$$

Here $Z/A$ is approximately $1/2$ for most nuclei, and $\delta_{Z/A}$ denotes its variation for different materials. Taking Be vs Ti for example, since Ti (Be) has 22 (4) protons and 26 (5) neutrons, the difference is $22/48 - 4/9 = 1.4\%$. More accurate calculations using $A = 47.87$ (9.012) gives 1.6%. In principle, $\delta_{Z/A}$ could be enhanced to as

large as 50% if Hydrogen ($Z = A = 1$) is used in combination with other $Z/A \approx 1/2$ material, though technically it is difficult to make test bodies of Hydrogen. In Fig. 3.5.2, below the solar neutrino line, we plot two lines by multiplying it with $\delta_{Z/A} = 10\%$ and $1\%$. If the direction-dependent signal of $V_{\nu-\text{force}}$ are submerged in various 24-hour noises, the material dependence of $V_{\nu-\text{force}}$, which is a factor of $\delta_{Z/A}$ weaker but more robust against noises, could be exploited to probe neutrino forces.

In addition to the aforementioned dependence on directions and materials, the difference between reactor-on and -off measurements could also be used to probe neutrino forces.

For supernova neutrinos, we plot a dashed line in Fig. 3.5.2 to present the magnitude. We assume that the supernova neutrino flux is $10^{12}$ cm$^{-2}$s$^{-1}$, corresponding to a 10 kpc core-collapse supernova neutrino burst [85]. The neutrino mean energy is about 10 MeV. Here we use a dashed line to remind the readers that such a neutrino burst lasts only for a short period of a few seconds, which might be too short for torsion balance experiments to reach the desired sensitivity (e.g. the torsional oscillation period of Washington 2007 is 798 s [78]). A dedicated analysis on such experiments taking the short duration into consideration might lead to a much weaker sensitivity, but this is beyond the scope of our work.

At last, we give some brief remarks on the background effects from atmospheric and accelerator neutrinos. The flux of atmospheric neutrinos is much smaller than those of the reactor and solar neutrinos [86]. As a result, the cor-

responding background potential is weaker than that of reactor neutrinos by 12 orders of magnitude. In addition, the flux from long-baseline accelerator neutrino experiments like DUNE [87] is also weaker than that of reactor neutrinos. The accelerator neutrino background potential at the near-detector location of DUNE is about 7 orders of magnitude smaller than that of reactor neutrinos. Therefore, the background potentials from both atmospheric and accelerator neutrinos are out of the reach with current experimental sensitivities.

## 3.6 Conclusions

In this chapter, we computed the background corrections to neutrino forces in a thermal or non-thermal neutrino background. We found that the presence of the background can significantly increase the strength of neutrino forces.

For the isotropic C$\nu$B in Eq. (3.13), we have derived general formulae of the background potential for both Dirac [Eq. (3.25)] and Majorana [Eq. (3.40)] neutrinos that are valid for arbitrary neutrino masses and distances. The main feature of the potential in the presence of the C$\nu$B is that, at large distances ($r \gg m_\nu^{-1}$), it is not exponentially suppressed, as opposed to the potential in vacuum. Therefore, when the distance between two particles exceeds the inverse mass of neutrinos, the neutrino force between them is dominated by the background contribution. However, since the number density of the cosmic neutrinos is very small today, the thermal effects of the C$\nu$B on the neutrino force are still far from the available

experimental sensitivities.

We then computed the neutrino force in a directional background. We parametrized the non-thermal and anisotropic background as monochromatic distribution function with a specific direction, $\alpha$. The general direction-dependent background potential is given by Eqs. (3.48) and (3.51). At $r \gg E_\nu^{-1}$ with $E_\nu$ being the typical energy of the neutrino flux, the background potential in the small $\alpha$ limit is proportional to $1/r$, which falls much slower than the $1/r^5$ potential in vacuum and in isotropic backgrounds. In particular, there is a potential significant enhancement of the vacuum force in the presence of directional energetic dense neutrino backgrounds.

We then turned to discuss the possibility of probing the neutrino force using torsion balance experiments that aim to precisely test the gravitational inverse-square law and the weak equivalence principle. Assuming the small $\alpha$ limit, the comparison of the neutrino force in reactor and solar neutrino backgrounds with experimental sensitivities is summarized in Fig. 3.5.2. The figure shows that, if Eq. (3.57) could be satisfied, the current experiments would be 2 or 3 orders of magnitude far from detecting neutrino forces in the reactor or solar neutrino background. With current technology, however, the condition in Eq. (3.57) is not satisfied and the energy and angular spread smear out the leading $1/r$ potential. While it is not clear to us how complicated and practical it is to design an experiment that can exploit the enhancement we discuss, the point to emphasize is that strong enhancement is present.

We conclude that the neutrino force in the solar or reactor neutrino background is much more experimentally accessible than the one in vacuum. Dedicated experimental efforts are called for to check if these enhancement factors can be exploit in order to detect the elusive neutrino force.

**Note added.** After we updated our work on arXiv to Version 2, Ref. [88] appeared on arXiv. The authors of that preprint commented that the finite size of the wave packets would destroy the leading $1/r$ potential in directional neutrino backgrounds that we found. However, the content of [88] was referring to Version 1 of our paper, while in Version 2 we have already addressed the smearing effect. To address the effect of the smearing, Ref. [88] took a different approach than ours. They included the energy spread in the wave packets first and then took a monochromatic directional flux and fixed $\alpha = 0$, while we consider the smearing effect by varying $E_\nu$ and $\alpha$ of the flux. While the details of our analyses are not identical, the results of the current version of our work are in agreement with the results of Ref. [88]. Yet, our conclusions have a different tone. While we emphasize the fact that there is indeed a strong enhancement when Eq. (3.57) is satisfied, Ref. [88] is worried about the feasibility of designing experiments that can use it.

CHAPTER 4

# FERMION PAIR RADIATION BY ACCELERATING CLASSICAL SYSTEMS

## 4.1 Introduction

Radiation by a classical system is a well-known phenomenon. Probably the most familiar example is the radiation of electromagnetic waves by an accelerating point-like particle. The power loss, in this case, is calculated using the famous Larmor formula [89, 28], which, in natural units, is given by

$$P_{\text{loss}} = \frac{1}{6\pi} q^2 \boldsymbol{a}^2, \tag{4.1}$$

where $q$ is the electric charge of the particle and $\boldsymbol{a}$ is its acceleration. The Larmor formula in Eq. (4.1) has been also generalized to other types of radiation by accelerating classical sources, such as radiation of massive vector and scalar bosons [90, 91, 92, 93, 94, 95, 96, 91].

Generalizations of the Larmor formula to exotic types of radiation are motivated, among other things, by their applications to new physics searches. The basic idea is that if a new physics radiation accompanies an accelerating astrophysical object, the power loss effect can be enhanced thanks to the large number density of an object, even if the coupling between the new physics and the Standard Model (SM) is very small. This expected enhancement can be used to obtain constraints on various new physics scenarios using astrophysical observations. One example is the radiation of an ultra-light gauged $L_\mu - L_\tau$ vector bo-

son [97, 98, 99, 100] by pulsar binaries. The measurement of the orbital period decay, when compared to the prediction due to the gravitational wave (GW) radiation, was used to constrain the mass of the $L_\mu - L_\tau$ gauge boson and its couplings to the SM [93, 92, 101, 102, 103, 104, 105].

In this chapter, we extend the previous work and derive the generalization of the Larmor formula to the case of fermion-antifermion pair radiation by classical systems. The interest in this scenario is twofold. First, it is interesting theoretically since it is one more example of a case where a fermion pair behaves like a boson (other cases are Cooper pairs in superconductors and the mediation of forces between objects via 2-fermion forces [6, 8, 58, 106]). Thus we can study the coherent radiation of fermions. The key point is that single-fermion emission changes the source and thus can not be treated classically. Fermion-pair emission, however, can take place without changing any quantum degrees of freedom of the emitting system (such as spin). Thus, fermion-pair emission (or emission of any even number of fermions) can be treated classically.

The second aspect is phenomenological. In particular, we consider radiation by astrophysical systems. In the SM, as we show below, the effect of the fermion pair radiation is negligible. In beyond the SM (BSM) theories, however, such processes can be enhanced, enabling us to probe various new physics scenarios using astrophysical observations. In particular, fermion-pair radiation can become significant in models with a new light mediator (a vector or scalar boson) that couples to some light fermionic degrees of freedom. These fermionic degrees of freedom

can be the well-known neutrinos or some new BSM fermions. The effects of this radiation can become relevant when the mediator is too heavy to be produced on-shell, but the fermions are much lighter and can be radiated out. Since fermion pairs can be produced via off-shell mediators, the fermion pair radiation can be used to probe broader regions of the parameter space of such models.

As a particular application of our result for the fermion-pair radiation, we consider two models: (*i*) a model with a gauged $L_\mu - L_\tau$ symmetry and (*ii*) a model with a muonophilic scalar that couples to the muon and the muon neutrino. We study the implications of these scenarios for the power loss by pulsar binaries and compare our results to the cases of on-shell vector boson radiation [93, 92, 90] and on-shell scalar radiation [90]. A stark difference is that the emission of neutrino pairs in a particular harmonic mode of the periodic system is not kinematically forbidden when the mediator mass becomes larger than the frequency of that particular mode. In the case of on-shell bosonic radiation, radiation from a harmonic mode is cut off once the boson mass exceeds the frequency of that particular mode due to energy conservation. We use the available period decay data for pulsar binaries to demonstrate how neutrino pair radiation, mediated by BSM bosons, can be used to probe a broader parameter space than the on-shell boson emission. We, however, do not perform a comprehensive study of other bounds on the models we consider.

This chapter is organized as follows: In Sec. 4.2, we discuss the general machinery required for calculating fermion-pair radiation from a classical system. In

Sec. 4.3, we discuss the main features of the power-loss formula. In Sec. 4.4, we perform the computation for the particular case where the classical system is a binary system. We then use available data to place constraints on the parameters of a few models. We conclude in Sec. 4.5. The detailed calculations are shown in the appendix.

## 4.2 Fermion pair radiation by a point-like object

In this section, we outline the calculation of the power of fermion-pair radiation that accompanies a non-relativistic point-like object. We formulate a general approach to the derivation of the power loss formula with a focus on the case of elliptical orbits. The fermion pair radiation is realized in our analysis via the coupling of the classical object to a massive boson: a vector, or a scalar, which is unstable and decays into a fermion pair. We consider the emission of Dirac fermions and generalize our result to the case of Weyl fermions when we discuss the application of our result to the SM in Section 4.3.3. While a point-like object is a purely theoretical entity, it is worthwhile to perform this calculation since the approximation of a radiating extended object as a point is valid in the limit of long-wavelength radiation.

### 4.2.1 General formalism

We describe a point-like object as a classical source using classical current, $J^{\mu}_{\rm cl}(x)$ and classical density, $\rho_{\rm cl}(x)$, which are given by

$$J^{\mu}_{\rm cl}(x) = Q\delta^3(\boldsymbol{x} - \boldsymbol{x}(t))u^{\mu}, \tag{4.2}$$

$$\rho_{\rm cl}(x) = N\delta^3(\boldsymbol{x} - \boldsymbol{x}(t)). \tag{4.3}$$

Here, $Q$ is the total charge of the object under the symmetry of interest, $N$ is the number of the relevant microscopic constituents, $\boldsymbol{x}(t)$ is its position as a function of time, $t$, and $u^{\mu}$ is its four-velocity.

Assuming motion in the $x - y$ plane, in the non-relativistic limit, the four-velocity of the object is given by

$$u^{\mu} = (1, \dot{x}, \dot{y}, 0)\,. \tag{4.4}$$

We focus on the case of the elliptical motion in the $x - y$ plane, which can be parametrically described by

$$x = a(\cos\xi - e), \qquad y = a\sqrt{1-e^2}\sin\xi, \qquad \Omega\, t = \xi - e\sin\xi, \tag{4.5}$$

where $e$ is the eccentricity, $a$ is the semi-major axis of the ellipse, and $\Omega$ is the fundamental frequency of revolution. One full revolution around the ellipse corresponds to changing the parameter $\xi$ from 0 to $2\pi$.

The power loss due to the fermion-pair radiation is calculated using

$$P_{\rm loss} = \int (\omega_1 + \omega_2)\, {\rm d}\Gamma, \tag{4.6}$$

where $\omega_1$ and $\omega_2$ are the energies of the emitted fermion and anti-fermion, respectively, and $\mathrm{d}\Gamma$ is the differential rate of the fermion-pair emission. The rate depends on the type of mediator, i.e., a scalar or a vector, and the specific form of the classical current or density.

In general, the acceleration is not constant. In the case of periodic orbits, the motion can be decomposed into harmonic modes with frequencies $\Omega_n = n\Omega$, where $\Omega$ is the fundamental frequency of revolution. The total emission rate can then be written as a sum of emission rates at different harmonics $n$,

$$\mathrm{d}\Gamma = \sum_n \mathrm{d}\Gamma_n \,. \tag{4.7}$$

The sum goes over all kinematically allowed harmonics $n > 2m_\psi/\Omega$, where $m_\psi$ is the mass of the emitted fermions. The emission rate at harmonic $n$ is found using

$$\mathrm{d}\Gamma_n = \sum_{s_1,s_2} |\mathcal{M}_n(s_1,s_2)|^2 (2\pi)\delta(\Omega_n - \omega_1 - \omega_2) \frac{\mathrm{d}^3\boldsymbol{k}_1}{(2\pi)^3\omega_1} \frac{\mathrm{d}^3\boldsymbol{k}_2}{(2\pi)^3\omega_2}. \tag{4.8}$$

Here, $k_1 = (\omega_1, \boldsymbol{k}_1)$ and $k_2 = (\omega_2, \boldsymbol{k}_2)$ are the four-momenta of the fermion and anti-fermion respectively, and $s_1(s_2)$ is the spin of the fermion (anti-fermion). The microscopic physics enters via $\mathcal{M}_n(s_1, s_2)$, which is the matrix element of the fermion-pair emission at harmonic $n$. At leading order, this matrix element is obtained from the diagram in Fig. 4.2.1. In the diagram, $\otimes$ denotes the classical source, which is given by the classical current, $J^\mu_{\mathrm{cl}}(x)$, in the case of vector mediator and by the density, $\rho_{\mathrm{cl}}(x)$, in the case of the scalar mediated radiation.

The total power loss via fermion-pair radiation is simply a sum of power losses

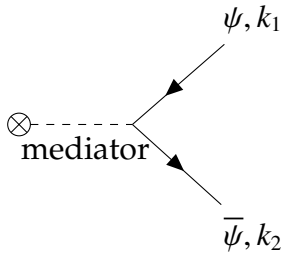


Feynman diagram for a fermion pair emission by a classical current.

over all harmonics

$$P_{\text{loss}} = \sum_n P_n, \qquad P_n = \int (\omega_1 + \omega_2)\, \mathrm{d}\Gamma_n. \tag{4.9}$$

Here, $P_n$ is the power loss of the $n$th harmonic.

In what follows, we consider two types of mediators: a massive gauge boson and a massive scalar. We only consider $s$-channel exchange and remark on $t$-channel exchange at the end of this subsection.

First, we consider a vector mediator, $A_\mu$, that corresponds to a broken U(1)′ and has mass $m_A$. This gauge boson couples to a classical current $J^\mu_{\text{cl}}(x)$, which has charge $Q$ under U(1)′. The gauge boson $A_\mu$ is unstable and decays into a fermion pair. The terms in the effective Lagrangian, relevant for the fermion-pair radiation via $A_\mu$, are

$$\mathcal{L}_{\text{eff}} \supset g A_\mu J^\mu_{\text{cl}} + g q_\psi \bar{\psi} \gamma^\mu A_\mu \psi \,, \tag{4.10}$$

where $q_\psi$ is the U(1)′ charge of the fermion $\psi$, $g$ is a dimensionless coupling constant, and $J^\mu_{\text{cl}}(x)$ is the classical current defined in Eq. (4.2). Both the vector boson and the fermions are assumed to be massive with masses $m_A$ and $m_\psi$, respectively.

The leading order matrix element for the emission, at the $n-$th harmonic, is given by

$$\mathcal{M}_n(s_1, s_2) = g^2 q_\psi \, \bar{u}(k_1, s_1)\gamma^\mu v(k_2, s_2) \, \frac{i(-\eta_{\mu\nu} + (k_1 + k_2)_\mu (k_1 + k_2)_\nu / m_A^2)}{(k_1 + k_2)^2 - m_A^2 + i m_A \Gamma_A} \, J^\nu_{\rm cl}(\Omega_n) \,, \quad (4.11)$$

where $J^\nu_{\rm cl}(\Omega_n)$ is the Fourier transform of $J^\nu_{\rm cl}(x)$, given by

$$J^\nu_{\rm cl}(\Omega_n) = \frac{\Omega}{2\pi} \int_0^{2\pi/\Omega} {\rm d}t \int {\rm d}^3\boldsymbol{x} \; e^{i(n\Omega t - \boldsymbol{p}\cdot\boldsymbol{x})} J^\nu_{\rm cl}(x) \quad (4.12)$$

with $\boldsymbol{p} = \boldsymbol{k}_1 + \boldsymbol{k}_2$, $\Gamma_A$ is the decay width of the gauge boson, and $2\pi/\Omega$ is the period. We assume that the decay into a $\bar{\psi}\psi$ pair is the only decay channel for the gauge boson $A_\mu$, and that the fermion mass $m_\psi$ is negligible compared to the gauge boson mass $m_A$. Under these assumptions, the decay width of $A_\mu$ is given by

$$\Gamma_A = \frac{g^2 q_\psi^2 m_A}{12\pi}. \quad (4.13)$$

The other case we consider is that of a scalar mediator, $\phi$, for which the relevant terms in the Lagrangian are

$$\mathcal{L} \supset g\phi\rho_{\rm cl} + g'\phi\bar{\psi}\psi, \quad (4.14)$$

where $g$ is the dimensionless coupling between the scalar $\phi$ and the classical source, $g'$ is the Yukawa coupling of the fermion $\psi$ to the scalar $\phi$, and $\rho_{\rm cl}(x)$ is the number density of relevant particles in the classical source. Both the scalar and the fermions are assumed to be massive with masses $m_\phi$ and $m_\psi$, respectively. The matrix element in this case is given by

$$\mathcal{M}_n(s_1, s_2) = g g' \bar{u}(k_1, s_1) v(k_2, s_2) \frac{i\rho_{\rm cl}(\Omega_n)}{(k_1 + k_2)^2 - m_\phi^2 + i m_\phi \Gamma_\phi}, \quad (4.15)$$

where $\rho_{\rm cl}(\Omega_n)$ is the Fourier transform of $\rho_{\rm cl}(x)$,

$$\rho_{\rm cl}(\Omega_n) = \frac{\Omega}{2\pi}\int_0^{2\pi/\Omega} {\rm d}t \int {\rm d}^3\boldsymbol{x}\; e^{i(n\Omega t - \boldsymbol{p}\cdot\boldsymbol{x})}\rho_{\rm cl}(x), \tag{4.16}$$

and the decay width of the scalar is $\Gamma_\phi$. As in the case of the vector mediator, we assume that the fermionic decay mode is the only available mode, and the fermion mass $m_\psi$ can be neglected compared to the mass of a scalar $m_\phi$. Thus we have

$$\Gamma_\phi = \frac{g'^2 m_\phi}{8\pi}. \tag{4.17}$$

So far, we have only considered the $s$-channel contribution to the fermion pair radiation. Fermion pair radiation via $t-$channel process mediated by a vector or scalar is also a possibility. Such contributions, however, are highly suppressed for $m_S \gg \Omega, m_M$, where $m_S$ is the mass of the particles in the source that couple to the fermion pairs $\bar{\psi}\psi$ at the microscopic level, and $m_M$ is the mediator mass. Since the emitted fermions have energy of the order of $\Omega$, the fundamental frequency of the system, the $t$-channel contribution to the momentum entering the propagator is of the order of $m_S - \Omega$. Thus the $t$-channel propagator is schematically given by

$$\Pi \sim \frac{1}{(m_S - \Omega)^2 - m_M^2}. \tag{4.18}$$

In the case where $m_S$ is much larger than both $\Omega$ and $m_M$, the propagator is dominated by the mass of the source particles, and the process is heavily suppressed. In this chapter, we assume that the mass hierarchy $m_S \gg \Omega, m_M$ and neglect the $t-$channel contributions to the fermion pair radiation everywhere.

### 4.2.2 Power loss formulae

Using Eqs. (4.8)–(4.15), we can calculate the power loss via fermion-pair radiation from a point-like object moving in an elliptical orbit. The detailed derivations are shown in Appendix C, and here we only quote the final result. The power loss due to fermion-pair emission in harmonic $n > 2m_\psi/\Omega$, for the cases of the vector and scalar mediator, can be written as

$$P_n^A = \frac{g^4 q_\psi^2 Q^2}{12\pi^3}\, a^2\Omega^4\, B_n^A(n_A, n_\psi, n_\Gamma), \tag{4.19}$$

$$P_n^\phi = \frac{g^2 g'^2 N^2}{12\pi^3}\, a^2\Omega^4\, B_n^\phi(n_\phi, n_\psi, n_\Gamma). \tag{4.20}$$

The functions $B_n^M(n_A, n_\psi, n_\Gamma)$, where $M = A, \phi$, are given by

$$B_n^M(n_M, n_\psi, n_\Gamma) \equiv \left(J_n'(ne)^2 + \frac{1-e^2}{e^2} J_n(ne)^2\right) \int_{n_\psi}^{n-n_\psi} \mathrm{d}x\, F^M(x, n, n_M, n_\psi, n_\Gamma). \tag{4.21}$$

Here

$$n_M \equiv m_M/\Omega, \qquad n_\psi \equiv m_\psi/\Omega, \qquad n_\Gamma \equiv \Gamma_M/\Omega, \tag{4.22}$$

and $J_n(ne)$ is a Bessel function of order $n$ with argument $ne$. The integration variable in Eq. (4.21) is defined by $x \equiv \omega_1/\Omega$, where $\omega_1$ is the energy of one of the final-state fermion. In what follows, for brevity, we use the notation

$$F^M(x) \equiv F^M(x, n, n_M, n_\psi, n_\Gamma), \qquad B_n^M \equiv B_n^M(n_M, n_\psi, n_\Gamma). \tag{4.23}$$

The functions $F^M(x)$ have the general form

$$\begin{aligned} F^M(x) = F_0^M(x) \quad &+ \quad \frac{F_1^M(x)}{n_M}\left[\tan^{-1}\left(\frac{a(x)+b(x)}{n_M}\right) - \tan^{-1}\left(\frac{a(x)-b(x)}{n_M}\right)\right] \\ &+ \quad F_2^M(x)\tanh^{-1}\left(\frac{2a(x)b(x)}{a(x)^2+b(x)^2+{n_M^2}^2}\right), \end{aligned} \tag{4.24}$$

with $a(x)$ and $b(x)$ being universal for both gauge boson and scalar mediators,

$$\begin{aligned} a(x) &= 2n_\psi^2 - n_M^2 + 2nx - 2x^2\,, \\ b(x) &= 2\sqrt{x^2 - n_\psi^2}\,\sqrt{(n-x)^2 - n_\psi^2}\,. \end{aligned} \tag{4.25}$$

The functions $F_0^M(x)$, $F_1^M(x)$, and $F_2^M(x)$ are different for the two cases. For a gauge boson mediator, we obtain

$$\begin{aligned} F_0^A(x) &= b(x)/2n\,, \\ F_1^A(x) &= \frac{1}{4n}\left(^4 + 4n^2n_\psi^2 - ^{2\,2} + 2^2n^2 - 4nx^2 + 4x^{22}\right), \\ F_2^A(x) &= \frac{1}{2n}\left(^2 + n^2 - 2nx + 2x^2\right), \end{aligned} \tag{4.26}$$

while for a scalar mediator,

$$\begin{aligned} F_0^\phi(x) &= -b(x)/2n\,, \\ F_1^\phi(x) &= \frac{1}{4n}\left(^{22} + (n^2 - ^2)(^2 - 4n_\psi^2)\right), \\ F_2^\phi(x) &= \frac{1}{4n}\left(n^2 + 4n_\psi^2 - 2^2\right). \end{aligned} \tag{4.27}$$

Eqs. (4.19)–(4.27) are the main results of our work. Analytical integration of $F^A(x)$ and $F^\phi(x)$ is challenging, but it still can be performed in certain limits. In Sec. 4.3.2, we consider two limiting cases: the case of $n_M \ll 1$, which reproduces the Larmor formula, and $n_M \gg 1$, which is relevant for the fermion pair radiation in the SM. In general, however, calculating the power loss requires numerical analysis. We perform such an analysis in Sec. 4.4 when we discuss a particular phenomenological application of our result.

## 4.3 Discussion of the power-loss formula

The power loss due to fermion-pair emission by a classical source on an elliptical orbit is given by Eqs. (4.19)-(4.27). Below we discuss the main features and the asymptotic behavior of this result.

### 4.3.1 General features of the power-loss formula

We start with the general features that hold for both the vector and scalar cases.

The radiation rate is proportional to the charge-squared; that is, the functions $P_n^A$ and $P_n^\phi$ depend on $Q^2$ and $N^2$, respectively. This is a manifestation of the fact that the fermion-pair radiation that we are considering is coherent.

The form of $F^M(x)$, with $M = A, \phi$, in Eq. (4.24) is somewhat general. We show in Appendix C that the overall form of $F^M(x)$, at the tree level, is the same for any renormalizable theory that couples fermions to a classical source moving in an elliptical orbit. Note that the functions $a(x)$ and $b(x)$ defined in Eq. (4.25) are purely kinematic and thus have the same form for any theory of fermion pair emission, while the form of $F_0^M(x), F_1^M(x)$, and $F_2^M(x)$ vary with the theory considered. For instance, considering non-renormalizable interactions would lead to a different momentum dependence of the matrix element that could, in principle, change the form of $F^M(x)$.

The power loss for both vector and scalar mediators behaves qualitatively the same way despite the different functional forms of $F_i^A(x)$ vs. $F_i^\phi(x)$, with $i = 0, 1, 2$. This is not surprising since there is nothing fundamentally different between the matrix elements for the vector and scalar cases.

Energy conservation implies that the functions $F^M(x)$ are invariant under $x \to (n-x)$ exchange. The reason is that the total energy radiated in fermion pairs in the $n$-th harmonic is $n\Omega$. The transformation $x \to (n-x)$ exchanges the energies of the emitted fermion and anti-fermion, and the emission rate is the same regardless of the order in which the integrals are carried out. This invariance results from the fact that the fermion-antifermion emission from a classical system is essentially a 2-body decay. Note that this has nothing to do with the details of the considered model.

For $< n$, the power loss has a very weak dependence on . This is true for the particular models that we chose here but is not expected to be true in general. For an example when this is not the case, see the discussion of Proca fields in Ref. [93], where dependence on  appears due to the absence of gauge symmetry.

There is an interplay of three energy scales: The mass of the mediator, $m_M$, the mass of the fermion, $m_\psi$, and the frequency of the harmonics, $n\Omega$. The fermions cannot be produced when $2m_\psi > n\Omega$. In the opposite limit, when $2m_\psi < n\Omega$, the production rate depends strongly on the mediator mass. For $m_M < 2m_\psi < n\Omega$, fermion production is strongly suppressed since the on-shell boson is kinematically forbidden from decaying into fermions. (Note that strictly speaking, our

result cannot be straightforwardly applied in this case as everywhere we assume $\Gamma_M > 0$.) For $2m_\psi < m_M < n\Omega$, the fermions are produced via decay of the on-shell mediator. Thus the power loss in the fermion-pair radiation is equal to that of the on-shell boson radiation. The region of the parameter space where $m_M > n\Omega > 2m_\psi$ is of the most interest to us, as in this region the fermions are kinematically allowed, the mediator is off-shell, and therefore the fermion pair emission is most significant.

As an example that illustrates the qualitative features of the power loss, consider Fig. 4.3.1. It shows $B_n^A$, defined in Eq. (4.21), as a function of $n_A$ for massless fermions for the first four harmonics. The most striking feature of the plots is a sharp drop at $n_A \sim n$. This behavior follows from the fact that at $n_A \sim n$, the radiation regime switches from the radiation dominated by on-shell boson production ($n_A < n$), which is proportional to $g^2$ to the off-shell production ($n_A > n$) proportional to $g^4$. The power loss in the regime dominated by fermion-pair radiation is thus suppressed by $g^2$ compared to the power loss in the regime dominated by the on-shell boson radiation. The power loss in the case of the scalar mediator exhibits the same behavior.

Comparing our results to the cases of vector [93, 92, 90] and scalar radiation [90], we note that from kinematic considerations alone, boson radiation drops to zero as soon as $n_M = n$. This is not what we observe for the fermion-pair emission. In the case of fermion-pair radiation, off-shell boson production is possible, even though there is an extra suppression by $g^2$ for a vector and $g'^2$ for a scalar

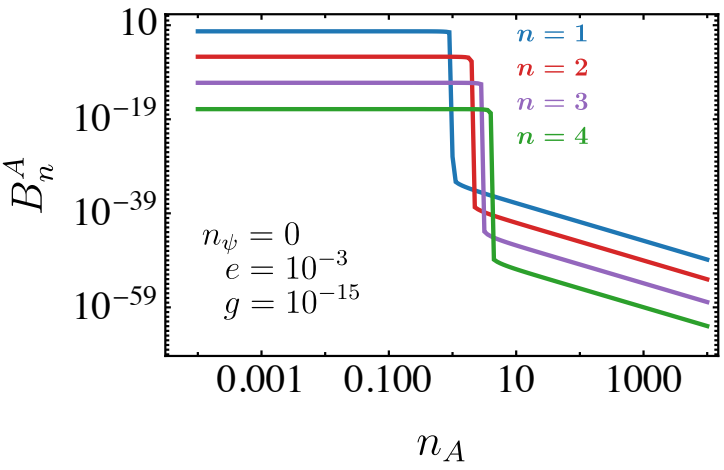


$B_n^A$ vs $n_A$ for fixed eccentricity, $e = 10^{-3}$, coupling constant $g = 10^{-15}$, and massless final state fermions, $m_\psi = 0$. See Eqs. (4.21)-(4.26) for the definition of $B_n^A$.

compared to on-shell boson radiation. As a result, the regime $n_M > n$ opens up new regions of the parameter space for each harmonic $n$ and is of particular phenomenological interest to us.

Next, we remark on the dependence of the power loss on the eccentricity in the case of orbits close to circular. For that, we note that the eccentricity only enters the power loss through the Bessel function prefactor of $B_n^M$ in Eq. (4.21), which we denote as $K(n, e)$,

$$K(n, e) = J_n'(ne)^2 + \frac{1 - e^2}{e^2} J_n(ne)^2 \,. \tag{4.28}$$

We recall that $J_n(z)$ and $J_n'(z)$ behave asymptotically, in the limit $z \ll 1$, as

$$J_n(z) \approx \frac{1}{n!}\left(\frac{z}{2}\right)^n, \qquad J_n'(z) \approx \frac{n}{n!}\frac{1}{2}\left(\frac{z}{2}\right)^{n-1} \approx \frac{n}{z} J_n(z), \qquad z \ll 1. \tag{4.29}$$

Using Eq. (4.29), we find for the eccentricity dependent prefactor $K(n, e)$, in the

limit $ne \ll 1$, that

$$K(n,e) = J_n'(ne)^2 + \frac{n^2-(ne)^2}{(ne)^2} J_n(z)^2 \approx J_n'(ne)^2 + \frac{n^2}{(ne)^2} J_n(z)^2$$
$$= 2\frac{n^2}{z^2} J_n(ne)^2 = \frac{(ne)^{2n-2}}{2^{2n-1}} \frac{n^2}{(n!)^2} = \frac{(ne)^{2n-2}}{2^{2n-1}\left((n-1)!\right)^2}. \tag{4.30}$$

Thus we learn that in the limit $ne \ll 1$, prefactor $K(n,e)$ scales with the eccentricity as

$$K(n,e) \propto (ne)^{2n-2}\,. \tag{4.31}$$

This shows that for small eccentricities (and thus orbits close to circular ones), the contributions from higher harmonics die away very fast as $n$ increases. For $n = 1$ and $e \ll 1$, we have $K(1,e) \approx 1/2$. For each subsequent harmonic power drops by a factor of order $e^2$, until the factorial in the denominator of $K(n,e)$ (see Eq. (4.30)) starts to dominate. Then the contributions from the higher harmonics start to decay away even faster. Fig. 4.3.1 illustrates the behavior of the power loss for the first four harmonics in the case of small eccentricity $e = 10^{-3}$.

The case of highly eccentric orbits $e \sim 1$ is significantly more involved. First, the contributions from different modes do not follow the simple hierarchy of the low eccentricity case. The contributions from higher modes can be of the same order or even larger than the first mode depending on the values of other parameters. See the left panel of Fig. 4.3.1 to compare the $n$-dependence of $B_n^A$ for different eccentricity values. Second, as Fig. 4.3.1 demonstrates, the hierarchy of modes in the on-shell dominated part of the parameter space does not carry into the off-shell dominated region. Consider the green line corresponding to a highly eccentric orbit with $e = 0.6$. For $n_A = 10^{-1}$ (left panel), the maximum contribution

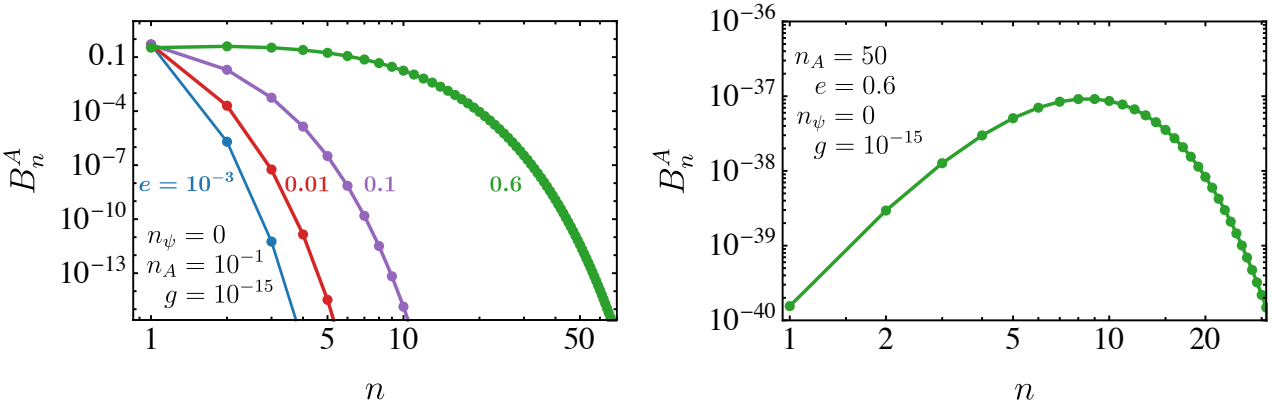


*Left:* $B_n^A$ as a function of $n$ in the regime where the radiation is dominated by on-shell boson production. Different colors correspond to different values of eccentricity. The values of $n_\psi$, $n_A$ and $g$ are fixed. *Right:* $B_n^A$ as a function of $n$ for a highly eccentric orbit with $e = 0.6$ in the regime where the radiation is dominated by off-shell boson production.

to the power loss comes from the mode with $n = 2$ and the first 5 modes contribute at about the same order. The situation is drastically different for $n_A = 50$ (right panel). The maximum contribution to the power loss comes from the $n = 8$ mode. We learn that for $e \sim 1$, generally speaking, the power loss per mode first increases as we increase $n$ and then starts decreasing after reaching a certain value of $n$. Where this maximum occurs depends on other parameters.

### 4.3.2 Asymptotic behavior for the case of circular orbits

We now move to the discussion of the asymptotic behaviour of the power loss in two limiting cases $m_M \ll \Omega$ and $m_M \gg \Omega$, where $m_M$ is the mass of the mediator, $M = A, \phi$. In this subsection, for simplicity we consider the straightforward case of circular orbits ($e = 0$) and massless fermions ($m_\psi = 0$). For the eccentricity dependent part of the power loss, $K(n, e)$, we have

$$\lim_{e \to 0} K(n, e) = \lim_{e \to 0} \left( J_n'(ne)^2 + \frac{1 - e^2}{e^2} J_n(ne)^2 \right) = \frac{1}{2} \delta_{n,1}. \tag{4.32}$$

Thus the only mode that contributes to the power loss in the circular orbit limit is the mode with $n = 1$.

First, let us consider the regime of light mediators, $m_M \ll \Omega$, or equivalently $n_M \ll 1$. In this limit, $F^M(x)$ defined in Eq. (4.24) is dominated by the second term. We thus neglect the first and the third terms of $F^M(x)$ and take the second term's limit $n_M \to 0$. After that, the integral in (4.21) can be performed analytically, yielding the following asymptotic expressions for the power radiated via vector and scalar, respectively:

$$P^A(m_A \ll \Omega) \approx \frac{g^2}{6\pi} Q^2 a^2 \Omega^4, \tag{4.33}$$

$$P^\phi(m_\phi \ll \Omega) \approx \frac{g^2}{12\pi} N^2 a^2 \Omega^4. \tag{4.34}$$

The asymptotic behavior that we find for $P^A$ and $P^\phi$ reproduces the known results for the on-shell vector [93, 92, 90] and scalar [90] radiation. This is expected as, in the regime $m_M \ll \Omega$, the fermion pair radiation is dominated by on-shell boson

production. Additionally, Eq. (4.33) also reproduces the Larmor formula for the power of the electromagnetic wave radiation given in Eq. (4.1). To see this, recall that the acceleration on a circular orbit is equal to $a\Omega^2$, where $a$ is the radius of the orbit and $\Omega$ is the frequency of revolution.

Next, we study the regime when on-shell boson production is kinematically forbidden, and the fermion pair radiation takes place through the off-shell mediator. This is the limit of heavy mediators, $m_M \gg \Omega$, or equivalently $n_M \gg 1$. In this case, we take the $n_M \to \infty$ limit of $F^M(x)$ and find that the resulting expression can be integrated analytically. Upon performing the integration, we find that the vector and scalar-mediated radiation behave as

$$P^A(m_A \gg \Omega) \approx \frac{g^4 q_\psi^2 Q^2}{210\pi^3} \frac{a^2\Omega^8}{m_A^4} = \frac{1}{35\pi^2} \frac{g^2 q_\psi^2 \Omega^4}{m_A^4} \times P^A(m_A \ll \Omega), \tag{4.35}$$

$$P^\phi(m_\phi \gg \Omega) \approx \frac{g^2 g'^2 N^2}{840\pi^3} \frac{a^2\Omega^8}{m_\phi^4} = \frac{1}{70\pi^2} \frac{g'^2 \Omega^4}{m_\phi^4} \times P^\phi(m_\phi \ll \Omega). \tag{4.36}$$

We learn that in the limit of heavy mediators, the fermion pair radiation is suppressed compared to on-shell boson radiation by the following factors:

1. A factor of $g^2 q_\psi^2$ or $g'^2$, which, at the amplitude level, comes from the coupling of the mediator to the fermion pair.
2. A factor of $\Omega^4/m_\phi^4$, which comes from the propagator of the mediator.
3. A phase space factor of $1/35\pi^2$ or $1/70\pi^2$, which arises from the fact that there are more particles in the final state in the case of the off-shell pair production than in the case of the on-shell boson production.

Note that Eqs. (4.35) and (4.36) can be interpreted as integrating out the heavy mediator, resulting in an effective 4-Fermi interaction with a coefficient proportional to $g^2/m_A^2$ or $gg'/m_\phi^2$. Thus, it is also valid for $t$-channel and $u$-channel interactions.

Last, we compare the results of the vector to that of the scalar mediators. Consider $m_A = m_\phi$, $Q^2 = N^2$ and $g' = gq_\psi$. In this case, the power radiated via the vector mediator is greater than the power radiated via the scalar mediator in both radiation regimes. In particular, we have

$$\frac{P^A(m_A \ll \Omega)}{P^\phi(m_\phi \ll \Omega)} \approx 2, \qquad \frac{P^A(m_A \gg \Omega)}{P^\phi(m_\phi \gg \Omega)} \approx 4. \tag{4.37}$$

These factors are related to the different number of degrees of freedom between the vector and scalar cases. There are two polarization states for an on-shell massless vector, while the scalar has only one. For the deeply off-shell mediator, the correspondence is not so clear, but it seems to us that it is related to the fact that off shell gauge boson, $A_\mu$, has four degrees of freedom

### 4.3.3 Fermion-pair radiation in the SM

The expression in Eq. (4.35) can be used to estimate the power loss due to fermion pair radiation by classical sources within the SM. In this subsection, we consider neutrino pair radiation mediated by $Z$-boson. The contribution due to $W$-boson mediated pair emission is qualitatively the same as the $Z$-boson contribution and

is expected to be of the same order. The main difference between the two contributions is due to the fact that $W$-boson mediated radiation is only relevant for leptons in the source while $Z$-boson contribution is present for all types of fermions.

Consider a source made of $N_\Psi$ fermions of type $\Psi$ with the total weak charge $Q = N_\Psi q_\Psi$. To apply Eq. (4.35) to the neutrino pair radiation in the SM, we need to recall that Eq. (4.35) was derived under the assumption of vectorial couplings, while the SM is a chiral theory. The relevant parts of the SM Lagrangian are different from the Lagrangian in Eq. (4.10); in particular, in the SM we have

$$\mathcal{L}_{\rm SM} \supset -i\frac{g}{2\cos\theta_W}\left(\bar{\Psi}\gamma^\mu(c_V^\Psi - c_A^\psi)\Psi + \bar{\nu}\gamma^\mu(c_V^\nu - c_A^\nu)\nu\right)Z_\mu. \tag{4.38}$$

Thus Eq. (4.35) yields the following expression for the $Z$-boson mediated power loss due to the neutrino pair radiation in the SM

$$P^Z(m_Z \gg \Omega) \approx \frac{1}{210\pi^3}\frac{g^4 q_\nu^2 q_\Psi^2 N_\Psi^2}{16\cos^4\theta_W}\frac{a^2\Omega^8}{m_Z^4}, \tag{4.39}$$

where we perform the replacement $g \to g/(2\cos\theta_W)$ in Eq. (4.35) and define

$$q_\psi^2 = q_\nu^2 = (c_V^\nu)^2 + (c_A^\nu)^2, \qquad q_\Psi = c_V^\Psi, \qquad m_A = m_Z\,. \tag{4.40}$$

Note that, for the source, only vectorial coupling $c_V^\Psi$ enters the power loss. This is because we consider coherent radiation.

The expression in Eq. (4.39) can be rewritten as

$$P^Z(m_Z \gg \Omega) \approx G_{\rm eff}^2 q_\Psi^2 q_\nu^2 N_\Psi^2 \frac{a^2\Omega^8}{210\pi^3}\,, \tag{4.41}$$

where $G_{\rm eff} = \sqrt{2}G_F$ and $G_F$ is the Fermi constant. When the power loss is written in the form of Eq. (4.41), it becomes clear that it is the same as what one would ob-

tain by performing the calculation for the effective Fermi theory with the effective Lagrangian given by

$$\mathcal{L}^{Z}_{\rm eff} \supset G_{\rm eff}[\bar{\Psi}\gamma^{\mu}(c^{\Psi}_{V} - c^{\Psi}_{A}\gamma^{5})\Psi][\bar{\nu}\gamma_{\mu}(c^{\nu}_{V} - c^{\nu}_{A}\gamma^{5})\nu]. \tag{4.42}$$

This, of course, is not surprising as we consider radiation at the energy $\Omega$, which is much less than the electroweak scale, $\Omega \ll m_Z$. In fact, the result in Eq. (4.41) applies to any effective 4-Fermi interaction. While we derive our results for $s$-channel exchange, in the limit where the mediator is much heavier than the orbit frequency, we do not need to distinguish between $s$-channel and $t$-channel. Thus, Eqs. (4.39) and (4.41) can also be used for $t$-channel $W$-exchange in the SM.

Finally, we discuss the situation when there are several different types of fermions in the source. In this case, we need to first add all the amplitudes that correspond to the radiation by different fermions $\Psi$ (for leptons, we add both $Z$-boson and $W$-boson contributions). Then, we square the sum of the relevant amplitudes to obtain the total emission rate.

We end this subsection with the following remark. The power loss due to neutrino pair radiation in the SM was estimated in Ref. [91] to be $P^{Z}_{SM} \sim G_F^2\Omega^6$. Using the explicit calculation, however, we find that $P^{Z}_{SM} \sim G_F^2 a^2\Omega^8$. That is, there is an extra factor of $a^2\Omega^2$ compared to the estimation of Ref. [91]. In fact, our result includes the semi-major axis $a$ as an additional energy scale of the system.

## 4.4 Fermion pair radiation by pulsar binaries

We now move to discuss the phenomenological applications of our results to astrophysical systems. We focus on the neutrino-pair emission from pulsar binaries [107, 108, 109, 110, 111, 112, 113, 114, 115, 116, 117]. A pulsar binary is a binary system of a pulsar and companion. This choice is motivated by the availability of extensive period decay data for such systems. In particular, we apply our results to two binaries: Hulse-Taylor binary PSR B1913+16 [118, 119, 120] (a system of a pulsar and a neutron star) and PSR J1738+0333 [113, 121] (a system of a pulsar and a white dwarf). The parameters characterizing the two systems are summarized in Table 4.4.

In what follows, we first discuss the applicability of our results of Section 4.2.2 to pulsar binaries in general. Then we estimate the contribution to the power loss due to neutrino pair emission in the SM and show that it is negligible compared to the gravitational wave radiation. We then consider neutrino pair radiation in two BSM scenarios via ultralight vector and scalar mediators and apply our results to the pulsar binaries with the parameters in Table 4.4.

| **Binary system** | **PSR B1913+16 [120]** | **PSR J1738+0333 [113]** |
|---|---|---|
| Eccentricity $e$ | 0.6171340(4) | $3.4(11) \times 10^{-7}$ |
| Pulsar mass $m_1$ ($M_\odot$) | 1.438(1) | 1.46(6) |
| Companion mass $m_2$ ($M_\odot$) | 1.390(1) | 0.181(8) |
| Binary period $T_b$ ($\mathrm{GeV}^{-1}$) | $4.240 \times 10^{28}$ | $4.657 \times 10^{28}$ |
| Intrinsic period decay $\dot{T}_b$ | $-2.398(4) \times 10^{-12}$ | $-2.59(32) \times 10^{-14}$ |
| Predicted period decay due to GW $\dot{T}_{GW}$ | $-2.40263(5) \times 10^{-12}$ | $-2.77(19) \times 10^{-14}$ |
| Ratio of period decays $\mathcal{R} = \dot{T}_b/\dot{T}_{GW}$ | 0.9983(16) | 0.94(13) |
| Orbital frequency $\Omega = 2\pi/T_b$ (GeV) | $1.482 \times 10^{-28}$ | $1.349 \times 10^{-28}$ |
| Semi-major axis $a$ ($\mathrm{GeV}^{-1}$) | $9.878 \times 10^{24}$ | $8.77 \times 10^{24}$ |

The relevant parameters for the PSR B1913+16 and PSR J1738+0333 binary systems. Figures in parenthesis are the $1\sigma$ uncertainties in the last quoted digit, where all the uncertainties are symmetrized. $M_\odot$ is the mass of the sun. The relative experimental error of the binary period $T_b$ is $\sim 10^{-12}$ for PSR B1913+16, and $\sim 10^{-11}$ for PSR J1738+0333. The double line separates binary parameters quoted in Ref. [120, 113] and the ones we derive. Values of the semi-major axis $a$ are calculated using Eq. (4.47).

### 4.4.1 Pulsar binaries as a classical source

The results for the fermion pair radiation, summarized in Eqs. (4.19)-(4.27), were derived for the case of classical current describing non-relativistic point-like object following an elliptical orbit. To justify the application of our results to pulsar binaries, we note the following:

1. A pulsar binary can be treated as a classical source. The typical size of a pulsar binary can be estimated as the size of the semi-major axis which varies between $10^6$ and $10^8$ km, that is, $a \sim 10^{24} - 10^{26}\,\mathrm{GeV}^{-1}$. The wavelength of the radiation is determined by the fundamental frequency of the orbit, and for a typical pulsar binary with periods in the range of $10^{-1} - 10^3$ days, the wavelength is $\lambda \sim 10^{28} - 10^{32}\,\mathrm{GeV}^{-1}$. Thus, $\lambda \gg a$ and we conclude that pulsar binaries can be treated as classical radiation sources.

2. Stars of the pulsar binary can be treated as point-like objects. Typical sizes of stars in a binary vary from $r \sim 10\,\mathrm{km} \sim 10^{19}\,\mathrm{GeV}^{-1}$, for neutron stars, and $r \sim 10^3\,\mathrm{km} \sim 10^{21}\,\mathrm{GeV}^{-1}$, for white dwarfs. Thus $r \ll a$, $\lambda$ and both pulsar and its companion can be treated as point-like objects. Moreover, $r \ll \lambda$ implies the coherence of the radiation.

3. The motion of the pulsar and its companion in the binary system is non-relativistic. We can roughly estimate the orbital velocity of the stars in a binary as $v \sim a\Omega$, which for characteristic values quoted above implies $v \lesssim 10^{-2}$.

4. For a wide range of pulsar binary systems, the observed power loss is such that it has no significant effect on the eccentricity of the orbit. Thus we can treat the orbit as elliptical over the time of observation. For example, the Hulse-Taylor binary has $e \sim 1$, with $T_b(\mathrm{d}e/\mathrm{d}t) \lesssim 10^{-11}$, where $T_b$ is the binary period and $\mathrm{d}e/\mathrm{d}t$ is the time derivative of the eccentricity [120].

Now that we have established that the results of Section 4.2.2 can be applied to pulsar binaries, we proceed in two steps. First, we modify our expressions for the classical current and number density in Eqs. (4.2) and (4.3) to the case of two point-like objects on an elliptical orbit. Second, we perform the standard reduction of the two-body problem to a one-body problem.

We write the classical current and number density as

$$J^{\mu}_{\mathrm{cl}}(x) = \sum_{b=1,2} Q_b \, \delta^3(\boldsymbol{x} - \boldsymbol{x}_b(t)) u^{\mu}_b, \tag{4.43}$$

and

$$\rho_{\mathrm{cl}}(x) = \sum_{b=1,2} N_b \, \delta^3(\boldsymbol{x} - \boldsymbol{x}_b(t)\,, \tag{4.44}$$

respectively. Here, $b = 1, 2$ is the index that labels the stars of the binary system, $\boldsymbol{x}_b(t)$ is the position of the $b$-th star at time $t$, and $u^{\mu}_b$ is its four-velocity.

Next, we move to the binary system's Center-of-Mass (CoM) frame. For that, we define $\boldsymbol{R}$, the coordinate of center of mass, and $\boldsymbol{r}$, the distance between the two stars,

$$\boldsymbol{R} = \frac{m_1}{m_1 + m_2}\boldsymbol{x}_1 + \frac{m_2}{m_1 + m_2}\boldsymbol{x}_2, \qquad \boldsymbol{r} = \boldsymbol{x}_1 - \boldsymbol{x}_2\,, \tag{4.45}$$

where $m_1$ and $m_2$ are the masses of the two stars.

As we are not concerned with the translational motion of the system as a whole, which is described by $\boldsymbol{R}$, we can solely focus on $\boldsymbol{r}$. This is the standard two-body to one-body problem reduction for central force motion. The non-relativistic classical trajectory of the stars in the CoM frame can thus be described by the vector $\boldsymbol{r} = (x, y, 0)$ and is given by elliptical orbits as in Eq. (4.4):

$$x = a(\cos\xi - e), \quad y = a\sqrt{1-e^2}\sin\xi, \quad \Omega t = \xi - e\sin\xi, \tag{4.46}$$

where $e$ is the eccentricity, $a$ is the semi-major axis of the elliptical orbit, and the fundamental frequency of revolution is given by

$$\Omega = \sqrt{\frac{G_N(m_1+m_2)}{a^3}}\,. \tag{4.47}$$

The results of Eqs. (4.19)-(4.27) generalize to the case of binary systems via the following replacements that follow from the 2-body to 1-body reduction procedure:

$$Q^2 \to M^2\left(\frac{Q_1}{m_1} - \frac{Q_2}{m_2}\right)^2, \qquad N^2 \to M^2\left(\frac{N_1}{m_1} - \frac{N_2}{m_2}\right)^2, \tag{4.48}$$

where

$$M = \frac{m_1 m_2}{m_1 + m_2} \tag{4.49}$$

is the reduced mass of the binary system. As a result we obtain the following expressions for the power loss in $n$-th harmonic for a vector and scalar mediators

respectively:

$$P_n^A = \frac{g^4 q_\psi^2}{12\pi^3} M^2 \left(\frac{Q_1}{m_1} - \frac{Q_2}{m_2}\right)^2 a^2 \Omega^4 \, B_n^A(n_A, n_\psi, n_\Gamma), \tag{4.50}$$

$$P_n^\phi = \frac{g^2 g'^2}{12\pi^3} M^2 \left(\frac{N_1}{m_1} - \frac{N_2}{m_2}\right)^2 a^2 \Omega^4 \, B_n^\phi(n_\phi, n_\psi, n_\Gamma), \tag{4.51}$$

where the functions $B_n^A$ and $B_n^\phi$ are defined in Eqs. (4.21)-(4.27).

### 4.4.2 Neutrino pair radiation by pulsar binaries in the SM

In the SM, for the pulsar binary, the power loss via electroweak mediators is discussed in Sec. 4.3.3. Here, we simply generalize it to the case of 2-body motion using Eq. (4.48). We obtain the following expression for the power loss in neutrino pair radiation via $Z$-exchange in the SM

$$P_{\rm SM} \approx \frac{G_F^2 \left(c_V^{\nu\,2} + c_A^{\nu\,2}\right)}{105\pi^3 \cos^2\theta_W} M^2 a^2 \Omega^8 \left(\frac{1}{m_1} \sum_{i=n,p,e,\ldots} c_V^i N_{1i} Q_{1i} - \frac{1}{m_2} \sum_{i=n,p,e,\ldots} c_V^i N_{2i} Q_{2i}\right)^2 \tag{4.52}$$

where the sum goes over all microscopic constituents of binary stars, such as neutrons ($n$), protons ($p$), electrons ($e$), etc. To perform a numerical estimate, we consider a pulsar binary with a neutron star companion and assume that all of the neutron star mass is in the form of neutrons. We consider a typical pulsar-neutron star binary with

$$m_{1,2} \sim M_\odot \sim 10^{57}\text{GeV}, \qquad a \sim 10^{25}\ \text{GeV}^{-1}, \qquad \Omega \sim 10^{-28}\ \text{GeV}, \tag{4.53}$$

and non-zero dipole moment

$$M^2 \left(\frac{Q_1}{m_1} - \frac{Q_2}{m_2}\right)^2 \sim Q_{1,2}^2 \sim 10^{114}, \tag{4.54}$$

where $Q_b = N_b(n) - N_b(\bar{n}) \approx N_b(n) \approx M_\odot/m_n \approx 10^{57}$, with $b = 1, 2$, are the neutron charges of the neutron stars, $N_b(n)$ and $N_b(\bar{n})$ are the numbers of neutrons and anti-neutrons respectively, $m_n$ is the neutron mass. Using $c_V^\nu = c_A^\nu = 1/2$, $c_V^n = -1/2$, and the measured values of $m_n$, $G_F$, and $\theta_W$, we find the following numerical estimate for the radiated power

$$P_{\rm SM} \sim 10^{-56}{\rm eV}^2. \tag{4.55}$$

To see if the above result is significant, we compare it to the power loss in the form of gravitational wave (GW) radiation. Using the quadrupole formula for the GW radiation [122] for the case of circular orbit ($e = 0$) we have

$$P_{\rm GW} = \frac{32}{5} G_N M^2 a^4 \Omega^6 \sim 10^8\,{\rm GeV}^2 \tag{4.56}$$

where $G_N$ is Newton's gravitational constant. The rough estimates in Eqs. (4.55) and (4.56) show that, in the SM, the fermion-pair radiation by astrophysical objects is completely negligible compared to the gravitational wave radiation.

We close the subsection with one remark. Within the SM, neutron stars also emit synchrotron radiation of fermion-antifermion pairs in their self-produced magnetic fields, as shown in Ref. [123]. This phenomenon is different from the one we consider here. Synchrotron radiation is an incoherent effect. Thus, the power loss, in this case, scales as $N$, the number of neutrons in the star. In the case we are considering, the radiation is coherent and comes from the star's acceleration as a whole. Then, the net power that is radiated is proportional to $N^2$.

### 4.4.3 New physics constraints from the neutrino pair radiation by pulsar binaries

Since extra radiation in the SM is negligible, any observed deviation from the gravitational wave radiation would be strong evidence for the physics beyond the SM. In particular, fermion-pair radiation can be enhanced in BSM models with light vector or scalar mediators, with $m_{A,\phi} \ll m_Z$. To explain why such light bosonic states have evaded detection so far, we must require that they have small couplings, thus evading all the available constraints. The smallness of couplings, however, still can be compensated in cases where the object has a large charge under the new symmetries. This can be the case for astrophysical objects. Thus, such objects are our prime focus in the rest of this work.

In particular, in this subsection, we demonstrate how our results can be used to derive new physics bounds from the neutrino pair radiation by pulsar binaries. As we mentioned above, we use two distinct pulsar binary systems, the Hulse-Taylor binary PSR B1913+16 and PSR J1738+0333. The relevant properties of the two systems are summarized in Table. 4.4. The Hulse-Taylor binary is a pulsar binary with a neutron star companion, it is highly eccentric, and the mass ratio of the two stars is close to 1. The PSR J1738+0333, on the other hand, is a pulsar-white dwarf binary with an almost circular orbit and a high pulsar-to-companion mass ratio. For both systems, the data on the orbital period decay is shown in Table 4.4. Both binaries lie within $1\sigma$ of the general relativity prediction.

In our analysis, we exploit the fact that typical neutron stars contain a very large number of muons, $N(\mu) \sim 10^{55}$ [124, 125, 126, 127]. Thus, the effects of muonophilic new physics can be significantly enhanced. The presence of the large muon number in neutron stars is attributed to the fact that when the electron chemical potential, $\mu_e$, is larger than the muon mass $\mu_e > m_\mu$, it becomes energetically favorable for relativistic electrons at the Fermi surface to decay into muons via $e^- \to \mu^- + \bar{\nu}_\mu + \nu_e$. Moreover, the muonic beta-decay $n \to p + \mu^- + \bar{\nu}_\mu$ and inverse beta-decay $p + \mu^- \to n + \nu_\mu$ reactions become energetically favorable, while the muon decay $\mu^- \to e^- + \bar{\nu}_e + \nu_\mu$ is forbidden by Fermi statistics.

Being motivated by the neutron star muonic content, we consider neutrino pair emission by pulsar binaries via the following two types of BSM mediators:

- $\mathrm{U}(1)_{L_\mu - L_\tau}$ massive gauge boson with

$$\mathcal{L} \supset g A_\alpha \left( \bar{\mu}\gamma^\alpha \mu - \bar{\tau}\gamma^\alpha \tau + \bar{\nu}_\mu \gamma^\alpha \nu_\mu - \bar{\nu}_\tau \gamma^\alpha \nu_\tau \right), \tag{4.57}$$

- Massive muonophilic scalar with

$$\mathcal{L} \supset g \phi \bar{\mu}\mu + g' \phi \bar{\nu}_\mu \nu_\mu \,. \tag{4.58}$$

It is known that at least two of the SM neutrinos are massive, while the third neutrino can be very light or massless. This means that only one neutrino mass eigenstate can be radiated in the two scenarios we consider here. A realistic treatment of neutrino emission would include insertions of the corresponding PMNS matrix elements [128], resulting in an additional factor of order one. Since we

already neglecting an $O(1)$ factor coming from the estimate of the muon number density in the neutron stars, we also ignore any PMNS factors in the rest of this section.

Note also that in a theory with general couplings to the left and right-handed neutrinos, i.e., $gA_\alpha \bar{\nu}\gamma^\alpha(c_V - c_A\gamma^5)\nu$, the results for the power loss are qualitatively similar. Moreover, in the case of massless neutrinos, the power loss for the case of the general coupling is the same as the power loss for the case of purely vectorial coupling up to $g^2 \to g^2(c_A^2 + c_V^2)$ replacement. This is why in what follows, for simplicity, we consider the case of the vectorial coupling only.

These two BSM models imply the possibility for the neutrino pair radiation at rates enhanced compared to the SM. Our results from Eqs. (4.50) and (4.51) thus can be used to set bounds on the coupling constants and masses of the new bosons.

The presence of the muonophilic new physics, however, not only alters the radiation patterns of pulsar binaries, but it also has important implications for the neutron star's equation of state. In particular, the presence of a repulsive (vector) or attractive (scalar) interaction between muons could affect the muon number, which depends on the coupling $g$ to the new physics. In the following, we write the muon number as $N(\mu, g)$ to keep the dependence on $g$ explicit.

The number of muons becomes $g$-dependent as the interactions change the muon chemical potential. The muon interaction due to the $L_\mu - L_\tau$ vector boson is

repulsive, and thus the chemical potential is increased compared to its SM value by $\varepsilon \sim g^2 N(\mu, g)/R$, where $R$ is the radius of the neutron star the boson mass is neglected. When the coupling $g$ is small, such that $\varepsilon \ll m_\mu$, the effect of the new interaction is insignificant, and the number of muons is approximately given by its value in the limit of no interaction $N(\mu, g = 0)$. When the interaction is strong, such that $\varepsilon \gg m_\mu$, it becomes energetically less favorable to have muons inside the neutron star and thus $N(\mu, g) < N(\mu, g = 0)$.

Similar reasoning applies to the case of the scalar mediator. The only difference is the sign of the interaction. In the scalar case, the interaction between muons is attractive. Thus the muon chemical potential is decreased by $\varepsilon$. This leads to the increase of the muon number for larger couplings $N(\mu, g) > N(\mu, g = 0)$. In both cases, the change from the regime when $N(\mu, g) \approx N(\mu, g = 0)$ to the situation when the interaction starts to affect the muon number happens for couplings such that $\varepsilon \sim m_\mu$, or numerically $g \sim 10^{-18}$ for a typical neutron star [92].

However, in what follows, we ignore the effect of the new physics on the muon number. Everywhere in our analysis, we use the muon number in the limit of no new physics interaction, that is we set $N(\mu) = N(\mu, g = 0) \sim 10^{55}$ [124, 125, 126, 127]. In principle, $g$-independence of muon number can be achieved in models with both vector and scalar mediators with fine-tuned coupling constants such that the repulsive and attractive interactions cancel each other.

To apply Eqs. (4.50) and (4.51), we define $N_b(\mu)$ and $N_b(\bar{\mu})$ as the number of muons and antimuons respectively in neutron star labeled by $b = 1, 2$. Then, as

there are almost no tau leptons in neutron stars, $Q_b = N_b(\mu) - N_b(\bar{\mu})$ is the total charge of the neutron star under the $L_\mu - L_\tau$ gauge symmetry, and $N_b = N_b(\mu) + N_b(\bar{\mu})$ is the total number of muons and anti-muons in the star. Additionally, since $N_b(\bar{\mu}) \approx 0$, we have $Q_b \approx N_b$.

The energy lost through radiation in a binary star system can be directly probed by measuring the decay of the orbital period. Assuming that the attractive gravitational force between the two stars is such that their orbits stay Keplerian, the decay rate of the period of revolution $T_b$ is related directly to the energy lost via radiation [93]:

$$\dot{T}_b = -6\pi a^{5/2} G_N^{-3/2} (m_1 m_2)^{-1} (m_1 + m_2)^{-1/2} \times P_{\text{loss}}, \tag{4.59}$$

where $\dot{T}_b$ is the time derivative of the binary period, $G_N$ is the gravitational constant, $m_1$ and $m_2$ are the masses of the stars in the binary system, $a$ is the semi-major axis of the elliptical orbit, and $P_{\text{loss}}$ is the total power radiated. The decay of the period per unit of time is dimensionless and is measured experimentally.

GW emission is the dominant source of power loss in a binary star system. Assuming that the GW emission and neutrino pair emission are the only sources of energy loss, we have

$$P_{\text{loss}} = P_{\text{GW}} + P_{\bar{\nu}\nu}, \tag{4.60}$$

where $P_{\bar{\nu}\nu}$ is the power loss due to the neutrino pair radiation and $P_{GW}$ is the power loss due to GW emission, which, to the leading order, is given by the GW

quadrupole radiation formula [122],

$$P_{\rm loss}^{GW} = \frac{32}{5} G\Omega^6 M^2 a^4 (1-e^2)^{-7/2} \left(1 + \frac{73}{24}e^2 + \frac{37}{96}e^4\right), \tag{4.61}$$

where $M$ is the reduced mass of the system, as defined in Eq. (4.49). The binary period decay $\dot{T}_b$ thus can be written as a sum of two contributions,

$$\dot{T}_b = \dot{T}_{\rm GW} + \dot{T}_{\bar{\nu}\nu}\,. \tag{4.62}$$

We next introduce the period decay ratio $\mathcal{R}$ as the ratio of the measured period decay to the theoretical prediction of the period decay due to GW radiation,

$$\mathcal{R} = \frac{\dot{T}_b}{\dot{T}_{\rm GW}} = 1 + \frac{\dot{T}_{\bar{\nu}\nu}}{\dot{T}_{\rm GW}}. \tag{4.63}$$

We use the measured value of $\mathcal{R}$ to set $2\sigma$ limits on the masses and couplings of the BSM mediators of neutrino pair radiation as

$$\frac{\dot{T}_{\bar{\nu}\nu}}{\dot{T}_{\rm GW}} \leq (\mathcal{R}-1) + 2\sigma\,. \tag{4.64}$$

The resulting constraints on the parameter space $(g, m_A)$ and $(g, m_\phi)$ that we derive from the period decay data for the Hulse-Taylor binary and PSR J1738+033 are shown in Fig. 4.4.3. When deriving the constraints, we use $Q_b = N_b = 10^{55}$ with $b = 1, 2$ and $q_\nu = 1$. For the gauge boson mediator (left panel), we calculate the period decay due to neutrino pair emission, $\dot{T}_{\bar{\nu}\nu}$, using Eqs. (4.50) and (4.59). As we take all three neutrinos to be massless, and as $L_\mu - L_\tau$ boson couples to two neutrino types, there is an extra factor of 2 in Eq. (4.50). Similarly, for the case of the scalar mediator (right panel), we use Eqs. (4.51) and (4.59). As there is no

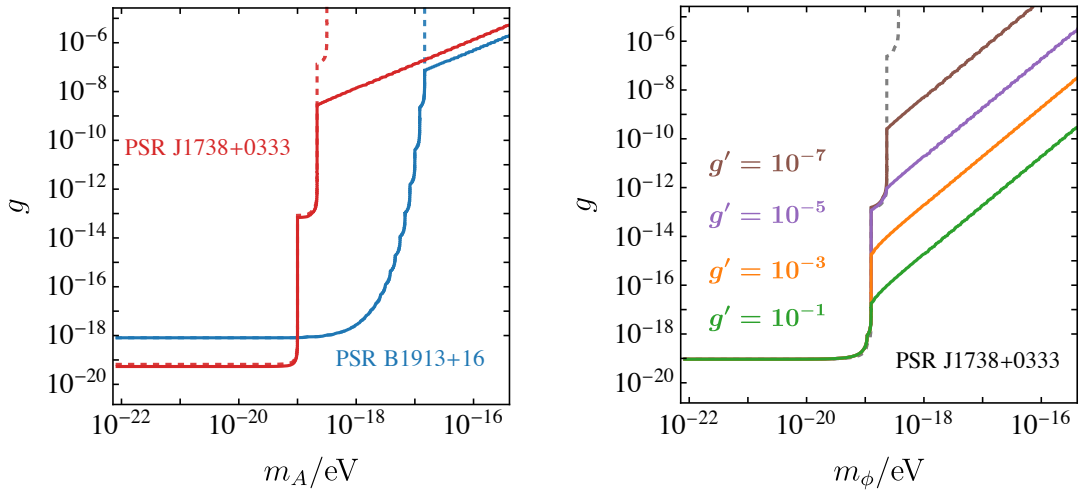


*Left:* Constraints on $g$ vs $m_A$ from the highly eccentric PSR B1913+16 (Hulse-Taylor) Bounds from the neutrino pair radiation (solid) and vector boson radiation (dashed) are shown such that the region above the curves is excluded by the measurements of the period decay. The system parameters are taken from Table 4.4. *Right:* Constraints on $g$ vs $m_\phi$ from PSR J1738+033. The dashed gray line corresponds to the bound set by the emission of the scalar boson only, while the solid lines show the bounds from including a coupling $g'$ to the neutrinos.

symmetry that requires equality of $g$ and $g'$ in the case of the scalar mediator, we present our results for the scalar case in the $(g, m_\phi)$ plane for four different values of $g'$ that vary from $10^{-7}$ to $10^{-1}$.

First, let us discuss the left panel of Fig. 4.4.3, which shows constraints on the mass and coupling of the gauge boson. For the PSR J1738+0333 (red line), whose orbit is very close to circular, the effect of neutrino pair radiation becomes

significant for the mediator masses greater than the second harmonic frequency, $m_A > 2\Omega$. For the highly eccentric Hulse-Taylor binary, off-shell radiation dominates for $m_A > 85\Omega$. In the region $m_A > 2\Omega$ ($m_A > 85\Omega$) for PSR J1738+0333 (Hulse-Taylor binary), the boundary of the excluded region is approximately quadratic in the mediator mass. This is in stark contrast with the case of the on-shell boson emission discussed in Ref. [93, 92, 90], where the boundary of the excluded region jumps in steps at $m_A = n\Omega$, with $n$ being an integer. For comparison, the dashed lines in Fig. 4.4.3 show the bounds due to the on-shell boson radiation.

Finally, we comment on the right panel of Fig. 4.4.3, which shows the constraints on the mass $m_\phi$ and coupling $g$ for different values of $g'$ in the case of the scalar mediated radiation. We only demonstrate the constraints for PSR J1738+0333; the results for the Hulse-Taylor binary are qualitatively the same. Depending on the value of $g'$ the off-shell scalar radiation starts to dominate for $m_\phi > \Omega$ ($g' \gtrsim 10^{-4}$) or $m_\phi > 2\Omega$ ($g' \lesssim 10^{-8}$). As one can see from the plot, $g' = 10^{-1}$ provides the strongest bound.

We conclude this section by noting that we do not perform a detailed analysis of the bounds on muonophilic light states. We only remark that very strong bounds on light states are derived from fifth force searches. Most of these bounds do not apply in our case as these experiments are done using materials made out of protons, neutrons, and electrons.

## 4.5 Conclusion

It is well known that fermion pairs can behave as bosons in several circumstances. In this work, we show that fermion pairs can also constitute classical radiation just like bosonic states do. We use this understanding to derive the generalization of the Larmor formula for the case of the fermion pair emission.

Being motivated by the potential of applying fermion pair radiation to astrophysical objects, we consider the case of classical sources following elliptical orbits. The most interesting regime of fermion pair radiation is when the mediator is off-shell, which takes place when the mass of the mediator is much smaller than the frequency of the periodic motion of the source. In this regime, the fermion pair emission takes over from on-shell boson production. This opens up a window into a broader region of parameter space for various models that allow for the fermion pair radiation by classical sources.

Subsequently, we apply our results to neutrino-antineutrino emission by two pulsar binary systems PSR B1913+16 and PSR J1738+0333. Neutrino pair emission by binary systems is highly suppressed in the SM compared to GW radiation, but can be significantly enhanced in various BSM scenarios. In particular, we consider two possibilities: light muonophilic vector and scalar mediators that couple to the SM neutrinos. Using period decay data for the two binary systems, we derive bounds on the parameters of the two models. While we did not perform a comprehensive study of the relevance of these bounds, the key point is that they

provide a demonstration of the fact that fermion pair radiation can be used to enhance BSM probes using astrophysical data.

There are several future directions to go from here. Here are a few that we find particularly interesting:

- A thorough and detailed study of the bounds that we find on specific models is called for. This, however, is complicated by the large uncertainties that come from the estimates on the neutron star constituents. In particular, new physics interactions alter the equation of state of a neutron star and, currently, there is no precise quantitative understanding of how this affects its content.
- It also would be interesting to see if we can find more systems to which our results can be applied. In particular, exotic astrophysical systems and exotic types of new physics models.
- In this work, we only consider fermion pair radiation; however, the results can be modified to also include bosonic pair radiation. All that needs to be done is to calculate the relevant matrix elements. It is expected to result in a different kinematic dependence.

We conclude with the main message of this chapter: If nature includes new light states, fermion pair radiation can be one more tool in our toolbox to probe them.

CHAPTER 5

# $K \to \mu^+\mu^-$ AS A CLEAN PROBE OF SHORT-DISTANCE PHYSICS

## 5.1 Introduction

Rare flavor changing neutral current (FCNC) kaon decays [129, 130, 131, 132, 133, 134, 135] provide a unique way to probe the flavor sector of the Standard Model (SM) and, in particular, CP-violating effects. The program to measure the decay rates of $K^+ \to \pi^+\nu\bar{\nu}$ [136] and $K_L \to \pi^0\nu\bar{\nu}$ [137] is aimed at determining the CKM parameters with very high theoretical precision. In particular, the $K_L \to \pi^0\nu\bar{\nu}$ decay rate can be used to extract [138, 139, 140]

$$|V_{ts}V_{td}\ \sin(\beta+\beta_s)| \approx |A^2\lambda^5\bar{\eta}|\,, \tag{5.1}$$

where $A$, $\lambda$, and $\bar{\eta}$ are the Wolfenstein parameters and $\beta+\beta_s$ is one of the angles in the $ds$ unitarity triangle such that [141]

$$\beta = \arg\left(-\frac{V_{cd}V_{cb}^*}{V_{td}V_{tb}^*}\right), \qquad \beta_s = \arg\left(-\frac{V_{ts}V_{tb}^*}{V_{cs}V_{cb}^*}\right), \qquad \beta+\beta_s-\pi = \arg\left(-\frac{V_{ts}V_{td}^*}{V_{cs}V_{cd}^*}\right). \tag{5.2}$$

Experimentally, working with decays that involve charged leptons is much simpler than the above-mentioned neutrino modes. Nonetheless, the focus of the current kaon program is on the neutrino final states, primarily because decays to charged leptons are believed not to be theoretically clean. There are so-called long-distance effects that introduce hadronic uncertainties, making extractions of clean theory parameters challenging.

In this work, we show that we can get very clean theoretical information from decays of kaons into charged leptons. This can be done only for the neutral kaons, by exploiting the interference effects between $K_S$ and $K_L$. We focus on $K \to \mu^+\mu^-$, for which the relevant CKM observable is that of Eq. (5.1). The theoretical precision in this case is superb, with hadronic uncertainties below the 1% level.

The importance of the interference terms in $K \to \mu^+\mu^-$ was emphasized in Ref. [142]. In this work, we generalize their results and demonstrate that one can get a very clean determination of the parameter combination in Eq. (5.1) by studying the interference terms.

Before we get into the details, below we explain the main idea. We first recall the situation with $K_L \to \pi^0\nu\bar{\nu}$. The reason that this decay mode is theoretically clean is that it is to a very good approximation pure CP-violating. As such, it is all calculable using perturbation theory and we do not have to worry about non-calculable long-distance effects, as they are to a very good approximation CP conserving.

The issue with $K \to \mu^+\mu^-$ is that the final state is a mixture of $\ell = 0$ and $\ell = 1$ partial wave configurations. Thus, both $K_S$ and $K_L$ decays are not pure CP-violating, and both decays have non-calculable long distance effects. Yet, if we could experimentally distinguish between the $\ell = 0$ and $\ell = 1$ final states, the situation would be similar to $K_L \to \pi^0\nu\bar{\nu}$, as we could separate the CP-violating part that we can calculate. In particular, the $\ell = 0$ amplitude has significant CP violation effects in the SM, and the decay mode $K_S \to (\mu^+\mu^-)_{\ell=0}$ is very clean theo-

retically. What we show in this work is that under some mild assumptions we can extract the rate, that is, $\mathcal{B}(K_S \to (\mu^+\mu^-)_{\ell=0})$ without separating the $\ell = 0$ and $\ell = 1$ final states. This can be done by isolating the interference terms.

Leptonic kaon decays have been studied for a long time [143, 144, 145, 146, 147, 148, 149, 150, 151, 152, 153, 150, 154, 155, 156, 157, 158, 159]. Rare kaon decays have a lot of potential for the discovery of physics beyond the SM [160, 161, 162, 163, 164, 165, 166, 167, 168, 169, 170, 171, 172, 173, 174, 175, 176, 177, 178]. Also on the experimental side a lot of advances took place in the quest for rare kaon decays [179, 180, 181, 182, 183, 137, 184, 136, 185].

The SM predictions for $K \to \mu^+\mu^-$ [186, 187, 142, 188] and the corresponding long-distance contributions [186, 189, 190, 191] have been studied in great detail. The same goes for $K_S \to \gamma\gamma$ and $K_S \to \gamma l^+ l^-$ [189] as well as kaon decays into four leptons [192]. See also the reviews Refs. [193, 194].

## 5.2 Notation and formalism

We use the following standard notation [195], where the two neutral kaon mass eigenstates, $|K_S\rangle$ and $|K_L\rangle$, are linear combinations of the flavor eigenstates:

$$|K_S\rangle = p|K^0\rangle + q|\overline{K}^0\rangle, \qquad |K_L\rangle = p|K^0\rangle - q|\overline{K}^0\rangle. \tag{5.3}$$

The mass and width averages and differences are denoted by

$$\begin{aligned} m &= \frac{m_L + m_S}{2}, \qquad \Gamma = \frac{\Gamma_L + \Gamma_S}{2}, \\ \Delta m &= m_L - m_S, \qquad \Delta\Gamma = \Gamma_L - \Gamma_S. \end{aligned} \tag{5.4}$$

We define the decay amplitudes of $|K^0\rangle$ and $|\overline{K}^0\rangle$ to a final state $f$,

$$A_f = \langle f|\mathcal{H}|K^0\rangle, \qquad \overline{A}_f = \langle f|\mathcal{H}|\overline{K}^0\rangle, \tag{5.5}$$

and the parameter $\lambda_f$,

$$\lambda_f \equiv \frac{q}{p}\frac{\overline{A}_f}{A_f}. \tag{5.6}$$

We use an arbitrary normalization, such that $A_f$ and $\overline{A}_f$ have the same normalization.

An amplitude is called *relatively real* if $\mathcal{I}m\lambda_f = 0$ and *relatively imaginary* if $\mathcal{R}e\lambda_f = 0$. Any amplitude can be written as a sum of a relatively real and a relatively imaginary part.

In any neutral meson system, the quantities $A_f$, $\overline{A}_f$, and $q/p$ depend on the phase convention. However, $|A_f|$, $|\overline{A}_f|$, $|q/p|$, and $\lambda_f$ are phase convention independent and are hence physical.

Consider a beam of neutral kaons. The time dependent decay rate as a function of proper time is given by [195]

$$\left(\frac{\mathrm{d}\Gamma}{\mathrm{d}t}\right) = \mathcal{N}_f f(t), \tag{5.7}$$

where $\mathcal{N}_f$ is a time-independent normalization factor and the function $f(t)$ is given as a sum of four functions

$$f(t) = C_L e^{-\Gamma_L t} + C_S\, e^{-\Gamma_S t} + 2\left[C_{sin}\sin(\Delta m t) + C_{cos}\cos(\Delta m t)\right] e^{-\Gamma t}. \tag{5.8}$$

The form of Eq. (7.13) is valid for any neutral kaon beam (that is, not only for a pure state) and also for a sum over several final states. We refer to the set of coefficients, $\{C_L, C_S, C_{sin}, C_{cos}\}$, as the *experimental parameters*. Note that $C_L$ is the coefficient of the $K_L$ decay term, $C_S$ of the $K_S$ decay term, while $C_{\rm sin}$ and $C_{\rm cos}$ come with the interference terms between $K_L$ and $K_S$. For convenience we also define

$$C^2_{Int.} = C^2_{cos} + C^2_{sin}\,. \tag{5.9}$$

The $C$ coefficients implicitly depend on the composition of the beam and on the relevant final states. The dependence on the final states enters via the parameters

$$\{|A_f|\,, \qquad |\overline{A}_f|\,, \qquad |q/p|\,, \qquad \arg(\lambda_f)\}. \tag{5.10}$$

We denote these as the *theory parameters*.

For an initial $|K^0\rangle$ and $|\overline{K}^0\rangle$ beam, respectively, and a single final state, $f$, the coefficients are explicitly given by [195]

$$\begin{aligned}
C_L^{K^0} &= \frac{1}{2}|A_f|^2\left(1 + |\lambda_f|^2 - 2\mathcal{R}e\lambda_f\right), & C_L^{\overline{K}^0} &= \frac{1}{2}|\overline{A}_f|^2\left(1 + |\lambda_f|^{-2} - 2\mathcal{R}e\lambda_f^{-1}\right),\\
C_S^{K^0} &= \frac{1}{2}|A_f|^2\left(1 + |\lambda_f|^2 + 2\mathcal{R}e\lambda_f\right), & C_S^{\overline{K}^0} &= \frac{1}{2}|\overline{A}_f|^2\left(1 + |\lambda_f|^{-2} + 2\mathcal{R}e\lambda_f^{-1}\right),\\
C_{\rm sin}^{K^0} &= -|A_f|^2\mathcal{I}m\lambda_f\,, & C_{\rm sin}^{\overline{K}^0} &= -|\overline{A}_f|^2\mathcal{I}m\lambda_f^{-1},\\
C_{\rm cos}^{K^0} &= \frac{1}{2}|A_f|^2\left(1 - |\lambda_f|^2\right), & C_{\rm cos}^{\overline{K}^0} &= \frac{1}{2}|\overline{A}_f|^2\left(1 - |\lambda_f|^{-2}\right).
\end{aligned} \tag{5.11}$$

In the following we focus on decays into CP-eigenstate final states. For a given final state, $f$, we define $\eta_f = 1$ if it is CP-even and $\eta_f = -1$ if it is CP-odd. We define the CP-even and CP-odd amplitudes

$$A_f^{\text{CP-even}} \equiv \frac{1}{\sqrt{2}} A_f \left(1 + \eta_f \lambda_f\right), \qquad A_f^{\text{CP-odd}} \equiv \frac{1}{\sqrt{2}} A_f \left(1 - \eta_f \lambda_f\right). \tag{5.12}$$

We make several assumptions and approximations as we go on. Our first approximation is

($i$) *CP violation (CPV) in mixing is negligible.*

Although our main interest is CP violating physics, CPV in mixing is subdominant in the effects we consider. We therefore neglect it throughout the chapter and work in the limit

$$\left|\frac{q}{p}\right| = 1. \tag{5.13}$$

This approximation is known to work to order $\epsilon_K \sim 10^{-3}$ which we neglect from this point on.

Under the above assumption, the full set of decay-mode-specific independent physical parameters can be taken to be

$$\{|A_f|, \qquad |\overline{A}_f|, \qquad \arg\left(\lambda_f\right)\}. \tag{5.14}$$

Furthermore, in the limit of no CPV in mixing, the CP amplitudes of Eq. (5.12) correspond to the amplitudes for the decays of $K_S$ and $K_L$. For example, for $f =$

$\pi^+\pi^-$, $\eta_f = 1$ and to a very good approximation $\lambda_f = 1$ and thus $A^{\text{CP-odd}}_{\pi^+\pi^-} = 0$. In the case of $K \to \pi\nu\bar{\nu}$, $\eta_f = 1$ and $\lambda_f$ is to a very good approximation a pure phase, so that the amplitude for $K_L \to \pi\nu\bar{\nu}$ gives sensitivity to the phase $\arg(\lambda_f)$ [160].

In the following it will be useful to replace the set of independent physical parameters of Eq. (5.14) with the equivalent set of physical parameters:

$$\{|A^{\text{CP-even}}_f|, \qquad |A^{\text{CP-odd}}_f|, \qquad \arg\left(A^{\text{CP-even}\,*}_f A^{\text{CP-odd}}_f\right)\}. \tag{5.15}$$

In particular, the time dependence for a beam of initial $|K^0\rangle$ into a CP-even final state is given by the coefficients

$$\begin{aligned} C^{K^0}_L &= |A^{\text{CP-odd}}_f|^2, & C^{K^0}_S &= |A^{\text{CP-even}}_f|^2, \\ C^{K^0}_{cos} &= \mathcal{R}e(A^{\text{CP-odd}*}_f A^{\text{CP-even}}_f), & C^{K^0}_{sin} &= -\mathcal{I}m(A^{\text{CP-odd}*}_f A^{\text{CP-even}}_f), \end{aligned} \tag{5.16}$$

For a CP-odd final state it is given by

$$\begin{aligned} C^{K^0}_L &= |A^{\text{CP-even}}_f|^2, & C^{K^0}_S &= |A^{\text{CP-odd}}_f|^2, \\ C^{K^0}_{cos} &= \mathcal{R}e(A^{\text{CP-odd}*}_f A^{\text{CP-even}}_f), & C^{K^0}_{sin} &= \mathcal{I}m(A^{\text{CP-odd}*}_f A^{\text{CP-even}}_f). \end{aligned} \tag{5.17}$$

For an initial $|\overline{K}^0\rangle$ state the result is obtained by multiplying $C_{cos}$ and $C_{sin}$ by $-1$ in Eqs. (5.16) and (5.17).

We also define

$$\varphi_f = \arg(A^{\text{CP-odd}*}_f A^{\text{CP-even}}_f), \tag{5.18}$$

such that we can write for a CP-even final state

$$C^{K^0}_{cos} = |A^{\text{CP-odd}*}_f A^{\text{CP-even}}_f| \cos\varphi_f\,, \qquad C^{K^0}_{sin} = -|A^{\text{CP-odd}*}_f A^{\text{CP-even}}_f| \sin\varphi_f\,. \tag{5.19}$$

For a CP-odd final state we have analogously

$$C_{cos}^{K^0} = |A_f^{\text{CP-odd}^*} A_f^{\text{CP-even}}| \cos\varphi_f\,, \qquad C_{sin}^{K^0} = |A_f^{\text{CP-odd}^*} A_f^{\text{CP-even}}| \sin\varphi_f\,. \tag{5.20}$$

## 5.3 The $K \to \mu^+\mu^-$ decay

In the decay of a neutral kaon into a pair of muons, there are two orthogonal final states that are allowed by conservation of angular momentum — muons with a symmetric wave function ($\ell = 0$) and muons with an anti-symmetric wave function ($\ell = 1$). Note that since the leptons are fermions, the state with $\ell = 0$ has negative parity and so it is CP odd, and the state with $\ell = 1$ is CP even. The four relevant amplitudes can be written in terms of the CP amplitudes of Eq. (5.12) as

$$A_\ell^{\text{CP-even}} = \frac{1}{\sqrt{2}} A_\ell \left(1 - (-1)^\ell \lambda_\ell\right), \qquad A_\ell^{\text{CP-odd}} = \frac{1}{\sqrt{2}} A_\ell \left(1 + (-1)^\ell \lambda_\ell\right), \tag{5.21}$$

with $\ell = 0, 1$. Note that we keep the normalization arbitrary, but if we want to maintain the same normalization for both $A_0$ and $A_1$ then we require a relative phase space factor between them, $\beta_\mu^2$, with

$$\beta_\mu \equiv \left(1 - \frac{4m_\mu^2}{m_K^2}\right)^{\frac{1}{2}}\,, \tag{5.22}$$

see for details Appendix D.2.

Note that under the approximation $|q/p| = 1$, Eq. (5.21) allows us to write the CP-even and -odd amplitudes as amplitudes for the decays of the mass eigenstates

$|K_S\rangle$ and $|K_L\rangle$:

$$\begin{aligned} A_0^{\text{CP-odd}} &= A(K_S \to \mu^+\mu^-)_{\ell=0}\,, \\ A_0^{\text{CP-even}} &= A(K_L \to \mu^+\mu^-)_{\ell=0}\,, \\ A_1^{\text{CP-odd}} &= A(K_L \to \mu^+\mu^-)_{\ell=1}\,, \\ A_1^{\text{CP-even}} &= A(K_S \to \mu^+\mu^-)_{\ell=1}. \end{aligned} \tag{5.23}$$

When measuring the total time dependent decay rate for $K \to \mu^+\mu^-$, the two di-muon configurations, $\ell = 0, 1$ add incoherently. The form of the function $f(t)$ defined in Eq. (7.13), is unchanged. Theoretically, each of the $C$'s is given by an implicit sum over the relevant amplitude expressions for different $\ell$'s. Thus we have two sets of decay-mode-specific physical theory parameters,

$$\{|A_\ell^{\text{CP-even}}|, \qquad |A_\ell^{\text{CP-odd}}|, \qquad \varphi_\ell \equiv \arg\left(A_\ell^{\text{CP-odd}*} A_\ell^{\text{CP-even}}\right)\}, \tag{5.24}$$

with $\ell = 0, 1$, bringing us to a total of six unknown physical parameters.

It is well known that the decay $K \to \mu^+\mu^-$ receives long-distance and short-distance contributions [196, 197, 198, 187]. The long-distance contribution is dominated by diagrams with two intermediate on-shell photons, while the short-distance contribution is defined as originating from the weak effective Hamiltonian. The distinction between long-distance and short-distance physics is somewhat ambiguous. It is clear that the short-distance physics is to a good approximation dispersive (real), since it is dominated by heavy particles in the loops. However, long-distance diagrams contribute both to the absorptive (imaginary) amplitude and, when taken off-shell, also to the dispersive amplitude.

In the following we make one extra simplifying assumption, which results in reducing the number of unknown parameters for $K \to \mu^+\mu^-$. We consider only models where

(*ii*) *The only source of CP violation is in the $\ell = 0$ amplitude.*

What we mean by this assumption is that only the $\ell = 0$ amplitude has $\mathcal{I}m(\lambda_\ell) \neq 0$.

As we discuss in Section 5.5 and in Appendix D.3, this assumption is fulfilled to a very good approximation within the SM and in any model in which the leading leptonic operator is vectorial.

We can then draw an important conclusion from the above assumption:

$$A_1^{\text{CP-odd}} = 0. \tag{5.25}$$

This implies that the number of unknown parameters is reduced by two, leaving a single parameter, $|A_1^{\text{CP-even}}|$, for the $\ell = 1$ final state. Thus, we are left with the following list of four unknown physical parameters,

$$|A_0^{\text{CP-odd}}|, \qquad |A_0^{\text{CP-even}}|, \qquad |A_1^{\text{CP-even}}|, \qquad \arg(A_0^{\text{CP-odd}*} A_0^{\text{CP-even}}). \tag{5.26}$$

In the rest of the work we demonstrate how it is possible to extract these parameters, and specifically $|A_0^{\text{CP-odd}}| = A(K_S \to \mu^+\mu^-)_{\ell=0}$, which, as we explain below, is a clean probe of the SM.

## 5.4 Extracting $\mathcal{B}(K_S \to \mu^+\mu^-)_{\ell=0}$

As portrayed in Eq. (7.13), the time-dependent decay rate for an arbitrary neutral kaon initial state is given in general by the sum of four independent functions of time that depend on the experimentally extracted parameters

$$\{C_L, \qquad C_S, \qquad C_{cos}, \qquad C_{sin}\}. \tag{5.27}$$

Within our assumptions, these coefficients depend on the following four theory parameters

$$\{|A_0^{\text{CP-odd}}|, \qquad |A_0^{\text{CP-even}}|, \qquad |A_1^{\text{CP-even}}|, \qquad \varphi_0 \equiv \arg(A_0^{\text{CP-odd}*} A_0^{\text{CP-even}})\}. \tag{5.28}$$

We consider a case of a beam that at $t = 0$ was a pure $K^0$ beam (that is, no $\overline{K}^0$). Using Eq. (5.11) we obtain that the result for this case is given by

$$\begin{aligned} C_L &= |A_0^{\text{CP-even}}|^2, \\ C_S &= |A_0^{\text{CP-odd}}|^2 + \beta_\mu^2 |A_1^{\text{CP-even}}|^2, \\ C_{cos} &= \mathcal{R}e(A_0^{\text{CP-odd}*} A_0^{\text{CP-even}}) = |A_0^{\text{CP-odd}*} A_0^{\text{CP-even}}| \cos\varphi_0, \\ C_{sin} &= \mathcal{I}m(A_0^{\text{CP-odd}*} A_0^{\text{CP-even}}) = |A_0^{\text{CP-odd}*} A_0^{\text{CP-even}}| \sin\varphi_0. \end{aligned} \tag{5.29}$$

We see that the four experimental parameters can be used to extract the four theory parameters. In particular, we find

$$|A_0^{\text{CP-odd}}|^2 = \frac{C_{cos}^2 + C_{sin}^2}{C_L} = \frac{C_{Int.}^2}{C_L}\,, \tag{5.30}$$

where $C^2_{Int.} = C^2_{cos} + C^2_{sin}$ was defined in Eq. (5.9). Having the magnitude of the amplitude we can deduce the branching ratio in terms of other observables,

$$\mathcal{B}(K_S \to \mu^+\mu^-)_{\ell=0} = \mathcal{B}(K_L \to \mu^+\mu^-) \times \frac{\tau_S}{\tau_L} \times \left(\frac{C_{int}}{C_L}\right)^2 . \tag{5.31}$$

Eq. (5.31) is our main result. It demonstrates that we can extract $\mathcal{B}(K_S \to \mu^+\mu^-)_{\ell=0}$ from the experimental time dependent decay rate.

A few comments are in order regarding Eq. (5.31):

1. Our ability to extract $\mathcal{B}(K_S \to \mu^+\mu^-)_{\ell=0}$ comes from the interference terms. It cannot be extracted from pure $K_L$ or $K_S$ terms.
2. A measurement of the interference terms additionally amounts to a measurement of the phase $\varphi_0$, which is not calculable from short-distance physics.
3. In order to extract $\mathcal{B}(K_S \to \mu^+\mu^-)_{\ell=0}$ we need only three of the four experimental parameters. The fourth parameter, $C_S$, can then be used to extract $|A_1^{\text{CP-even}}|$, or equivalently $\mathcal{B}(K_S \to \mu^+\mu^-)_{\ell=1}$. Yet, this is not our main interest, as $|A_1^{\text{CP-even}}|$ is not calculable from short-distance physics.
4. For a pure $\overline{K}^0$ beam, $C_S$ and $C_L$ in Eq. (7.14) are unchanged while $C_{cos}$ and $C_{sin}$ pick up a minus sign, and Eq. (5.31) is unchanged.

While we have only discussed a pure $K^0$ beam in this section, as long as we have sensitivity to the interference terms, it is possible to determine $|A_0^{\text{CP-odd}}|$. In

particular, as long as the kaon decays in vacuum, one can write the branching ratio $\mathcal{B}(K_S \to \mu^+\mu^-)_{\ell=0}$ in terms of $\mathcal{B}(K_L \to \mu^+\mu^-)$ in the following way:

$$\mathcal{B}(K_S \to \mu^+\mu^-)_{\ell=0} = \mathcal{D}_F \times \mathcal{B}(K_L \to \mu^+\mu^-) \times \frac{\tau_S}{\tau_L} \times \left(\frac{C_{int}}{C_L}\right)^2 . \tag{5.32}$$

where $\mathcal{D}_F$ is a dilution factor that takes into account the particular composition of the kaon beam. We discuss two cases, that of a mixed beam, and of a $K_L$ beam with regeneration, in Appendix D.1.

## 5.5 Calculating $\mathcal{B}(K_S \to \mu^+\mu^-)_{\ell=0}$

We move to discuss the theoretical calculation of $\mathcal{B}(K_S \to \mu^+\mu^-)_{\ell=0}$.

### 5.5.1 General calculation

We define

$$A_\ell = A_\ell^{SD} + A_\ell^{LD}. \tag{5.33}$$

The short-distance (SD) amplitude, $A_\ell^{SD}$, is the one that can be calculated perturbatively from the effective Hamiltonian of any model. Note that at leading order in the perturbative calculation it carries no strong phase. By definition, the long-distance (LD) amplitude, $A_\ell^{LD}$, is the part that is not captured by that calculation.

In general, it carries a strong phase. We further define

$$\lambda_\ell^{SD} = \frac{q}{p}\frac{\overline{A}_\ell^{SD}}{A_\ell^{SD}}, \qquad \lambda_\ell^{LD} = \frac{q}{p}\frac{\overline{A}_\ell^{LD}}{A_\ell^{LD}}. \tag{5.34}$$

Note that since we assume that the SD amplitude carries no strong phase, we have $|\lambda_\ell^{SD}| = 1$.

We now adopt one more working assumption, that is, we consider only models where:

(*iii*) *The long-distance physics is CP conserving.*

That is, we only consider cases where $A_\ell^{LD}$ is relatively real, that is, $\mathcal{I}m\left(\lambda_\ell^{LD}\right) = 0$.

In particular, this assumption implies that we can trust the perturbative calculation for the CP-violating amplitude, using specific operators described by quarks.

We are now ready to discuss the CP-odd amplitudes. Because of assumption (*ii*) we have $A_1^{\text{CP-odd}} = 0$. Thus we only need to consider the $\ell = 0$ CP-odd amplitude. Using Eqs. (5.12) and (5.21) we write it as

$$A_0^{\text{CP-odd}} = \frac{1}{\sqrt{2}} A_0^{SD}\left(1 + \lambda_0^{SD}\right). \tag{5.35}$$

Then, using the fact that $|\lambda_0^{SD}| = 1$, we get

$$|A_0^{\text{CP-odd}}|^2 = |A_0^{SD}|^2\left[1 + \text{Re}(\lambda_0^{SD})\right] = |A_0^{SD}|^2\left[1 - \cos\left(2\phi_0^{SD}\right)\right] = 2|A_0^{SD}|^2 \sin^2\phi_0^{SD}\,. \tag{5.36}$$

where we define

$$\phi_0^{SD} = \frac{1}{2}\arg\left(-\lambda_0^{SD}\right). \tag{5.37}$$

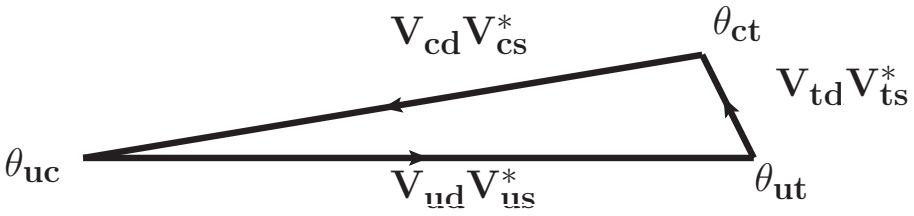


The "ds" unitarity triangle, see Refs. [199, 141]. The plot is not to scale.

Note that the result is independent of the way we choose to split the amplitude into long- and short-distance physics as long as the part we call "long-distance" is relatively real. Moreover, we can subtract from $A_0^{SD}$ any part that is relatively real without affecting the result. We use this freedom below when we discuss the SM prediction.

We conclude that in any model that satisfies our assumptions, we need to calculate $|A_0^{SD}|^2$ and $\sin^2\phi_0^{SD}$ in order to make a prediction for $\mathcal{B}(K_S \to \mu^+\mu^-)_{\ell=0}$.

### 5.5.2 SM calculation

Next we discuss the situation in the SM and remark on more generic models. The SM short-distance prediction has been discussed in Ref. [187]. Here we do not present any new arguments, but instead we review the results in the literature, explicitly stating the assumptions made, and present the results in a basis independent way.

In order to discuss the situation in the SM we look at the "ds" unitarity triangle,

that we plot in Fig. 5.5.2. The angles are given as [141]:

$$\theta_{ct} \equiv \arg\left(-\frac{V_{td}V_{ts}^*}{V_{cd}V_{cs}^*}\right) = \pi - \beta - \beta_s \sim \lambda^0\,, \tag{5.38}$$

$$\theta_{ut} = \arg\left(-\frac{V_{ud}V_{us}^*}{V_{td}V_{ts}^*}\right) = \beta + \beta_s - \theta_{uc} \sim \lambda^0\,, \tag{5.39}$$

$$\theta_{uc} = \arg\left(-\frac{V_{cd}V_{cs}^*}{V_{ud}V_{us}^*}\right) \sim \lambda^4\,. \tag{5.40}$$

In what follows, when we discuss the SM prediction, we make one more approximation:

(*iv*) We neglect effects of $O(\lambda^4)$. In particular, we set $\theta_{uc} = 0$.

With this approximation we then write

$$\frac{q}{p} = -\left(\frac{V_{cd}V_{cs}^*}{V_{cd}^*V_{cs}}\right)\left[1 + O(\lambda^4)\right] \approx -\left(\frac{V_{cd}V_{cs}^*}{V_{cd}^*V_{cs}}\right). \tag{5.41}$$

where in the last step we used $\theta_{uc} = 0$.

We are now ready to show that in the SM the long-distance amplitude is CP conserving, complying with assumption (iii) above. The claim is that the CKM factors in the long-distance amplitudes are to a good approximation $V_{us}V_{ud}^*$. The reason is that rescattering effects, which are what results in the long-distance contributions, are dominated by tree level decays followed by QCD rescattering. The most important one is $K \to \gamma\gamma$, which is dominated by the $\pi^0$ poles [190, 187]. We thus have

$$\lambda_0^{LD} = \frac{q}{p}\frac{\overline{A}_0^{LD}}{A_0^{LD}} = -\left(\frac{V_{cd}V_{cs}^*}{V_{cd}^*V_{cs}}\right)\left(\frac{V_{ud}V_{us}^*}{V_{ud}^*V_{us}}\right) \quad \Rightarrow \quad \mathcal{I}m(\lambda_0^{LD}) = 0. \tag{5.42}$$

where in the last step we use $\theta_{uc} = 0$. The fact that $\mathcal{I}m(\lambda_0^{LD}) = 0$ implies that the long-distance amplitude is CP conserving.

We next discuss working assumption (ii) above, that is, that CP violation enters only for $\ell = 0$. Within the SM the short-distance effects are due to the following Hamiltonian

$$\mathcal{H}_{\rm eff} = -\frac{G_F}{\sqrt{2}} \frac{\alpha}{2\pi \sin^2\theta_W} \left[V_{cs}^* V_{cd} Y_{NL} + V_{ts}^* V_{td} Y(x_t)\right] \left[(\bar{s}d)_{V-A} (\bar{\mu}\mu)_{V-A}\right] + h.c., \tag{5.43}$$

with $x_t = m_t^2/m_W^2$, and the loop function $Y(x_t) \approx 0.950 \pm 0.049$ and $Y_{NL} = O(10^{-4})$ [200, 188]. Thus the leading SM short-distance physics operator is

$$(\bar{s}d)_{V-A} (\bar{\mu}\mu)_{V-A} + h.c.\,. \tag{5.44}$$

This operator contributes only to the $\ell = 0$ final state [187]. For completeness, we provide a short derivation of this known result in Appendix D.3.

A few comments are in order:

1. Scalar operators could also lead to CP violation in the $\ell = 1$ amplitude through short-distance effects. However, in the SM, the contribution of these operators to the rate are suppressed with respect to the operator in Eq. (6.59) by a factor of $(m_K/m_W)^2 \sim 10^{-5}$ [201], and can be safely neglected for the extraction of SM parameters.
2. Only the axial-times-axial part of the hadronic times leptonic currents of Eq. (5.44) is relevant for $K \to \mu^+\mu^-$ (see Appendix D.3).

We conclude that the approximations and assumptions we work under are valid in the SM up to very small deviations, of order $\lambda^4 \sim \epsilon_K \sim 10^{-3}$. Thus, within the SM, the only source of a CP violating phase is the weak effective Hamiltonian given in Eq. (6.59). Moreover, any extension of the SM in which the leptonic operator remains vectorial rather than a scalar would satisfy our set of assumptions. For example also models with right-handed currents fall under this category. Thus, within the SM and any such extension it is straightforward to extract a prediction for $\mathcal{B}(K_S \to \mu^+\mu^-)_{\ell=0}$ purely from short-distance physics.

We are now ready to discuss the SM prediction for $\mathcal{B}(K_S \to \mu^+\mu^-)_{\ell=0}$. We recover the result, given in Ref. [187], using phase convention independent expressions (see Appendix D.2). We first redefine $A_0^{SD}$ by subtracting the charm contribution, which is relatively real under the approximation $\theta_{uc} = 0$. Then we can write

$$\lambda_0^{SD} = \frac{q}{p}\frac{\overline{A}_0^{SD}}{A_0^{SD}} = -\left(\frac{V_{cd}V_{cs}^*}{V_{cd}^*V_{cs}}\right)\left(\frac{V_{td}^*V_{ts}}{V_{td}V_{ts}^*}\right) = -e^{-2i\theta_{ct}} \quad \Rightarrow \quad \sin^2\phi_0^{SD} = \sin^2\theta_{ct}. \tag{5.45}$$

The calculation of $|A_0^{SD}|^2$ and the phase space integral is reviewed in Appendix D.2. The result is given in Eq. (D.18):

$$\begin{aligned}\mathcal{B}(K_S \to \mu^+\mu^-)_{\ell=0} &= \frac{\beta_\mu \tau_S}{16\pi m_K}\left|\frac{G_F}{\sqrt{2}}\frac{2\alpha_{em}}{\pi\sin^2\theta_W} m_K m_\mu \times Y(x_t) \times f_K \times V_{ts}V_{td}\sin\theta_{ct}\right|^2 \\ &\approx 1.64\cdot 10^{-13} \times \left|\frac{V_{ts}V_{td}\sin\theta_{ct}}{(A^2\lambda^5\bar{\eta})_{\text{best fit}}}\right|^2 ,\end{aligned} \tag{5.46}$$

where we use

$$(A^2\lambda^5\bar{\eta})_{\text{best fit}} = 1.33\cdot 10^{-4}. \tag{5.47}$$

Eq. (5.46) is very precise. There are a few sources of uncertainties that enter here. They are all under control:

1. The only hadronic parameter is the kaon decay constant, which is well known from charged kaon decays. Isospin breaking effects can also be incorporated in lattice QCD if needed [202], reducing the ultimate hadronic uncertainties below the 1% level.
2. We have neglected subleading terms, that is, we neglected the term proportional to $Y_{NL} \sim 10^{-4}$ from Eq. (6.59), as well as CPV effects of order $\epsilon_K$.
3. Parametric errors, including the dependence of the loop function $Y(x_t)$ on $m_t/m_W$, are small, as the errors on the top and $W$ masses are below the 1% level.
4. Only leading order results in the loop expansion are used. Higher order terms are expected to be suppressed by a loop factor, which is of order 1%. If needed, higher orders in the loop function can be incorporated in order to reduce this uncertainty.
5. We only consider the leading SM operator, which is vectorial. At higher order scalar operators are also present, but these effects are suppressed by $O(m_K^2/m_W^2)$ [201].

We conclude that a measurement of $\mathcal{B}(K_S \to \mu^+\mu^-)_{\ell=0}$ would be a very clean independent measurement of the following combination of CKM elements

$$|V_{ts}V_{td}\ \sin\theta_{ct}| = |V_{ts}V_{td}\ \sin(\beta+\beta_s)| \approx A^2\lambda^5\bar{\eta}\,, \tag{5.48}$$

which coincides with Eq. (5.1).

A similar analysis can be done in any model that satisfies the assumptions we have made. In particular, these results hold in any model that generates the same operator as in the SM. In such a model the prediction would be amended by replacing the SM values for the CKM parameters and the loop function with the respective values in the model under consideration.

We end this section with two remarks

1. There are models where we can have a significant contribution to the CP-odd amplitude from scalar operators [165], in which case our assumption (*ii*) is not satisfied.
2. In addition to our quantity of interest, $\mathcal{B}(K_S \to \mu^+\mu^-)_{\ell=0}$, under the same set of assumptions it is also possible to calculate the short-distance contribution to $A_0^{\text{CP-even}}$, that is, $A(K_L \to \mu^+\mu^-)^{SD}_{\ell=0}$. Then, assuming given values for the CKM parameters, the measurement of the interference terms is also a measurement of the long-distance amplitude $A(K_L \to \mu^+\mu^-)^{LD}_{\ell=0}$, and in particular of its unknown sign [142].

## 5.6 Experimental considerations

We now turn to discuss the feasibility of the extraction of $\mathcal{B}(K_S \to \mu^+\mu^-)_{\ell=0}$. As is apparent from Eq. (5.31) we need to experimentally extract $C_{Int.}$ and $C_L$. Of

these, $C_L$ has already been measured, and we can expect that in the future it will be measured with even higher precision. The question is how well can $C_{Int.}$ be extracted.

Below we estimate the number of kaons that is needed to perform the measurement assuming the SM. For that we need the values in the SM of the relevant amplitudes. While the method we discuss does not require any estimation of the amplitudes, we use these estimates to illustrate the expected magnitude of the interference terms, and to estimate the needed statistics to perform the measurements. Of the three amplitudes, $|A_0^{\text{CP-odd}}|$ can be calculated perturbatively, $|A_0^{\text{CP-even}}|$ can be extracted directly from the measured value of $\mathcal{B}(K_L \to \mu^+\mu^-)$, and $|A_1^{\text{CP-even}}|$ can only be estimated a priori by relying on non-perturbative calculations from the literature, that suffer from large hadronic uncertainties. We provide the details of these estimations in Appendix D.2. They result in the following values for the experimental parameters:

$$\begin{aligned} (C_L^{K^0})_{\text{SM}} &= |A_0^{\text{CP-even}}|^2 \equiv 1, \\ (C_S^{K^0})_{\text{SM}} &= |A_0^{\text{CP-odd}}|^2 + \beta_\mu^2 |A_1^{\text{CP-even}}|^2 \approx 0.43, \\ (C_{Int.}^{K^0})_{\text{SM}} &= |A_0^{\text{CP-even}}||A_0^{\text{CP-odd}}| \approx 0.12, \end{aligned} \tag{5.49}$$

where we have used a normalization such that the coefficient $(C_L^{K^0})_{\text{SM}}$ is set to be unity. Using these estimates, we plot the time dependence of the rate in Fig. 5.6, for two values of the unknown phase, $\varphi_0 = \arg(A_0^{\text{CP-odd}^*} A_0^{\text{CP-even}})$. For illustration, we also plot the time dependence excluding the interference terms (see caption). We use the range $t \lesssim 6\tau_S$ as for larger times the beam is almost a pure $K_L$ beam. The

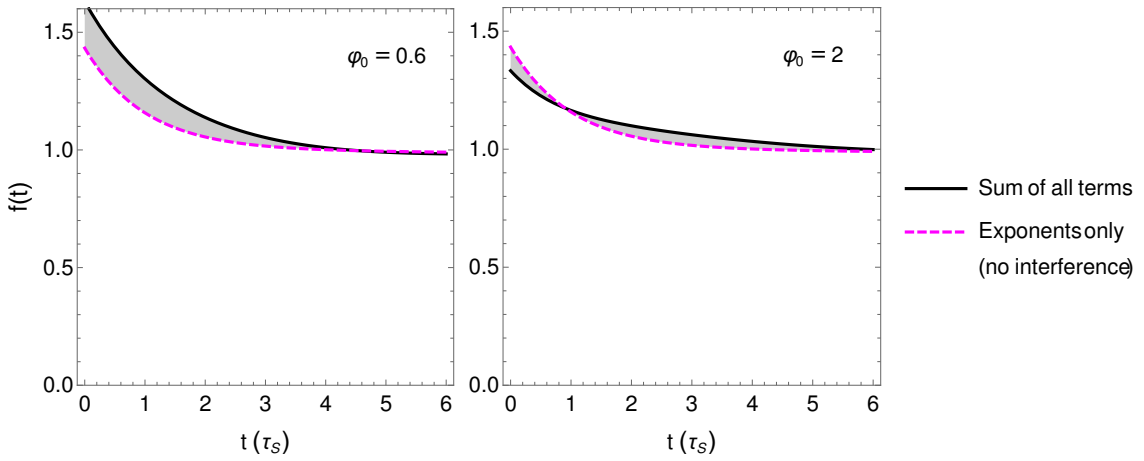


The expected approximate time dependence within the SM, using the coefficients of Eq. (5.49), for two values of $\varphi_0 = \arg(A_0^{\text{CP-odd}*} A_0^{\text{CP-even}})$. The difference between the dashed magenta curve and the solid black one is a measure of interference effects.

relative magnitude of the interference terms is apparent in the difference between the two plotted curves. We find the relative integrated effect to be of order 3% to 6%, depending on the value of $\varphi_0$.

Based on the above, we can roughly estimate the number of required kaons. We have $\mathcal{B}(K_L \to \mu^+\mu^-) = (6.84 \pm 0.11) \cdot 10^{-9}$ [195], and only about 1% of the $K_L$ particles decay inside our region of interest, $t \lesssim 6\tau_S$. Since the coefficients in Eq. (5.49) are not very small, we can use this to estimate that the number of useful events is roughly a fraction of $10^{-10}$ out of the kaons. Thus, for example, in order to get $O(1000)$ events in the interesting region we need $O(10^{13})$ $K^0$ particles to start with. We do not expect this preliminary estimate to be strongly affected

by backgrounds or reconstruction efficiencies.

Experimentally, it is not easy to produce a pure neutral kaon beam. Experiments currently running enjoy a very high luminosity of kaons of order $10^{14}$ kaons a year (see Ref. [203] for NA62, Ref. [137] for KOTO, and Ref. [204] for LHCb). However, these kaons are either charged (NA62), or to a good approximation a pure $K_L$ (KOTO), or come with an almost equal mix of $K^0$ and $\overline{K}^0$ (LHCb).

Thus, for the purpose of the analysis we are considering, we need to turn to a mixed beam or a regenerated beam. As discussed in Appendix D.1, in the case of a mixed beam with non-zero production asymmetry, the sensitivity to the interference terms is diluted by a factor of $D$. The use of matter effects, for example in the case of a $K_L$ beam going through a regenerator, introduces suppression that is proportional to the regeneration parameter, $r$. Thus, the number of kaons that are needed in these cases compared to the pure kaon beam, are larger by roughly $1/D$ or $1/r$ as we need to overcome these suppression effects.

Several approaches that could be useful in acquiring the needed sensitivity to the interference terms appear in the literature:

1. There are cases with QCD production where both $K^0$ and $\overline{K}^0$ are produced, but there is an asymmetry, that is $D \neq 0$. One example is the "high intensity $K_S$-run" at the NA48 experiment, which reported $10^{10}$ $K_S$ decays with $D \sim 0.3$ [205].
2. Regeneration in $K_L$ beams [206, 207, 208, 209]. Numerically, typical values

for $r$ range from $O(10^{-2})$ to a few times $10^{-1}$, depending on the material and on the relevant kaon momentum.

3. The use of a charge exchange target in order to generate pure $K^0$ beams from $K^+$ beams [210, 211].

4. Post-selection using tagging in high energy production, for example, by looking at the charge of the pion in $K^*$ decays, or by tagging $\Lambda^0$ and $K^-$ in $pp \to K^0 K^- X$ and $pp \to K^0 \Lambda^0 X$ decays [142].

We do not discuss these options in any detail. The high yields of currently running experiments is encouraging in terms of the ability of future endeavors to reach the desired sensitivity, should some of these methods be implemented. Clearly, a detailed study of the experimental requirements is needed in order to arrive at a reliable estimate for the expected sensitivity.

We close this section with a remark about the time dependence. A measurement of the full time dependence would result in the best sensitivity. However, in principle, a measurement of the integral over four different time intervals suffices to get the needed information. In practice, $C_L$ is already known, $C_S$ can be extracted from a beam with $D = 0$, and then we would need two time intervals using a beam with $D \neq 0$ or $r \neq 0$.

## 5.7 Conclusion and Outlook

We have demonstrated how, under well-motivated approximations and assumptions, it is possible to cleanly test the SM using a measurement of the time-dependent decay rate of $K \to \mu^+\mu^-$. A necessary ingredient is sensitivity to the interference between the $K_L$ and $K_S$ amplitudes, as can be seen from Eq. (5.31), which is our main result. The relevant SM parameter of interest is

$$|V_{ts}V_{td}\ \sin(\beta + \beta_s)|\,, \tag{5.50}$$

which is exactly the CKM parameter combination that appears in $K_L \to \pi^0\nu\bar{\nu}$ . Thus, our proposal is to use $K \to \mu^+\mu^-$ as an additional independent measurement of the same SM quantity.

As we discuss in detail, the point to emphasize is that the extraction is theoretically very clean. There are several assumptions that were made in setting up the method, as well as in the calculation within the SM. All of these are valid within the SM to a few per-mill, giving a total uncertainty below the 1% level. This is comparable to the best probing methods for the angle $\beta$ and related quantities, that is, the CP asymmetries in $B \to \psi K_S$ and the decay rate of $K_L \to \pi^0\nu\bar{\nu}$. The assumptions we rely on are additionally respected by any extension of the SM in which the relevant leptonic current is vectorial.

The approach we discuss can in principle be extended to other decay modes. Most promising are the decays $K \to \pi e^+e^-$ and $K \to \pi\mu^+\mu^-$. The generalization is not trivial as these decays involve more partial waves beyond $\ell = 0, 1$. We plan to

discuss these modes in a future publication.

Our very preliminary estimates indicate that these measurements can be carried out in next generation kaon experiments. This is encouraging, and more detailed feasibility studies are called for.

CHAPTER 6

# A PRECISION RELATION BETWEEN $\Gamma(K \to \mu^+\mu^-)(t)$ AND $\mathcal{B}(K_L \to \mu^+\mu^-)/\mathcal{B}(K_L \to \gamma\gamma)$

## 6.1 Introduction

A recent proposal has shown that short-distance parameters of the decay $K \to \mu^+\mu^-$ can be cleanly extracted from a measurement of the $K_L$–$K_S$ time-dependent rate [142, 2, 212]. The time-dependent rate for a beam of initial $K^0$ particles can be written as

$$\frac{1}{\mathcal{N}}\frac{d\Gamma(K^0 \to \mu^+\mu^-)}{dt} = f(t) \equiv C_L\, e^{-\Gamma_L t} + C_S\, e^{-\Gamma_S t} + 2\, C_{\text{Int.}} \cos(\Delta M_K t - \varphi_0) e^{-\frac{\Gamma_L+\Gamma_S}{2}t}\,, \quad (6.1)$$

where $\mathcal{N}$ is a normalization factor, $\Gamma_L$ ($\Gamma_S$) is the $K_L$ ($K_S$) decay width, and $\Delta M_K$ is the $K_L$–$K_S$ mass difference. Then, the four experimental parameters characterizing the time dependence,

$$\{C_L,\, C_S,\, C_{\text{Int}},\, \varphi_0\}\,, \quad (6.2)$$

are directly related to the four theory parameters describing the system [2],

$$\{|A(K_S)_{\ell=0}|,\ |A(K_L)_{\ell=0}|,\ |A(K_S)_{\ell=1}|,\ \arg\left[A(K_S)^*_{\ell=0}\, A(K_L)_{\ell=0}\right]\}\,, \quad (6.3)$$

where the subscripts $\ell = 0$ ($s$-wave symmetric wave function) and $\ell = 1$ ($p$-wave anti-symmetric wave function) correspond to the CP-odd and -even ($\mu^+\mu^-$) final states, respectively. The relations between the experimental and theory parame-

ters are given by

$$\begin{aligned} C_L &= |A(K_L)_{\ell=0}|^2\,, \\ C_S &= |A(K_S)_{\ell=0}|^2 + \beta_\mu^2 |A(K_S)_{\ell=1}|^2\,, \\ C_{\text{Int.}} &= |A(K_S)^*_{\ell=0}\, A(K_L)_{\ell=0}| = |A(K_S)_{\ell=0}||A(K_L)_{\ell=0}|\,, \\ \varphi_0 &= \arg\left[A(K_S)^*_{\ell=0}\, A(K_L)_{\ell=0}\right], \end{aligned} \tag{6.4}$$

with

$$\beta_\mu = \sqrt{1 - \frac{4m_\mu^2}{m_{K^0}^2}}\,. \tag{6.5}$$

The experimental parameter $\varphi_0$, which is the phase shift of the oscillating rate in Eq. (6.1), is a combination of the relative weak and strong phases between the $K_S$ and $K_L$ amplitudes to the CP-odd final state. In this work, we demonstrate that this phase shift is closely related to the proportionality coefficient in the ratio between the rates of $K_L \to \mu^+\mu^-$ and $K_L \to \gamma\gamma$.

The ratio between the rates of $K_L \to \mu^+\mu^-$ and $K_L \to \gamma\gamma$ is of historical significance. Using CPT invariance, unitarity, and the well-motivated assumption that the absorptive part of the $K_L \to \mu^+\mu^-$ amplitude is dominated by the two-photon intermediate state, the ratio between the rates of $K_L \to \mu^+\mu^-$ and $K_L \to \gamma\gamma$ is bounded by the lower limit [146, 159, 213, 214]

$$R_{K_L} \equiv \frac{\Gamma(K_L \to \mu^+\mu^-)}{\Gamma(K_L \to \gamma\gamma)} \geq 1.195 \times 10^{-5}\,. \tag{6.6}$$

However, back in the 1970's, this conflicted with the contemporary experimental upper bound of $0.4 \times 10^{-5}$ [215, 216], leading to the so-called "$K_L \to \mu^+\mu^-$ puzzle" [159, 217] that gained much attention. But today, this ratio is measured in the

experiment as [218]

$$R_{K_L}^{\text{exp}} = (1.250 \pm 0.022) \times 10^{-5} \,. \tag{6.7}$$

This means that the observed branching ratio $\mathcal{B}(K_L \to \mu^+\mu^-) = (6.84 \pm 0.11) \times 10^{-9}$ [218], along with $\mathcal{B}(K_L \to \gamma\gamma) = (5.47 \pm 0.04) \times 10^{-4}$ [218] known today obey the lower limit prescribed by CPT invariance and unitarity.

In this chapter, we show that the phase $\varphi_0$ is cleanly predicted in the Standard Model (SM), up to a four-fold discrete ambiguity, making its measurement a potent test of the SM. The discrete ambiguity can be partially resolved by using further theory input from the literature in the large-$N_C$ limit of chiral perturbation theory (ChPT). This result is additionally significant for sensitivity estimations of a future measurement of the short-distance parameters.

Leptonic kaon decays have been a field that received a lot of attention in the literature recently. Effects from CPV in kaon mixing on $K \to \mu^+\mu^-$ have been taken into account in Refs. [142, 212], and implications for physics beyond the SM have been studied in Refs. [165, 163, 3]. Another future high precision test of the SM employing the ratio $\mathcal{B}(K_S \to \mu^+\mu^-)_{\ell=0}/\mathcal{B}(K_L \to \pi^0\nu\bar{\nu})$ has been identified in Ref. [219]. Advances in calculating $K_L \to \mu^+\mu^-$ and $K_L \to \gamma\gamma$ on the lattice can be found in Refs. [220, 221, 222]. On the experimental side, the LHCb collaboration recently found an improved bound on $K_S \to \mu^+\mu^-$ [223] and $K_{S,L} \to 2(\mu^+\mu^-)$ [224].

In Sec. 7.3 we introduce our notation and summarize key results from the literature. In Sec. 6.3 we determine $\cos^2\varphi_0$, which predicts $\varphi_0$ up to a four-fold am-

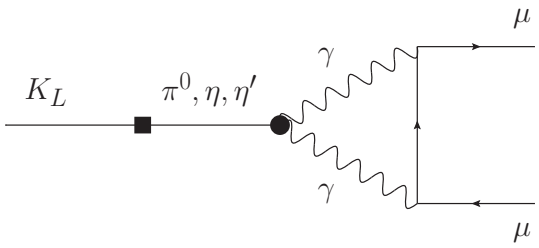


Leading order Feynman diagram of the long-distance two-photon contribution to $K_L \to \mu^+\mu^-$.

biguity, in a model-independent way, only assuming that the long-distance contributions are SM-like. In Sec. 6.4 we reduce this ambiguity to a two-fold one by using the large-$N_C$ limit and assuming that the short-distance physics is known. We demonstrate that the remaining ambiguity cannot be resolved using current knowledge in Sec. 6.5. We conclude in Sec. 7.6.

## 6.2 Setup and notation

We work within a framework defined by the following approximations, as detailed in Ref. [2]:

(i) We neglect CPV in mixing, which is a sub-dominant effect for our purposes. Note that when considering higher order corrections, this effect can be taken into account consistently [212].

(ii) We neglect CPV in the long-distance contribution.

(iii) We assume that the leptonic current is (axial-)vectorial, *i.e.*, given by $\bar{\mu}\gamma^{\mu}(a + b\gamma^{5})\mu$.

In the SM, all three approximations are fulfilled within the precision relevant for our findings. In addition, in the following we assume that

(iv) The long-distance contribution to the $K_L \to \mu^+\mu^-$ amplitude is SM-like. That is, the only non-negligible intermediate state is the di-photon state.

Regarding the short-distance contribution, we explicitly state whenever our results are relevant regardless of any assumption on the nature of the short-distance physics, and when SM input is used.

Adopting this setup, it has been shown that the decay of $K_S$ to the CP-odd final state, $(\mu^+\mu^-)_{\ell=0}$ involves only short-distance physics. Additionally, the $K_L \to \mu^+\mu^-$ decay proceeds only to the CP-odd final state, $(\mu^+\mu^-)_{\ell=0}$. However, the latter involves two contributions of different underlying physics:

1. A short-distance (SD) contribution, arising to leading order from box and electroweak penguin diagrams, for which the ingredients for a precise SM prediction are straight-forward to derive.
2. A long-distance (LD) contribution, strongly dominated by the on-shell two photon intermediate state, see Fig. 6.2.

The on-shell two photon contribution is known to be significantly larger in magnitude than both the SD contribution and the off-shell part of the LD contribution.

The $K^0 \to (\mu^+\mu^-)_{\ell=0}$ and $\overline{K}^0 \to (\mu^+\mu^-)_{\ell=0}$ amplitudes can be written as a sum of two general contributions, with corresponding weak and strong phases,

$$\begin{aligned} A_{\ell=0} &= |A_{SD}|e^{i\theta_{SD}}e^{i\delta_{SD}} + |A_{LD}|e^{i\theta_{LD}}e^{i\delta_{LD}}\,, \\ \overline{A}_{\ell=0} &= -\left(|A_{SD}|e^{-i\theta_{SD}}e^{i\delta_{SD}} + |A_{LD}|e^{-i\theta_{LD}}e^{i\delta_{LD}}\right), \end{aligned} \tag{6.8}$$

where the overall minus sign for $\overline{A}_{\ell=0}$ is due to the CP nature of the final state. Using the convention

$$|K_S\rangle = p|K^0\rangle + q|\overline{K}^0\rangle\,, \qquad |K_L\rangle = p|K^0\rangle - q|\overline{K}^0\rangle\,, \tag{6.9}$$

the mass eigenstate amplitudes are related to $A_{\ell=0}$ and $\overline{A}_{\ell=0}$ by [2]

$$\begin{aligned} A(K_S)_{\ell=0} &= \frac{1}{\sqrt{2}}\left[A_{SD}(1+\lambda_{SD}) + A_{LD}(1+\lambda_{LD})\right], \\ A(K_L)_{\ell=0} &= \frac{1}{\sqrt{2}}\left[A_{SD}(1-\lambda_{SD}) + A_{LD}(1-\lambda_{LD})\right], \end{aligned} \tag{6.10}$$

where

$$A_{SD} \equiv |A_{SD}|e^{i\theta_{SD}}e^{i\delta_{SD}}\,, \qquad A_{LD} \equiv |A_{LD}|e^{i\theta_{LD}}e^{i\delta_{LD}}\,, \tag{6.11}$$

$$\overline{A}_{SD} \equiv -|A_{SD}|e^{-i\theta_{SD}}e^{i\delta_{SD}}\,, \qquad \overline{A}_{LD} \equiv -|A_{LD}|e^{-i\theta_{LD}}e^{i\delta_{LD}}\,, \tag{6.12}$$

and

$$\lambda_{SD} \equiv \frac{q}{p}\frac{\overline{A}_{SD}}{A_{SD}}\,, \qquad \lambda_{LD} \equiv \frac{q}{p}\frac{\overline{A}_{LD}}{A_{LD}}\,. \tag{6.13}$$

As we focus here mainly on amplitudes with $\ell = 0$ final states, compared to the notation of Ref. [2] we use for brevity the notation

$$\lambda_{SD} \equiv \lambda_0^{SD}\,, \qquad \lambda_{LD} \equiv \lambda_0^{LD}\,, \tag{6.14}$$

$$A(K_S) \equiv A(K_S)_{\ell=0}\,, \qquad A(K_L) \equiv A(K_L)_{\ell=0}\,. \tag{6.15}$$

The amplitudes are normalized such that

$$\mathcal{B}(K_{S,L} \to \mu^+\mu^-)_{\ell=0} = \frac{\tau_K \beta_\mu}{16\pi m_K} |A(K_{S,L})|^2\,. \tag{6.16}$$

We also use

$$\mathcal{B}(K_L \to \gamma\gamma) = \frac{\tau_K}{32\pi m_K} |A(K_L \to \gamma\gamma)|^2\,. \tag{6.17}$$

Up to this point, the labels LD and SD are just naming. However, in the following we will treat them as corresponding to what we think of as long-distance and short-distance amplitudes. It is important to note that the separation into LD and SD contributions is not well-defined. We think of short-distance physics as having no sources for a strong phase, while long-distance physics can go on-shell. However, any on-shell intermediate state can also be considered to contribute off-shell. Therefore there is no way to unambiguously define the separation. In the following we keep the strong phases general, while we insert knowledge of the SM weak phase of the long-distance contribution.

We then have [2]

$$\lambda_{LD} = -\left(\frac{V_{cd}V_{cs}^*}{V_{cd}^*V_{cs}}\right)\left(\frac{V_{ud}^*V_{us}}{V_{ud}V_{us}^*}\right) = -e^{-2i\theta_{uc}}\,. \tag{6.18}$$

Equation (6.18) corrects a typo in Eq. (42) of Ref. [2]. Here,

$$\theta_{uc} \equiv \arg\left(-\frac{V_{cd}V_{cs}^*}{V_{ud}V_{us}^*}\right) = \mathcal{O}(\lambda^4)\,, \tag{6.19}$$

such that, to $\mathcal{O}(\lambda^4)$,

$$\arg\lambda_{LD} = -2\theta_{LD} + \pi = \pi\,, \tag{6.20}$$

that is

$$\theta_{LD} = 0\,, \qquad \lambda_{LD} = -1\,. \tag{6.21}$$

No assumptions are made for the short-distance phase,

$$\arg\lambda_{SD} = -2\theta_{SD} + \pi\,. \tag{6.22}$$

We have therefore

$$A(K_S) = \frac{1}{\sqrt{2}}A_{SD}(1+\lambda_{SD}) = i\sqrt{2}|A_{SD}|\sin\theta_{SD}e^{i\delta_{SD}}\,, \tag{6.23}$$

$$A(K_L) = \frac{1}{\sqrt{2}}\left[A_{SD}(1-\lambda_{SD}) + 2A_{LD}\right] = \sqrt{2}\Big(|A_{LD}|e^{i\delta_{LD}} + |A_{SD}|\cos\theta_{SD}e^{i\delta_{SD}}\Big)\,. \tag{6.24}$$

Note that $A(K_S)$ is pure short-distance and is manifestly CP-odd. The oscillation term in the rate is then controlled by the interference term:

$$A(K_S)^*A(K_L) \;=\; -2i|A_{SD}|\sin\theta_{SD}\left(|A_{LD}|e^{i\Delta\delta} + |A_{SD}|\cos\theta_{SD}\right)\,, \tag{6.25}$$

where $\Delta\delta \equiv \delta_{LD} - \delta_{SD}$.

## 6.3 Determination of $\cos^2\varphi_0$: model-independent

From Eqs. (6.4) and (6.25), we have

$$\cos^2\varphi_0 \;=\; \frac{\mathrm{Re}[A(K_S)^* A(K_L)]^2}{|A(K_S)A(K_L)|^2} = \frac{(\sqrt{2}|A_{LD}|\sin\Delta\delta)^2}{|A(K_L)|^2} \;= \frac{[A(K_L)_{\mathrm{absorptive}}]^2}{|A(K_L)|^2}\,, \tag{6.26}$$

where

$$A(K_L)_{\mathrm{absorptive}} \equiv \mathrm{Im}[A(K_L)]\,, \tag{6.27}$$

and we define the imaginary part relative to the strong phase of the SD amplitude (or in the basis in which the SD amplitude carries no strong phase, hence $\delta_{LD} = \Delta\delta$). This convention corresponds to choosing $C_{\mathrm{had.}}$, introduced in Sec. 6.4 below, to be real without loss of generality.

The numerator is simply the on-shell long-distance contribution to the $K_L$ amplitude. Under the assumption that the only non-negligible intermediate state is the di-photon state [143], this absorptive part is equal to the discontinuity of the three-point diagram (see Fig. 6.2), which can be computed in a straightforward way using Cutkosky rules,

$$\left|\sqrt{2}|A_{LD}|\sin\Delta\delta\right| = \left|A(K_L)_{\mathrm{absorptive}}\right| = \left|\frac{1}{2i}\mathrm{Disc}(K_L\to\gamma\gamma\to\mu^+\mu^-)\right|\,. \tag{6.28}$$

Furthermore, the discontinuity is directly related to the measured rate of $K_L\to\gamma\gamma$, meaning that its magnitude can be extracted completely model independently (using only QED for the $\gamma\gamma\to\mu^+\mu^-$ half of the diagram). We can write

$$\cos^2\varphi_0 = \frac{[A(K_L)_{\mathrm{absorptive}}]^2}{|A(K_L)|^2} = C^2_{\mathrm{QED}}\frac{\Gamma(K_L\to\gamma\gamma)}{\Gamma(K_L\to\mu^+\mu^-)}\,, \tag{6.29}$$

*i.e.*,

$$\cos^2\varphi_0\,\mathcal{B}(K_L\to\mu^+\mu^-)\;=\;C^2_{\rm QED}\,\mathcal{B}(K_L\to\gamma\gamma)\,, \tag{6.30}$$

where $C_{\rm QED}$ describes the $\gamma\gamma\to\mu^+\mu^-$ transition and is given as [143]

$$C_{\rm QED}=\frac{\alpha_{em}m_\mu}{\sqrt{2\beta_\mu}m_K}\,\log\left(\frac{1-\beta_\mu}{1+\beta_\mu}\right)+O(\alpha^2_{em})\,. \tag{6.31}$$

Equation (6.30) demonstrates that $\cos^2\varphi_0$ is simply the proportionality factor parameterizing to what extent is the $K_L\to\mu^+\mu^-$ rate saturated by the absorptive contribution from the intermediate $\gamma\gamma$ state. Using the measured ratio of rates $R_{K_L}$, see Eq. (6.6), we have a clean SM prediction for the phase $\varphi_0$, up to a four-fold discrete ambiguity,

$$\cos^2\varphi_0\quad=\quad\frac{C^2_{\rm QED}}{R^{\rm exp}_{K_L}}\,. \tag{6.32}$$

This SM prediction is dependent only on

1. The measurement of $R_{K_L}$, currently with an uncertainty of $O(2\%)$;
2. A QED calculation, here taken up to relative corrections of $O(\alpha_{em})$;
3. The assumption that other intermediate on-shell contributions ($3\pi$, $\pi\pi\gamma$) are negligible [143].

Inserting

$$C^2_{\rm QED}=1.195\times10^{-5}[1+O(\alpha_{em})], \tag{6.33}$$

and

$$R_{K_L}^{\text{exp}} = (1.250 \pm 0.022) \times 10^{-5}\,, \tag{6.34}$$

which we obtain, not taking into account any correlations, from [218]

$$\mathcal{B}(K_L \to \mu^+\mu^-) = (6.84 \pm 0.11) \times 10^{-9}\,, \tag{6.35}$$

$$\mathcal{B}(K_L \to \gamma\gamma) = (5.47 \pm 0.04) \times 10^{-4}\,, \tag{6.36}$$

using Gaussian error propagation, we arrive at $\cos^2\varphi_0 = 0.96 \pm 0.02$ , where the quoted error reflects only the experimental error on $R_{K_L}^{\text{exp}}$.

There are two sources of theoretical errors. One of the them is the higher order QED calculation, resulting in an error of order $\alpha_{em} \sim 1\%$. This error is reducible, that is, if needed the calculation of the higher-order corrections can be done. The other source of uncertainty are the intermediate states that we neglected, such as $3\pi$ and $\pi\pi\gamma$ [143]. These contributions are estimated to be at most 1% of the two-photon state that we considered. Each of the two effects results in about 1% error, and thus we conservatively add them linearly resulting in a total theory error of 0.02 to arrive at our final estimate,

$$\cos^2\varphi_0 = 0.96 \pm 0.02_{\text{exp}} \pm 0.02_{\text{th}}\,. \tag{6.37}$$

Combining the experimental and theoretical errors in quadrature we then have

$$\cos^2\varphi_0 = 0.96 \pm 0.03. \tag{6.38}$$

Note that the error quoted in Eq. (6.38) is therefore to be interpreted as an estimate of the total uncertainty, rather than as a statistical error only.

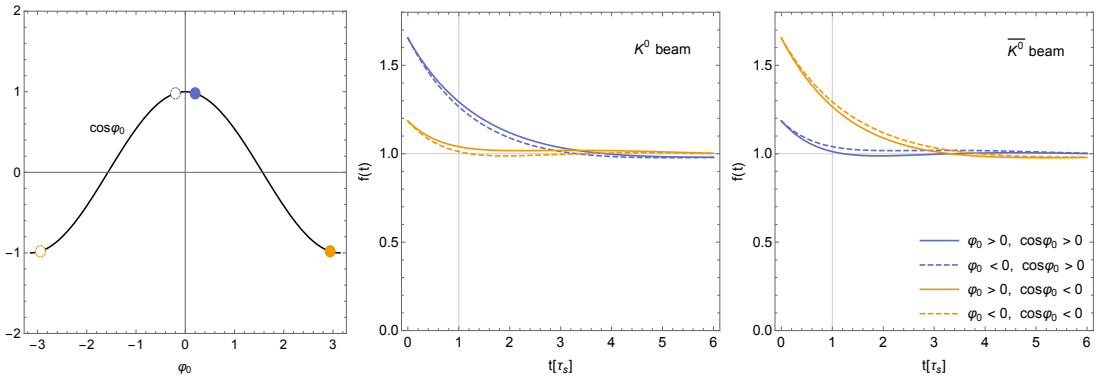


(a) (b) (c)

(a) Illustration of the four-fold ambiguity arising from $\cos^2\varphi_0 = 0.96$. (b) The time dependence of the $K^0(t) \to \mu^+\mu^-$ rate, $f(t)$, as defined in Eq. (6.1), for the four values of $\varphi_0$. We have used a normalization in which $C_L$ of Eq. (6.1) is set to unity. (c) The same for an initial pure $\overline{K}^0$ beam.

Given the value of $\cos^2\varphi_0$ there are four possible values for the phase shift, $\varphi_0$. Two of them correspond to overall constructive interference in the time-dependent rate and two correspond to destructive interference, depending on the sign of $\cos\varphi_0$. We plot the time-dependent rate for the four possibilities in Fig. 6.3 for both a $K^0$ or a $\overline{K}^0$ beam. Note that, for a $K^0$ beam, a positive (negative) $\cos\varphi_0$ results in constructive (destructive) interference. As pointed out in Ref. [142], the situation is reversed for a $\overline{K}^0$ beam where a negative (positive) $\cos\varphi_0$ results in constructive (destructive) interference.

## 6.4 Determination of $\cos\varphi_0$: model dependent

The four-fold ambiguity cannot be resolved in a model-independent way. Thus, in this section we use input from theory in order to try to reduce it. We first consider the sign of $\cos\varphi_0$. We discuss below how chiral perturbation theory (ChPT) and lattice QCD and can help in this regard.

### 6.4.1 Chiral perturbation theory

Within chiral perturbation theory and using the large-$N_C$ limit, it has been shown that the sign of the absorptive amplitude relative to the short-distance contribution, which determines the sign of $\cos\varphi_0$, can be determined [190, 187].

In the following, we relate our notation for the long-distance contribution to that appearing in the literature in order to apply existing results, primarily of Refs. [187, 190, 191, 198]. We rewrite the long-distance amplitude for $K_L \to \mu^+\mu^-$ as

$$\begin{aligned}\sqrt{2}|A_{LD}|e^{i\Delta\delta} &= [A_{LD}]_{\text{dispersive}} + i[A_{LD}]_{\text{absorptive}} \\ &\equiv C_{\text{had.}}\Big[(A_{LD}^{\text{local}} + \text{Re}A_{LD}^{\gamma\gamma}) + i\,\text{Im}A_{LD}^{\gamma\gamma}\Big], \end{aligned} \tag{6.39}$$

where $C_{\text{had.}}$ encodes the hadronic behavior of the effective $K_L\gamma\gamma$ vertex. Without loss of generality, we take $C_{\text{had.}}$ to be real, consistent with Eq. (6.27). The dispersive

part is split in two parts to be consistent with the literature,

$$[A_{LD}]_{\text{dispersive}} = C_{\text{had.}} \left( A_{LD}^{\text{local}} + \text{Re}A_{LD}^{\gamma\gamma} \right) , \tag{6.40}$$

$$[A_{LD}]_{\text{absorptive}} = C_{\text{had.}} \, \text{Im}A_{LD}^{\gamma\gamma} , \tag{6.41}$$

where $A_{LD}^{\text{local}}$ denotes the local counterterm, which is real [187]. Using the fact that the decay $K_L \to \gamma\gamma$ has the same hadronic behavior, we define

$$A(K_L \to \gamma\gamma) \equiv C_{\text{had.}} \, A_{\gamma\gamma} . \tag{6.42}$$

Note that $A_{\gamma\gamma} \neq A_{LD}^{\gamma\gamma}$. The former is part of the $K_L \to \gamma\gamma$ amplitude, while the latter is the two-photon contribution to $K_L \to \mu^+\mu^-$. Then we have

$$\begin{aligned} \frac{\Gamma(K_L \to \mu^+\mu^-)}{\Gamma(K_L \to \gamma\gamma)} &= 2\beta_\mu \left| \frac{\sqrt{2}|A_{LD}|e^{i\Delta\delta} + \sqrt{2}|A_{SD}| \cos\theta_{SD}}{A(K_L \to \gamma\gamma)} \right|^2 \\ &= 2\beta_\mu \frac{\left( A_{LD}^{\text{local}} + \text{Re}A_{LD}^{\gamma\gamma} + \sqrt{2}|A_{SD}| \cos\theta_{SD}/C_{\text{had.}} \right)^2 + (\text{Im}A_{LD}^{\gamma\gamma})^2}{|A_{\gamma\gamma}|^2} . \end{aligned} \tag{6.43}$$

Note that $C_{\text{had.}}$ now appears as a factor accompanying the short-distance contribution. We can now easily relate to the notations of Ref. [187], with (the superscript "IU" denotes the initials of the authors of Ref. [187])

$$\frac{A_{LD}^{\text{local}}}{|A_{\gamma\gamma}|} = \frac{\alpha_{em} m_\mu}{\pi m_K} [\chi_{\gamma\gamma}(\mu)]^{\text{IU}} , \tag{6.44}$$

$$\frac{\text{Re}A_{LD}^{\gamma\gamma}}{|A_{\gamma\gamma}|} = \frac{\alpha_{em} m_\mu}{\pi m_K} \left[ \text{Re}C_{\gamma\gamma} - \frac{5}{2} + \frac{3}{2} \log\left( \frac{m_\mu^2}{\mu^2} \right) \right]^{\text{IU}} , \tag{6.45}$$

$$\frac{\sqrt{2}|A_{SD}| \cos\theta_{SD}}{C_{\text{had.}}|A_{\gamma\gamma}|} = \frac{\alpha_{em} m_\mu}{\pi m_K} [\chi_{\text{short}}]^{\text{IU}} , \tag{6.46}$$

$$\frac{\text{Im}A_{LD}^{\gamma\gamma}}{|A_{\gamma\gamma}|} = \frac{\alpha_{em} m_\mu}{\pi m_K} [\text{Im}C_{\gamma\gamma}]^{\text{IU}} = \frac{1}{\sqrt{2\beta_\mu}} C_{\text{QED}} . \tag{6.47}$$

The assumptions and findings of the literature, as conveyed in Refs. [187, 190], can now be summarized as the following:

1. Using results in the large-$N_C$ limit, Refs. [187, 190] find destructive interference between the short-distance and the local long-distance contributions,

$$\frac{\cos\theta_{SD}}{C_{\text{had.}}A_{LD}^{\text{local}}} < 0\,. \tag{6.48}$$

2. Ref. [187] uses phenomenological analyses of the form factor in $K_L \to \gamma e^+e^-$, $K_L \to \gamma\mu^+\mu^-$ and $K_L \to e^+e^-\mu^+\mu^-$ from data, together with theory considerations, to estimate the local counter term. Using up-to-date inputs, we update their estimation (see App. E) and find

$$[\chi_{\gamma\gamma}(m_\rho)]^{\text{IU}} = \frac{\pi m_K}{\alpha_{em}m_\mu}\frac{A_{LD}^{\text{local}}}{|A_{\gamma\gamma}|} = (6.10 \pm 1.01) > 0\,, \tag{6.49}$$

where we have set $\mu^2 = m_\rho^2$ here and in the following whenever we make use of specific numerical estimates. Hence, using Eq. (6.48),

$$\text{sgn}[C_{\text{had.}}] = -\text{sgn}[\cos\theta_{SD}]\,. \tag{6.50}$$

3. This, in turn, determines the sign of the absorptive long-distance amplitude relative to the short-distance contribution,

$$\text{sgn}\left([A_{LD}]_{\text{absorptive}}\right) = \text{sgn}[\cos\theta_{SD}]\,, \tag{6.51}$$

where we used the fact that $\text{sgn}\left[\text{Im}A_{LD}^{\gamma\gamma}\right] = \text{sgn}\left[C_{\text{QED}}\right] = -1$.

We conclude that within a model for the short-distance contribution, and adopting the assumptions in the literature regarding the long-distance physics, *i.e.*, the large-$N_C$ limit, the sign of $\cos\varphi_0$ is determined,

$$\begin{aligned} \mathrm{sgn}\Big[\cos\varphi_0\Big] &= \mathrm{sgn}\left[\frac{\mathrm{Re}[A(K_S)^* A(K_L)]}{|A(K_S)A(K_L)|}\right] \\ &= \mathrm{sgn}\left[\frac{[A(K_L)]_{\text{absorptive}}\,\mathrm{sgn}[\sin\theta_{SD}]}{|A(K_L)|}\right] \\ &= \mathrm{sgn}\Big[\tan\theta_{SD}\Big]\,. \end{aligned} \tag{6.52}$$

### 6.4.2 Detailed assumptions within ChPT

The considerations leading to the assumption of destructive interference between the short-distance and the local long-distance contributions, as conveyed in Eq. (6.48), involve some details of the structure of the $K_L \to \gamma\gamma$ amplitude within the ChPT. According to Ref. [193], the on-shell tensor amplitude for $K_L \to \gamma\gamma$ starts from at $O(p^6)$ in the ChPT as

$$-iA(K_L \to \gamma\gamma) = \varepsilon^{\mu\nu\rho\sigma}\epsilon_{1\mu}(q_1)\epsilon_{2\nu}(q_2)q_{1\rho}q_{2\sigma}\,c^{(6)}(0,0)\,, \tag{6.53}$$

where

$$c^{(6)}(0,0) \;=\; -\frac{2}{\pi}\alpha_{em}F_0\,(G_8 - G_{27})\,\frac{1}{1-r_\pi^2}c^{(6)}_{\text{red}}\,, \tag{6.54}$$

and a dimensionless reduced amplitude $c_{\rm red}^{(6)}$ is

$$\begin{aligned} c_{\rm red}^{(6)} =& 1 + \frac{1-r_\pi^2}{3\left(1-r_\eta^2\right)}\left[(1+\xi)\,c_\theta + 2\sqrt{2}\,\hat{\rho}\,s_\theta\right]\left(\frac{F_\pi}{F_{\eta_8}}c_\theta - 2\sqrt{2}\frac{F_\pi}{F_{\eta_1}}s_\theta\right) \\ & - \frac{1-r_\pi^2}{3\left(1-r_{\eta'}^2\right)}\left[2\sqrt{2}\,\hat{\rho}\,c_\theta - (1+\xi)\,s_\theta\right]\left(\frac{F_\pi}{F_{\eta_8}}s_\theta + 2\sqrt{2}\frac{F_\pi}{F_{\eta_1}}c_\theta\right), \end{aligned} \tag{6.55}$$

with $\sqrt{2}F_0 = \sqrt{2}F_\pi = f_\pi = (130.2 \pm 0.8)$ MeV [225], $F_{\eta_8} = (1.27 \pm 0.02)\,F_\pi$, $F_{\eta_1} = (1.14 \pm 0.05)\,F_\pi$ [226, 227], and $r_P \equiv m_P/m_K$. Combining the above formulae gives

$$-iA(K_L \to \gamma\gamma) = -\frac{\sqrt{2}\alpha_{em} f_\pi\,(G_8 - G_{27})}{\pi\,(1-r_\pi^2)} c_{\rm red}^{(6)} \varepsilon^{\mu\nu\rho\sigma} \epsilon_{1\mu}(q_1)\epsilon_{2\nu}(q_2) q_{1\rho} q_{2\sigma}\,. \tag{6.56}$$

Here, the point is that $O(p^4)$ contributions vanish within the ChPT, which are proportional to $c_{\rm red}^{(4)}$ and

$$c_{\rm red}^{(4)} \;=\; 1 + \frac{1-r_\pi^2}{3\left(1-r_{\eta_8}^2\right)} \;=\; \frac{4-3r_{\eta_8}^2-r_\pi^2}{3\left(1-r_{\eta_8}^2\right)} \;=\; 0\,, \tag{6.57}$$

where the Gell-Mann–Okubo mass formula, $4m_K^2 = 3m_{\eta_8}^2 + m_\pi^2$, is used. Therefore, $c_{\rm red}^{(6)}$ amplitudes correspond to the violation of the Gell-Mann–Okubo formula implying that the sign of $c_{\rm red}^{(6)}$ is sensitive to the $\eta$–$\eta'$ mixing angle $\theta$ in the octet–singlet basis, the $SU(3)_F$ breaking $\xi$ [228, 229], the nonet symmetry breaking $\hat{\rho}$ [230, 231, 232], and their higher-order corrections. $(1+\xi)$ is proportional to the $K_L \to \eta_8$ form factor, while $\hat{\rho}$ is proportional to the $K_L \to \eta_1$ one. However, by considering the typical parameter regions; $\theta \approx -20^\circ$, $\xi \sim 0.0$–$0.2$, and $\hat{\rho} \approx 0.8$ [193], one can predict $\mathrm{sgn}[c_{\rm red}^{(6)}] > 0$, which leads to

$$\mathrm{sgn}\Big[A(K_L \to \gamma\gamma)\Big] = \mathrm{sgn}\Big[A(K_L \to \pi^0 \to \gamma\gamma)\Big]\,. \tag{6.58}$$

Combining this relation with $\mathrm{sgn}[G_8 - G_{27}]$ which can be extracted from the $\Delta S = 1$ effective Lagrangian in the large-$N_C$ limit [233, 187, 234], $\mathrm{sgn}[C_{\rm had.}] > 0$ can be predicted, see Eq. (6.50), where, in the SM we have $\cos\theta_{SD}^{\rm SM} < 0$.

### 6.4.3 Lattice QCD

In the last decade, lattice QCD made paramount progress in the treatment of $K \to \pi\pi$ [235, 236, 237, 238]. Moreover, recently, lattice QCD made advances in the calculation of $K_L \to \mu^+\mu^-$ and $K_L \to \gamma\gamma$ [220, 221, 222]. ChPT parameters like $G_8$ can now also be extracted from fits to lattice results, as shown in Ref. [239].

While it seems to us that the data is available to extract the sign, we were unable to find it from the available publications. It would be interesting to use the available lattice data to obtain it. Such an extraction would be interesting to confront the ChPT results.

### 6.4.4 SM prediction for the short-distance physics

Within the SM, the short distance contribution arises from the following effective Hamiltonian [200]

$$\mathcal{H}_{\text{eff}} = -\frac{G_F}{\sqrt{2}}\frac{\alpha_{em}}{2\pi\sin^2\theta_W}\left[V_{ts}^* V_{td} Y(x_t) + V_{cs}^* V_{cd} Y_{NL}\right]\left[(\bar{s}d)_{V-A}(\bar{\mu}\mu)_{V-A}\right] + \text{h.c.}\,. \tag{6.59}$$

We can then write (in the basis where $\delta_{SD} = 0$)

$$\begin{aligned} A(K_L)_{SD}^{\text{SM}} &= \left(\sqrt{2}|A_{SD}|\cos\theta_{SD}\right)^{\text{SM}} \\ &= \frac{\sqrt{2}G_F\alpha_{em}}{\pi\sin^2\theta_W}\left|V_{ts}^* V_{td} Y(x_t) + V_{cs}^* V_{cd} Y_{NL}\right| f_K m_\mu m_K \cos\theta_{SD}^{\text{SM}}\,, \end{aligned} \tag{6.60}$$

where we identify

$$\theta_{SD}^{\text{SM}} = \arg\left(-\frac{V_{ts}^* V_{td} + V_{cs}^* V_{cd} Y_{NL}/Y(x_t)}{V_{cs}^* V_{cd}}\right). \tag{6.61}$$

We therefore find,

$$\tan\theta_{SD}^{\rm SM} \;=\; -\frac{\eta}{(1-\rho)+\frac{1}{A^2\lambda^4}\frac{Y_{NL}}{Y(x_t)}} + O(\lambda^6) \;<\; 0\,. \tag{6.62}$$

Hence, from Eq. (6.52), within the SM and under the aforementioned model-dependent assumptions, we have

$$[\cos\varphi_0]^{\rm SM}_{\text{large}\,N_C} \;<\; 0\,. \tag{6.63}$$

Together with the result of section 6.3, $\cos^2\varphi_0 = 0.96 \pm 0.03$, we have

$$[\cos\varphi_0]^{\rm SM}_{\text{large}\,N_C} \;=\; -0.98 \pm 0.02\,. \tag{6.64}$$

Note that the error combines both a statistical error from experiment as well as a theory component, *i.e.* is to be interpreted as an estimate of the total uncertainty.

## 6.5 Going beyond the two-fold ambiguity

In order to determine the sign of $\sin\varphi_0$ and get rid of the remaining ambiguity, we would need to determine the signs and magnitudes of the competing short-distance and long-distance dispersive contributions,

$$\begin{aligned}\sin\varphi_0 &= \frac{\text{Im}[A(K_S)^* A(K_L)]}{|A(K_S)A(K_L)|} \\ &= -\frac{\Big([A_{LD}]_{\text{dispersive}} + \sqrt{2}|A_{SD}|\cos\theta_{SD}]\Big)\,\text{sgn}[\sin(\theta_{SD})]}{|A(K_L)|}\,.\end{aligned} \tag{6.65}$$

We recall that $[A_{LD}]_{\text{dispersive}}$ can be written as

$$[A_{LD}]_{\text{dispersive}} = \sqrt{2}|A_{LD}|\cos\Delta\delta = C_{\text{had.}}\left(A_{LD}^{\text{local}} + \text{Re}A_{LD}^{\gamma\gamma}\right), \tag{6.66}$$

see Eq. (6.39). Existing semi-phenomenological theory estimations of $[A_{LD}]_{\text{dispersive}}$ come with large theory uncertainties. Using the estimate of Ref. [187] as in Eq. (6.49), updated with existing data (see App. E), we have for the long-distance contribution,

$$\begin{aligned}\frac{[A_{LD}]_{\text{dispersive}}}{|A(K_L\to\mu^+\mu^-)|} &= \frac{C_{\text{had.}}}{|A(K_L\to\mu^+\mu^-)|}\left(A_{LD}^{\text{local}} + \text{Re}A_{LD}^{\gamma\gamma}\right) \\ &= \frac{C_{\text{had.}}|A_{\gamma\gamma}|}{|A(K_L\to\mu^+\mu^-)|}\frac{\alpha_{em}m_\mu}{\pi m_K}\left([\chi_{\gamma\gamma}(m_\rho)]^{\text{IU}} + \left[\text{Re}C_{\gamma\gamma} - \frac{5}{2} + \frac{3}{2}\log\left(\frac{m_\mu^2}{m_\rho^2}\right)\right]^{\text{IU}}\right) \\ &= \text{sgn}\,[C_{\text{had.}}]\sqrt{\frac{2\beta_\mu}{R_{K_L}}}\frac{\alpha_{em}m_\mu}{\pi m_K}\,[(6.10\pm1.01) - 5.14] \in [-0.009,\, 0.37]\,,\end{aligned} \tag{6.67}$$

where $\text{sgn}[C_{\text{had.}}] > 0$ derived in the previous section is used.

For the short-distance SM contribution, we have (see Eq. (6.60))

$$\begin{aligned}\frac{A(K_L)_{SD}^{\text{SM}}}{|A(K_L\to\mu^+\mu^-)|} &= \frac{\sqrt{2}G_F\alpha_{em}(m_Z)}{\pi\sin^2\theta_W}\frac{\left|V_{ts}^*V_{td}Y(x_t) + V_{cs}^*V_{cd}Y_{NL}\right|f_K m_\mu m_K\,\cos\theta_{SD}^{\text{SM}}}{|A(K_L\to\mu^+\mu^-)|} \\ &= -0.331\pm0.008\,,\end{aligned} \tag{6.68}$$

where we use the following inputs,

$$
\begin{aligned}
&Y(x_t) = 0.931 \pm 0.005\ [212]\,, && Y_{\rm NL} = (2.95 \pm 0.46) \times 10^{-4}\ [188]\,, \\
&A = 0.790^{+0.017}_{-0.012}\,, && \lambda = 0.22650 \pm 0.00048\,, \\
&\bar{\rho} = 0.141^{+0.016}_{-0.017}\,, && \bar{\eta} = 0.357 \pm 0.011\,, \\
&m_K = 497.61\,\text{MeV}\,, && m_\mu = 105.658\,\text{MeV}\,, \\
&G_F = 1.166378 \times 10^{-5}\,\text{GeV}^{-2}\,, && f_K = 155.7\,\text{MeV}\,, \\
&\alpha_{em} = 1/137\,, && \alpha_{em}(m_Z) = 1/129\,, \\
&\sin^2\theta_W = 0.23\,, && m_\rho = 775.26\,\text{MeV}\,.
\end{aligned}
\tag{6.69}
$$

In particular, the CKM input results in $\cos\theta_{SD}^{\rm SM} = -0.94$.

Hence, the large theory uncertainty on the dispersive long-distance contribution, as reflected in the range given in Eq. (6.67), does not allow to determine if it is larger or smaller than the short-distance SM contribution, Eq. (6.68). We conclude that with current knowledge on the dispersive long-distance contribution the sign of $\sin\varphi_0$ cannot be determined.

Therefore, we have, using Gaussian error propagation,

$$
[\cos\varphi_0]^{\rm SM}_{\text{large}\,N_C} = -0.98 \pm 0.02\,, \qquad [\sin\varphi_0]^{\rm SM}_{\text{large}\,N_C,\,\text{theory}} = \pm(0.21 \pm 0.07)\,. \tag{6.70}
$$

We note that due to the nature of the theoretical error, the error should not be interpreted as a statistical error but rather as an estimate of the uncertainty.

## 6.6 Discussion and Conclusions

In this work we have related the phase shift, $\varphi_0$, appearing in the time-dependent decay rate of a neutral kaon to a dimuon pair to the ratio of integrated rates of $K_L \to \mu^+\mu^-$ and $K_L \to \gamma\gamma$. This relation holds to an excellent approximation under the well-motivated assumption that the two-photon intermediate state dominates the absorptive contribution, and within any model in which the short-distance leptonic current is axial or vectorial, as in the SM. The only input required other than the ratio of integrated rates is a coefficient calculated within QED. We find that $\cos^2\varphi_0$ is precisely predicted model independently, and given by

$$\cos^2\varphi_0 \;=\; 0.96 \pm 0.02_{\rm exp} \pm 0.02_{\rm th}\,. \tag{6.71}$$

The experimental error comes from the error of $R_{K_L}$ and the theory error is our estimate of the size of higher order QED corrections and the contribution from other intermediate states beside the di-photon state. The result leaves a four-fold ambiguity in $\varphi_0$.

The phase shift, $\varphi_0$, is also of experimental significance since it controls the integrated number of interference events. For a $K^0$ beam a positive value of $\cos\varphi_0$ is preferred as it enhances the interference and improves the feasibility of extracting clean short-distance information from the interference term. For a $\overline{K}^0$ beam the situation is reversed, and a negative value of $\cos\varphi_0$ is preferred. Thus, for experiments employing a proton beam on target, where the number of $K^0$ particles is expected to exceed that of $\overline{K}^0$ particles, a positive $\cos\varphi_0$ would be preferred.

We were unable to determine the sign of $\cos\varphi_0$ completely model independently. Thus, with the use of several assumptions, that is, within the framework of ChPT and using a typical parameter region (motivated by the large-$N_C$ limit, as detailed in Sec. 6.4.2), the sign of $\cos\varphi_0$, relative to the short-distance contribution, can be predicted. We find that within this framework, and assuming that the short-distance contribution is SM-like, there is a theory preference towards $\cos\varphi_0 < 0$. New Physics can potentially yield a different sign for $\cos\varphi_0$. A measurement of the angle $\varphi_0$ is therefore a test of the validity of several assumptions, pertaining to both the short-distance physics and the ChPT description of the dispersive long-distance physics.

Given the assumptions that were made to arrive to the conclusion about the sign of $\cos\varphi_0$, and the fact that the prediction can be modified for models beyond the SM, we conclude that neither solution is unequivocally theoretically favored. That is, we cannot conclude that we know the sign of $\cos\varphi_0$ to high confidence. Thus, when planing to perform the experiment we encourage the experimental collaborations to consider both possible signs for $\cos\varphi_0$ for purposes of sensitivity estimations.

We therefore conclude by emphasizing that the time dependence of the kaon decay rate to two muons provides two very clean SM predictions:

1. The coefficient of the interference term allows the extraction of the theoretically clean decay rate $\mathcal{B}(K_S \to \mu^+\mu^-)_{\ell=0}$. In the SM, this observable is proportional to the CKM combination $|V_{ts}V_{td}\sin(\beta+\beta_s)|$.

2. Although it includes long-distance as well as short-distance physics, the phase shift in the interference term, $\varphi_0$, is predicted cleanly up to a four-fold ambiguity.

Thus, an experiment that performs the time-dependence studies of the $K \to \mu^+\mu^-$ decay rate provides two independent tests of the SM from the same measurement. While the phase $\varphi_0$ is not determined model independently, it directly impacts the measurement of the $K \to \mu^+\mu^-$ time dependent rate as it affects the interference between the $K_S$ and $K_L$ amplitudes in the total rate. The phase shift $\varphi_0$ is therefore a quantity of critical importance in kaon physics, as a way to test the SM, and in extension, as a probe of new physics beyond the SM because of its sensitivity to short distance effects.

CHAPTER 7

# $K \to \mu^+\mu^-$ BEYOND THE STANDARD MODEL

## 7.1 Introduction

A recent proposal has demonstrated that short-distance (SD) parameters of the decay $K \to \mu^+\mu^-$ can be cleanly extracted from a measurement of the $K_S - K_L$ interference term in the time dependent rate [142, 2]. This statement is true to a very good approximation within the SM and any New Physics (NP) model in which the leptonic ($\mu^+\mu^-$) current is of similar CP structure. As shown in Ref. [2], once such a measurement is carried out, its results can be interpreted as a measurement of standard model (SM) CKM parameters. Recently, Ref. [219] has pointed out that within the SM, the ratio, $\mathcal{B}(K_S \to \mu^+\mu^-)_{\ell=0}/\mathcal{B}(K_L \to \pi^0\bar{\nu}\nu)$ is independent of any SM parameter except for the well-measured $|V_{us}|$ and $m_t$ (and in particular gets rid of any parametric dependence on $|V_{cb}|$). In this work we show that a measurement of $\mathcal{B}(K_S \to \mu^+\mu^-)_{\ell=0}$ can also serve as a probe of possible NP scenarios.

$K \to \mu^+\mu^-$ is a flavor-changing-neutral-current (FCNC) process, making it a very potent probe of physics beyond the SM, sensitive to high NP scales. The prospects of having a theoretically clean measurement of its parameters are therefore very exciting. In the following, we investigate the NP reach of this proposed measurement. In other words, we ask the question of to what extent and within which models can the CP-violating mode, $\mathcal{B}(K_S \to \mu^+\mu^-)_{\ell=0}$, be significantly en-

hanced compared to the SM.

We first discuss a model-independent generic bound in Sec. 7.2, we review the basic setup in Sec. 7.3, then we derive relations to other modes using an EFT approach in Sec. 7.4, and analyze specific examples of relevant NP models in Sec. 7.5. We conclude in Sec. 7.6.

## 7.2 Generic bound

The 2020 LHCb bound on $K_S \to \mu^+\mu^-$ reads [223]

$$\mathcal{B}(K_S \to \mu^+\mu^-) < 2.1 \cdot 10^{-10} \equiv \mathcal{B}(K_S \to \mu^+\mu^-)_{lim.}\,. \tag{7.1}$$

Within the SM, the prediction for $K_S \to \mu^+\mu^-$ involves a large CP-conserving contribution, dominated by long-distance physics, and a much smaller CP-violating contribution, dominated by short-distance physics. Since these two contributions result in final states of opposite CP, they do not interfere and we have

$$\mathcal{B}(K_S \to \mu^+\mu^-) = \mathcal{B}(K_S \to \mu^+\mu^-)^{(\mathrm{LD})}_{\mathrm{CPC}} + \mathcal{B}(K_S \to \mu^+\mu^-)^{(\mathrm{SD})}_{\mathrm{CPV}}\,. \tag{7.2}$$

The bound of Eq. (7.1) can then be read as a conservative bound on the CP-violating (CPV) short-distance contribution alone,

$$\mathcal{B}(K_S \to \mu^+\mu^-)_{\mathrm{CPV}} < \mathcal{B}(K_S \to \mu^+\mu^-)_{lim.}\,. \tag{7.3}$$

The short-distance CPV contribution to $K_S \to \mu^+\mu^-$ can be identified with the decay of $K_S$ into the CP-odd final state $(\mu^+\mu^-)_{\ell=0}$, where $\ell$ denotes the orbital angular

momentum of the dimuon pair. The SM prediction is given by $\mathcal{B}(K_S \to \mu^+\mu^-)^{\rm SM}_{\ell=0} = 1.64 \times 10^{-13}$ [2], leaving much room for possible NP contributions,

$$R(K_S \to \mu^+\mu^-)_{\ell=0} \equiv \frac{\mathcal{B}(K_S \to \mu^+\mu^-)_{\ell=0}}{\mathcal{B}(K_S \to \mu^+\mu^-)^{\rm SM}_{\ell=0}} \leq \frac{\mathcal{B}(K_S \to \mu^+\mu^-)_{lim.}}{\mathcal{B}(K_S \to \mu^+\mu^-)^{\rm SM}_{\ell=0}} \approx 1280\,. \tag{7.4}$$

As laid out in detail in Ref. [2], within the SM, the decay $K_L \to \mu^+\mu^-$ is CP-conserving, and involves only the $(\mu^+\mu^-)_{\ell=0}$ final state. In this case we have

$$|A(K_L)_{\ell=1}| = 0\,, \tag{7.5}$$

which implies that the $K_S - K_L$ interference term involves only $\ell = 0$,

$$\Gamma_{int.} \propto |A(K_S)_{\ell=0}||A(K_L)_{\ell=0}|\,. \tag{7.6}$$

The observable

$$\frac{\Gamma^2_{int.}}{\mathcal{B}(K_L \to \mu^+\mu^-)} \propto |A(K_S)_{\ell=0}|^2, \tag{7.7}$$

then provides a clean measurement of the short-distance, CP-violating parameter $|A(K_S)_{\ell=0}|$.

Any NP that honors the assumption which the analysis of Ref. [2] hinges on, that is, keeps $|A(K_L)_{\ell=1}| = 0$, retains the form of Eqs. (7.6) and (7.7).

We can deduce the experimentally allowed range for NP in $\Gamma_{int.}$ from Eqs. (7.4) and (7.7), using the fact that $\mathcal{B}(K_L \to \mu^+\mu^-)$ is well-measured. We find that

$$\frac{\Gamma_{int.}}{\Gamma^{\rm SM}_{int.}} = \sqrt{R(K_S \to \mu^+\mu^-)_{\ell=0}}36\,, \tag{7.8}$$

suggesting that a direct measurement of the $K_S - K_L$ interference term from the time-dependent rate would be sensitive to viable NP scenarios.

## 7.3 Notation and setup

We use the following standard notation [**?**], where the two neutral kaon mass eigenstates, $|K_S\rangle$ and $|K_L\rangle$, are linear combinations of the flavor eigenstates:

$$|K_S\rangle = p|K^0\rangle + q|\overline{K}^0\rangle, \qquad |K_L\rangle = p|K^0\rangle - q|\overline{K}^0\rangle. \tag{7.9}$$

For the purposes of our analysis, CPV in mixing, which is an $O(\varepsilon_K) \sim 10^{-3}$ effect, can be safely neglected and we work in the limit

$$\left|\frac{q}{p}\right| = 1\,. \tag{7.10}$$

In this limit, the kaon mass eigenstates are also CP eigenstates, and therefore for final states that have definite CP, the decay amplitude is either purely CP-violating or purely CP-conserving. The dimuon final state is a CP eigenstate, which can be in one of two possible configurations of different orbital angular momentum: CP-odd ($\ell = 0$) and CP-even ($\ell = 1$).

Within the SM, and any extension of it in which the leptonic current inducing the dimuon final state is CP-odd (vectorial, axial-vectorial and pseudoscalar currents all fall under this category), CP-violating short-distance effects only contribute to $(\mu^+\mu^-)_{\ell=0}$. In addition, all long-distance contributions are CP-conserving to $O(10^{-3})$, see Ref. [2] for details. It follows that in this context:

1. Only the $\ell = 0$ final state appears in the $K_L$ decay,

$$|A(K_L)_{\ell=1}| = 0\,. \tag{7.11}$$

2. A measurement of $K_S - K_L$ interference involves only the $\ell = 0$ amplitudes, and is proportional to $A(K_S)_{\ell=0} \times A(K_L)^*_{\ell=0}$.

Thus, as long as NP does not introduce CP-even leptonic operators, the measurement proposed in Ref. [2] is a clean measurement of the short-distance amplitude $|A(K_S)_{\ell=0}|$, which is equivalent to a measurement of $\mathcal{B}(K_S \to \mu^+\mu^-)_{\ell=0}$.

The time dependent decay rate as a function of proper time for a neutral kaon beam is given by [**?**]

$$\left(\frac{\mathrm{d}\Gamma}{\mathrm{d}t}\right) = \mathcal{N}_f f(t), \tag{7.12}$$

where $\mathcal{N}_f$ is a time-independent normalization factor and the function $f(t)$ is given as a sum of four functions

$$f(t) = C_L e^{-\Gamma_L t} + C_S\, e^{-\Gamma_S t} + 2\left[C_{sin}\sin(\Delta m t) + C_{cos}\cos(\Delta m t)\right] e^{-\Gamma t}. \tag{7.13}$$

For a pure $K^0$ beam, the coefficients are given by [2]

$$\begin{aligned}
C_L &= |A(K_L)_{\ell=0}|^2, \\
C_S &= |A(K_S)_{\ell=0}|^2 + \beta_\mu^2 |A(K_S)_{\ell=1}|^2, \\
C_{cos} &= \mathcal{R}e(A(K_S)^*_{\ell=0} A(K_L)_{\ell=0}) = |A(K_S)^*_{\ell=0} A(K_L)_{\ell=0}|\,\cos\varphi_0, \\
C_{sin} &= \mathcal{I}m(A(K_S)^*_{\ell=0} A(K_L)_{\ell=0}) = |A(K_S)^*_{\ell=0} A(K_L)_{\ell=0}|\,\sin\varphi_0.
\end{aligned} \tag{7.14}$$

where $\varphi_0 \equiv \arg(A(K_S)^*_{\ell=0} A(K_L)_{\ell=0})$. The interference effects are embodied by $C_{cos}$ and $C_{sin}$,

$$\Gamma_{int.} \propto \sqrt{C_{cos}^2 + C_{sin}^2}\,. \tag{7.15}$$

## 7.4 Model-independent analysis using effective operators

We consider the effective $|\Delta S| = 1$ Hamiltonian,

$$\mathcal{H}_{eff.}^{|\Delta S|=1} = \sum_i C_i O_i, \tag{7.16}$$

where the flavor indices are implicit. The following six operators are relevant for $K \to \mu^+\mu^-$:

- Vectorial operators

$$\begin{aligned} O_{VLL} &= (\overline{Q}_L\gamma^\mu Q_L)(\overline{L}_L\gamma_\mu L_L); \qquad O_{VLR} = (\overline{Q}_L\gamma^\mu Q_L)(\overline{e}_R\gamma_\mu e_R), \\ O_{VRL} &= (\overline{d}_R\gamma^\mu d_R)(\overline{L}_L\gamma_\mu L_L); \qquad O_{VRR} = (\overline{d}_R\gamma^\mu d_R)(\overline{e}_R\gamma_\mu e_R), \end{aligned} \tag{7.17}$$

- Scalar operators

$$\begin{aligned} O_{SLR} &= (\overline{Q}_L d_R)(\overline{e}_R L_L), \\ O_{SRL} &= (\overline{d}_R Q_L)(\overline{L}_L e_R)\,. \end{aligned} \tag{7.18}$$

Since the quark indices we are interested in are non-diagonal, $O_{SLR}$ and $O_{SRL}$ are two distinct operators, not related by hermitian conjugation. For concreteness, we consider the quark flavor indices to always be $(2, 1)$ unless otherwise indicated. Note that we do not include tensor operators here, since tensor operators do not contribute to the 2-body decay of a pseudoscalar, as is the case at hand.

We obtain the following general expression for the $K_S \to (\mu^+\mu^-)_{\ell=0}$ rate, in units

of the SM expectation,

$$R(K_S \to \mu^+\mu^-)_{\ell=0} = \left(1 + \frac{1}{|C^{\rm SM}_{VLL}|\sin\theta_{ct}}\left[A_S\left(|C^{\rm NP}_{SLR}|\sin\Theta_{SLR} + |C^{\rm NP}_{SRL}|\sin\Theta_{SRL}\right)\right.\right. \tag{7.19}$$
$$\left.\left. + |C^{\rm NP}_{VLL}|\sin\Theta_{VLL} - |C^{\rm NP}_{VLR}|\sin\Theta_{VLR} - |C^{\rm NP}_{VRL}|\sin\Theta_{VRL} + |C^{\rm NP}_{VRR}|\sin\Theta_{VRR}\right]\right)^2 ,$$

where $A_S \equiv \frac{m_K^2/m_\mu}{2(m_s+m_d)}$ is the so-called scalar enhancement factor (see, for example, the discussion around Eq. (28) of Ref. [**?**]), $\Theta_i$ is the basis independent phase between the mixing and the Wilson coefficient,

$$\Theta_i \equiv \frac{1}{2}\arg\left(\frac{q}{p}\right) - \arg(C_i^{\rm NP}) , \tag{7.20}$$

and [2]

$$|C^{\rm SM}_{VLL}|\sin\theta_{ct} = \left|\frac{G_F}{\sqrt{2}}\frac{2\alpha Y(x_t)}{\pi\sin^2_W}\mathcal{I}m\left(-\frac{V^*_{ts}V_{td}}{V^*_{cs}V_{cd}}\right)\right| . \tag{7.21}$$

It is important to note, that the scalar operators, $O_{SLR}$ and $O_{SRL}$, induce both the $\ell = 0$ and the $\ell = 1$ final states, since they include both pseudo-scalar ($P$) and scalar ($S$) leptonic currents. Only the combination ($O_{SRL} + O_{SLR}$) can in general protect the assumption of $|A(K_L)_{\ell=1}| = 0$.

By taking any Wilson coefficient to be $\mathcal{O}(1/\Lambda^2)$, where $\Lambda$ is the scale of NP, we learn that a measurement of $\mathcal{B}(K_S \to \mu^+\mu^-)_{\ell=0}$ that saturates the current experimental upper bound would be sensitive to NP scales of up to $\Lambda \sim 40\,\text{TeV}$ for vectorial operators, and up to $\Lambda \sim 130\,\text{TeV}$ for scalar operators.

### 7.4.1 The relation between $K_S \to (\mu^+\mu^-)_{\ell=0}$ and $K_L \to \pi^0\bar{\nu}\nu$

Of the six operators, $O_{VLL}$ and $O_{VRL}$ contribute additionally to $K_L \to \pi^0\nu\bar{\nu}$. The general expression for $K_L \to \pi^0\bar{\nu}\nu$, assuming diagonal couplings in flavor space, is given by:

$$R(K_L \to \pi^0\bar{\nu}\nu) = \frac{1}{3}\sum_{i=e,\mu,\tau}\left(1 + \frac{|(C^{\rm NP}_{VLL})_i|\sin\Theta_{VLL,i} + |(C^{\rm NP}_{VRL})_i|\sin\Theta_{VRL,i}}{|C^{\rm SM}_{VLL}|\sin\theta_{ct}}\right)^2, \quad (7.22)$$

where $R(X)$ denotes the rate of $X$ in units of the SM prediction.

- **Models with lepton-flavor universality.**

  $K_S \to (\mu^+\mu^-)_{\ell=0}$ and $K_L \to \pi^0\bar{\nu}\nu$ are both CPV processes and both arise in the SM from a single operator, $O_{VLL}$. This leads to simple relations between their rates, in the case of models that are lepton flavor universal (LFU), and involve only the lepton-doublet vectorial operators, $\{O_{VLL}, O_{VRL}\}$. We have,

$$R(K_S \to \mu^+\mu^-)^{\{O_{VLL},O_{VRL}\}}_{\ell=0} = \left(1 + \frac{|C^{\rm NP}_{VLL}|\sin\Theta^{\rm NP}_{VLL} - |C^{\rm NP}_{VRL}|\sin\Theta^{\rm NP}_{VRL}}{|C^{\rm SM}_{VLL}|\sin\theta_{ct}}\right)^2, \quad (7.23)$$

$$R(K_L \to \pi^0\bar{\nu}\nu)^{\rm LFU} = \left(1 + \frac{|C^{\rm NP}_{VLL}|\sin\Theta^{\rm NP}_{VLL} + |C^{\rm NP}_{VRL}|\sin\Theta^{\rm NP}_{VRL}}{|C^{\rm SM}_{VLL}|\sin\theta_{ct}}\right)^2 .$$

  The sign differences in the two expressions result entirely from the fact that the first process is sensitive only to the axial hadronic current, while the second is only sensitive to the vector hadronic current. We conclude the following:

  1. In models where only $C^{\rm NP}_{VLL}$ is turned on, we have

$$R(K_S \to \mu^+\mu^-)^{C_{VLL}}_{\ell=0} = R(K_L \to \pi^0\bar{\nu}\nu)^{C_{VLL}}_{\rm LFU} . \quad (7.24)$$

Then, by using the Grossman–Nir (GN) bound [160] to place an experimental constraint on $R(K_L \to \pi^0 \bar{\nu}\nu)$,

$$R(K_L \to \pi^0 \bar{\nu}\nu)^{C_{VLL}}_{\text{LFU}} \underset{\text{GN}}{} \frac{4.3 \cdot \mathcal{B}(K^+ \to \pi^+ \bar{\nu}\nu)}{\mathcal{B}(K_L \to \pi^0 \bar{\nu}\nu)_{\text{SM}}} 26\,, \tag{7.25}$$

the following bound can be set on the deviation from the SM in $\mathcal{B}(K_S \to \mu^+\mu^-)_{\ell=0}$,

$$R(K_S \to \mu^+\mu^-)^{C_{VLL}}_{\ell=0} \underset{\text{GN}}{} 26\,. \tag{7.26}$$

2. In models where only $C^{\text{NP}}_{VRL}$ is turned on,

$$\frac{R(K_S \to \mu^+\mu^-)^{C_{VRL}}_{\ell=0}}{R(K_L \to \pi^0 \bar{\nu}\nu)^{C_{VRL}}_{\text{LFU}}} = \frac{\left(1 - \frac{|C^{\text{NP}}_{VRL}|}{|C^{\text{SM}}_{VLL}|} \frac{\sin\Theta^{\text{NP}}_{VRL}}{\sin\theta_{ct}}\right)^2}{\left(1 + \frac{|C^{\text{NP}}_{VRL}|}{|C^{\text{SM}}_{VLL}|} \frac{\sin\Theta^{\text{NP}}_{VRL}}{\sin\theta_{ct}}\right)^2}\,. \tag{7.27}$$

Then, the GN bound on $R(K_L \to \pi^0 \bar{\nu}\nu)$ results in

$$R(K_S \to \mu^+\mu^-)^{C_{VRL}}_{\ell=0} \underset{\text{GN}}{} 50\,. \tag{7.28}$$

3. Hence, if NP is discovered in a future measurement of $R(K_S \to \mu^+\mu^-)_{\ell=0}$, with a larger value than the above bounds, we will be able to exclude models that turn on only one of $\{O_{VLL}, O_{VRL}\}$.
4. If, on the other hand, a future bound is set on $R(K_S \to \mu^+\mu^-)_{\ell=0}$ that is more stringent than the above, it has the potential to become the leading constraint on $R(K_L \to \pi^0 \bar{\nu}\nu)$ in the framework of a single LFU operator.
5. If more than one operator is turned on, or if any of the operators involving right-handed leptons or scalar currents ($\{O_{VLR}, O_{VRR}, O_{SLR}, O_{SRL}\}$) are at play, then the two modes are in general completely independent.

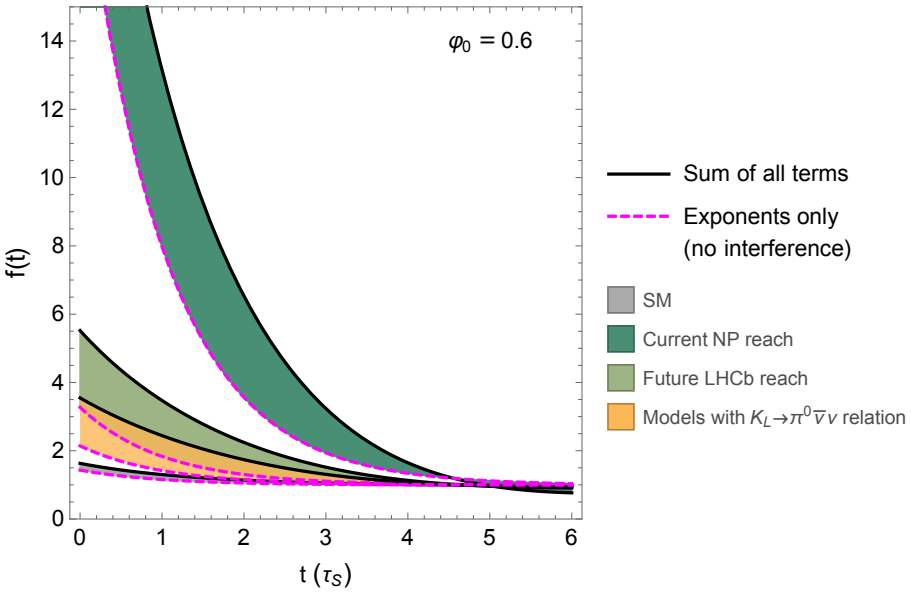


The time dependence in the decay of a $K^0$ beam into $\mu^+\mu^-$, as given by Eq. (7.12), for magnitudes of the $K_S \to (\mu^+\mu^-)_{\ell=0}$ amplitude given by: the SM prediction (gray), the current experimental upper bound (dark green), the upper bound for models where the rate is correlated with $K_L \to \pi^0\bar{\nu}\nu$ (yellow), and the expected future reach at LHCb (light green). The integral between the solid and dashed curves corresponds to the magnitude of interference effects.

We note that similar relations are expected to apply between $K_S \to (\mu^+\mu^-)_{\ell=0}$ and the direct CPV contributions in $K_L \to \pi^0\mu^+\mu^-$ and $K_S \to \pi^0\pi^0\mu^+\mu^-$. These would apply for any single operator that affects $K_S \to (\mu^+\mu^-)_{\ell=0}$. We leave a detailed discussion of these modes to a future work.

- **Models that break lepton-flavor universality.**

  In general, there could be operators that contribute to $K_L \to \pi^0\nu\bar{\nu}$ but not to $K \to \mu^+\mu^-$. These are analogous to $O_{VLL}$, $O_{VRL}$ with lepton flavor indices

different from $(2, 2)$.

We note further that the experimental signature for $K_L \to \pi^0 \nu\bar{\nu}$ involves missing energy, hence it also captures scenarios with exotic undetected particles, to which $K_S \to (\mu^+\mu^-)_{\ell=0}$ is insensitive.

The time dependent rate of Eq. (7.12) for a pure $K^0$ beam, for a choice of the unknown phase $\varphi_0 \equiv \arg(A(K_S)^*_{\ell=0} A(K_L)_{\ell=1})$ is plotted in Fig. 2. It is apparent that both the total rate and the effect of interference (depicted by the area between the dashed and solid curves) can be greatly enhanced compared to the SM. The estimate for the future reach of LHCb $\mathcal{B}(K_S \to \mu^+\mu^-)$ searches is taken from Ref. [**?**].

## 7.5 Explicit NP models

In this section we present a few examples of simple models in which $\mathcal{B}(K_S \to \mu^+\mu^-)_{\ell=0}$ is enhanced compared to the SM expectation, and discuss the relevant constraints in each. We present three models: two scalar leptoquark representations, each inducing a different vectorial effective operator, and a model with an extra scalar doublet, which introduces the scalar effective operators. Many other possible models beyond the SM exist that can affect $K \to \mu^+\mu^-$, and some may have unavoidable implications on additional constraints untouched by our choice of toy models. For example, models with flavor changing $Z$ couplings can enhance $\mathcal{B}(K_S \to \mu^+\mu^-)_{\ell=0}$, but introduce additional strong constraints from $\varepsilon'/\varepsilon$ that

generally restrict the contribution to $\mathcal{B}(K_S \to \mu^+\mu^-)_{\ell=0}$ to be small. We therefore do not discuss this further here.

### 7.5.1 Scalar Leptoquark : $\tilde{S}_1(\bar{3}, 1, 4/3)$

As a first example of a simple model that can contribute to $K_S \to (\mu^+\mu^-)_{\ell=0}$, we consider a scalar leptoquark. A detailed review of leptoquarks and their phenomenology can be found, for example, in Ref. [**?**]. Here we discuss two examples of scalar leptoquark representations which demonstrate some of the characteristic features of the $K \to \mu^+\mu^-$ phenomenology.

We first consider a scalar leptoquark in the following SM gauge group representation,

$$\tilde{S}_1 \sim (\bar{3}, 1)_{4/3}\,. \tag{7.29}$$

The relevant Lagrangian terms are given by

$$\mathcal{L}_{\tilde{S}_1} \supset g_{12}\,\tilde{S}_1 \overline{d}_R^C \mu_R + g_{22}\,\tilde{S}_1 \overline{s}_R^C \mu_R \;+\; h.c.\,, \tag{7.30}$$

with $\psi^C = C\overline{\psi}^T$, $C = i\gamma^2\gamma^0$. After integrating out the leptoquark field, we are left with the following dimension six operator,

$$\frac{g_{12}g_{22}^*}{2M_{\tilde{S}_1}^2}(\overline{d}_R^C \mu_R)(\overline{\mu}_R s_R^C) = \frac{g_{12}g_{22}^*}{4M_{\tilde{S}_1}^2}(\overline{s}_R\gamma^\mu d_R)(\overline{\mu}_R\gamma_\mu\mu_R), \tag{7.31}$$

where in the last step we used a Fierz transformation. In the language of the effective operators of section 7.4, this model induces the operator $O_{VRR}$, with $C_{VRR}^{\rm NP} = \frac{g_{12}g_{22}^*}{4M_{\tilde{S}_1}^2}$.

We then have,

$$R(K_S \to \mu^+\mu^-)^{\tilde{S}_1}_{\ell=0} \;=\; \left(1 \,+\, \frac{|g_{12}g_{22}|\sin\Theta_{\tilde{S}_1}}{4M^2_{\tilde{S}_1}|C^{\rm SM}_{VLL}|\sin\theta_{ct}}\right)^2 , \tag{7.32}$$

where, as in Eq. (7.20), the angle $\Theta_{\tilde{S}_1}$ is defined as the phase between the Wilson coefficient and the mixing,

$$\Theta_{\tilde{S}_1} \equiv \frac{1}{2}\arg\left(\frac{q}{p}\right) - \arg(g_{12}g^*_{22}), \tag{7.33}$$

and $|C^{\rm SM}_{VLL}|$ is defined in Eq. (7.21). In order to saturate the experimental bound, $R(K_S \to \mu^+\mu^-)_{\ell=0} \approx 1280$, we require

$$\left|g_{12}g_{22}\sin\Theta_{\tilde{S}_1}\right| \approx 3.4\cdot 10^{-3}\left(\frac{M_{\tilde{S}_1}}{\rm TeV}\right)^2 . \tag{7.34}$$

There are several constraints on the model parameters. Direct searches at ATLAS and CMS for leptoquark states with $O(1)$ branching ratios into a muon and a light quark result in lower bounds on the leptoquark mass of [**?**, **?**]

$$M_{\tilde{S}_1} \gtrsim 1.7\,{\rm TeV}\,. \tag{7.35}$$

Therefore Eq. (7.34) can be rewritten as

$$\left|g_{12}g_{22}\sin\Theta_{\tilde{S}_1}\right| \approx 3.4\cdot 10^{-3}\left(\frac{M_{\tilde{S}_1}}{\rm TeV}\right)^2 \gtrsim 9.3\cdot 10^{-3}\,. \tag{7.36}$$

The same operator of Eq. (7.31) induces $K^0 - \overline{K}^0$ mixing via loop diagrams [162], inducing a contribution to $M_{12}$,

$$M_{12} = M^{\rm SM}_{12} + \frac{f_K^2\hat{B}_K m_K}{384\pi^2 M^2_{\tilde{S}_1}}(g^*_{12}g_{22})^2. \tag{7.37}$$

We use

$$\Delta m_K = \frac{4\mathcal{R}e(M_{12}\Gamma_{12}^*)}{\Delta\Gamma}, \qquad |\varepsilon_K| \approx -\frac{\mathcal{I}m(M_{12}\Gamma_{12}^*)}{\sqrt{2}|M_{12}\Gamma_{12}|}\,, \tag{7.38}$$

together with the fact that in the kaon system we have $\Gamma_{12} \approx \bar{A}_0 A_0^*$, where $A_0$ is the decay amplitude of $K^0$ into $(\pi\pi)_{I=0}$. This allows us to identify the relevant physical phase in the NP contribution, and relate it to the physical phase relevant for $K \to \mu\mu$,

$$\arg\left(M_{12}^{\rm NP}\Gamma_{12}^*\right) \approx \arg\left(M_{12}^{\rm NP}\bar{A}_0^* A_0\right) \approx \arg\left(\left[g_{12}^* g_{22}\right]^2 \frac{q}{p}\right) = -2\Theta_{\tilde{S}_1}. \tag{7.39}$$

where in the next to last step we used the fact that CPV in $K \to \pi\pi$ is negligible, which is equivalent to neglecting CPV in mixing, as in Eq. (7.10).

The allowed regions due to mixing are plotted in Fig. 7.5.1. The measurement of $|\varepsilon_K|$ bounds $|g_{12}g_{22}|^2 \sin\Theta_{\tilde{S}_1}\cos\Theta_{\tilde{S}_1}$, inducing an inverse relation between the magnitudes of the $\sin\Theta_{\tilde{S}_1}$ and $\cos\Theta_{\tilde{S}_1}$, and the constraint from $\Delta m_K$ bounds $|g_{12}g_{22}|^2\left|\cos^2\Theta_{\tilde{S}_1} - \sin^2\Theta_{\tilde{S}_1}\right|$. The constraint from $|\varepsilon_K|$ ensures that for larger values of $\sin\Theta_{\tilde{S}_1}$, such that the bound on $\mathcal{B}(K_S \to \mu^+\mu^-)_{\ell=0}$ is saturated, $\cos\Theta_{\tilde{S}_1}$ has to be small, such that the contribution to $\mathcal{B}(K_L \to \mu^+\mu^-)_{\ell=0}$ is well below the theoretical error. The allowed ranges, such that all constraints are satisfied and the bound on $\mathcal{B}(K_S \to \mu^+\mu^-)_{\ell=0}$ is saturated, can be summarized as

$$|g_{12}g_{22}| \gtrsim 9.3\cdot 10^{-3} \qquad \text{AND} \qquad |\cos\Theta_{\tilde{S}_1}|0.08\,. \tag{7.40}$$

We deduce that the $\tilde{S}_1$ model can saturate the experimental bound of $R(K_S \to \mu^+\mu^-)_{\ell=0} \leq 1.3\times 10^3$, without violating the constraints from mixing and direct

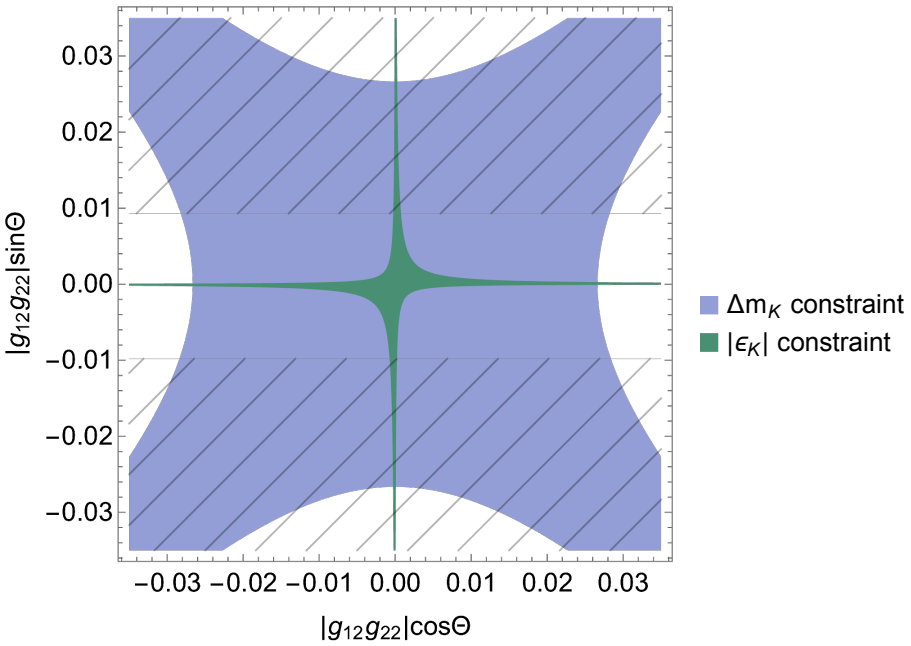


Allowed regions from $K^0 - \overline{K}^0$ mixing. The hatched regions are where the bound on $\mathcal{B}(K_S \to \mu^+\mu^-)_{\ell=0}$ can be saturated (see Eq. (7.36)).

searches. The interference term could be enhanced by $O(30)$ compared to the SM within this model.

### 7.5.2 $S_3(\bar{3}, 3, 1/3)$

Next we consider an SU(2) triplet leptoquark,

$$S_3 \sim (\bar{3}, 3)_{1/3} . \tag{7.41}$$

The relevant Lagrangian term is

$$\mathcal{L}_{S_3} \supset g^{QL}\,(\overline{Q}_L^C)^a \epsilon_{ab} (\tau_i S_3^{\,i})^{bc} (L_L)_c \;+\; h.c.\,, \tag{7.42}$$

where $\tau_i$ are pauli matrices in $\mathrm{SU}(2)_L$ space.

After EWSB, we have

$$\begin{aligned}\mathcal{L}_{S_3} \;\supset\; & g_{12}^{QL}\left[\overline{d}_L^C\left(S_3^{(4/3)}\mu_L + S_3^{(1/3)}\nu_{\mu L}\right) + (\overline{u}_L^c)_i V_{id}\left(S_3^{(1/3)}\mu_L - S_3^{(-2/3)}\nu_{\mu L}\right)\right] \\ +\; & g_{22}^{QL}\left[\overline{s}_L^C\left(S_3^{(4/3)}\mu_L + S_3^{(1/3)}\nu_{\mu L}\right) + (\overline{u}_L^c)_i V_{si}\left(S_3^{(1/3)}\mu_L - S_3^{(-2/3)}\nu_{\mu L}\right)\right] + \; h.c.\,,\end{aligned} \tag{7.43}$$

where $(\overline{u}_L)_i = (\bar{u}_L, \bar{c}_L, \bar{t}_L)$, and $V$ is the CKM matrix. Integrating out the leptoquark states, we are left with a list of effective 4-fermion operators. Mediating $d \to s$ transitions, we have:

$$\begin{aligned}\frac{g_{12}^{QL} g_{22}^{QL*}}{2M^2_{S_3^{(4/3)}}}(\overline{d}_L^C \mu_L)(\overline{\mu}_L s_L^C) \;+\; & \frac{g_{12}^{QL} g_{22}^{QL*}}{2M^2_{S_3^{(1/3)}}}(\overline{d}_L^C \nu_{\mu L})(\overline{\nu_{\mu L}} s_L^C) \\ =\; & \frac{g_{12}^{QL} g_{22*}^{QL}}{4M^2_{S_3^{(4/3)}}}(\bar{s}_L\gamma^\mu d_L)(\bar{\mu}_L\gamma_\mu\mu_L) + \frac{g_{12}^{QL} g_{22}^{QL*}}{4M^2_{S_3^{(1/3)}}}(\bar{s}_L\gamma^\mu d_L)(\overline{\nu_{\mu L}}\gamma_\mu\nu_{\mu L}).\end{aligned} \tag{7.44}$$

There are also $u_i \to u_j$, $u_i \to s$, and $u_i \to d$ transitions induced in this model, but they do not introduce relevant bounds.

In the $SU(2)_L$ limit, $M_{S_3}^{(4/3)} = M_{S_3}^{(1/3)}$, the effective operator generated by this model is $O_{VLL}$, with $C_{VLL}^{\mathrm{NP}} = \frac{g_{12}^{QL} g_{22}^{QL*}}{4M^2_{S_3}}$. Therefore, as expected, the limit on $R(K_L \to \pi^0\bar{\nu}\nu)$ (Eq. (7.25)) translates into a limit on $R(K_S \to \mu^+\mu^-)_{\ell=0}$,

$$R(K_S \to \mu^+\mu^-)_{\ell=0} \;=\; R(K_L \to \pi^0\bar{\nu}\nu) = \left(1 \;+\; \frac{|g_{12}^{QL} g_{22}^{QL}|\sin\Theta_{S_3}}{4M^2_{S_3}|C_{VLL}^{\mathrm{SM}}|\sin\theta_{ct}}\right)^2 26\,. \tag{7.45}$$

The bounds from mixing and from direct searches are the same as in the case of the model of Section 7.5.1, implying that $R(K_S \to \mu^+\mu^-)_{\ell=0} \approx 26$ can be saturated. The interference term in this case could thus be enhanced compared to the SM by a factor of $O(5)$.

### 7.5.3 Scalar doublet (2HDM)

Another example of a simple model that can contribute to $K_S \to (\mu^+\mu^-)_{\ell=0}$ is a two-Higgs-doublet model (2HDM), in which a second scalar doublet is added to the SM,

$$\Phi \sim (1,2)_{\frac{1}{2}} = \begin{pmatrix} \phi^+ \\ \phi_0 \end{pmatrix}. \tag{7.46}$$

If $\phi_0$ couples to either $(\bar{s}_L d_R)$ or $(\bar{d}_L s_R)$, and to $(\bar{\mu}_L \mu_R)$, it would contribute to $K_S \to (\mu^+\mu^-)_{\ell=0}$. Without loss of generality, we choose to align the neutral state with the down-type mass eigenstates, The relevant Lagrangian terms are then,

$$\mathcal{L}_\Phi \supset \lambda^d_{ij}\left[\phi_0(\bar{d}_L)_i(d_R)_j + \phi^+(\bar{u}_L)_k V_{ki}(d_R)_j + h.c.\right] + \lambda^e_{22}\left[\phi_0\bar{\mu}_L\mu_R + \phi^+\bar{\nu}_{\mu L}\mu_R + h.c.\right], \tag{7.47}$$

with $(i,j) = (1,2),(2,1)$. After integrating out the $\Phi$ fields, the effective dimension six operators $O_{SLR}, O_{SRL}$ are generated, with coefficients

$$C^\Phi_{SLR} = \frac{\lambda^d_{21}\lambda^{e\,*}_{22}}{M^2_\phi}, \qquad C^\Phi_{SRL} = \frac{\lambda^d_{12}\lambda^{e\,*}_{22}}{M^2_\phi}. \tag{7.48}$$

The contribution to $R(K_S \to \mu^+\mu^-)_{\ell=0}$ is given by Eq. (7.19),

$$R(K_S \to \mu^+\mu^-)^\Phi_{\ell=0} = \left(1 + \frac{m^2_K/m_\mu}{(m_s+m_d)}\frac{(|\lambda^d_{21}\lambda^e_{22}|\sin\Theta_{\phi_{21}} + |\lambda^d_{12}\lambda^e_{22}|\sin\Theta_{\phi_{12}})}{M^2_\phi |C^{\rm SM}_{VLL}|\sin\theta_{ct}}\right)^2, \tag{7.49}$$

where

$$\Theta_{\phi_{21(12)}} \equiv \frac{1}{2}\arg\left(\frac{q}{p}\right) - \arg(\lambda^d_{21(12)}\lambda^{e\,*}_{22})\,. \tag{7.50}$$

In order to saturate the current upper bound, $R(K_S \to \mu^+\mu^-)_{\ell=0} \approx 1280$, we require

$$|\lambda^e_{22}|(|\lambda^d_{21}|\sin\Theta_{\phi_{21}} + |\lambda^d_{12}|\sin\Theta_{\phi_{12}}) \approx 3\cdot 10^{-5}\left(\frac{M_\phi}{\text{TeV}}\right)^2\,. \tag{7.51}$$

This model induces $K^0 - \overline{K}^0$ mixing at tree level. We find the following constraints on the magnitude of couplings [**?**],

$$\begin{aligned} |\lambda^d_{12}|^2,\ |\lambda^d_{21}|^2 \qquad & 10^{-8}\left(\frac{M_\phi}{\text{TeV}}\right)^2\,, \\ |\lambda^d_{12}\lambda^d_{21}| \qquad & 10^{-9}\left(\frac{M_\phi}{\text{TeV}}\right)^2\,. \end{aligned} \tag{7.52}$$

From Eq. (7.51), and assuming a perturbative coupling, $|\lambda^e_{22}|1$, we deduce that in order to saturate the bound we need at least one of the couplings $\lambda^d_{12}, \lambda^d_{21}$ to obey

$$|\lambda^d_{ij}| \geq |\lambda^e_{22}\lambda^d_{ij}|\sin\Theta_{\phi_{ij}} \approx 3\cdot 10^{-5}\left(\frac{M_\phi}{\text{TeV}}\right)^2\,, \tag{7.53}$$

which can be accommodated together with the constraints of Eq. (7.52), independently of $M_\phi$. Loop diagrams involving a muon loop in principle constrain the phases $\Theta_{\phi_{12}}$, $\Theta_{\phi_{21}}$, however, these are strongly suppressed and do not result in relevant bounds.

Models that induce scalar dimension six operators are prone to break the assumption of $|A(K_L)_{\ell=1}| = 0$, since they introduce, in general, both pseudo-scalar (CP-odd) and scalar (CP-even) leptonic currents. We therefore comment on two scenarios:

- Models with $\lambda^d_{12} = \lambda^d_{21}$ :

  In this scenario we have $C_{SLR} = C_{SRL}$, which implies that only the CP-odd leptonic current ($\bar{\mu}\gamma^5\mu$) is generated, and no contribution exists for the $(\mu^+\mu^-)_{\ell=1}$ final state, so that the assumption of $|A(K_L)_{\ell=1}| = 0$ is fulfilled. This ensures that the clean short-distance parameter $|A(K_S)_{\ell=0}|$ can be extracted from the time dependent $K \to \mu^+\mu^-$ rate.

- Models with $\lambda^d_{12} \neq \lambda^d_{21}$ :

  If no symmetry protects $\lambda^d_{12} = \lambda^d_{21}$, this model generally induces $|A(K_L)_{\ell=1}| \neq 0$ (unless $\mathcal{R}e(\lambda^d_{12}\lambda^e_{22}\,(p/q)^{1/2})$, $\mathcal{R}e(\lambda^d_{21}\lambda^e_{22}\,(p/q)^{1/2}) = 0$, that is, $\cos\Theta_{\phi_{12}}$, $\cos\Theta_{\phi_{21}} = 0$). This breaks the assumption needed in order to extract short-distance parameters from the measurement of the interference terms. The observable of Eq. (7.7) is no longer a pure measurement of a short-distance parameter, but is polluted by irreducible long-distance effects.

We conclude that models with a second scalar doublet can significantly enhance the $\mathcal{B}(K_S \to \mu^+\mu^-)_{\ell=0}$ rate, saturating the current experimental bound. If no symmetry protects the relation $\lambda^d_{12} = \lambda^d_{21}$, these models will generally lead to non-zero $|A(K_L)_{\ell=1}|$, which extinguishes the ability to extract $\mathcal{B}(K_S \to \mu^+\mu^-)_{\ell=0}$ from a measurement of $\Gamma_{int.}$. The total rate, $\mathcal{B}(K_S \to \mu^+\mu^-)$, could still exhibit significant enhancement compared to the SM, signaling NP is at play.

## 7.6 Discussion and Conclusion

Following the recent understanding that short-distance parameters of the SM can be cleanly extracted from a measurement of interference effects in $K \to \mu^+\mu^-$ [2, 142], we have addressed the question of what can be learned from such a measurement beyond the SM. Any NP contribution in which the leptonic current is CP-odd, as is the case to a good approximation within the SM, keeps effects of CPV limited to a single partial wave configuration, $(\mu^+\mu^-)_{\ell=0}$, which enables the extraction of the purely short-distance observable, $\mathcal{B}(K_S \to \mu^+\mu^-)_{\ell=0}$. NP that induces also CP-even leptonic currents, as is the case in general when scalar operators are induced, can also result in large enhancements to $\mathcal{B}(K_S \to \mu^+\mu^-)_{\ell=0}$, but would not allow its clean extraction from interference effects.

The current model-independent bound on $\mathcal{B}(K_S \to \mu^+\mu^-)_{\ell=0}$ is determined by the LHCb bound on the total branching ratio and given by

$$R(K_S \to \mu^+\mu^-)_{\ell=0} 1280\,, \tag{7.54}$$

leaving room for enhancement of up to $O(30)$ compared to the SM, at the amplitude level. In the future, LHCb is expected to improve its reach by an order of magnitude, allowing to probe amplitude enhancements of $O(10)$ times the SM contribution.

We note, however, that a measurement of the total branching ratio is a measurement of the sum, $\mathcal{B}(K_S \to \mu^+\mu^-)_{\ell=0} + \mathcal{B}(K_S \to \mu^+\mu^-)_{\ell=1}$. Therefore, while it can probe the existence of large NP contributions, it cannot allow the extraction

of short-distance parameters. A dedicated measurement of $K_S - K_L$ interference effects in $K \to \mu^+\mu^-$ is required in order to obtain a clean evaluation of the pure short-distance quantity, $\mathcal{B}(K_S \to \mu^+\mu^-)_{\ell=0}$.

We have formulated relations between $K_S \to (\mu^+\mu^-)_{\ell=0}$ and $K_L \to \pi^0\bar{\nu}\nu$ within several EFT scenarios. We find that within models with lepton-flavor universality in which a single vectorial dimension six operator is present, involving the lepton doublet, the two modes are correlated. However, if scalar operators are at play, or if more than one vectorial operator is present, the two modes are independent. CPV in additional modes, such as $K_L \to \pi^0\mu^+\mu^-$ and $K_S \to \pi^0\pi^0\mu^+\mu^-$, is expected to have analogous relations. We leave the study of these relations to a future work.

Within specific NP models, constraints from additional observables are relevant, arising from $K^0 - \overline{K}^0$ mixing and from direct searches for NP resonances. We have presented examples of simple explicit models in which large enhancements to $\mathcal{B}(K_S \to \mu^+\mu^-)_{\ell=0}$ are possible. We find that models in which a scalar leptoquark is added to the SM, as well as a 2HDM, can allow large enhancements without violating existing constraints. Of the three models, two can saturate the current experimental bound on $\mathcal{B}(K_S \to \mu^+\mu^-)_{\ell=0}$, while the third is an example where a relation to $\mathcal{B}(K_L \to \pi^0\bar{\nu}\nu)$ implies a constraint coming from the GN bound.

The models we consider, while non-generic, affect the kaon sector alone, and cannot be probed by measurements in other sectors. This provides additional motivation for dedicated kaon programs in next-generation experiments. Initial estimates of the feasibility of reaching SM sensitivity in a measurement of interfer-

ence effects in $K \to \mu^+\mu^-$ in next-generation experiments are very encouraging [2]. Our results indicate that such a measurement would be a unique and potent probe of physics beyond the SM.

CHAPTER 8

# $SU(3)_F$ ANALYSIS OF BEAUTY BARYON DECAYS

## 8.1 Introduction

A tremendous amount of $b$-baryons is produced at the LHC [185]. This allows for angular analyses of $\Lambda_b$ decays at LHCb [240] and ATLAS [241] and has led to evidence of CP violation in $\Lambda_b$ decays [242]. It is now feasible to scrutinize rare or suppressed $b$-baryon decays: Recent results include the first observation of $\Lambda_b \to \Lambda\gamma$ [243] and the analysis of the isospin suppressed $\Lambda_b \to \Sigma^0 J/\psi$ decay and the Cabibbo-suppressed decay $\Xi_b^0 \to \Lambda J/\psi$ [244].

These increasingly precise measurements of baryon decays motivate us to perform an $SU(3)_F$ analysis of $b \to c\bar{c}q$ (with $q = s, d$) decays of the heavy $b$-baryon $\overline{\mathbf{3}}$ to the light baryon $\mathbf{8}$ and an $SU(3)_F$ singlet, $\overline{\mathbf{3}}_b \to \mathbf{8}_b \otimes \mathbf{1}$. From the perspective of $SU(3)_F$ it makes no difference if the singlet, which we denote as $S$, is a $J/\psi$ or any final state particle that does not carry any $SU(3)_F$ flavor, for example, a photon or a lepton pair.

We start our analysis using two separate assumptions: (1) We work in the $SU(3)_F$ limit and (2) we treat the $\Lambda$ and $\Sigma^0$ as isospin eigenstates. We emphasize that these assumptions are not connected to each other. We later relax these assumptions and take into account corrections to the $SU(3)_F$ limit as well as deviations of the mass eigenstates of $\Lambda$ and $\Sigma^0$ from their isospin eigenstates.

At leading order the decays $\overline{\mathbf{3}}_b \to \mathbf{8}_b \otimes \mathbf{1}$ are mediated by tree-level $b \to c\bar{c}q$ transitions. These correspond to a $\mathbf{3}$ operator. In full generality however, we have to take into account additional contributions from loops that generate effective $b \to t\bar{t}q$ and $b \to u\bar{u}q$ transitions. The contribution from $b \to t\bar{t}q$ can be neglected as it is a penguin and therefore suppressed and it gives only another $\mathbf{3}$ under $\mathrm{SU}(3)_F$. In contrast, the up quarks in $b \to u\bar{u}q$ can induce intermediate on-shell states leading to nontrivial effects from rescattering. Specifically, the $b \to u\bar{u}q$ transition has a more complicated isospin and $\mathrm{SU}(3)_F$ structure and induces the higher $\mathrm{SU}(3)_F$ representations $\overline{\mathbf{6}}$ and $\mathbf{15}$. Therefore, as higher $\mathrm{SU}(3)_F$ representations stem from rescattering, in the literature it is often assumed that these are suppressed.

Our strategy is to start with a very general model-independent viewpoint and then introduce additional assumptions step by step. While we mainly concentrate in this chapter on the case where $S = J/\psi$, the general nature of our results make it possible to apply them also to radiative and semileptonic decays.

CKM-leading $\mathrm{SU}(3)_F$ limit Clebsch-Gordan coefficients for $\overline{\mathbf{3}}_b \to \mathbf{8}_b \otimes \mathbf{1}$ in $b \to s$ transitions have been presented in Refs. [245, 246, 247]. In Refs. [246, 248, 249, 250] hadronic models based on QCD factorization have been utilized, and in Refs. [251, 247] a covariant confined quark model has been applied. An $\mathrm{SU}(3)_F$ analysis of $b$-baryon antitriplet decays to the light baryon octet and the $\eta_1$ singlet can be found in Ref. [252].

Further applications of $\mathrm{SU}(3)_F$ to $b$ baryon decays can be found in Refs. [253, 254, 255, 256, 257, 258]. Works on $b$ baryon decays beyond their $\mathrm{SU}(3)_F$ treatment

are given in Refs. [259, 260, 261, 262, 263]. Applications of $SU(3)_F$ methods on non-$b$ baryon decays can be found in Refs. [264, 265, 266, 267, 268, 269, 270, 271, 272, 273, 274, 275]. Further literature on baryon decays is given in Refs. [276, 277, 278]. Discussions of baryonic form factors can be found in Refs. [279, 280, 281, 282, 283, 284, 285, 286, 287, 288].

We present our $SU(3)_F$ analysis including isospin and $SU(3)_F$ breaking in Sec. 8.2. After that we estimate in Sec. 8.3 the effect of $\Sigma^0$–$\Lambda$ mixing in $\Lambda_b$ decays, which is in general scale- and process-dependent, i.e. non-universal. We compare with recent experimental results in Sec. 8.4 and conclude in Sec. 8.5.

## 8.2 $SU(3)_F$ Analysis

### 8.2.1 General $SU(3)_F$ Decomposition

The $b \to c\bar{c}q$ (with $q = s, d$) decays of $\Lambda_b$, $\Xi_b^-$ and $\Xi_b^0$, which form the heavy baryon $\bar{\mathbf{3}}$, into a singlet $S$ (e.g. $S = J/\psi, \gamma, l^+l^-, \ldots$) and a member of the light baryon $\mathbf{8}$, share a common set of reduced $SU(3)_F$ matrix elements after the application of the Wigner-Eckart theorem. These decays are specifically:

- $b \to sc\bar{c}$ transitions:

$$\Lambda_b \to \Lambda S\,, \qquad \Lambda_b \to \Sigma^0 S\,, \qquad \Xi_b^0 \to \Xi^0 S\,, \qquad \Xi_b^- \to \Xi^- S\,. \tag{8.1}$$

- $b \to dc\bar{c}$ transitions:

$$\Xi_b^0 \to \Lambda S\,, \qquad \Xi_b^0 \to \Sigma^0 S\,, \qquad \Lambda_b \to nS\,, \qquad \Xi_b^- \to \Sigma^- S\,. \tag{8.2}$$

Note that there are two additional allowed decays $\Lambda_b \to \Xi^0 J/\psi$ and $\Xi_b^0 \to nJ/\psi$ which are however highly suppressed by two insertions of weak effective operators, so we do not consider them in our study here. The $\mathrm{SU}(3)_F$ quantum numbers and masses are given in Table 8.5. In this section we discuss the $\mathrm{SU}(3)_F$ limit, $\mathrm{SU}(3)_F$-breaking effects are treated in Sec. 8.2.5.

We can write the $\mathrm{SU}(3)_F$ structure of the relevant $b \to s$ and $b \to d$ Hamiltonians as [289]

$$\begin{aligned}
\mathcal{H}^{b\to s} &= \lambda_{cs}(\bar{c}b)(\bar{s}c) + \lambda_{us}(\bar{u}b)(\bar{s}u) + \lambda_{ts}(\bar{t}b)(\bar{s}t) \\
&= \lambda_{cs}\,(\mathbf{3})^c_{0,0,-\frac{2}{3}} + \lambda_{us}\left((\mathbf{3})^u_{0,0,-\frac{2}{3}} + \left(\bar{\mathbf{6}}\right)^u_{1,0,-\frac{2}{3}} + \sqrt{6}\,(\mathbf{15})^u_{1,0,-\frac{2}{3}} + \sqrt{3}\,(\mathbf{15})^u_{0,0,-\frac{2}{3}}\right), \qquad (8.3)\\
\mathcal{H}^{b\to d} &= \lambda_{cd}(\bar{c}b)(\bar{d}c) + \lambda_{ud}(\bar{u}b)(\bar{d}u) + \lambda_{td}(\bar{t}b)(\bar{d}t) \\
&= \lambda_{cd}\,(\mathbf{3})^c_{\frac{1}{2},-\frac{1}{2},\frac{1}{3}} + \lambda_{ud}\left((\mathbf{3})^u_{\frac{1}{2},-\frac{1}{2},\frac{1}{3}} - \left(\overline{\mathbf{6}}\right)^u_{\frac{1}{2},-\frac{1}{2},\frac{1}{3}} + \sqrt{8}\,(\mathbf{15})^u_{\frac{3}{2},-\frac{1}{2},\frac{1}{3}} + (\mathbf{15})^u_{\frac{1}{2},-\frac{1}{2},\frac{1}{3}}\right). \qquad (8.4)
\end{aligned}$$

See also Refs. [290] and [291] for the application of these Hamiltonians to $B \to J/\psi K$ and $B \to DD$, respectively. The notation for the subindices are such that $(\mathbf{N})_{I,I_3,Y}$ refers to the irreducible representation $\mathbf{N}$ of $\mathrm{SU}(3)_F$ using the quantum numbers of strong isospin $I$, $I_3$ and strong hypercharge $Y$. In the standard basis of the Gell-Mann matrices $I_3$ and $Y$ correspond to the eigenvalues of $\lambda_3$ and $\lambda_8$,

respectively. We further use the notation

$$\lambda_{cs} \equiv V_{cb}^* V_{cs} \sim \lambda^2\,, \qquad \lambda_{us} \equiv V_{ub}^* V_{us} \sim \lambda^4\,, \qquad \lambda_{ts} \equiv V_{tb}^* V_{ts} \sim \lambda^2\,, \tag{8.5}$$

$$\lambda_{cd} \equiv V_{cb}^* V_{cd} \sim \lambda^3\,, \qquad \lambda_{ud} \equiv V_{ub}^* V_{ud} \sim \lambda^3\,, \qquad \lambda_{td} \equiv V_{tb}^* V_{td} \sim \lambda^3\,, \tag{8.6}$$

for the CKM matrix element combinations, where we indicate the hierarchies using the Wolfenstein parameter $\lambda$.

Note that in Eqs. (8.3) and (8.4) it is understood that $\mathrm{SU}(3)_F$ operators in front of different CKM matrix elements have to be differentiated as they stem from different underlying operators. For instance, even if the two triplets generate linearly dependent Clebsch-Gordan coefficients, the respective matrix elements themselves are independent. They can, for example, have a relative strong phase.

We write the reduced $\mathrm{SU}(3)_F$ limit matrix elements as $A_q^k$, where $k$ is the respective $\mathrm{SU}(3)_F$ representation in the Hamiltonian and $q$ denotes the operator it stems from. The initial state is always a $|\overline{\mathbf{3}}\rangle$ and the final state is always a $|\mathbf{8}\rangle$, so that we are left with four reduced matrix elements in the $\mathrm{SU}(3)_F$ limit:

$$A_c^3\,, \qquad A_u^3\,, \qquad A_u^{\overline{6}}\,, \qquad A_u^{15}\,. \tag{8.7}$$

The $\mathrm{SU}(3)_F$ limit decomposition is given in Table 8.5. The CKM-leading part of the $b \to s$ transitions agrees with Refs. [245, 246, 247]. The Clebsch-Gordan coefficients are obtained using Refs. [292, 293, 294]. The normalization of the amplitudes is such that

$$\mathcal{B}(B_1 \to B_2 S) = |\mathcal{A}(B_1 \to B_2 S)|^2 \times \mathcal{P}(B_1, B_2, S)\,, \tag{8.8}$$

with the two-body decay phase space factors

$$\mathcal{P}(B_1, B_2, S) \equiv \frac{\tau_{B_1}}{16\pi m_{B_1}^3} \sqrt{(m_{B_1}^2 - (m_{B_2} - m_S)^2)(m_{B_1}^2 - (m_{B_2} + m_S)^2)}\,. \tag{8.9}$$

Note that in cases where the $SU(3)_F$ singlet $S$ is a multibody state, e.g. $S = l^+ l^-$, we imply the appropriate phase space integration in Eq. (8.8). Note further, that we still work in the $SU(3)_F$ limit of the decay amplitudes. Eq. (8.9) only accounts for the trivial $SU(3)_F$ breaking from phase space effects. Additional $SU(3)_F$ breaking contributions are discussed in Sec. 8.2.5. Therein, we estimate $SU(3)_F$ breaking effects to be of order 20%. Note that the amplitudes in Eq. (8.8) have a mass dimension, but we always care about ratios, so we can think about them as dimensionless quantities. Note that phase space effects are of order 3% and thus they are well within the errors and could or could not be taken into account. For a model-dependent way to estimate these effects one can, for example, employ form factor results in Refs. [295, 247].

The reduced $SU(3)_F$ matrix elements can in principle be matched on a color suppressed tree diagram $C$, an exchange diagram $E$ and penguin diagrams $P_q$ with quark $q$ running in the loop. As examples we show the topological diagrams for $\Lambda_b \to \Lambda J/\psi$ and $\Lambda_b \to \Sigma^0 J/\psi$ in Fig. 8.5. In the following, however, we only perform the group theory treatment.

The combined matrix of Clebsch-Gordan coefficients of $b \to s$ and $b \to d$ de-

cays in Table 8.5 has matrix rank four, i.e., there are four sum rules, which read

$$-\sqrt{\frac{3}{2}}\mathcal{A}(\Lambda_b \to \Lambda S) + \frac{1}{\sqrt{2}}\mathcal{A}(\Lambda_b \to \Sigma^0 S) + \mathcal{A}(\Xi_b^0 \to \Xi^0 S) = 0\,, \quad (\mathrm{SU}(3)_F \text{ sum rule}) \tag{8.10}$$

$$\sqrt{\frac{3}{2}}\mathcal{A}(\Xi_b^0 \to \Lambda S) - \frac{1}{\sqrt{2}}\mathcal{A}(\Xi_b^0 \to \Sigma^0 S) + \mathcal{A}(\Lambda_b \to n S) = 0\,, \quad (\mathrm{SU}(3)_F \text{ sum rule}) \tag{8.11}$$

$$-\sqrt{2}\mathcal{A}(\Lambda_b \to \Sigma^0 S)\frac{\lambda_{ud}}{\lambda_{us}} + \sqrt{6}\mathcal{A}(\Xi_b^0 \to \Lambda S) + \mathcal{A}(\Lambda_b \to n S) = 0\,, \quad (\mathrm{SU}(3)_F \text{ sum rule}) \tag{8.12}$$

$$\begin{aligned}\sqrt{\frac{3}{2}}\mathcal{A}(\Lambda_b \to \Lambda S)\frac{\lambda_{ud}}{\lambda_{us}} - \frac{3}{\sqrt{2}}\mathcal{A}(\Lambda_b \to \Sigma^0 S)\frac{\lambda_{ud}}{\lambda_{us}} \\ -\mathcal{A}(\Xi_b^- \to \Xi^- S)\frac{\lambda_{ud}}{\lambda_{us}} + \sqrt{6}\mathcal{A}(\Xi_b^0 \to \Lambda S) + \mathcal{A}(\Xi_b^- \to \Sigma^- S) = 0\,, \quad (\mathrm{SU}(3)_F \text{ sum rule})\end{aligned} \tag{8.13}$$

all of which are $\mathrm{SU}(3)_F$ sum rules, and there is no isospin sum rule. Note that there are two sum rules which mix $b \to s$ and $b \to d$ decays and two which do not. These sum rules are valid in the $\mathrm{SU}(3)_F$ limit irrespective of the power counting of the CKM matrix elements, assumptions on the reduced matrix elements, or the particular $\mathrm{SU}(3)_F$ singlet $S$, i.e. they are completely generic.

### 8.2.2 Assumptions on CKM Hierarchy and Rescattering

We now make some assumptions, which are not completely generic, i.e. their validity can for example depend on the particular considered $\mathrm{SU}(3)_F$ singlet $S$, e.g. if $S = J/\psi$ or $S = \gamma$.

We first neglect the CKM-suppressed amplitude in $b \to s$ decays, that is we set $\lambda_{us}/\lambda_{cs} \to 0$. In the isospin and SU(3)$_F$ limit for $b \to s$ decays we have then only one contributing reduced matrix element:

$$\mathcal{A}(\Lambda_b \to \Sigma^0 S) = 0\,, \qquad \text{(isospin sum rule)} \tag{8.14}$$

$$\mathcal{A}(\Xi_b^0 \to \Xi^0 S) = \mathcal{A}(\Xi_b^- \to \Xi^- S)\,, \qquad \text{(isospin sum rule)} \tag{8.15}$$

$$\mathcal{A}(\Xi_b^0 \to \Xi^0 S) = \sqrt{\frac{3}{2}}\mathcal{A}(\Lambda_b \to \Lambda S)\,. \qquad \text{(SU(3)}_F\text{ sum rule)} \tag{8.16}$$

We now move to make another assumption and that is to also neglect the $\lambda_{ud}$ terms for the $b \to d$ transitions. Despite the formal power counting Eq. (8.6), that is $|\lambda_{ud}| \simeq |\lambda_{cd}|$, numerically we actually have [296]

$$\left|\frac{\lambda_{ud}}{\lambda_{cd}}\right| \approx 0.38\,. \tag{8.17}$$

Moreover, it is plausible that $A_u^{\overline{6}}$ and $A_u^{15}$ are suppressed because they result from light quarks stemming from $b \to u\bar{u}s(d)$ which induce intermediate on-shell states that rescatter into $c\bar{c}$, see also Refs. [297, 298, 299, 300, 301]. Under the assumption that these terms are more or equally suppressed as SU(3)$_F$-breaking effects we have many more relations. All seven non-zero decays we considered in Table 8.5 are then simply related by the Clebsch-Gordan coefficients in the first column. In

addition to the sum rules Eqs. (8.14)–(8.16), we have then

$$\sqrt{2}\,\mathcal{A}(\Xi_b^0 \to \Sigma^0 S) = \mathcal{A}(\Xi_b^- \to \Sigma^- S)\,, \qquad \text{(isospin sum rule)} \tag{8.18}$$

$$\mathcal{A}(\Xi_b^0 \to \Xi^0 S) = -\sqrt{6}\,\mathcal{A}(\Xi_b^0 \to \Lambda S)\frac{\lambda_{cs}}{\lambda_{cd}}\,, \qquad (\mathrm{SU}(3)_F \text{ sum rule}) \tag{8.19}$$

$$-\sqrt{6}\,\mathcal{A}(\Xi_b^0 \to \Lambda S) = \sqrt{2}\,\mathcal{A}(\Xi_b^0 \to \Sigma^0 S)\,, \qquad (\mathrm{SU}(3)_F \text{ sum rule}) \tag{8.20}$$

$$\sqrt{2}\,\mathcal{A}(\Xi_b^0 \to \Sigma^0 S) = \mathcal{A}(\Lambda_b \to nS)\,, \qquad (\mathrm{SU}(3)_F \text{ sum rule}) \tag{8.21}$$

$$\mathcal{A}(\Lambda_b \to nS) = \mathcal{A}(\Xi_b^- \to \Sigma^- S)\,. \qquad (\mathrm{SU}(3)_F \text{ sum rule}) \tag{8.22}$$

### 8.2.3 Isospin and $U$-Spin Decompositions

For comprehensiveness, we give also the isospin and $U$-spin decompositions of the Hamiltonians, which read

$$\mathcal{H}_{b\to s} = \lambda_{cs}(0,0)_I^c + \lambda_{us}\left((0,0)_I^u + (1,0)_I^u\right) \tag{8.23}$$

$$= \lambda_{cs}\left(\frac{1}{2},-\frac{1}{2}\right)_U^c + \lambda_{us}\left(\frac{1}{2},-\frac{1}{2}\right)_U^u\,, \tag{8.24}$$

and

$$\mathcal{H}_{b\to d} = \lambda_{cd}\left(\frac{1}{2},-\frac{1}{2}\right)_I^c + \lambda_{ud}\left(\left(\frac{3}{2},-\frac{1}{2}\right)_I^u + \left(\frac{1}{2},-\frac{1}{2}\right)_I^u\right) \tag{8.25}$$

$$= \lambda_{cd}\left(\frac{1}{2},\frac{1}{2}\right)_U^c + \lambda_{ud}\left(\frac{1}{2},\frac{1}{2}\right)_U^u\,, \tag{8.26}$$

where we use the notation

$$(i,j)_I^q \equiv O^{\Delta I=i}_{\Delta I_3=j}\,, \qquad (i,j)_U^q \equiv O^{\Delta U=i}_{\Delta U_3=j}\,, \tag{8.27}$$

where $q$ denotes the quark content of the operator the representation stems from and we absorbed Clebsch-Gordan coefficients into operators.

Using the isospin and $U$-spin states in Table 8.5, we obtain the isospin decompositions in Tables 8.5 and 8.5 and the $U$-spin decomposition in Table 8.5. We note that the SU(3)$_F$ decomposition includes more information than the isospin and $U$-spin tables each on their own. An example is the ratio

$$\left|\frac{\mathcal{A}(\Xi_b^0 \to \Lambda S)}{\mathcal{A}(\Xi_b^0 \to \Xi^0 S)}\right| = \frac{1}{\sqrt{2}}\left|\frac{\langle 0|\frac{1}{2}|\frac{1}{2}\rangle}{\langle \frac{1}{2}|0|\frac{1}{2}\rangle}\right|\left|\frac{\lambda_{cd}}{\lambda_{cs}}\right| . \tag{8.28}$$

where the appearing reduced matrix elements are not related, e.g. the final states belong to different isospin representations. That means we really need SU(3)$_F$ to find the relation Eq. (8.19).

We can make this completely transparent by writing out the implications of Eq. (8.14) for the corresponding $U$-spin decomposition. From Table 8.5 and Eq. (8.14) it follows for the $U$-spin matrix elements

$$-\frac{\sqrt{3}}{2\sqrt{2}}\left\langle 0\left|\frac{1}{2}\right|\frac{1}{2}\right\rangle^c + \frac{1}{2\sqrt{2}}\left\langle 1\left|\frac{1}{2}\right|\frac{1}{2}\right\rangle^c = 0 . \tag{8.29}$$

Inserting this relation into the $U$-spin decomposition of the decay $\Xi_b^0 \to \Lambda S$ in Table 8.5, we obtain

$$\mathcal{A}(\Xi_b^0 \to \Lambda S) = \frac{1}{\sqrt{6}}\lambda_{cd}\left\langle 1\left|\frac{1}{2}\right|\frac{1}{2}\right\rangle^c . \tag{8.30}$$

Comparing this expression with the $U$-spin decomposition of the decay $\Xi_b^0 \to \Xi^0 S$ in Table 8.5, we arrive again at the sum rule Eq. (8.19).

In order that Eq. (8.19) holds we need not only the suppression of other $SU(3)_F$ limit contributions as discussed above, but also the suppression of both isospin and $U$-spin violating contributions. A non-vanishing dynamic isospin breaking contribution to $\Lambda_b \to \Sigma^0 S$ would also be reflected in isospin and $SU(3)_F$-breaking violations of Eq. (8.19). We make this correlation explicit in Sec. 8.2.5.

### 8.2.4 CP Asymmetry Sum Rules

Due to a general sum rule theorem given in Ref. [302] that relates direct CP asymmetries of decays connected by a complete interchange of $d$ and $s$ quarks [302, 303, 304, 305], we can directly write down two $U$-spin limit sum rules:

$$\frac{a_{CP}^{\rm dir}(\Xi_b^0 \to \Xi^0 S)}{a_{CP}^{\rm dir}(\Lambda_b \to n S)} = -\frac{\tau(\Xi_b^0)}{\tau(\Lambda_b)} \frac{\mathcal{B}(\Lambda_b \to n S)}{\mathcal{B}(\Xi_b^0 \to \Xi^0 S)}\,, \tag{8.31}$$

$$\frac{a_{CP}^{\rm dir}(\Xi_b^- \to \Xi^- S)}{a_{CP}^{\rm dir}(\Xi_b^- \to \Sigma^- S)} = -\frac{\mathcal{B}(\Xi_b^- \to \Sigma^- S)}{\mathcal{B}(\Xi_b^- \to \Xi^- S)}\,, \tag{8.32}$$

where the branching ratios imply CP averaging. Note that the general U-spin rule leading to Eqs. (8.31) and (8.32) also applies to multi-body final states, as pointed out in Refs. [302, 306, 264]. It follows that Eqs. (8.31) and (8.32) apply also when $S$ is a multi-body state like $S = l^+ l^-$.

Note that although the quark content of the $\Lambda$ and $\Sigma$ is $uds$, this does not mean that a complete interchange of $d$ and $s$ quarks gives the identity. The reason is given by the underlying quark wave functions [307]

$$|\Lambda\rangle \sim \frac{1}{\sqrt{2}}\,(ud - du)\,s\,, \qquad |\Sigma^0\rangle \sim \frac{1}{\sqrt{2}}\,(ud + du)\,s\,, \tag{8.33}$$

where we do not write the spin wave function. Eq. (8.33) shows explicitly that a complete interchange of $d$ and $s$ quarks in $\Lambda$ or $\Sigma^0$ does not result again in a $\Lambda$ or $\Sigma^0$ wave function, respectively. This is similar to the situation for $\eta$ and $\eta'$, where no respective particles correspond to a complete interchange of $d$ and $s$ quarks [308], see e.g. the quark wave functions given in Ref. [309].

We can put this into a different language, namely that in the $U$-spin basis the large mixing of $|1,0\rangle_U$ and $|0,0\rangle_U$ to the $U$-spin states of $\Lambda$ and $\Sigma^0$, see Table 8.5, destroys two sum rules which exist for the $U$-spin eigenstates. To be explicit, we define $U$-spin eigenstates which are not close to mass eigenstates

$$|X\rangle = |0,0\rangle_U\,, \quad |Y\rangle = |1,0\rangle_U\,. \tag{8.34}$$

For these, we obtain the $U$-spin decomposition given in Table 8.5. From that it is straightforward to obtain another two CP asymmetry sum rules. These are however impractical, because there is no method available to prepare $\Lambda$ and $\Sigma^0$ as $U$-spin eigenstates, instead of approximate isospin eigenstates. Consequently, we are left only with the two CP asymmetry sum rules Eqs. (8.31) and (8.32).

Note that CKM-leading $\mathrm{SU}(3)_F$ breaking by itself cannot contribute to CP violation, because it comes only with relative strong phases but not with the necessary relative weak phase. Therefore, the individual CP asymmetries can be written as

$$a_{CP}^{\mathrm{dir}} = \mathrm{Im}\frac{\lambda_{uq}}{\lambda_{cq}}\mathrm{Im}\frac{A_u}{A_c}\,, \tag{8.35}$$

where $A_{u,c}$ have only a strong phase and to leading order in Wolfenstein-$\lambda$ we

have [296]

$$\mathrm{Im}\left(\frac{\lambda_{us}}{\lambda_{cs}}\right) \approx \lambda^2\bar{\eta} \approx 0.02\,, \qquad \mathrm{Im}\left(\frac{\lambda_{ud}}{\lambda_{cd}}\right) \approx \bar{\eta} \approx 0.36\,. \tag{8.36}$$

Additional suppression from rescattering implies that on top of Eq. (8.36) we have $|A_u| \ll |A_c|$, i.e. the respective imaginary part is also expected to be small. This implies that we do not expect to see a nonvanishing CP asymmetry in these decays any time soon. The other way around, this prediction is also a test of our assumption that the $\lambda_{uq}$-amplitude is suppressed.

### 8.2.5 SU(3)$_F$ Breaking

We consider now isospin and SU(3)$_F$ breaking effects in the CKM-leading part of the $b \to s$ and $b \to d$ Hamiltonians. This will become useful once we have measurements of several $b$-baryon decays that are precise enough to see deviations from the SU(3)$_F$ limit sum rules. SU(3)$_F$ breaking effects for charm and beauty decays have been discussed in the literature for a long time [310, 311, 264, 312, 313, 314, 315, 316, 317, 290, 318, 319, 320, 321, 322, 323, 314, 324, 320, 310]. They are generated through the spurion $\Phi$, given by

$$\Phi = \begin{pmatrix} \frac{m_u}{\Lambda} - \frac{2}{3}\alpha & 0 & 0 \\ 0 & \frac{m_d}{\Lambda} + \frac{1}{3}\alpha & 0 \\ 0 & 0 & \frac{m_s}{\Lambda} + \frac{1}{3}\alpha \end{pmatrix} \tag{8.37}$$

$$= \frac{1}{3}\frac{m_u + m_d + m_s}{\Lambda}\mathbf{1} - \frac{1}{2}\left(\frac{m_d - m_u}{\Lambda} + \alpha\right)\lambda_3 + \frac{1}{2\sqrt{3}}\left(\frac{m_u + m_d - 2m_s}{\Lambda} - \alpha\right)\lambda_8\,, \tag{8.38}$$

with the unity **1** and the Gell-Mann matrices $\lambda_3$ and $\lambda_8$. The part of Eq. (8.38) that is proportional to 1 can be absorbed into the SU(3)$_F$ limit part. It follows that the isospin and SU(3)$_F$-breaking tensor operator is given as

$$\delta\,(\mathbf{8})_{1,0,0} + \varepsilon\,(\mathbf{8})_{0,0,0}\,, \tag{8.39}$$

with

$$\delta = \frac{1}{2}\left(\frac{m_d - m_u}{\Lambda} + \alpha\right), \qquad \varepsilon = \frac{1}{2\sqrt{3}}\left(\frac{m_u + m_d - 2m_s}{\Lambda} - \alpha\right), \tag{8.40}$$

where $\alpha$ is the electromagnetic coupling and we generically expect the size of isospin and SU(3)$_F$ breaking to be $\delta \sim 1\%$ and $\varepsilon \sim 20\%$, respectively. Note that the scale-dependence of the quark masses, as well as the fact that we do not know how to define the scale $\Lambda$ make it impossible to quote decisive values for $\delta$ and $\varepsilon$. Eventually, they will have to be determined experimentally for each process of interest separately as they are not universal.

For the tensor products of the perturbation with the CKM-leading SU(3)$_F$ limit operator it follows:

$$(\mathbf{8})_{1,0,0} \otimes (\mathbf{3})^c_{0,0,-\frac{2}{3}} = \sqrt{\frac{1}{2}}\,(\overline{\mathbf{6}})_{1,0,-\frac{2}{3}} + \sqrt{\frac{1}{2}}\,(\mathbf{15})_{1,0,-\frac{2}{3}}\,, \tag{8.41}$$

$$(\mathbf{8})_{0,0,0} \otimes (\mathbf{3})^c_{0,0,-\frac{2}{3}} = \frac{1}{2}\,(\mathbf{3})_{0,0,-\frac{2}{3}} + \frac{\sqrt{3}}{2}\,(\mathbf{15})_{0,0,-\frac{2}{3}}\,, \tag{8.42}$$

$$\begin{aligned}(\mathbf{8})_{1,0,0} \otimes (\mathbf{3})^c_{\frac{1}{2},-\frac{1}{2},\frac{1}{3}} = {} & \frac{\sqrt{3}}{4}\,(\mathbf{3})_{\frac{1}{2},-\frac{1}{2},\frac{1}{3}} - \sqrt{\frac{1}{8}}\,(\overline{\mathbf{6}})_{\frac{1}{2},-\frac{1}{2},\frac{1}{3}} \\ & - \sqrt{\frac{1}{48}}\,(\mathbf{15})_{\frac{1}{2},-\frac{1}{2},\frac{1}{3}} + \sqrt{\frac{2}{3}}\,(\mathbf{15})_{\frac{3}{2},-\frac{1}{2},\frac{1}{3}}\,,\end{aligned} \tag{8.43}$$

$$(\mathbf{8})_{0,0,0} \otimes (\mathbf{3})^c_{\frac{1}{2},-\frac{1}{2},\frac{1}{3}} = -\frac{1}{4}\,(\mathbf{3})_{\frac{1}{2},-\frac{1}{2},\frac{1}{3}} - \sqrt{\frac{3}{8}}\,(\overline{\mathbf{6}})_{\frac{1}{2},-\frac{1}{2},\frac{1}{3}} + \frac{3}{4}\,(\mathbf{15})_{\frac{1}{2},-\frac{1}{2},\frac{1}{3}}\,, \tag{8.44}$$

so that we arrive at the $\mathrm{SU}(3)_F$ breaking Hamiltonians

$$\mathcal{H}_X^{b\to s} \equiv \lambda_{cs}\,\delta\left(\sqrt{\frac{1}{2}}\left(\overline{\mathbf{6}}\right)_{1,0,-\frac{2}{3}} + \sqrt{\frac{1}{2}}\left(\mathbf{15}\right)_{1,0,-\frac{2}{3}}\right) + \lambda_{cs}\,\varepsilon\left(\frac{1}{2}\left(\mathbf{3}\right)_{0,0,-\frac{2}{3}} + \frac{\sqrt{3}}{2}\left(\mathbf{15}\right)_{0,0,-\frac{2}{3}}\right), \tag{8.45}$$

$$\mathcal{H}_X^{b\to d} \equiv \lambda_{cd}\,\delta\left(\frac{\sqrt{3}}{4}\left(\mathbf{3}\right)_{\frac{1}{2},-\frac{1}{2},\frac{1}{3}} - \sqrt{\frac{1}{8}}\left(\overline{\mathbf{6}}\right)_{\frac{1}{2},-\frac{1}{2},\frac{1}{3}} - \sqrt{\frac{1}{48}}\left(\mathbf{15}\right)_{\frac{1}{2},-\frac{1}{2},\frac{1}{3}} + \sqrt{\frac{2}{3}}\left(\mathbf{15}\right)_{\frac{3}{2},-\frac{1}{2},\frac{1}{3}}\right) + \lambda_{cd}\,\varepsilon\left(-\frac{1}{4}\left(\mathbf{3}\right)_{\frac{1}{2},-\frac{1}{2},\frac{1}{3}} - \sqrt{\frac{3}{8}}\left(\overline{\mathbf{6}}\right)_{\frac{1}{2},-\frac{1}{2},\frac{1}{3}} + \frac{3}{4}\left(\mathbf{15}\right)_{\frac{1}{2},-\frac{1}{2},\frac{1}{3}}\right). \tag{8.46}$$

This gives rise to three additional matrix elements

$$B^{3}\,, \qquad B^{\overline{6}}\,, \qquad B^{15}\,. \tag{8.47}$$

The CKM-leading decomposition for $b \to s$ and $b \to d$ decays including isospin and $\mathrm{SU}(3)_F$ breaking is given in Table 8.5. The complete $4 \times 4$ matrix of the $b \to s$ matrix has rank four, i.e. there is no $b \to s$ sum rule to this order. As discussed in Sec. 8.2 after Eq. (8.30) we see from Table 8.5 explicitly that isospin breaking contributions to $\mathcal{A}(\Lambda_b \to \Sigma^0 S)$ lead at the same time to a deviation of the ratio $|\mathcal{A}(\Xi_b^0 \to \Lambda S)|/|\mathcal{A}(\Xi_b^0 \to \Xi^0 S)|$ from the result Eq. (8.19).

Comparing to results present in the literature, in Ref. [252] two separate coefficient matrices of $b \to s$ and $b \to d$ decays are given in terms of the isoscalar coefficients, i.e. where the isospin quantum number is still kept in the corresponding reduced matrix element. We improve on that by giving instead the $\mathrm{SU}(3)_F$ Clebsch-Gordan coefficient table that makes transparent the corresponding sum rules in a direct way and furthermore reveals directly the correlations between

$b \to s$ and $b \to d$ decays. We also find the complete set of sum rules, and discuss how further assumptions lead to additional sum rules. We note that the first two sum rules in Eq. (43) in Ref. [252] are sum rules for coefficient matrix vectors but do not apply to the corresponding amplitudes because of the different CKM factors involved.

## 8.3 $\Sigma^0$–$\Lambda$ Mixing in $\Lambda_b$ decays

### 8.3.1 General Considerations

In this section we study the ratio

$$R \equiv \frac{\mathcal{A}(\Lambda_b \to \Sigma^0_{\rm phys} J/\psi)}{\mathcal{A}(\Lambda_b \to \Lambda_{\rm phys} J/\psi)} = \frac{\langle J/\psi \Sigma^0_{\rm phys}|\mathcal{H}|\Lambda_b\rangle}{\langle J/\psi \Lambda_{\rm phys}|\mathcal{H}|\Lambda_b\rangle}\,. \tag{8.48}$$

In order to do this we need the matrix elements appearing in Eq. (8.48). In the limit where isospin is a good symmetry and $\Sigma^0_{\rm phys}$ is an isospin eigenstate, $R$ vanishes, and therefore we are interested in the deviations from that limit. We study leading order effects in isospin breaking.

We first note that we can neglect the deviation of $\Lambda_b$ from its isospin limit. The reason is that regarding the mixing of heavy baryons, for example $\Sigma_b$–$\Lambda_b$, $\Xi_c^0$–$\Xi_c^{\prime 0}$ or $\Xi_c^+$–$\Xi_c^{\prime +}$, in the quark model one obtains a suppression of the mixing angle with the heavy quark mass [325, 326, 327, 328, 329, 330]. It follows that for our purposes we can safely neglect the mixing between $\Lambda_b$ and $\Sigma_b$ as it is not only

isospin suppressed but on top suppressed by the $b$ quark mass.

We now move to discuss the mixing of the light baryons. It has already been pointed out in Ref. [329], that a description with a single mixing angle captures only part of the effect. The reason is because isospin breaking contributions will affect not only the mixing between the states but also the decay amplitude. The non-universality is also reflected in the fact that the $\Lambda_b \to \Sigma^0$ transition amplitude vanishes in the heavy quark limit at large recoil, i.e. in the phase space when $\Sigma^0$ carries away a large fraction of the energy [285], see also Ref. [263] for the heavy quark limit of similar classes of decays.

To leading order in isospin breaking we consider two effects, the mixing between $\Lambda$ and $\Sigma^0$ as well as the correction to the Hamiltonian. We discuss these two effects below.

Starting with the wave function mixing angle $\theta_m$ , this is defined as the mixing angle between the isospin limit states $|\Sigma^0\rangle = |1,0\rangle_I$ and $|\Lambda\rangle = |0,0\rangle_I$, see Eq. (8.33), into the physical states (see Refs. [331, 332, 333, 334, 335, 336])

$$|\Lambda_{\text{phys}}\rangle = \cos\theta_m|\Lambda\rangle - \sin\theta_m|\Sigma^0\rangle\,, \tag{8.49}$$

$$|\Sigma^0_{\text{phys}}\rangle = \sin\theta_m|\Lambda\rangle + \cos\theta_m|\Sigma^0\rangle\,. \tag{8.50}$$

The effect stems from the non-vanishing mass difference $m_d - m_u$ as well as different electromagnetic charges [307] which lead to a hyperfine mixing between the isospin limit states. A similar mixing effect takes place for the light mesons in form of singlet octet mixing of $\pi^0$ and $\eta^{(\prime)}$ [337, 338, 339, 340, 341, 342].

As for the Hamiltonian, we write $\mathcal{H} = \mathcal{H}_0 + \mathcal{H}_1$ where $\mathcal{H}_0$ is the isospin limit one and $\mathcal{H}_1$ is the leading order breaking. In general for decays into final states $\Lambda f$ and $\Sigma^0 f$ we can write

$$\begin{aligned}\langle f\,\Sigma^0_{\rm phys}|\mathcal{H}|\Lambda_b\rangle &= \sin\theta_m\langle f\,\Lambda|\mathcal{H}|\Lambda_b\rangle + \cos\theta_m\langle f\,\Sigma^0|\mathcal{H}|\Lambda_b\rangle \;\approx \\ &\theta_m\langle f\,\Lambda|\mathcal{H}_0|\Lambda_b\rangle + \langle f\,\Sigma^0|\mathcal{H}_1|\Lambda_b\rangle\,, \\ \langle f\,\Lambda_{\rm phys}|\mathcal{H}|\Lambda_b\rangle &= \cos\theta_m\langle f\,\Lambda|\mathcal{H}|\Lambda_b\rangle - \sin\theta_m\langle f\,\Sigma^0|\mathcal{H}|\Lambda_b\rangle \;\approx \langle f\,\Lambda|\mathcal{H}_0|\Lambda_b\rangle\,,\end{aligned} \tag{8.51}$$

where we use the isospin eigenstates $|\Lambda\rangle$ and $|\Sigma^0\rangle$. It follows that we can write

$$R \approx \theta_f \equiv \theta_m + \theta_f^{\rm dyn}\,, \qquad \theta_f^{\rm dyn} \equiv \frac{\langle f\,\Sigma^0|\mathcal{H}_1|\Lambda_b\rangle}{\langle f\,\Lambda|\mathcal{H}_0|\Lambda_b\rangle}. \tag{8.52}$$

We learn that the angle $\theta_f$ has contributions from two sources: A universal part $\theta_m$ from wave function overlap, which we call "static" mixing, and a non-universal contribution $\theta_f^{\rm dyn}$ that we call "dynamic" mixing. We can think of $\theta_f$ as a decay dependent "effective" mixing angle relevant for the decay $\Lambda_b \to \Sigma^0 f$. It follows

$$\frac{\mathcal{B}(\Lambda_b \to \Sigma^0 J/\psi)}{\mathcal{B}(\Lambda_b \to \Lambda J/\psi)} = \frac{\mathcal{P}(\Lambda_b, \Sigma^0, J/\psi)}{\mathcal{P}(\Lambda_b, \Lambda, J/\psi)} \times \left|\theta_f\right|^2\,. \tag{8.53}$$

Our aim in the next section is to find $\theta_f$.

### 8.3.2 Anatomy of $\Sigma^0$–$\Lambda$ Mixing

We start with $\theta_m$. Because of isospin and SU(3)$_F$ breaking effects, the physical states $|\Lambda_{\rm phys}\rangle$ and $|\Sigma^0_{\rm phys}\rangle$ deviate from their decomposition into their SU(3)$_F$ eigen-

states both in the $U$-spin and in the isospin basis. As isospin is the better symmetry, we expect generically the scaling

$$\theta_m \sim \frac{\delta}{\varepsilon} \,. \tag{8.54}$$

This scaling can be seen explicitly in some of the estimates of the effect. In the quark model, the QCD part of the isospin breaking corrections comes from the strong hyperfine interaction generated by the chromomagnetic spin-spin interaction as [327]

$$\theta_m = \frac{\sqrt{3}}{4} \frac{m_d - m_u}{m_s - (m_u + m_d)/2} \,, \tag{8.55}$$

see also Refs. [343, 307, 344, 345, 346, 347], and where constituent quark masses are used. Eq. (8.55) agrees with our generic estimate from group-theory considerations, Eq. (8.54). The same analytic result, Eq. (8.55), is also obtained in chiral perturbation theory [344, 348].

Within the quark model, the mixing angle can also be related to baryon masses via [327, 332, 334]

$$\tan\theta_m = \frac{(m_{\Sigma^0} - m_{\Sigma^+}) - \left(m_n - m_p\right)}{\sqrt{3}(m_\Sigma - m_\Lambda)} \,, \tag{8.56}$$

or equally [327, 349, 334]

$$\tan\theta_m = \frac{(m_{\Xi^-} - m_{\Xi^0}) - (m_{\Xi^{*-}} - m_{\Xi^{*0}})}{2\sqrt{3}(m_\Sigma - m_\Lambda)} \,. \tag{8.57}$$

In Ref. [327] Eqs. (8.55)-(8.57) have been derived within the generic "independent quark model" [**?**, **?**]. Furthermore, Ref. [327] provides SU(3)-breaking corrections to Eq. (8.56) within this model.

Note that Eqs. (8.56) and (8.57) automatically include also QED corrections through the measured baryon masses. Recently, lattice calculations of $\theta_m$ have become available that include QCD and QED effects [336], and which we consider as the most reliable and robust of the quoted results.

The various results for the mixing angle from the literature are summarized in Table 8.5. It turns out that the quark-model predictions agree quite well with modern lattice QCD calculations. Note however, that the lattice result of Ref. [336] (see Table 8.5) demonstrates that the QED correction is large, contrary to the quark model expectation in Ref. [307], and amounts to about 50% of the total result [336].

In the literature the mixing angle has often been assumed to be universal and employed straight forward for the prediction of decays, see Refs. [332, 347, 350, 351]. It was already pointed out in Refs. [347, 352] that the $\Sigma^0$–$\Lambda$ mixing angle can also be extracted from semileptonic $\Sigma^- \to \Lambda l^- \nu$ decays. The angle has also been directly related to the $\pi$–$\eta$ mixing angle [351, 353]. The ratio on the right hand side of Eq. (8.55) can be extracted from $\eta \to 3\pi$ decays [353] or from the comparison of $K^+ \to \pi^0 e^+ \nu_e$ and $K_L^0 \to \pi^- e^+ \nu_e$ [353]. For pseudoscalar mesons it has been shown [354, 355] that the reduction of isospin violation from $(m_d - m_u)/(m_d + m_u)$ to the ratio in Eq. (8.55) is related to the Adler-Bell-Jackiw anomaly [356, 357] of QCD.

Note that in principle also $\theta_m$ is scale dependent [347], as was observed for the similar case of $\pi^0$–$\eta$ mixing in Ref. [358]. Furthermore, $\theta_m$ has an electromagnetic component. Depending on the relevant scale of the process in principle the QED

correction can be large. We see from the lattice results in Table 8.5 that this is the case for $\theta_m$. Very generally, at high energy scales electromagnetic interactions will dominate over QCD ones [359].

### 8.3.3 The Dynamic Contribution

The dynamical contributions to isospin breaking can be parametrized as part of the isospin- and SU(3)$_F$-breaking expansion, see Sec. 8.2.5. Explicitly we found

$$\theta^{\rm dyn}_{J/\psi} \equiv \frac{\langle J/\psi\,\Sigma^0|\mathcal{H}_1|\Lambda_b\rangle}{\langle J/\psi\,\Lambda|\mathcal{H}_0|\Lambda_b\rangle} = \delta \times \left[\sqrt{\frac{1}{5}}\frac{B^{15}}{A_c^3} - \sqrt{\frac{1}{2}}\frac{B^{\bar{6}}}{A_c^3}\right]. \tag{8.58}$$

We expect that $B^{15} \sim B^{\bar{6}} \sim A_c^3$. The important result is that these effects are order $\delta$. Taking everything into account, very schematically we expect therefore the power counting

$$\theta_f \sim \left(\frac{\delta}{\varepsilon}\right)_m + \delta_f \sim \theta_m\left[1 + O(\varepsilon_f)\right]. \tag{8.59}$$

where $\delta_f$ and $\varepsilon_f$ refer to isospin and $SU(3)$ breaking parameters that depend on $f$.

### 8.3.4 Prediction for $\mathcal{B}(\Lambda_b \to \Sigma^0 J/\psi)$

We see from the power counting in Eq. (8.59) that the static component $\theta_m$ dominates, as it is relatively enhanced by the inverse of the size of SU(3)$_F$ breaking. Employing this assumption we obtain for

$$\theta_f \sim \theta_m \sim 1^\circ \tag{8.60}$$

the prediction

$$\left|\frac{\mathcal{A}(\Lambda_b \to \Sigma^0 J/\psi)}{\mathcal{A}(\Lambda_b \to \Lambda J/\psi)}\right| = \left|\theta_f\right| \sim 0.02\,. \tag{8.61}$$

A confirmation of our prediction would imply the approximate universality of the $\Sigma^0$–$\Lambda$ mixing angle in $b$-baryon decays. In that case we would expect that likewise

$$\left|\frac{\mathcal{A}(\Lambda_b \to \Sigma^0 J/\psi)}{\mathcal{A}(\Lambda_b \to \Lambda J/\psi)}\right| = \left|\frac{\mathcal{A}(\Lambda_b \to \Sigma^0 \gamma)}{\mathcal{A}(\Lambda_b \to \Lambda \gamma)}\right| = \left|\frac{\mathcal{A}(\Lambda_b \to \Sigma^0 l^+ l^-)}{\mathcal{A}(\Lambda_b \to \Lambda l^+ l^-)}\right| = \left|\frac{\mathcal{A}(\Sigma_b^0 \to \Lambda J/\psi)}{\mathcal{A}(\Sigma_b^0 \to \Sigma^0 J/\psi)}\right| \sim 0.02\,, \tag{8.62}$$

up to $\mathrm{SU}(3)_F$ breaking. Note that $\Lambda_b$ and $\Sigma_b$ are not in the same $\mathrm{SU}(3)_F$ multiplet, so that there is no relation between their reduced matrix elements.

The above predictions are based on the assumption that the dynamic contribution is smaller by a factor of the order of the SU(3) breaking. In practice, these effects may be large enough to be probed experimentally. Thus, we can hope that precise measurements of these ratios will be able to test these assumptions.

## 8.4 Comparison with recent data

We move to compare the general results of Sections 8.2 and 8.3 to the recent LHCb data for the case $S = J/\psi$ [244]. Particularly relevant to the experimental findings is the sum rule Eq. (8.19) which we rephrase as

$$\left|\frac{\mathcal{A}(\Xi_b^0 \to \Lambda J/\psi)}{\mathcal{A}(\Xi_b^0 \to \Xi^0 J/\psi)}\right| = \frac{1}{\sqrt{6}}\,(1 + O(\varepsilon))\left|\frac{\lambda_{cd}}{\lambda_{cs}}\right| \approx 0.41\,\left|\frac{\lambda_{cd}}{\lambda_{cs}}\right|\,, \tag{8.63}$$

where in the last step we only wrote the central value. The error is expected to be roughly of order $\varepsilon \sim 20\%$. The estimate in Eq. (8.63) agrees very well with the recent measurement [244]

$$\left|\frac{\mathcal{A}(\Xi_b^0 \to \Lambda J/\psi)}{\mathcal{A}(\Xi_b^0 \to \Xi^0 J/\psi)}\right| = (0.44 \pm 0.06 \pm 0.02)\left|\frac{\lambda_{cd}}{\lambda_{cs}}\right| . \tag{8.64}$$

This suggests that the assumptions made in Sec. 8.2 are justified. However, from the $SU(3)_F$-breaking contributions which we calculated in Sec. 8.2.5, we expect generically an order 20% correction to Eq. (8.63). The measurement Eq. (8.64) is not yet precise enough to probe and learn about the size of these corrections. However, $SU(3)_F$ breaking seems also not to be enhanced beyond the generic 20%.

The only other theory result for the ratio Eq. (8.64) that we are aware of in the literature can be obtained from the branching ratios provided in Ref. [247], where a covariant confined quark model has been employed. From the branching ratios given therein we extract the central value

$$\left|\frac{\mathcal{A}(\Xi_b^0 \to \Lambda J/\psi)}{\mathcal{A}(\Xi_b^0 \to \Xi^0 J/\psi)}\right| \sim 0.34\,\frac{\lambda_{cd}}{\lambda_{cs}}\,, \tag{8.65}$$

where an error of $\sim$ 20% is quoted in Ref. [247] for the branching ratios. This estimate is also in agreement with the data, Eq. (8.64) (see for details in Ref. [247]).

Finally, our prediction Eq. (8.61)

$$\left|\frac{\mathcal{A}(\Lambda_b \to \Sigma^0 J/\psi)}{\mathcal{A}(\Lambda_b \to \Lambda J/\psi)}\right| = \left|\theta_f\right| \sim 0.02\,, \tag{8.66}$$

is only about a factor two below the bound provided in Ref. [244],

$$\left|\frac{\mathcal{A}(\Lambda_b \to \Sigma^0 J/\psi)}{\mathcal{A}(\Lambda_b \to \Lambda J/\psi)}\right| < 1/20.9 = 0.048 \quad \text{at } 95\% \text{ CL.} \tag{8.67}$$

A deviation from Eq. (8.61) would indicate the observation of a non-universal contribution to the effective mixing angle, i.e. an enhancement of isospin violation in the dynamical contribution $\theta_{J/\Psi}^{\text{dyn}}$. It seems that a first observation of isospin violation in $\Lambda_b$ decays is feasible for LHCb in the near future.

## 8.5 Conclusions

We perform a comprehensive SU(3)$_F$ analysis of two-body $b \to c\bar{c}s(d)$ decays of the $b$-baryon antitriplet to baryons of the light octet and an SU(3)$_F$ singlet, including a discussion of isospin and SU(3)$_F$ breaking effects as well as $\Sigma^0$–$\Lambda$ mixing. Our formalism allows us to interpret recent results for the case $S = J/\psi$ by LHCb, which do not yet show signs of isospin violation or SU(3)$_F$ breaking. We point out several sum rules which can be tested in the future and give a prediction for the ratios $|\mathcal{A}(\Lambda_b \to \Sigma^0 J/\psi)|/|\mathcal{A}(\Lambda_b \to \Lambda J/\psi)| \sim 0.02$ and $\left|\mathcal{A}(\Xi_b^0 \to \Lambda J/\psi)/\mathcal{A}(\Xi_b^0 \to \Xi^0 J/\psi)\right| \approx 1/\sqrt{6}\left|V_{cb}^* V_{cd}/(V_{cb}^* V_{cs})\right|$. More measurements are needed in order to probe isospin and SU(3)$_F$ breaking corrections to these and many more relations that we laid out in this work.

| Particle | Quark Content | $SU(3)_F$ State | Isospin | $U$-spin | Hadron Mass [MeV] |
|---|---|---|---|---|---|
| $u$ | $u$ | $\|\mathbf{3}\rangle_{\frac{1}{2},\frac{1}{2},\frac{1}{3}}$ | $\|\frac{1}{2},\frac{1}{2}\rangle_I$ | $\|0,0\rangle_U$ | n/a |
| $d$ | $d$ | $\|\mathbf{3}\rangle_{\frac{1}{2},-\frac{1}{2},\frac{1}{3}}$ | $\|\frac{1}{2},-\frac{1}{2}\rangle_I$ | $\|\frac{1}{2},\frac{1}{2}\rangle_U$ | n/a |
| $s$ | $s$ | $\|\mathbf{3}\rangle_{0,0,-\frac{2}{3}}$ | $\|0,0\rangle_I$ | $\|\frac{1}{2},-\frac{1}{2}\rangle_U$ | n/a |
| $\|\Lambda_b\rangle$ | $udb$ | $\|\bar{\mathbf{3}}\rangle_{0,0,\frac{2}{3}}$ | $\|0,0\rangle_I$ | $\|\frac{1}{2},\frac{1}{2}\rangle_U$ | $5619.60 \pm 0.17$ |
| $\|\Xi_b^-\rangle$ | $dsb$ | $\|\bar{\mathbf{3}}\rangle_{\frac{1}{2},-\frac{1}{2},-\frac{1}{3}}$ | $\|\frac{1}{2},-\frac{1}{2}\rangle_I$ | $\|0,0\rangle_U$ | $5797.0 \pm 0.9$ |
| $\|\Xi_b^0\rangle$ | $usb$ | $\|\bar{\mathbf{3}}\rangle_{\frac{1}{2},\frac{1}{2},-\frac{1}{3}}$ | $\|\frac{1}{2},\frac{1}{2}\rangle_I$ | $\|\frac{1}{2},-\frac{1}{2}\rangle_U$ | $5791.9 \pm 0.5$ |
| $\|\Lambda\rangle$ | $uds$ | $\|\mathbf{8}\rangle_{0,0,0}$ | $\|0,0\rangle_I$ | $\frac{\sqrt{3}}{2}\|1,0\rangle_U - \frac{1}{2}\|0,0\rangle_U$ | $1115.683 \pm 0.006$ |
| $\|\Sigma^0\rangle$ | $uds$ | $\|\mathbf{8}\rangle_{1,0,0}$ | $\|1,0\rangle_I$ | $\frac{1}{2}\|1,0\rangle_U + \frac{\sqrt{3}}{2}\|0,0\rangle_U$ | $1192.642 \pm 0.024$ |
| $\|\Sigma^-\rangle$ | $dds$ | $\|\mathbf{8}\rangle_{1,-1,0}$ | $\|1,-1\rangle_I$ | $\|\frac{1}{2},\frac{1}{2}\rangle_U$ | $1197.449 \pm 0.0030$ |
| $\|\Sigma^+\rangle$ | $uus$ | $\|\mathbf{8}\rangle_{1,1,0}$ | $\|1,1\rangle_I$ | $\|\frac{1}{2},-\frac{1}{2}\rangle_U$ | $1189.37 \pm 0.07$ |
| $\|\Xi^0\rangle$ | $uss$ | $\|\mathbf{8}\rangle_{\frac{1}{2},\frac{1}{2},-1}$ | $\|\frac{1}{2},\frac{1}{2}\rangle_I$ | $\|1,-1\rangle_U$ | $1314.86 \pm 0.20$ |
| $\|\Xi^-\rangle$ | $dss$ | $\|\mathbf{8}\rangle_{\frac{1}{2},-\frac{1}{2},-1}$ | $\|\frac{1}{2},-\frac{1}{2}\rangle_I$ | $\|\frac{1}{2},-\frac{1}{2}\rangle_U$ | $1321.71 \pm 0.07$ |
| $\|n\rangle$ | $udd$ | $\|\mathbf{8}\rangle_{\frac{1}{2},-\frac{1}{2},1}$ | $\|\frac{1}{2},-\frac{1}{2}\rangle_I$ | $\|1,1\rangle_U$ | $939.565413 \pm 0.000006$ |
| $\|p\rangle$ | $uud$ | $\|\mathbf{8}\rangle_{\frac{1}{2},\frac{1}{2},1}$ | $\|\frac{1}{2},\frac{1}{2}\rangle_I$ | $\|\frac{1}{2},\frac{1}{2}\rangle_U$ | $938.2720813 \pm 0.0000058$ |
| $\|J/\psi\rangle$ | $c\bar{c}$ | $\|\mathbf{1}\rangle_{0,0,0}$ | $\|0,0\rangle_I$ | $\|0,0\rangle_U$ | $3096.900 \pm 0.006$ |

$SU(3)_F$, isospin and $U$-spin wave functions [292, 360, 296, 361, 362] and masses [296]. For the indices of the $SU(3)_F$ states we use the convention $|\mu\rangle_{I,I_3,Y}$. The lifetimes of the members of the heavy baryon triplet are $\tau_{\Lambda_b}/\tau_{B^0} = 0.964 \pm 0.007$ , where $\tau_{B^0} = (1519 \pm 4) \times 10^{-15} s$ , $\tau_{\Xi_b^0} = (1.480 \pm 0.030) \times 10^{-12}\ s$ , $\tau_{\Xi_b^-} = (1.572 \pm 0.040) \cdot 10^{-12}\ s$ . [296]. Note that the exact form of the $\Sigma^0$–$\Lambda$ mixing is phase convention dependent [362]. Our convention agrees with Refs. [362, 363]. Another convention can be found e.g. in Ref. [364] in the form of $|\Lambda\rangle = \frac{\sqrt{3}}{2}|1,0\rangle_U - \frac{1}{2}|0,0\rangle_U$ and $|\Sigma^0\rangle = -\frac{1}{2}|1,0\rangle_U - \frac{\sqrt{3}}{2}|0,0\rangle_U$ .

| Decay ampl. $\mathcal{A}$ | $A_c^3$ | $A_u^3$ | $A_u^{\overline{6}}$ | $A_u^{15}$ |
|---|---|---|---|---|
| | | $b \to s$ | | |
| $\mathcal{A}(\Lambda_b \to \Lambda S)$ | $\sqrt{\frac{2}{3}}\lambda_{cs}$ | $\sqrt{\frac{2}{3}}\lambda_{us}$ | $0$ | $\sqrt{\frac{6}{5}}\lambda_{us}$ |
| $\mathcal{A}(\Lambda_b \to \Sigma^0 S)$ | $0$ | $0$ | $-\sqrt{\frac{2}{3}}\lambda_{us}$ | $2\sqrt{\frac{2}{5}}\lambda_{us}$ |
| $\mathcal{A}(\Xi_b^0 \to \Xi^0 S)$ | $\lambda_{cs}$ | $\lambda_{us}$ | $\sqrt{\frac{1}{3}}\lambda_{us}$ | $\sqrt{\frac{1}{5}}\lambda_{us}$ |
| $\mathcal{A}(\Xi_b^- \to \Xi^- S)$ | $\lambda_{cs}$ | $\lambda_{us}$ | $-\sqrt{\frac{1}{3}}\lambda_{us}$ | $-\frac{3}{\sqrt{5}}\lambda_{us}$ |
| | | $b \to d$ | | |
| $\mathcal{A}(\Xi_b^0 \to \Lambda S)$ | $-\sqrt{\frac{1}{6}}\lambda_{cd}$ | $-\sqrt{\frac{1}{6}}\lambda_{ud}$ | $-\frac{1}{\sqrt{2}}\lambda_{ud}$ | $\sqrt{\frac{3}{10}}\lambda_{ud}$ |
| $\mathcal{A}(\Xi_b^0 \to \Sigma^0 S)$ | $\frac{1}{\sqrt{2}}\lambda_{cd}$ | $\frac{1}{\sqrt{2}}\lambda_{ud}$ | $-\frac{1}{\sqrt{6}}\lambda_{ud}$ | $\sqrt{\frac{5}{2}}\lambda_{ud}$ |
| $\mathcal{A}(\Lambda_b \to nS)$ | $\lambda_{cd}$ | $\lambda_{ud}$ | $\frac{1}{\sqrt{3}}\lambda_{ud}$ | $\frac{1}{\sqrt{5}}\lambda_{ud}$ |
| $\mathcal{A}(\Xi_b^- \to \Sigma^- S)$ | $\lambda_{cd}$ | $\lambda_{ud}$ | $-\frac{1}{\sqrt{3}}\lambda_{ud}$ | $-\frac{3}{\sqrt{5}}\lambda_{ud}$ |

SU(3)$_F$-limit decomposition.

| $b \to s$ | | | | | | |
|---|---|---|---|---|---|---|
| Decay Ampl. $\mathcal{A}$ | $\langle 0\|0\|0\rangle^c$ | $\langle \frac{1}{2}\|0\|\frac{1}{2}\rangle^c$ | $\langle 0\|0\|0\rangle^u$ | $\langle 1\|1\|0\rangle^u$ | $\langle \frac{1}{2}\|1\|\frac{1}{2}\rangle^u$ | $\langle \frac{1}{2}\|0\|\frac{1}{2}\rangle^u$ |
| $\mathcal{A}(\Lambda_b \to \Lambda S)$ | $\lambda_{cs}$ | $0$ | $\lambda_{us}$ | $0$ | $0$ | $0$ |
| $\mathcal{A}(\Lambda_b \to \Sigma^0 S)$ | $0$ | $0$ | $0$ | $\lambda_{us}$ | $0$ | $0$ |
| $\mathcal{A}(\Xi_b^0 \to \Xi^0 S)$ | $0$ | $\lambda_{cs}$ | $0$ | $0$ | $-\sqrt{\frac{1}{3}}\lambda_{us}$ | $\lambda_{us}$ |
| $\mathcal{A}(\Xi_b^- \to \Xi^- S)$ | $0$ | $\lambda_{cs}$ | $0$ | $0$ | $\sqrt{\frac{1}{3}}\lambda_{us}$ | $\lambda_{us}$ |

Isospin decomposition for $b \to s$ transitions.

| $b \to d$ | | | | | | | |
|---|---|---|---|---|---|---|---|
| Decay ampl. $\mathcal{A}$ | $\langle 0\|\frac{1}{2}\|\frac{1}{2}\rangle^c$ | $\langle 0\|\frac{1}{2}\|\frac{1}{2}\rangle^u$ | $\langle 1\|\frac{1}{2}\|\frac{1}{2}\rangle^c$ | $\langle 1\|\frac{1}{2}\|\frac{1}{2}\rangle^u$ | $\langle \frac{1}{2}\|\frac{1}{2}\|0\rangle^c$ | $\langle \frac{1}{2}\|\frac{1}{2}\|0\rangle^u$ | $\langle 1\|\frac{3}{2}\|\frac{1}{2}\rangle^u$ |
| $\mathcal{A}(\Xi_b^0 \to \Lambda S)$ | $-\frac{1}{\sqrt{2}}\lambda_{cd}$ | $-\frac{1}{\sqrt{2}}\lambda_{ud}$ | $0$ | $0$ | $0$ | $0$ | $0$ |
| $\mathcal{A}(\Xi_b^0 \to \Sigma^0 S)$ | $0$ | $0$ | $\frac{1}{\sqrt{2}}\lambda_{cd}$ | $\frac{1}{\sqrt{2}}\lambda_{ud}$ | $0$ | $0$ | $-\frac{1}{\sqrt{2}}\lambda_{ud}$ |
| $\mathcal{A}(\Lambda_b \to nS)$ | $0$ | $0$ | $0$ | $0$ | $\lambda_{cd}$ | $\lambda_{ud}$ | $0$ |
| $\mathcal{A}(\Xi_b^- \to \Sigma^- S)$ | $0$ | $0$ | $\lambda_{cd}$ | $\lambda_{ud}$ | $0$ | $0$ | $\frac{1}{2}\lambda_{ud}$ |

Isospin decomposition for $b \to d$ transitions.

| Decay ampl. $\mathcal{A}$ | $\langle 0\vert\frac{1}{2}\vert\frac{1}{2}\rangle^c$ | $\langle 0\vert\frac{1}{2}\vert\frac{1}{2}\rangle^u$ | $\langle 1\vert\frac{1}{2}\vert\frac{1}{2}\rangle^c$ | $\langle 1\vert\frac{1}{2}\vert\frac{1}{2}\rangle^u$ | $\langle\frac{1}{2}\vert\frac{1}{2}\vert 0\rangle^c$ | $\langle\frac{1}{2}\vert\frac{1}{2}\vert 0\rangle^u$ |
|---|---|---|---|---|---|---|
| | | | $b \to s$ | | | |
| $\mathcal{A}(\Lambda_b \to \Lambda S)$ | $\frac{1}{2\sqrt{2}}\lambda_{cs}$ | $\frac{1}{2\sqrt{2}}\lambda_{us}$ | $\frac{\sqrt{3}}{2\sqrt{2}}\lambda_{cs}$ | $\frac{\sqrt{3}}{2\sqrt{2}}\lambda_{us}$ | 0 | 0 |
| $\mathcal{A}(\Lambda_b \to \Sigma^0 S)$ | $-\frac{\sqrt{3}}{2\sqrt{2}}\lambda_{cs}$ | $-\frac{\sqrt{3}}{2\sqrt{2}}\lambda_{us}$ | $\frac{1}{2\sqrt{2}}\lambda_{cs}$ | $\frac{1}{2\sqrt{2}}\lambda_{us}$ | 0 | 0 |
| $\mathcal{A}(\Xi_b^0 \to \Xi^0 S)$ | 0 | 0 | $\lambda_{cs}$ | $\lambda_{us}$ | 0 | 0 |
| $\mathcal{A}(\Xi_b^- \to \Xi^- S)$ | 0 | 0 | 0 | 0 | $\lambda_{cs}$ | $\lambda_{us}$ |
| | | | $b \to d$ | | | |
| $\mathcal{A}(\Xi_b^0 \to \Lambda S)$ | $-\frac{1}{2\sqrt{2}}\lambda_{cd}$ | $-\frac{1}{2\sqrt{2}}\lambda_{ud}$ | $\frac{\sqrt{3}}{2\sqrt{2}}\lambda_{cd}$ | $\frac{\sqrt{3}}{2\sqrt{2}}\lambda_{ud}$ | 0 | 0 |
| $\mathcal{A}(\Xi_b^0 \to \Sigma^0 S)$ | $\frac{\sqrt{3}}{2\sqrt{2}}\lambda_{cd}$ | $\frac{\sqrt{3}}{2\sqrt{2}}\lambda_{ud}$ | $\frac{1}{2\sqrt{2}}\lambda_{cd}$ | $\frac{1}{2\sqrt{2}}\lambda_{ud}$ | 0 | 0 |
| $\mathcal{A}(\Lambda_b \to nS)$ | 0 | 0 | $\lambda_{cd}$ | $\lambda_{ud}$ | 0 | 0 |
| $\mathcal{A}(\Xi_b^- \to \Sigma^- S)$ | 0 | 0 | 0 | 0 | $\lambda_{cd}$ | $\lambda_{ud}$ |

$U$-spin decomposition.

| Decay ampl. $\mathcal{A}$ | $\langle 0\vert\frac{1}{2}\vert\frac{1}{2}\rangle^c$ | $\langle 0\vert\frac{1}{2}\vert\frac{1}{2}\rangle^u$ | $\langle 1\vert\frac{1}{2}\vert\frac{1}{2}\rangle^c$ | $\langle 1\vert\frac{1}{2}\vert\frac{1}{2}\rangle^u$ | $\langle\frac{1}{2}\vert\frac{1}{2}\vert 0\rangle^c$ | $\langle\frac{1}{2}\vert\frac{1}{2}\vert 0\rangle^u$ |
|---|---|---|---|---|---|---|
| | | | $b \to s$ | | | |
| $\mathcal{A}(\Lambda_b \to XS)$ | $-\frac{1}{\sqrt{2}}\lambda_{cs}$ | $-\frac{1}{\sqrt{2}}\lambda_{us}$ | 0 | 0 | 0 | 0 |
| $\mathcal{A}(\Lambda_b \to YS)$ | 0 | 0 | $\frac{1}{\sqrt{2}}\lambda_{cs}$ | $\frac{1}{\sqrt{2}}\lambda_{us}$ | 0 | 0 |
| | | | $b \to d$ | | | |
| $\mathcal{A}(\Xi_b^0 \to XS)$ | $\frac{1}{\sqrt{2}}\lambda_{cd}$ | $\frac{1}{\sqrt{2}}\lambda_{ud}$ | 0 | 0 | 0 | 0 |
| $\mathcal{A}(\Xi_b^0 \to YS)$ | 0 | 0 | $\frac{1}{\sqrt{2}}\lambda_{cd}$ | $\frac{1}{\sqrt{2}}\lambda_{ud}$ | 0 | 0 |

(Unpractical) $U$-spin decomposition for the $U$-spin eigenstates $|X\rangle$ and $|Y\rangle$, see Eq. (8.34) and discussion in the text.

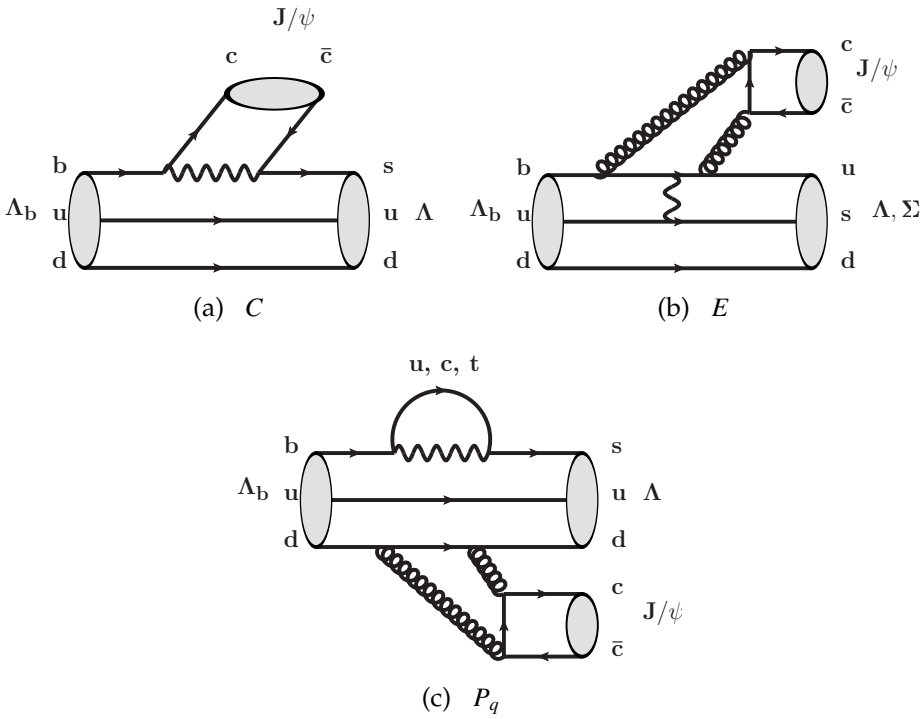


Topological diagrams for the decays $\Lambda_b \to \Lambda J/\psi$ and $\Lambda_b \to \Sigma J/\psi$. Note that in the exchange diagram one gluon alone can not create the $J/\psi$ because it is a color singlet.

| Method | Mixing Angle $\theta_m$ [°] | Ref. |
|---|---|---|
| Quark model: Relation to Baryon masses | 0.86 ± 0.06 | [332, 334] |
| Quark model: Hyperfine splitting + EM interactions | $\simeq$ 0.57 | [307] |
| Lattice QCD+QED A | 1.00 ± 0.32 | [336] |
| Lattice QCD+QED B | 0.96 ± 0.31 | [336] |
| Lattice QCD without QED | 0.55 ± 0.03 | [336] |

Results for the $\Sigma^0$–$\Lambda$ mixing angle. Note that we adjusted the sign conventions for the results to match always the one of Ref. [332], see also the corresponding comment in Ref. [336]. For older lattice results for the "QCD only" scenario see Refs. [333, 335]. Note that with alternate quark mass input taken from Ref. [202] the result for the "Lattice QCD without QED" scenario is changed to $\theta_m = 0.65 \pm 0.03$ [336].

| Decay ampl. $\mathcal{A}$ | $A_c^3$ | $B^3$ | $B^{15}$ | $B^{\bar{6}}$ |
|---|---|---|---|---|
| | | $b \to s$ | | |
| $\mathcal{A}(\Lambda_b \to \Lambda S)/\lambda_{cs}$ | $\sqrt{\frac{2}{3}}$ | $\frac{1}{2}\sqrt{\frac{1}{3}}\,\varepsilon$ | $\sqrt{\frac{3}{10}}\,\varepsilon$ | $0$ |
| $\mathcal{A}(\Lambda_b \to \Sigma^0 S)/\lambda_{cs}$ | $0$ | $0$ | $\sqrt{\frac{2}{15}}\,\delta$ | $-\sqrt{\frac{1}{3}}\,\delta$ |
| $\mathcal{A}(\Xi_b^0 \to \Xi^0 S)/\lambda_{cs}$ | $1$ | $\frac{1}{2}\,\varepsilon$ | $\sqrt{\frac{1}{15}}\,\delta - \frac{1}{2\sqrt{5}}\,\varepsilon$ | $\sqrt{\frac{1}{6}}\,\delta$ |
| $\mathcal{A}(\Xi_b^- \to \Xi^- S)/\lambda_{cs}$ | $1$ | $\frac{1}{2}\,\varepsilon$ | $-\sqrt{\frac{1}{15}}\,\delta - \frac{1}{2\sqrt{5}}\,\varepsilon$ | $-\sqrt{\frac{1}{6}}\,\delta$ |
| | | $b \to d$ | | |
| $\mathcal{A}(\Xi_b^0 \to \Lambda S)/\lambda_{cd}$ | $-\frac{1}{\sqrt{6}}$ | $-\frac{1}{4\sqrt{2}}\delta + \frac{1}{4\sqrt{6}}\varepsilon$ | $-\frac{1}{4\sqrt{10}}\delta + \frac{3}{4}\sqrt{\frac{3}{10}}\varepsilon$ | $-\frac{1}{4}\delta - \frac{\sqrt{3}}{4}\varepsilon$ |
| $\mathcal{A}(\Xi_b^0 \to \Sigma^0 S)/\lambda_{cd}$ | $\frac{1}{\sqrt{2}}$ | $\frac{1}{4}\sqrt{\frac{3}{2}}\delta - \frac{1}{4\sqrt{2}}\varepsilon$ | $\frac{11}{4\sqrt{30}}\delta - \frac{1}{4\sqrt{10}}\varepsilon$ | $-\frac{1}{4\sqrt{3}}\delta - \frac{1}{4}\varepsilon$ |
| $\mathcal{A}(\Lambda_b \to n S)/\lambda_{cd}$ | $1$ | $\frac{\sqrt{3}}{4}\delta - \frac{1}{4}\varepsilon$ | $-\frac{1}{4\sqrt{15}}\delta + \frac{3}{4\sqrt{5}}\varepsilon$ | $\frac{1}{2\sqrt{6}}\delta + \frac{1}{2\sqrt{2}}\varepsilon$ |
| $\mathcal{A}(\Xi_b^- \to \Sigma^- S)/\lambda_{cd}$ | $1$ | $\frac{\sqrt{3}}{4}\delta - \frac{1}{4}\varepsilon$ | $-\frac{1}{4}\sqrt{\frac{5}{3}}\delta - \frac{1}{4\sqrt{5}}\varepsilon$ | $-\frac{1}{2\sqrt{6}}\delta - \frac{1}{2\sqrt{2}}\varepsilon$ |

CKM-leading SU(3)$_F$ decomposition including isospin- and SU(3)$_F$-breaking.

APPENDIX A

# ATOMIC PARITY VIOLATION AND THE NEUTRINO FORCE

## A.1 Calculation of the parity violating force between the electron and the proton

Our approach here closely follows the methodology of [7]. For the sake of simplicity, we start by assuming just one flavor for the neutrino. In that case we find the following four-Fermi operator for two fermions of type $\psi$ and two neutrinos by summing over the $Z$ and $W$ diagrams:

$$O_4 = -\frac{G_F}{\sqrt{2}}[\bar{\psi}\gamma^\mu(a^\psi - b^\psi\gamma^5)\psi][\bar{\nu}\gamma_\mu(1-\gamma^5)\nu], \tag{A.1}$$

where $a^\psi$ and $b^\psi$ are the effective couplings to the $Z$ as defined in Eqs. (2.20) and (2.21). They depend on the particular fermion in question, depending on whether the $W$ exchange contributes, the $Z$ exchange contributes, or both.

The two-neutrino potential can be calculated by a double insertion of this operator, and the evaluation of the resulting amplitude, and by taking the Fourier transform of the amplitude. The Feynman diagram that is relevant is given in Fig. 2.1. The corresponding matrix element is given by

$$i\mathcal{M} = -\frac{(-iG_F)^2}{2}\bar{e}\bar{N}\left[\Gamma^e_\mu\Gamma^N_\nu\right]\int\frac{\mathrm{d}^4k\mathrm{d}^4k'}{(2\pi)^4}\delta^4(q-k-k')\mathrm{Tr}\left[i\Gamma^\mu\frac{i(-\not{k}'+m)}{k'^2-m^2}i\Gamma^\nu\frac{i(\not{k}+m)}{k^2-m^2}\right]eN. \tag{A.2}$$

Here, $\Gamma^f_\mu = \gamma_\mu(a_f - b_f\gamma^5)$, with $a_f$ and $b_f$ depending on the type of fermion in question. $N$ stands for nucleus, which in our case is just the proton. We can write the matrix element as $i\mathcal{M} = \bar{e}\bar{N}iFeN$, where:

$$F = -i\frac{G_F^2}{2}\left[\Gamma^e_\mu\Gamma^N_\nu\right]\int\frac{\mathrm{d}^4k\mathrm{d}^4k'}{(2\pi)^4}\delta^4(q-k-k')\mathrm{Tr}\left[\Gamma^\mu\frac{(-\not{k}'+m)}{k'^2-m^2}\Gamma^\nu\frac{(\not{k}+m)}{k^2-m^2}\right]. \tag{A.3}$$

We then evaluate the trace, and consider only the symmetric part, since the anti-symmetric part is odd in $k$, and hence evaluates to 0 in the loop integral,

$$\begin{aligned} F &= i\frac{G_F^2}{2}\left[\Gamma^e_\mu\Gamma^N_\nu\right]2\mathrm{Tr}\left[\gamma^\mu\gamma^\rho\gamma^\nu\gamma^\sigma\right]\int\frac{\mathrm{d}^4k\mathrm{d}^4k'}{(2\pi)^4}\delta^4(q-k-k')\frac{k_\sigma k'_\rho}{(k^2-m^2)(k'^2-m^2)}, \qquad \text{(A.4)}\\ &= i\frac{G_F^2}{2}\left[\Gamma^e_\mu\Gamma^N_\nu\right]C^{\mu\nu;\rho\sigma}I_{\sigma\rho}, \end{aligned}$$

where,

$$C^{\mu\nu;\rho\sigma} \equiv 2\mathrm{Tr}\left[\gamma^\mu\gamma^\rho\gamma^\nu\gamma^\sigma\right], \tag{A.5}$$

$$I_{\sigma\rho} \equiv \int\frac{\mathrm{d}^4k\mathrm{d}^4k'}{(2\pi)^4}\delta^4(q-k-k')\frac{k_\sigma k'_\rho}{(k^2-m^2)(k'^2-m^2)} = A'g_{\rho\sigma} + B'q_\sigma q_\rho. \tag{A.6}$$

We can therefore write, after contracting $I_{\sigma\rho}$ with $g_{\rho\sigma}$ and $q_\sigma q_\rho$ respectively,

$$4A' + B't = \int\frac{\mathrm{d}^4k\mathrm{d}^4k'}{(2\pi)^4}\delta^4(q-k-k')\frac{k.k'}{(k^2-m^2)(k'^2-m^2)} \equiv J_0, \tag{A.7}$$

$$A't + B't^2 = \int\frac{\mathrm{d}^4k\mathrm{d}^4k'}{(2\pi)^4}\delta^4(q-k-k')\frac{(q.k)(q.k')}{(k^2-m^2)(k'^2-m^2)} \equiv J_1, \tag{A.8}$$

where $t$ is the Mandelstam variable.

To calculate the force, we find the discontinuity in the matrix element across the branch cut in the complex $t$ plane, using the Cutkosky cutting rules, which

yields

$$\tilde{J}_0 = -\frac{1}{(2\pi)^2}\int \mathrm{d}^4k\mathrm{d}^4k'\delta^4(q-k-k')\theta(k^0)\theta(k'^0)\delta(k^2-m^2)\delta(k'^2-m^2)(k\cdot k'), \quad (A.9)$$

$$\tilde{J}_1 = -\frac{1}{(2\pi)^2}\int \mathrm{d}^4k\mathrm{d}^4k'\delta^4(q-k-k')\theta(k^0)\theta(k'^0)\delta(k^2-m^2)\delta(k'^2-m^2)(k\cdot q)(k'\cdot q), \quad (A.10)$$

Here, the tilde denotes the discontinuity of a quantity across the branch cut. Writing

$$C^{\mu\nu;\rho\sigma}\left(A' g_{\rho\sigma} + B' q_\sigma q_\rho\right) = A g^{\mu\nu} + B' q^\mu q^\nu,$$

we obtain

$$A = -8\,(2A' + B' t), \quad B = 16\,B'. \quad (A.11)$$

We have then,

$$F = i\frac{G_F^2}{2}\left(\Gamma^e\cdot\Gamma^N A + q^\mu q^\nu \Gamma^e_\mu \Gamma^N_\nu B\right), \quad (A.12)$$

$$\tilde{F} = i\frac{G_F^2}{2}\left(\Gamma^e\cdot\Gamma^N \tilde{A} + q^\mu q^\nu \Gamma^e_\mu \Gamma^N_\nu \tilde{B}\right). \quad (A.13)$$

What we need is to calculate the discontinuity in the matrix element since the spectral function $\rho$ is given by:

$$\rho = \frac{\tilde{\mathcal{M}}}{2i}. \quad (A.14)$$

We evaluate the integrals above in the CM frame of momentum transfer, i.e, the frame where $q = (\sqrt{t}, 0, 0, 0)$, and hence $k = (\omega, \vec{k})$, $k' = (\omega', -\vec{k})$.

Performing the integrals, in the case of equal masses of the neutrino in both propagators of the loop, we have

$$\tilde{J}_0 = -\frac{1}{16\pi}\sqrt{1-\frac{4m^2}{t}}(t-2m^2), \quad \tilde{J}_1 = -\frac{t^2}{32\pi}\sqrt{1-\frac{4m^2}{t}}. \quad (A.15)$$

Which yields

$$\tilde{A}' = -\sqrt{1-\frac{4m^2}{t}}\left(\frac{t-4m^2}{96\pi}\right), \quad \tilde{B}' = -\sqrt{1-\frac{4m^2}{t}}\left(\frac{t^2+2m^2t}{32\pi t^2}\right), \tag{A.16}$$

and translates to

$$\tilde{A} = \sqrt{1-\frac{4m^2}{t}}\left(\frac{t-m^2}{3\pi}\right), \quad \tilde{B} = -\sqrt{1-\frac{4m^2}{t}}\left(\frac{1+\frac{2m^2}{t}}{3\pi}\right). \tag{A.17}$$

We now need to deal with Eq. (A.13), and evaluate the spinor products in the non-relativistic limit. For the purpose of calculating the velocity-dependent terms in the potential, it is necessary to evaluate the spinors upto first order in momentum $\vec{p}$. This calculation seems most convenient in the Pauli-Dirac basis where the non-relativistic limit is much easier to work with. In the Pauli-Dirac basis, a Dirac spinor is given by

$$u_s(\vec{p}) = \sqrt{p^0+m}\begin{pmatrix} \xi_s \\ \frac{\vec{\sigma}\cdot\vec{p}}{p^0+m}\xi_s \end{pmatrix}. \tag{A.18}$$

The gamma matrices, in this basis, are given by

$$\gamma^0 = \begin{pmatrix} \mathbf{1} & 0 \\ 0 & -\mathbf{1} \end{pmatrix}, \quad \gamma^i = \begin{pmatrix} 0 & \sigma^i \\ -\sigma^i & 0 \end{pmatrix}, \quad \gamma^5 = \begin{pmatrix} 0 & \mathbf{1} \\ \mathbf{1} & 0 \end{pmatrix}. \tag{A.19}$$

In the non-relativistic limit, $p^0 + m \to 2m$, and therefore, for the electron,

$$u_s(\vec{p}) \approx \sqrt{2m}\begin{pmatrix} \xi_s \\ \frac{\vec{\sigma}\cdot\vec{p}}{2m}\xi_s \end{pmatrix} = \sqrt{2m}\begin{pmatrix} \xi_s \\ \frac{\vec{\sigma}\cdot\vec{v}}{2}\xi_s \end{pmatrix}, \tag{A.20}$$

where $\xi_s$ is a 2-component vector that encodes the spin state. For the nucleus, which has mass $M \gg m$, we can write

$$u_r(\vec{p}) \approx \sqrt{2M}\begin{pmatrix} \xi_r \\ 0 \end{pmatrix}. \tag{A.21}$$

We use the above approximation for evaluating $\mathcal{M}$. Our plan is to evaluate the integral that gives us the long-range potential from the spectral function.

The $q_\mu q_\nu$ term does not give a parity violating term when evaluated explicitly using spinors. Thus, we only need to evaluate the $\Gamma^e \cdot \Gamma^N$ term. We suppress writing the spin states $\xi$, and assume that the incoming and outgoing electrons have 3-momenta $\vec{p}$ and $\vec{p}\,'$ respectively, while the incoming and outgoing nuclei have 3-momenta $\vec{k}$ and $\vec{k}'$ (note, as usual that $q = p - p' = k' - k$, let us not confuse the $k$'s here with the integration variables used before — those $k$'s have no relevance in the upcoming discussion). To compute the leading radial dependence of the potential, we need the spin and momentum independent parity conserving term in $F$. This is found to be $2im_eMa_ea_NG_F^2A$. The discontinuity in the matrix element for the spin-independent part is

$$\tilde{\mathcal{M}} = 2m_eMia_ea_NG_F^2\tilde{A} = 2m_eMia_ea_NG_F^2\sqrt{1-\frac{4m^2}{t}}\left(\frac{t-m^2}{3\pi}\right). \tag{A.22}$$

The spectral function is therefore (ignoring the spin states)

$$\rho(t) \;=\; \frac{\tilde{\mathcal{M}}}{2i} = m_eMa_ea_NG_F^2\sqrt{1-\frac{4m^2}{t}}\left(\frac{t-m^2}{3\pi}\right). \tag{A.23}$$

Thus, the spin-independent parity conserving potential is given by the formula

$$\begin{aligned} V(r) &= \frac{1}{16\pi^2 m_eMr}\int_{t_0}^{\infty} \mathrm{d}t\,\rho(t)e^{-\sqrt{t}r}, \\ &= \frac{m_eMa_ea_NG_F^2}{16\pi^2 m_eMr}\int_{4m^2}^{\infty}\mathrm{d}t\,e^{-\sqrt{t}r}\sqrt{1-\frac{4m^2}{t}}\left(\frac{t-m^2}{3\pi}\right), \\ &= \frac{a_ea_NG_F^2}{4\pi^3}\frac{m^3K_3(2mr)}{r^2}, \\ &= a_ea_NV_{\gamma\gamma}(r), \end{aligned} \tag{A.24}$$

where $V_{\nu\nu}(r)$ is given in Eq. (2.2) (the Dirac case).

We also calculate the parity violating parts, as below:

$$\frac{\bar{e}\bar{N}\Gamma^e.\Gamma^N eN}{4m_e M} \supset a_N b_e \left(\frac{1}{2m_e}+\frac{1}{2M}\right)\vec{\sigma}_e\cdot\vec{q} - a_e b_N\left(\frac{1}{2m_e}+\frac{1}{2M}\right)\vec{\sigma}_N\cdot\vec{q} + \frac{a_e b_N}{m_e}\vec{\sigma}_N\cdot\vec{p} - \frac{a_N b_e}{m_e}\vec{\sigma}_e\cdot\vec{p} + i\left(\frac{a_e b_N}{2m_e}+\frac{a_N b_e}{2M}\right)\vec{\sigma}_e\cdot(\vec{\sigma}_N\times\vec{q}). \tag{A.25}$$

The parity violating parts of $F$ are therefore given by:

$$\frac{F}{2iG_F^2 m_e M} \supset \left[a_N b_e\left(\frac{1}{2m_e}+\frac{1}{2M}\right)\vec{\sigma}_e\cdot\vec{q}\right]A - \left[a_e b_N\left(\frac{1}{2m_e}+\frac{1}{2M}\right)\vec{\sigma}_N\cdot\vec{q}\right]A + \left[\frac{a_e b_N}{m_e}\vec{\sigma}_N\cdot\vec{p}\right]A - \left[\frac{a_N b_e}{m_e}\vec{\sigma}_e\cdot\vec{p}\right]A + i\left[\left(\frac{a_e b_N}{2m_e}+\frac{a_N b_e}{2M}\right)\vec{\sigma}_e\cdot(\vec{\sigma}_N\times\vec{q})\right]A. \tag{A.26}$$

$V_{\nu\nu}(r)$ is basically the Fourier transform of the spin-independent part of the matrix element $\mathcal{M}$, i.e, it can be thought of as the Fourier transform of $A$, upto the non-relativistic normalization of the Dirac spinors. But observe that the spin-dependent part of the matrix element is obtained by multiplying the spin independent term $A$ to the terms in Eq. (A.25). Thus, to obtain the spin dependent parts of the potential, we need to take the Fourier transforms of quantities such as $(\vec{\sigma}\cdot\vec{q})A$ and so on. In essence, we replace $\vec{q}$ 's by gradients.

Let us look at the particular case of the hydrogen atom. We incorporate flavor mixing as in sec. 2.4, and get the couplings $a^e_{ii}$, $b^e_{ii}$, $a^p_{ii}$ and $b^p_{ii}$ as in Eq. (2.28).

For sake of cleanliness, below we drop one index $i$ from the above couplings, since no sum is assumed anyway. The analog of Eq. (A.25) in the hydrogen atom

is therefore (the Hermitian conjugate is implicitly added)

$$\begin{aligned}\frac{\bar{e}\bar{P}\Gamma^e.\Gamma^P eP}{4m_e m_p} &= a_i^p b_i^e\left(\frac{1}{2m_e}+\frac{1}{2m_p}\right)\vec{\sigma}_e\cdot\vec{q} - a_i^e b_i^p\left(\frac{1}{2m_e}+\frac{1}{2m_p}\right)\vec{\sigma}_p\cdot\vec{q} + \frac{a_i^e b_i^p}{m_e}\vec{\sigma}_p\cdot\vec{p} \\ &\quad - \frac{a_i^p b_i^e}{m_e}\vec{\sigma}_e\cdot\vec{p} + i\left(\frac{a_i^e b_i^p}{2m_e}+\frac{a_i^p b_i^e}{2m_p}\right)\vec{\sigma}_e\cdot(\vec{\sigma}_p\times\vec{q}), \\ &\approx \frac{a_i^e b_i^p}{2m_e}\left[2\vec{\sigma}_p\cdot\vec{p} - \vec{\sigma}_p\cdot\vec{q} + i\vec{\sigma}_e\cdot(\vec{\sigma}_p\times\vec{q})\right], \\ &= \frac{G_A}{2m_e}\left(-\frac{1}{4}+\sin^2\theta_W+\frac{1}{2}|U_{ei}|^2\right)\left[2\vec{\sigma}_p\cdot\vec{p} - \vec{\sigma}_p\cdot\vec{q} + i\vec{\sigma}_e\cdot(\vec{\sigma}_p\times\vec{q})\right].\end{aligned}$$

Here, we used the fact that $\sin^2\theta_W \approx 0.23$ so that $a_i^p \sim 0$ and that $m_e \ll m_p$. The parity-violating potential that comes out of this with a Fourier transform is given by (we remember to add in the Hermitian conjugate and implicitly sum over $i$)

$$\begin{aligned}V_{PNC}^{\text{loop}} &= \frac{G_A}{m_e}\left(-\frac{1}{4}+\sin^2\theta_W+\frac{1}{2}|U_{ei}|^2\right)\left[(2\vec{\sigma}_p\cdot\vec{p})V_{\nu_i\nu_i}(r) + \vec{\sigma}_e\cdot(\vec{\sigma}_p\times\vec{\nabla})V_{\nu_i\nu_i}(r)\right], \\ &= \frac{G_A}{m_e}\left(-\frac{1}{4}+\sin^2\theta_W+\frac{1}{2}|U_{ei}|^2\right)\left[(2\vec{\sigma}_p\cdot\vec{p})V_{\nu_i\nu_i}(r) + (\vec{\sigma}_e\times\vec{\sigma}_p)\cdot\vec{\nabla}V_{\nu_i\nu_i}(r)\right] \quad \text{(A.27)}\end{aligned}$$

## A.2 Details of the calculation in Sec. 2.7

In Sec. 2.7, we computed $R$, for the $E1$ and $M1$ transitions between the "base" states $|A\rangle$ and $|B\rangle$. Both of these states were corrected by the "correction state" $|\Delta\rangle$. Other corrections were ignored because they are much smaller than the correction due to $|\Delta\rangle$.

Using the machinery of angular-momentum addition, we can write

$$
\begin{aligned}
|A\rangle = |4,3,3,5/2,3\rangle &\equiv -\frac{1}{\sqrt{7}}\psi_{432}|\uparrow\uparrow\rangle + \sqrt{\frac{6}{7}}\psi_{433}|\downarrow\uparrow\rangle, \\
|B\rangle = |4,3,3,7/2,3\rangle &\equiv -\frac{1}{2}\sqrt{\frac{3}{7}}\psi_{432}|\uparrow\uparrow\rangle + \frac{1}{2}\sqrt{\frac{7}{2}}\psi_{433}|\uparrow\downarrow\rangle - \frac{1}{2\sqrt{14}}\psi_{433}|\downarrow\uparrow\rangle, \\
|\Delta\rangle = |4,3,3,5/2,2\rangle &\equiv \psi_{422}|\uparrow\uparrow\rangle,
\end{aligned}
\tag{A.28}
$$

where $\psi_{nlm}$ are the unperturbed energy eigenstates of hydrogen, given by

$$
\psi_{nlm} = \langle r,\theta,\phi|nlm\rangle = \sqrt{\left(\frac{2}{na_0}\right)^3 \frac{(n-l-1)!}{2n[(n+l)!]^3}} e^{-r/na_0}\left[L^{2l+1}_{n-l-1}(2r/na_0)\right] Y^m_l(\theta,\phi). \tag{A.29}
$$

Using these three states, we can write the corrected states in the spirit of Eq. (2.39) as:

$$
|A'\rangle = |A\rangle + \frac{\langle\Delta|V_{PNC}|A\rangle}{E_A - E_\Delta}|\Delta\rangle + \cdots = |A\rangle + C_{A\Delta}|\Delta\rangle + \cdots, \tag{A.30}
$$

where $C_{A\Delta}$ is the correction coefficient. Similarly,

$$
|B'\rangle = |B\rangle + \frac{\langle\Delta|V_{PNC}|B\rangle}{E_B - E_\Delta}|\Delta\rangle + \cdots = |B\rangle + C_{B\Delta}|\Delta\rangle + \ldots \tag{A.31}
$$

In the end, we add the contributions from both terms in the potential. Our states therefore become

$$
|A'\rangle = |B\rangle + (C^{sc}_{A\Delta} + C^{h}_{A\Delta})|\Delta\rangle + \cdots, \tag{A.32}
$$

$$
|B'\rangle = |B\rangle + (C^{sc}_{B\Delta} + C^{h}_{B\Delta})|\Delta\rangle + \cdots. \tag{A.33}
$$

Here $C^{sc}$ is the correction coefficient for the spin-cross term alone, while $C^h$ is the coefficient for the "helicity" term alone.

Using the two terms in $V_{PNC}^{\text{loop}}(r)$, we compute the corrections up to second order in the small parameter $v_i$. To calculate the energy differences between the states, we use Eq. (2.35). We obtain ($s_W \equiv \sin\theta_W$)

$$C_{A\Delta}^{\text{sc}} = i\frac{G_A G_F^2 m_p m_e^3 \alpha^2}{\pi^3 g_p}\left(-\frac{1}{4}+s_W^2+\frac{1}{2}|U_{ei}|^2\right)\left(\frac{21\sqrt{7}v_i^2}{10816}-\frac{35\sqrt{7}}{64896}\right), \tag{A.34}$$

$$C_{B\Delta}^{\text{sc}} = i\frac{G_A G_F^2 m_p m_e^4 \alpha^2}{\pi^3(29 g_p m_e - 21609000 m_p)}\left(-\frac{1}{4}+s_W^2+\frac{1}{2}|U_{ei}|^2\right)\times\left(-\frac{7\sqrt{\frac{7}{3}}v_i^2}{64}+\frac{35\sqrt{\frac{7}{3}}}{1152}\right), \tag{A.35}$$

$$C_{A\Delta}^{\text{h}} = \left(-\frac{1}{4}+s_W^2+\frac{1}{2}|U_{ei}|^2\right)\frac{7i\sqrt{7}\alpha^2 m_e^3\left(36v_i^2-5\right)m_p G_A G_F^2}{129792\pi^3 g_p}, \tag{A.36}$$

$$C_{B\Delta}^{\text{h}} = \left(-\frac{1}{4}+s_W^2+\frac{1}{2}|U_{ei}|^2\right)\frac{7i\sqrt{\frac{7}{3}}\alpha^2 m_e^4\left(1122v_i^2-115\right)M G_A G_F^2}{27648\pi^3(29 g_p m_e - 21609000 m_p)}. \tag{A.37}$$

We are interested in the ratio between the electric and magnetic dipole moment matrix elements for the states $|A'\rangle$ and $|B'\rangle$. These two transition matrix elements have the same dependence on the magnetic quantum numbers in hydrogen, and so the ratio is independent of the orientation of the atom. As such, in our calculations, we only look at the magnetic and electric dipole moments along the $z$ direction,

$$\hat{P} = -ez = -(4\pi\alpha)^{1/2} r\cos\theta,$$
$$\hat{M} = \frac{e}{2m_e}(\hat{L}_z + 2\hat{S}_z) = \frac{(4\pi\alpha)^{1/2}}{2m_e}(\hat{L}_z + 2\hat{S}_z).$$

Using this form of electric and magnetic dipole moment operators in Eq. (2.50) leads to the final result in Eq. (2.53).

APPENDIX B

# NEUTRINO FORCES IN BACKGROUNDS - SOME MORE DETAILS

## B.1 The background effect on fermion propagators

The neutrino propagator in a background with finite neutrino number density in Eq. (3.4) can be found in various references including books and reviews on finite temperature field theory [62, 63, 64, 65, 66]. In this appendix, we provide a simple and pedagogical re-derivation of the formula *without using finite temperature field theory*, aiming at providing a physical interpretation of the background effect.

Let us start with the propagator of a generic fermion in vacuum, which is defined as

$$S_F(x-y) \equiv \langle 0|T\psi(x)\overline{\psi(y)}|0\rangle\,, \tag{B.1}$$

where $T$ indicates that it is a time-ordered product. Using

$$\psi = \int \frac{d^3\mathbf{p}}{(2\pi)^3}\frac{1}{\sqrt{2E_\mathbf{p}}}\sum_s \left[a^s_\mathbf{p} u^s(p)e^{-ip\cdot x} + b^{s\dagger}_\mathbf{p} v^s(p)e^{ip\cdot x}\right], \tag{B.2}$$

where we follow the standard notation of Ref. [365], and assuming $x^0 > y^0$ so that $T$ can be removed, we obtain

$$S_F \propto \int \frac{d^3\mathbf{p}}{(2\pi)^3}\int \frac{d^3\mathbf{k}}{(2\pi)^3}\frac{1}{\sqrt{2E_\mathbf{p}}}\frac{1}{\sqrt{2E_\mathbf{k}}}e^{-ip\cdot x+ik\cdot y}\langle 0|a_\mathbf{p}a^\dagger_\mathbf{k}|0\rangle + \cdots\,, \tag{B.3}$$

where for brevity we have neglected $u^s$, $v^s$, and the script $s$ (they only affect the structure of Dirac spinors). The "$\cdots$" denote terms proportional to $\langle 0|a_\mathbf{p}b_\mathbf{k}|0\rangle$,

$\langle 0|b_{\mathbf{p}}^\dagger a_{\mathbf{k}}^\dagger|0\rangle$, or $\langle 0|b_{\mathbf{p}}^\dagger b_{\mathbf{k}}|0\rangle$, all being zero. Since $\langle 0|a_{\mathbf{p}} a_{\mathbf{k}}^\dagger|0\rangle = (2\pi)^3\delta^3(\mathbf{p}-\mathbf{k})$, Eq. (B.3) gives

$$S_F \propto \int \frac{d^3\mathbf{p}}{(2\pi)^3}\frac{1}{2E_{\mathbf{p}}}e^{-ip\cdot(x-y)} = \int \frac{d^4p}{(2\pi)^4}\frac{i}{p^2-m^2+i\epsilon}e^{-ip\cdot(x-y)}\,. \tag{B.4}$$

The last step is simply the reverse process of computing the contour integral of $p^0$, with the underlying assumption that $x^0 > y^0$. For $x^0 < y^0$, the time ordering guarantees the same result.

Now we shall replace $|0\rangle$ with a background state. Let us first consider a single-particle state which contains a particle with an almost certain position and an almost certain momentum. The two cannot be simultaneously fixed at exact values due to the uncertainty principle, but one can nevertheless introduce a wave package function $w(\mathbf{p})$ so that both $w(\mathbf{p})$ and its Fourier transform $\int w(\mathbf{p})e^{i\mathbf{p}\cdot\mathbf{x}}d^3\mathbf{x}$ are limited in a small region of their respective space—for further elucidation, see e.g. Appendix A of Ref. [366]. The single particle state is then defined as

$$|w\rangle = \int \frac{d^3\mathbf{p}}{(2\pi)^3}w(\mathbf{p})a_{\mathbf{p}}^\dagger|0\rangle\,,\ \langle w|w\rangle = \int \frac{d^3\mathbf{p}}{(2\pi)^3}|w(\mathbf{p})|^2 \equiv 1\,, \tag{B.5}$$

where the last step is defined as the normalization condition of $w(\mathbf{p})$.

Replacing $|0\rangle \to |w\rangle$ in Eq. (B.3), we obtain

$$S_F \propto \int_{\mathbf{pk}} \langle w|a_{\mathbf{p}}a_{\mathbf{k}}^\dagger|w\rangle = \int_{\mathbf{pk}} \left\langle w\left|\left((2\pi)^3\delta^3(\mathbf{p}-\mathbf{k}) - a_{\mathbf{k}}^\dagger a_{\mathbf{p}}\right)\right|w\right\rangle\,, \tag{B.6}$$

where $\int_{\mathbf{pk}}$ standards for $\int \frac{d^3\mathbf{p}}{(2\pi)^3}\int \frac{d^3\mathbf{k}}{(2\pi)^3}\frac{1}{\sqrt{2E_{\mathbf{p}}}}\frac{1}{\sqrt{2E_{\mathbf{k}}}}e^{-ip\cdot x+ik\cdot y}$. Since $\langle w|w\rangle = 1$, the first term leads to the same result as the vacuum case and the second term represents the

background effect. We denote the contribution of the latter by $S_F^{\rm bkg}$:

$$S_F^{\rm bkg} \propto -\int_{\mathbf{pk}} \langle w|a_{\mathbf{k}}^\dagger a_{\mathbf{p}}|w\rangle = -\int_{\mathbf{pk}} w^*(\mathbf{k})w(\mathbf{p})\,, \tag{B.7}$$

where we have used $a_{\mathbf{p}}|w\rangle = w(\mathbf{p})|0\rangle$. Note that $w(\mathbf{p})$ has been defined in such a way that the particle's position and momentum are nearly fixed at certain values (say $\mathbf{x}_0$ and $\mathbf{p}_0$). One can perform spatial translation of the wave package $w(\mathbf{p}) \to w_{\Delta\mathbf{x}}(\mathbf{p}) \equiv e^{i\mathbf{p}\cdot\Delta\mathbf{x}}w(\mathbf{p})$ so that its position is changed to $\mathbf{x}_0 + \Delta\mathbf{x}$ while the momentum is unchanged. Now, if we randomly choose $\Delta\mathbf{x}$ with a uniform probability distribution in a large volume $V$ (much larger than the distribution of each wave package), the position of the particle would be evenly smeared in $V$. For $w^*(\mathbf{k})w(\mathbf{p})$ in Eq. (B.7), the smearing leads to

$$\begin{aligned} w^*(\mathbf{k})w(\mathbf{p}) \xrightarrow{\text{smearing}} & \frac{1}{V}\int w^*_{\Delta\mathbf{x}}(\mathbf{k})w_{\Delta\mathbf{x}}(\mathbf{p})d^3\Delta\mathbf{x} \\ &= \frac{1}{V}\int w^*(\mathbf{k})w(\mathbf{p})e^{i(\mathbf{p}-\mathbf{k})\cdot\Delta\mathbf{x}}d^3\Delta\mathbf{x} \\ &= \frac{(2\pi)^3\delta^3(\mathbf{p}-\mathbf{k})}{V}|w(\mathbf{p})|^2 \\ &= (2\pi)^3\delta^3(\mathbf{p}-\mathbf{k})n_+(\mathbf{p})\,, \end{aligned} \tag{B.8}$$

where in the last step we have identified $|w(\mathbf{p})|^2/V$ as $n_+(\mathbf{p})$ because $\int \frac{d^3\mathbf{p}}{(2\pi)^3}|w(\mathbf{p})|^2 = 1$ and the number density after smearing is $\int \frac{d^3\mathbf{p}}{(2\pi)^3}n_+(\mathbf{p}) = 1/V$.

Substituting Eq. (B.8) into Eq. (B.7), we obtain

$$\begin{aligned} -\int_{\mathbf{pk}} w^*(\mathbf{k})w(\mathbf{p}) \xrightarrow{\text{smearing}} & -\int \frac{d^3\mathbf{p}}{(2\pi)^3}\frac{e^{-ip\cdot(x-y)}}{2E_{\mathbf{p}}}n_+(\mathbf{p}) \\ &= -\int \frac{d^4p}{(2\pi)^4}e^{-ip\cdot(x-y)}(2\pi)\delta\left(p^2-m^2\right)\Theta\left(p^0\right)n_+(\mathbf{p})\,. \end{aligned} \tag{B.9}$$

Combining Eq. (B.9) with the vacuum part in Eq. (B.4), we obtain

$$S_F \propto \int \frac{d^4p}{(2\pi)^4} e^{-ip\cdot(x-y)} \left\{ \frac{i}{p^2 - m^2 + i\epsilon} - (2\pi)\delta\left(p^2 - m^2\right)\Theta\left(p^0\right) n_+(\mathbf{p}) \right\} . \tag{B.10}$$

For an anti-particle background, the above calculation is similar except that some minus signs are flipped. In the presence of both particles and anti-particles in the background, we obtain

$$\begin{aligned} S_F(p) &= \left(\not{p} + m\right) \left\{ \frac{i}{p^2 - m^2 + i\epsilon} - (2\pi)\delta\left(p^2 - m^2\right)\Theta\left(p^0\right)\left[n_+(\mathbf{p}) - n_-(\mathbf{p})\right] \right\} \\ &= \left(\not{p} + m\right) \left\{ \frac{i}{p^2 - m^2 + i\epsilon} - (2\pi)\delta\left(p^2 - m^2\right)\left[\Theta\left(p^0\right) n_+(\mathbf{p}) + \Theta\left(-p^0\right) n_-(\mathbf{p})\right] \right\}, \end{aligned}$$

where $S_F(p)$ is the propagator in the momentum space [i.e. the Fourier transform of $S_F(x-y)$], the prefactor $\left(\not{p} + m\right)$ can be inferred from the vacuum propagator. The result is the same as the fermion propagator derived in finite temperature field theory.

From the above calculation, one can see that the background effect comes from the second term in Eq. (B.6), proportional to $\langle w|a^\dagger_{\mathbf{k}} a_{\mathbf{p}}|w\rangle$. Recall that the annihilation operator $a_{\mathbf{p}}$ acting on $|w\rangle$ can be interpreted as reducing one particle in the background. Hence $\langle w|a^\dagger_{\mathbf{k}} a_{\mathbf{p}}|w\rangle$ corresponds to first absorbing a particle of momentum $\mathbf{p}$ from the background ($a_{\mathbf{p}}|w\rangle = w(\mathbf{p})|0\rangle$), and returning a particle of momentum $\mathbf{k}$ back to the background. Smearing the single particle state in Eq. (B.8) leads to $\delta^3(\mathbf{p} - \mathbf{k})$, which guarantees that the particle being returned has the same momentum as the one being absorbed.

Intuitively, the modified propagator in Eq. (3.4) can be understood as the vacuum expectation value of two fermion fields with the vacuum state $|0\rangle$ replaced by

the modified background state $|w\rangle$, which is the vacuum equipped with some on-shell background fermions. Then the Wick contraction can be carried out not only between the two internal fermion fields (leading to the vacuum propagator), but also among the internal fields and the background fermions (leading to the modified term). Therefore, the modified term is naturally proportional to the number density of background fermions, with the factor $2\pi\delta(p^2 - m^2)\Theta(p^0)$ coming from cutting the propagator to put it on-shell (optical theorem). Notice that the above arguments should be valid in any background and do not require the distribution to be thermal.

## B.2 Integrals

In this appendix, we present the details about some integrals in calculating neutrino forces in the neutrino backgrounds.

### B.2.1 Derivation of the general background potential $V_{\rm bkg}(r)$ in Eq. (3.9)

We first show how to obtain the general expression of the background potential with an arbitrary distribution function.

As has been stated above, when both neutrino propagators in Eq. (3.6) take the

first part, it corresponds to the vacuum potential $V_0(r)$, which is independent of the background distribution functions. When both propagators take the second part, the result always vanishes because of the existence of two delta functions. Therefore, the background contribution comes from the cross terms, i.e., $S_\nu(k)$ takes the first (second) part and $S_\nu(k+q)$ takes the second (first) part:

$$\begin{aligned}
\mathcal{A}_{\rm bkg}(q) &= -\pi G_F^2 g_V^1 g_V^2 \int \frac{d^4k}{(2\pi)^4}\delta\left(k^2-m_\nu^2\right)\left[\Theta\left(k^0\right)n_+(\mathbf{k})+\Theta\left(-k^0\right)n_-(\mathbf{k})\right] \\
&\quad\times\left\{\frac{\mathrm{Tr}\left[\gamma^0(1-\gamma_5)\left(\not{k}+m_\nu\right)\gamma^0(1-\gamma_5)\left(\not{k}+\not{q}+m_\nu\right)\right]}{(k+q)^2-m_\nu^2}\right. \\
&\quad\left.+\frac{\mathrm{Tr}\left[\gamma^0(1-\gamma_5)\left(\not{k}-\not{q}+m_\nu\right)\gamma^0(1-\gamma_5)\left(\not{k}+m_\nu\right)\right]}{(k-q)^2-m_\nu^2}\right\}, \\
&= -8\pi G_F^2 g_V^1 g_V^2 \int \frac{d^4k}{(2\pi)^4}\delta\left(k^2-m_\nu^2\right)\left[\Theta\left(k^0\right)n_+(\mathbf{k})+\Theta\left(-k^0\right)n_-(\mathbf{k})\right] \\
&\quad\times\left[\frac{2k^0\left(k^0+q^0\right)-\left(k\cdot q+k^2\right)}{(k+q)^2-m_\nu^2}+\frac{2k^0\left(k^0-q^0\right)+\left(k\cdot q-k^2\right)}{(k-q)^2-m_\nu^2}\right]. \qquad \text{(B.11)}
\end{aligned}$$

Taking advantage of the identity

$$\delta\left(k^2-m_\nu^2\right)=\delta\left(\left(k^0\right)^2-E_k^2\right)=\frac{1}{2E_k}\left[\delta\left(k^0-E_k\right)+\delta\left(k^0+E_k\right)\right],$$

one can first integrate $k^0$ in Eq. (B.11). In addition, the NR approximation requires $q\simeq(0,\mathbf{q})$. Thus the integral in Eq. (B.11) can be reduced to Eq. (3.8)

$$\mathcal{A}_{\rm bkg}(\mathbf{q})=4G_F^2 g_V^1 g_V^2\int\frac{d^3\mathbf{k}}{(2\pi)^3}\frac{n_+(\mathbf{k})+n_-(\mathbf{k})}{2E_k}\left[\frac{2|\mathbf{k}|^2+m_\nu^2+\mathbf{k}\cdot\mathbf{q}}{2\mathbf{k}\cdot\mathbf{q}+|\mathbf{q}|^2}+(\mathbf{k}\to-\mathbf{k})\right]. \qquad \text{(B.12)}$$

Furthermore, for an isotropic distribution, $n_\pm(\mathbf{k})=n_\pm(\kappa)$ with $\kappa\equiv|\mathbf{k}|$, one can first integrate out the angular part in Eq. (B.12) and obtains

$$\mathcal{A}_{\rm bkg}(\rho)=\frac{G_F^2 g_V^1 g_V^2}{\pi^2}\int_0^\infty d\kappa\frac{\kappa^2}{\sqrt{\kappa^2+m_\nu^2}}\left[n_+(\kappa)+n_-(\kappa)\right]\int_{-1}^1 d\xi\frac{m_\nu^2+2\kappa^2\left(1-\xi^2\right)}{\rho^2-4\kappa^2\xi^2}, \qquad \text{(B.13)}$$

where we have defined $\rho \equiv \left|\vec{q}\right|$ and $\xi \equiv \cos\theta$ with $\theta$ being the angel between $\mathbf{k}$ and $\mathbf{q}$. Then the background potential is given by

$$\begin{aligned} V_{\rm bkg}(r) &= -\int \frac{d^3\mathbf{q}}{(2\pi)^3} e^{i\mathbf{q}\cdot\mathbf{r}} \mathcal{A}_{\rm bkg}(\rho) = -\frac{1}{2\pi^2 r}\int_0^\infty d\rho\rho \sin(\rho r)\,\mathcal{A}_{\rm bkg}(\rho) \\ &= -\frac{G_F^2 g_V^1 g_V^2}{2\pi^4 r}\int_0^\infty d\kappa \frac{\kappa^2}{\sqrt{\kappa^2+m_\nu^2}}\left[n_+(\kappa)+n_-(\kappa)\right]\int_{-1}^1 d\xi\left[m_\nu^2+2\kappa^2\left(1-\xi^2\right)\right]\int_0^\infty d\rho\frac{\rho\sin(\rho r)}{\rho^2-4\kappa^2\xi^2} \\ &= -\frac{G_F^2 g_V^1 g_V^2}{4\pi^3 r}\int_0^\infty d\kappa \frac{\kappa^2}{\sqrt{\kappa^2+m_\nu^2}}\left[n_+(\kappa)+n_-(\kappa)\right]\int_{-1}^1 d\xi\left[m_\nu^2+2\kappa^2\left(1-\xi^2\right)\right]\cos(2\kappa r\xi) \\ &= -\frac{G_F^2 g_V^1 g_V^2}{4\pi^3 r^4}\int_0^\infty \frac{d\kappa\kappa}{\sqrt{\kappa^2+m_\nu^2}}\left[n_+(\kappa)+n_-(\kappa)\right]\left[\left(1+m_\nu^2 r^2\right)\sin(2\kappa r)-2\kappa r\cos(2\kappa r)\right] , \end{aligned} \quad \text{(B.14)}$$

which is just Eq. (3.9).

### B.2.2 Calculation of the integral $\mathcal{I}(\ell,\alpha)$ in Eq. (3.50)

Here, we calculate the integral $\mathcal{I}(\ell,\alpha)$ appearing in the reactor neutrino background. Without loss of generality, we can assume

$$\mathbf{k}_0 = E_\nu(0,0,1) , \quad \mathbf{r} = r(s_\alpha,0,c_\alpha) , \quad \mathbf{q} = \rho\left(s_\theta c_\varphi, s_\theta s_\varphi, c_\theta\right) , \qquad \text{(B.15)}$$

where $(c_x, s_x) \equiv (\cos x, \sin x)$ have been defined. With the above coordinates, we have

$$\mathbf{q}\cdot\mathbf{r} = \rho r\left(s_\alpha s_\theta c_\varphi + c_\alpha c_\theta\right) , \quad \xi \equiv \frac{\mathbf{k_0}\cdot\mathbf{q}}{|\mathbf{k_0}|\,|\mathbf{q}|} = c_\theta , \quad \int d^3\mathbf{q} = \int_0^\infty \rho^2 d\rho \int_{-1}^1 d\xi \int_0^{2\pi} d\varphi \qquad \text{(B.16)}$$

The integral in Eq. (3.50) turns out to be

$$\begin{aligned}\mathcal{I} &\equiv \frac{1}{E_\nu}\int d^3\mathbf{q}e^{i\mathbf{q}\cdot\mathbf{r}}\frac{1-\xi^2}{\rho^2-4E_\nu^2\xi^2} = \frac{1}{E_\nu}\int_0^{2\pi}d\varphi\int_{-1}^{1}d\xi\int_0^{\infty}d\rho e^{i\rho r(s_\alpha s_\theta c_\varphi + c_\alpha c_\theta)}\frac{\rho^2\left(1-\xi^2\right)}{\rho^2-4E_\nu^2\xi^2} \\ &= \frac{1}{E_\nu}\left(\int_0^{2\pi}d\varphi\int_0^{1}d\xi\int_0^{\infty}d\rho + \int_0^{2\pi}d\varphi\int_{-1}^{0}d\xi\int_0^{\infty}d\rho\right)e^{i\rho r(s_\alpha s_\theta c_\varphi + c_\alpha c_\theta)}\frac{\rho^2\left(1-\xi^2\right)}{\rho^2-4E_\nu^2\xi^2}\,.\end{aligned} \tag{B.17}$$

In the second term in the bracket of Eq. (B.17), changing the variables as $\rho \to -\rho$ and $\xi \to -\xi$ one obtains

$$\begin{aligned}\mathcal{I} &= \frac{1}{E_\nu}\int_0^{2\pi}d\varphi\int_0^{1}d\xi\left[\int_0^{\infty}d\rho e^{i\rho r(s_\alpha s_\theta c_\varphi + c_\alpha c_\theta)} + \int_{-\infty}^{0}d\rho e^{i\rho r(-s_\alpha s_\theta c_\varphi + c_\alpha c_\theta)}\right]\frac{\rho^2\left(1-\xi^2\right)}{\rho^2-4E_\nu^2\xi^2} \\ &= \frac{1}{E_\nu}\int_0^{\pi}d\varphi\int_0^{1}d\xi\left[\int_0^{\infty}d\rho e^{i\rho r(s_\alpha s_\theta c_\varphi + c_\alpha c_\theta)} + \int_{-\infty}^{0}d\rho e^{i\rho r(-s_\alpha s_\theta c_\varphi + c_\alpha c_\theta)}\right]\frac{\rho^2\left(1-\xi^2\right)}{\rho^2-4E_\nu^2\xi^2} \\ &+ \frac{1}{E_\nu}\int_\pi^{2\pi}d\varphi\int_0^{1}d\xi\left[\int_0^{\infty}d\rho e^{i\rho r(s_\alpha s_\theta c_\varphi + c_\alpha c_\theta)} + \int_{-\infty}^{0}d\rho e^{i\rho r(-s_\alpha s_\theta c_\varphi + c_\alpha c_\theta)}\right]\frac{\rho^2\left(1-\xi^2\right)}{\rho^2-4E_\nu^2\xi^2}\,.\end{aligned} \tag{B.18}$$

In the last line of Eq. (B.18) changing the variable $\varphi \to \varphi - \pi$ one obtains

$$\begin{aligned}\mathcal{I} &= \frac{1}{E_\nu}\int_0^{\pi}d\varphi\int_0^{1}d\xi\left[\int_0^{\infty}d\rho e^{i\rho r(s_\alpha s_\theta c_\varphi + c_\alpha c_\theta)} + \int_{-\infty}^{0}d\rho e^{i\rho r(-s_\alpha s_\theta c_\varphi + c_\alpha c_\theta)}\right]\frac{\rho^2\left(1-\xi^2\right)}{\rho^2-4E_\nu^2\xi^2} \\ &+ \frac{1}{E_\nu}\int_0^{\pi}d\varphi\int_0^{1}d\xi\left[\int_0^{\infty}d\rho e^{i\rho r(-s_\alpha s_\theta c_\varphi + c_\alpha c_\theta)} + \int_{-\infty}^{0}d\rho e^{i\rho r(s_\alpha s_\theta c_\varphi + c_\alpha c_\theta)}\right]\frac{\rho^2\left(1-\xi^2\right)}{\rho^2-4E_\nu^2\xi^2} \\ &= \frac{1}{E_\nu}\int_0^{\pi}d\varphi\int_0^{1}d\xi\left(1-\xi^2\right)\int_{-\infty}^{\infty}d\rho\left[e^{i\rho r(s_\alpha s_\theta c_\varphi + c_\alpha c_\theta)} + e^{i\rho r(-s_\alpha s_\theta c_\varphi + c_\alpha c_\theta)}\right]\frac{\rho^2}{\rho^2-4E_\nu^2\xi^2}\,.\end{aligned} \tag{B.19}$$

What we have done is to change the integral to the standard form of one-dimensional Fourier transform. Then one can use the following Fourier trans-

form:

$$\int_{-\infty}^{\infty} d\rho e^{i\rho x} \frac{\rho^2}{\rho^2 - 4E_\nu^2 \xi^2} = 2\pi \left[\delta(x) - \mathrm{sgn}(x) E_\nu \xi \sin\left(2E_\nu \xi x\right)\right] \ , \tag{B.20}$$

from which one obtains

$$\begin{aligned}
\mathcal{I} &= \frac{2\pi}{E_\nu} \int_0^\pi d\varphi \int_0^1 d\xi \left(1-\xi^2\right) \left[\delta\left(x_+\right) - \mathrm{sgn}\left(x_+\right) E_\nu \xi \sin\left(2E_\nu \xi x_+\right)\right. \\
&\quad \left. + \delta\left(x_-\right) - \mathrm{sgn}\left(x_-\right) E_\nu \xi \sin\left(2E_\nu \xi x_-\right)\right] \\
&= \frac{2\pi}{E_\nu} \int_{-1}^1 d\xi \left(1-\xi^2\right) \int_0^\pi d\varphi \left[\delta\left(x_+\right) - \mathrm{sgn}\left(x_+\right) E_\nu \xi \sin\left(2E_\nu \xi x_+\right)\right]
\end{aligned} \tag{B.21}$$

where $x_\pm \equiv r(\pm s_\alpha s_\theta c_\varphi + c_\alpha c_\theta)$. The first term in Eq. (B.21) involving $\delta$ function can be analytically integrated out

$$\begin{aligned}
& \frac{2\pi}{E_\nu} \int_{-1}^1 d\xi \left(1-\xi^2\right) \int_0^\pi d\varphi \delta\left[r\left(s_\alpha s_\theta c_\varphi + c_\alpha c_\theta\right)\right] \\
= \ & \frac{2\pi}{rE_\nu} \int_{-1}^1 d\xi \left(1-\xi^2\right) \int_0^\pi d\varphi \delta\left(s_\alpha \sqrt{1-\xi^2} c_\varphi + c_\alpha \xi\right) \\
\overset{t=c_\varphi}{=} \ & \frac{2\pi}{\ell s_\alpha} \int_{-1}^1 d\xi \left(1-\xi^2\right) \frac{1}{\sqrt{1-\xi^2}} \int_{-1}^1 \frac{dt}{\sqrt{1-t^2}} \delta\left(t + \frac{\xi}{\sqrt{1-\xi^2}} \cot\alpha\right) \\
= \ & \frac{2\pi}{\ell s_\alpha} \int_{-\frac{1}{\sqrt{1+\cot^2\alpha}}}^{\frac{1}{\sqrt{1+\cot^2\alpha}}} d\xi \frac{1-\xi^2}{\sqrt{1-\left(1+\cot^2\alpha\right)\xi^2}} \\
= \ & \frac{\pi^2}{2\ell} \left(3 + \cos 2\alpha\right) \ ,
\end{aligned} \tag{B.22}$$

where we have defined the dimensionless quantity $\ell \equiv rE_\nu$. The second term in Eq. (B.21) cannot be analytically integrated. So finally one obtains the directional integral

$$\begin{aligned}
\mathcal{I}\left(\ell, \alpha\right) &= \frac{\pi^2}{2\ell} \left(3 + \cos 2\alpha\right) \\
&\quad -2\pi \int_{-1}^1 d\xi \, \xi \left(1-\xi^2\right) \int_0^\pi d\varphi \, \mathrm{sgn}\left(s_\alpha \sqrt{1-\xi^2} c_\varphi + c_\alpha \xi\right) \sin\left[2\ell\xi \left(s_\alpha \sqrt{1-\xi^2} c_\varphi + c_\alpha \xi\right)\right] \\
&= \frac{\pi^2}{2\ell} \left(3 + \cos 2\alpha\right) - 2\pi \int_{-1}^1 d\xi \, \xi \left(1-\xi^2\right) \int_0^\pi d\varphi \, \sin\left(2\ell\xi \left|s_\alpha \sqrt{1-\xi^2} c_\varphi + c_\alpha \xi\right|\right) \ ,
\end{aligned} \tag{B.23}$$

which is the result of Eq. (3.51). Then the directional background potential is given by

$$V_{\rm bkg}(r,\alpha) = -\frac{g_V^1 g_V^2}{\pi^3} G_F^2 \Phi_0 E_\nu^2 \times \mathcal{I}\left(rE_\nu, \alpha\right) \ . \tag{B.24}$$

## B.3 Energy distribution function with a finite spread

In this appendix, we consider a directional neutrino flux with a finite energy spread instead of the monochromatic case we considered in the main text in Eq. (3.44).

Neglecting the neutrino mass, which is much smaller than the typical energy of neutrino flux, the general directional neutrino flux can be written as

$$n_\pm\left(\mathbf{k}\right) = (2\pi)^3 f(E) \delta\left(\hat{\mathbf{k}} - \hat{\mathbf{k}}_0\right) \ , \tag{B.25}$$

where $\hat{\mathbf{k}}$ denotes the unit vector of the three momentum $\mathbf{k}$, while $\hat{\mathbf{k}}_0$ represents a certain direction. Without loss of generality, we take $\hat{\mathbf{k}}_0 = (0,0,1)$ and such that the delta function enforces $\mathbf{k} = (0,0,E)$. The energy distribution function $f(E)$ should satisfy the normalization condition:

$$\int \frac{d^3\mathbf{k}}{(2\pi)^3} n_\pm\left(\mathbf{k}\right) = \Phi_0 \ , \tag{B.26}$$

with $\Phi_0$ being the total flux of neutrinos.

For example, a Gaussian-like distribution reads

$$f_g(E) = \frac{\Phi_0}{2\pi B} \exp\left[-\frac{\left(E - E_0^2\right)}{2\sigma_E^2}\right] \ , \tag{B.27}$$

where $E_0$ is the mean energy and $\sigma_E$ denotes the spread of energy. The normalization factor $B$ is given by

$$\begin{aligned} B &= \int_0^\infty dE E^2 \exp\left[-\frac{(E-E_0)^2}{2\sigma_E^2}\right] \\ &= E_0\sigma_E^2 \exp\left(-\frac{E_0^2}{2\sigma_E^2}\right) + \sqrt{\frac{\pi}{2}}\sigma_E\left(E_0^2+\sigma_E^2\right)\left[1+\mathrm{Erf}\left(\frac{E_0}{\sqrt{2}\sigma_E}\right)\right] \\ &= \sqrt{2\pi}E_0^2\sigma_E + O\left(\sigma_E^3\right) . \end{aligned} \tag{B.28}$$

It can be verified explicitly that the distribution in Eq. (B.27) satisfies the normalization in Eq. (B.26). In particular, in the limit of $\sigma_E \to 0$ one obtains

$$f_g(E)\delta\left(\hat{\mathbf{k}}-\hat{\mathbf{k}}_0\right) \to \frac{\Phi_0}{2\pi E_0^2}\delta\left(E-E_0\right)\delta\left(\hat{\mathbf{k}}-\hat{\mathbf{k}}_0\right) = \delta^3\left(\mathbf{k}-\mathbf{k}_0\right)\Phi_0 , \tag{B.29}$$

which reduces to the monochromatic case in Eq. (3.44).

Below we compute the background potential without the specific form of $f(E)$ for the purpose of generality. Substituting Eq. (B.25) in Eq. (3.8), one obtains

$$\mathcal{A}_{\mathrm{bkg}}(\mathbf{q}) = 2G_F^2 g_V^1 g_V^2 \int d^3\mathbf{k}\frac{f(E)}{E}\delta\left(\hat{\mathbf{k}}-\hat{\mathbf{k}}_0\right)\left[\frac{2|\mathbf{k}|^2+\mathbf{k}\cdot\mathbf{q}}{2\mathbf{k}\cdot\mathbf{q}+|\mathbf{q}|^2}+(\mathbf{k}\to-\mathbf{k})\right] . \tag{B.30}$$

Then using the decomposition

$$\int d^3\mathbf{k}\delta\left(\hat{\mathbf{k}}-\hat{\mathbf{k}}_0\right)f(E) = 2\pi\int_{-1}^1 dz\delta\left(z-1\right)\int_0^\infty dE E^2 f(E) , \tag{B.31}$$

where $z \equiv \hat{\mathbf{k}}\cdot\hat{\mathbf{k}}_0$, we have

$$\begin{aligned} \mathcal{A}_{\mathrm{bkg}}(\mathbf{q}) &= 4\pi G_F^2 g_V^1 g_V^2 \int_{-1}^1 dz\delta\left(z-1\right)\int_0^\infty dE E f(E)\left[\frac{2E^2+E\rho\xi}{2E\rho\xi+\rho^2}+\frac{2E^2-E\rho\xi}{-2E\rho\xi+\rho^2}\right] \\ &= 16\pi G_F^2 g_V^1 g_V^2 \int_0^\infty dE E^3 f(E)\frac{1-\xi^2}{\rho^2-4E^2\xi^2} . \end{aligned} \tag{B.32}$$

Notice that $\rho \equiv |\mathbf{q}|$ and $\xi \equiv \frac{\mathbf{k}\cdot\mathbf{q}}{|\mathbf{k}||\mathbf{q}|}$ have been defined. The background potential turns out to be

$$\begin{aligned} V_{\rm bkg}(\mathbf{r}) &= -\int \frac{d^3\mathbf{q}}{(2\pi)^3} e^{i\mathbf{q}\cdot\mathbf{r}} \mathcal{A}_{\rm bkg}(\mathbf{q}) = -\frac{2}{\pi^2} G_F^2 g_V^1 g_V^2 \int_0^\infty dE E^3 f(E) \int d^3\mathbf{q} e^{i\mathbf{q}\cdot\mathbf{r}} \frac{1-\xi^2}{\rho^2 - 4E^2\xi^2} \\ &= -\frac{2}{\pi^2} G_F^2 g_V^1 g_V^2 \int_0^\infty dE E^4 f(E)\, \mathcal{I}\,(Er, \alpha) \ , \end{aligned} \tag{B.33}$$

where the dimensionless integral is defined as

$$\mathcal{I}\,(Er, \alpha) \equiv \frac{1}{E} \int d^3\mathbf{q} e^{i\mathbf{q}\cdot\mathbf{r}} \frac{1-\xi^2}{\rho^2 - 4E^2\xi^2} \ , \tag{B.34}$$

whose result has been given by Eq. (3.51) with the substitution $\ell = Er$. In particular, in the monochromatic limit, the background potential reduces to Eq. (3.48):

$$f(E) \to \frac{\Phi_0}{2\pi E_0^2} \delta\,(E - E_0) \ , \qquad V_{\rm bkg}(\mathbf{r}) \to -\frac{1}{\pi^3} G_F^2 g_V^1 g_V^2 \Phi_0 E_0^2\, \mathcal{I}\,(E_0 r, \alpha) \ . \tag{B.35}$$

To sum up, the background potential in a directional neutrino flux with an arbitrary finite energy spread is given by Eq. (B.33), with the integral $\mathcal{I}$ being computed in Eq. (3.51).

## B.4 Flavor- and material-dependence of the background potential

In Sec. 3.5 we have neglected the effects of neutrino flavors and materials of test bodies when computing the directional neutrino background potential. Here we compute a complete expression for the neutrino force between two objects with

masses $m_1$ and $m_2$, as a function of the background neutrino flavor distribution and their respective atomic and mass numbers. We present the expression under the following assumptions:

1. Let the masses be pure elements of atomic numbers $Z_1$ and $Z_2$ respectively. Let their mass numbers be $A_1$ and $A_2$ respectively.
2. We further assume that the mass of the objects are constituted entirely by the masses of the neutrons and protons in the object, i.e, we ignore electron mass $m_e \ll m_p \approx m_n$, where the subscripts $p$ and $n$ stand for proton and neutron respectively.
3. We assume the massless limit for the neutrinos, where the mass eigenstates are identical to the flavor eigenstates.
4. We see in the text how finite spread of the masses weakens the $1/r$ behavior of the neutrino background potential. In this appendix, we assume that the angular spread $\alpha^2 \ll 1/\Delta(E_\nu r)$, where $r$ is the distance between the masses and $E_\nu$ is defined in the text [see Eq. (3.57)].

Given masses $m_i$ (for $i = 1, 2$), the number of protons, neutrons and electrons in each mass is given by

$$N_p^i \equiv \frac{m_i Z_i}{A_i m_p} = N_e^i \,, \qquad N_n^i \equiv \frac{m_i (A_i - Z_i)}{A_i m_p} \,. \tag{B.36}$$

The effective $g_V$'s for each mass can then be computed simply by adding up the $g_V$'s of each of the constituent species and multiplying by the corresponding number of that species in the mass. The effective $g_V$ depends on which neutrino is being exchanged between the masses. For instance, when the neutrinos exchanged are electron neutrinos, we get:

$$g^i_{Ve} = N^i_p(1/2 - 2s^2_W) + N^i_e(1/2 + 2s^2_W) - N^i_n/2 = N^i_p - N^i_n/2 \ , \tag{B.37}$$

where $s_W$ is the sine of the Weinberg angle $\theta_W$. For other neutrinos being exchanged the effective coupling is:

$$g^i_{V\mu/\tau} = N^i_p(1/2 - 2s^2_W) + N^i_e(-1/2 + 2s^2_W) - N^i_n/2 = -N^i_n/2 \ . \tag{B.38}$$

Note that, in the presence of electron neutrino background, the electrons in the material need to be considered when calculating the force.

In the end, the neutrino background potential between the two masses is given by (we have taken $\alpha = 0$ like what we did in Eq. (3.62)] in accordance with assumption 4 above):

$$V_{\rm bkg}(r) = -\frac{G^2_F \Phi E_\nu}{\pi r}\left[n_e g^1_{Ve} g^2_{Ve} + (1 - n_e)\, g^1_{V\mu/\tau} g^2_{V\mu/\tau}\right], \tag{B.39}$$

where $n_e$ is the fraction of electron neutrinos in the flux $\Phi$. After some algebra this can be written as:

$$V_{\rm bkg}(r) = -\frac{G^2_F \Phi E_\nu}{\pi r}\frac{m_1 m_2}{m^2_p} \times f(A_1, A_2, Z_1, Z_2, n_e) \ , \tag{B.40}$$

where

$$f(A_1, A_2, Z_1, Z_2, n_e) = \frac{1}{4}\left[n_e\left(\frac{3Z_1}{A_1} - 1\right)\left(\frac{3Z_2}{A_2} - 1\right) + (1 - n_e)\left(1 - \frac{Z_1}{A_1}\right)\left(1 - \frac{Z_2}{A_2}\right)\right]. \quad \text{(B.41)}$$

The net potential between these two masses is therefore given by:

$$V_{\text{net}} = V_{\text{grav}} + V_{\text{bkg}} = -\frac{m_1 m_2}{r}\left[G_N + \frac{G_F^2 \Phi E_\nu}{\pi m_p^2} f(A_1, A_2, Z_1, Z_2, n_e)\right], \quad \text{(B.42)}$$

where $G_N$ is the gravitational constant. We have ignored the $1/r^5$ term from the vacuum neutrino force since at the distances we are talking about that force is negligible. Note that the Weinberg angle does not feature in our final expression for the neutrino force.

The ratio of the neutrino force to the gravitational force between these two masses at some distance $r \gg E_\nu^{-1}$ is independent of $r$,

$$\frac{V_{\text{bkg}}(r)}{V_{\text{grav}}(r)} = \frac{G_F^2 \Phi E_\nu f(A_1, A_2, Z_1, Z_2, n_e)}{\pi G_N m_p^2}\,. \quad \text{(B.43)}$$

Below we mention some special cases:

1. Consider the special case $Z_1 = Z_2 = Z, A_1 = A_2 = A$ and $n_e = 1$, i.e, the background is purely electron neutrino. In this case, the ratio reads:

$$\frac{V_{\text{bkg}}(r)}{V_{\text{grav}}(r)} = \frac{G_F^2 \Phi E_\nu}{4\pi G_N m_p^2}\left(\frac{3Z}{A} - 1\right)^2. \quad \text{(B.44)}$$

Note that this ratio is maximized when $Z = A$, i.e, for Hydrogen.

Putting in the numbers we get (using $\Phi \sim 10^{14}\text{cm}^{-2}\text{s}^{-1}$ and $E_\nu \sim 1$ MeV):

$$\frac{V_{\text{bkg}}(r)}{V_{\text{grav}}(r)} \sim 10^{-13} \, . \tag{B.45}$$

The gravitational force is thus 13 orders of magnitude greater than the neutrino background force in this limit. This corresponds to the purple line (reactor 10m) in Fig. 3.5.2.

2. Consider the special case $Z_1 = Z_2 = Z, A_1 = A_2 = A$ and $n_e = 0$, i.e, the background is purely muon/tau neutrino. In this case we note that force is entirely due to the number of neutrons in the masses, and the ratio:

$$\frac{V_{\text{bkg}}(r)}{V_{\text{grav}}(r)} = \frac{G_F^2 \Phi E_\nu}{4\pi G_N m_p^2} \left(1 - \frac{Z}{A}\right)^2 . \tag{B.46}$$

In the special case of Hydrogen we see that we shall not find any additional force due to background neutrinos. However in other elements we can see this effect.

To finish this section, we show how the force varies for different materials. For a given $\Phi$ and $E_\nu$, and assuming that $A \approx 2Z$ as is usually the case for most elements, we have,

$$\frac{\delta V_{\text{bkg}}}{V_{\text{bkg}}} \approx 4\,(4n_e - 1)\,\delta_{Z/A} \, , \tag{B.47}$$

where $\delta_{Z/A}$ refers to the variation of $Z/A$ for different materials, as in Eq. (3.63).

APPENDIX C

# FERMION PAIR RADIATION FROM CLASSICAL SYSTEMS - DERIVATION OF THE POWER LOSS FORMULA

We present below an explicit derivation of the power loss formula for the fermion pair radiation by a point-like classical object on an elliptical orbit. We perform the calculation separately for the case of vector and scalar mediators. In our calculation, we follow closely the analysis in Ref. [93].

## C.1 The case of a vector boson mediator

The power loss is a sum over different harmonics, as given by Eqs. (4.8) and (4.9). The matrix element, at leading order, for a vector boson mediator, is given by Eq. (4.11). It includes the Fourier Transform of the classical current $J^{\mu}_{\rm cl}(x)$ defined in Eq. (4.2). We rewrite it here for convenience:

$$\mathcal{M}_n(s_1, s_2) = g^2 Q_\psi \, \bar{u}(k_1, s_1)\gamma^\mu v(k_2, s_2) \, \frac{i(-\eta_{\mu\nu} + (k_1+k_2)_\mu (k_1+k_2)_\nu / m_A^2)}{(k_1+k_2)^2 - m_A^2 + i m_A \Gamma_A} \, J^\nu_{\rm cl}(\Omega_n) \,, \quad \text{(C.1)}$$

where $\eta_{\mu\nu}$ is the Minkowski metric tensor. Note that the contribution from the $(k_1+k_2)_\mu (k_1+k_2)_\nu$ term vanishes by means of the Dirac equation since the fermions are on-shell, that is,

$$\bar{u}(\not{k}_1 + \not{k}_2)v = \bar{u}(m_\psi - m_\psi)v = 0. \quad \text{(C.2)}$$

Squaring the amplitudes corresponding to different harmonics and summing over spins, we find

$$
\begin{aligned}
|\overline{\mathcal{M}_n}|^2 &= \sum_{s_1,s_2} |\mathcal{M}_n|^2 = \frac{g^4 Q_\psi^2}{\left((k_1+k_2)^2 - m_A^2\right)^2 + m_A^2\Gamma_A^2} J^\mu_{\rm cl}(\Omega_n) J^{*\nu}_{\rm cl}(\Omega_n)\,\mathrm{Tr}\left[(\not{k}_1 + m_\nu)\gamma_\mu(\not{k}_2 - m_\nu)\gamma_\nu\right] \\
&= \frac{4g^4 Q_\psi^2}{\left((k_1+k_2)^2 - m_A^2\right)^2 + m_A^2\Gamma_A^2} J^\mu_{\rm cl}(\Omega_n) J^{*\nu}_{\rm cl}(\Omega_n)\left(k_{1\mu}k_{2\nu} + k_{1\nu}k_{2\mu} - \frac{1}{2}(k_1+k_2)^2\eta_{\mu\nu}\right). \quad \text{(C.3)}
\end{aligned}
$$

Finally, we are ready to write the expression for the rate of energy loss due to $\psi\bar{\psi}$ emission at harmonic $n$ by the classical source as

$$
\begin{aligned}
P_n = \left(\frac{dE}{dt}\right)_n &= \int \Omega_n\, d\Gamma_n \\
&= \Omega_n \int \frac{\mathrm{d}^3\boldsymbol{k}_1}{(2\pi)^3(2\omega_1)} \frac{\mathrm{d}^3\boldsymbol{k}_2}{(2\pi)^3(2\omega_2)} (2\pi)\delta(\Omega_n - \omega_1 - \omega_2)|\overline{\mathcal{M}_n}|^2 \\
&= \Omega_n \int \mathrm{d}\Phi_1 \mathrm{d}\Phi_2 \frac{|\boldsymbol{k}_1|\mathrm{d}\omega_1}{2(2\pi)^3} \frac{|\boldsymbol{k}_2|\mathrm{d}\omega_2}{2(2\pi)^3} (2\pi)\delta(\Omega_n - \omega_1 - \omega_2)|\overline{\mathcal{M}_n}|^2\,, \quad \text{(C.4)}
\end{aligned}
$$

where $|\boldsymbol{k}_{1,2}| = \sqrt{\omega_{1,2}^2 - m_\psi^2}$, we used $\Omega_n = \omega_1 + \omega_2$ for the total energy carried away by the fermion pair, $d\Phi_{1,2}$ are the differential elements of solid angles in the fermion's direction of flight, and $\left|\overline{\mathcal{M}_n}\right|^2$ is given in Eq. (C.3). The total power radiated is found by summing over all kinematically allowed harmonics:

$$
P = \sum_n P_n. \quad \text{(C.5)}
$$

To calculate the power radiated in fermion pairs by a point-like source in an elliptical orbit, we need to evaluate the integrals in Eq. (C.4), after substituting in the explicit form of $J^\mu_{\rm cl}(\Omega_n)$ in Eq. (C.3). Using Eqs. (4.2) and (4.5), we find the Fourier Transform $J^\mu_{\rm cl}(\Omega_n)$ as:

$$
J^i_{\rm cl}(\Omega_n) = a\Omega Q j^i_n, \qquad J^0_{\rm cl}(\Omega_n) = a\Omega Q\left(\frac{\boldsymbol{j}_n \cdot \boldsymbol{p}}{n\Omega}\right), \quad \text{(C.6)}
$$

where the 3-vector $\boldsymbol{j}_n$ is defined as

$$\boldsymbol{j}_n = \left(-iJ_n'(ne), \frac{\sqrt{1-e^2}}{e} J_n(ne), 0\right), \tag{C.7}$$

with $J_n(z)$ denoting a Bessel function, and $\boldsymbol{p} = \boldsymbol{k}_1 + \boldsymbol{k}_2$.

The terms in the numerator of $|\overline{\mathcal{M}}|^2$ in Eq. (C.3), are then given by

$$\left(J^{\mu}_{\rm cl}(\Omega_n)k_{1\mu}\right)\left(J^{\nu *}_{\rm cl}(\Omega_n)k_{2\nu}\right) = a^2\Omega^2 Q^2 j_n^i j_n^{j*}\left[\frac{\omega_1\omega_2}{(n\Omega)^2}p^i p^j - \frac{\omega_1}{n\Omega}p^i k_2^j - \frac{\omega_2}{n\Omega}k_1^i p^j + k_1^i k_2^j\right], \tag{C.8}$$

and

$$|J^{\mu}_{\rm cl}(\Omega_n)|^2 = |J^0_{\rm cl}(\Omega_n)|^2 - |\boldsymbol{J}_{\rm cl}(\Omega_n)|^2 = a^2\Omega^2 Q^2 j_n^i j_n^{j*}\left[\frac{p^i p^j}{(\Omega n)^2} - \delta^{ij}\right], \tag{C.9}$$

where we used $\Omega_n = n\Omega$. Note that all quantities above are 3-vectors with Latin indices $i = 1, 2, 3$, and a sum over $i$ and $j$ is implicit. The expression for $\left(J^{\mu}_{\rm cl}(\Omega_n)k_{2\mu}\right)\left(J^{\nu *}_{\rm cl}(\Omega_n)k_{1\nu}\right)$ is obtained from Eq. (C.8) via complex conjugation.

Next we note that the denominator of $|\overline{\mathcal{M}_n}|^2$, see Eq. (C.3), depends only on $m_A$, $\Gamma_A$, $\omega_{1,2}$, the magnitudes $|\boldsymbol{k}_{1,2}|$ and the relative angle between the two momenta $\boldsymbol{k}_1$, and $\boldsymbol{k}_2$ that we denote as $\gamma$. Because of this, it is convenient to perform the change of coordinates in the integral in Eq. (C.4) from the integration over the solid angles $\mathrm{d}\Phi_1\mathrm{d}\Phi_2$ to the integration over $\mathrm{d}\Phi_1\mathrm{d}\Phi_2^r$ where the solid angle of the second neutrino is measured relative to the direction of $\boldsymbol{k}_1$, hence the super index $r$. (Equivalently, one can also choose to integrate over $\mathrm{d}\Phi_1^r\mathrm{d}\Phi_2$.) The Jacobian of this coordinate change is unity since the transformation is simply a coordinate rotation, and thus

$$\mathrm{d}\Phi_1\mathrm{d}\Phi_2 = \mathrm{d}\Phi_1\mathrm{d}\Phi_2^r. \tag{C.10}$$

Defining

$$\mathrm{d}\Phi_b = \sin\theta_b \mathrm{d}\theta_b \mathrm{d}\phi_b, \qquad \mathrm{d}\Phi_2^r = \sin\gamma \mathrm{d}\gamma \mathrm{d}\delta, \qquad b = 1, 2\,, \tag{C.11}$$

we find the following relations between the two sets of integration variables

$$\begin{aligned} \cos\gamma &= \cos\theta_1 \cos\theta_2 + \sin\theta_1 \sin\theta_2 \cos\left(\phi_2 - \phi_1\right), \\ \sin\delta &= \frac{\sin\theta_2 \sin\left(\phi_2 - \phi_1\right)}{\sin\gamma}\,. \end{aligned} \tag{C.12}$$

Since, out of all the angular variables, the denominator only depends on the relative angle $\gamma$, the integrals over $\theta_1$, $\phi_1$ and $\delta$ can be taken easily using the following relations

$$\begin{aligned} \int \mathrm{d}\Phi_1 \mathrm{d}\Phi_2 k_a^i k_a^j &= \int \mathrm{d}\Phi_1 \mathrm{d}\Phi_2^r k_a^i k_a^j = \delta^{ij} \frac{8\pi^2}{3} \boldsymbol{k}_a^2 \int \sin\gamma \mathrm{d}\gamma, \\ \int \mathrm{d}\Phi_1 \mathrm{d}\Phi_2 k_1^i k_2^j &= \int \mathrm{d}\Phi_1 \mathrm{d}\Phi_1^r k_1^i k_2^j = \delta^{ij} \frac{8\pi^2}{3} (\boldsymbol{k}_1 \cdot \boldsymbol{k}_2) \int \sin\gamma \mathrm{d}\gamma, \\ \int \mathrm{d}\Phi_1 \mathrm{d}\Phi_2 &= \int \mathrm{d}\Phi_1 \mathrm{d}\Phi_2^r = 8\pi^2 \int \sin\gamma \mathrm{d}\gamma\,. \end{aligned} \tag{C.13}$$

Using this and the results of Eqs. (C.8) and (C.9), we perform the integration over $\theta_1$, $\phi_1$ and $\delta$ in Eq. (C.4), and find the following expression for the power radiated in harmonic $n$,

$$\begin{aligned} P_n = \frac{g^4 (n\Omega)}{12\pi^3} a^2 \Omega^2 Q_\psi^2 Q^2 \left|\boldsymbol{j}_n\right|^2 \int & \frac{\delta(n\Omega - \omega_1 - \omega_2)}{\left((k_1 + k_2)^2 - m_A^2\right)^2 + m_A^2 \Gamma_A^2} \times \\ & \left[ -\frac{1}{2} (k_1 + k_2)^2 \left[ (\boldsymbol{k}_1 + \boldsymbol{k}_2)^2 / \left( (n\Omega)^2 - 3 \right) \right] + 2 \frac{\omega_1 \omega_2}{(n\Omega)^2} (\boldsymbol{k}_1 + \boldsymbol{k}_2)^2 \right. \\ & \left. -2 \frac{\omega_1}{n\Omega} \left( \boldsymbol{k}_2^2 + \boldsymbol{k}_1 \cdot \boldsymbol{k}_2 \right) - 2 \frac{\omega_2}{n\Omega} \left( \boldsymbol{k}_1^2 + \boldsymbol{k}_1 \cdot \boldsymbol{k}_2 \right) + 2 \boldsymbol{k}_1 \cdot \boldsymbol{k}_2 \right] \times \\ & \omega_1 \omega_2 \left( 1 - \frac{m_\psi^2}{\omega_1^2} \right)^{1/2} \left( 1 - \frac{m_\psi^2}{\omega_2^2} \right)^{1/2} \sin\gamma \, \mathrm{d}\gamma \mathrm{d}\omega_1 \mathrm{d}\omega_2\,, \end{aligned} \tag{C.14}$$

where the only integrals left are the integrals over $\gamma$, $\omega_1$ and $\omega_2$.

Next, we introduce the following dimensionless variables and parameters

$$x_1 = \frac{\omega_1}{\Omega}, \quad x_2 = \frac{\omega_2}{\Omega}, \quad n_\psi = \frac{m_\psi}{\Omega}, \quad n_A = \frac{m_A}{\Omega}, \quad n_\Gamma = \frac{\Gamma_A}{\Omega}. \tag{C.15}$$

Performing the change of variables in Eq. (C.14) from $(\omega_1, \omega_2)$ to $(x_1, x_2)$, we rewrite the expression for the power radiated in harmonic $n$ as follows:

$$P_n = \frac{g^4}{12\pi^3} a^2 \Omega^4 Q_\psi^2 |\boldsymbol{\jmath}_n|^2 \int \sin\gamma \, \mathrm{d}\gamma \, \mathrm{d}x_1 \, \mathrm{d}x_2 \, \delta(n - x_1 - x_2) \, \mathcal{F}(\cos\gamma, x_1, x_2) \, . \tag{C.16}$$

Upon taking the integral over $x_2$ and performing the replacement $x_1 \to x$, we obtain

$$P_n = \frac{g^4}{12\pi^3} a^2 \Omega^4 Q_\psi^2 Q^2 |\boldsymbol{\jmath}_n|^2 \int_{n_\psi}^{n-n_\psi} \mathrm{d}x \int_{-1}^{1} \mathrm{d}(\cos\gamma) \, \mathcal{F}(\cos\gamma, x) \, , \tag{C.17}$$

where function $\mathcal{F}(\cos\gamma, x)$ is given by

$$\mathcal{F}(\cos\gamma, x) = \frac{b(x)}{2n} \frac{\frac{1}{2} b^2(x) \cos^2\gamma + b(x) c(x) \cos\gamma + d(x)}{(a(x) - b(x)\cos\gamma)^2 + g^2} \, , \tag{C.18}$$

with

$$\begin{aligned}
a(x) &= 2n_\psi^2 + 2x(n-x) - n_A^2 \, , \\
b(x) &= 2\sqrt{x^2 - n_\psi^2}\sqrt{(n-x)^2 - n_\psi^2} \, , \\
c(x) &= -\left(n^2 + 2n_\psi^2\right) , \\
d(x) &= 2(x(n^3 - 2n^2 x + 2nx^2 - x^3) + 2n^2 n_\psi^2 + n_\psi^4) , \\
g^2 &= n_A^2 n_\Gamma^2 \, .
\end{aligned} \tag{C.19}$$

The variable $x$ here is the ratio of the energy of one of the fermions to the fundamental oscillation frequency. It can be at least $n_\psi$ or at most $n-$, hence the limits

on the integral. Also note that $F$ also depends on the parameters of the problem namely $n_A$, $n_\psi$, $n_\Gamma$ defined in Eq. (C.15), but we do not write them explicitly for brevity. Lastly, note that the $\gamma$-dependence of the numerator of function $\mathcal{F}$ is through a term quadratic in $\cos\gamma$ and a term linear in $\cos\gamma$. This behavior is attributed to the theory that we pick – renormalizable theories such as in the case considered here would only contribute at most two powers of momentum in the matrix element, leading to a $\cos\gamma$ dependence that is at most quadratic. However non-renormalizable theories have more momenta in the matrix element, and will give us a different $\cos\gamma$ dependence in the $\mathcal{F}$.

Now, we define

$$F^A(x) \equiv F^A(n, x, , , ) = \int_{-1}^{1} \mathrm{d}\,(\cos\gamma)\,\mathcal{F}\,(\cos\gamma, x, n)\,, \tag{C.20}$$

where the superscript $A$ denotes the vector boson mediator.

The integral over $\cos\gamma$ can be taken analytically. Then, we find that the function $F^A(x)$, has the form:

$$\begin{aligned} F^A(x) = F_0^A(x) \;&+\; \frac{F_1^A(x)}{n_M}\left[\tan^{-1}\left(\frac{a(x)+b(x)}{n_M}\right) - \tan^{-1}\left(\frac{a(x)-b(x)}{n_M}\right)\right] \\ &+\; F_2^A(x)\tanh^{-1}\left(\frac{2a(x)b(x)}{a(x)^2 + b(x)^2 + n_M^{2\,2}}\right), \end{aligned} \tag{C.21}$$

with:

$$\begin{aligned} F_0^A(x) &= b(x)/2n\,, \\ F_1^A(x) &= \frac{1}{4n}\left({}^4 + 4n^{22} - {}^{2\,2} + 2^2n^2 - 4nx^2 + 4x^{22}\right), \\ F_2^A(x) &= \frac{1}{2n}\left({}^2 + n^2 - 2nx + 2x^2\right). \end{aligned} \tag{C.22}$$

Consequently, the power loss formula of each mode with $n > 2n_\psi$ becomes

$$P_n = \frac{2g^4 Q_\psi^2 Q^2}{3(2\pi)^3} a^2 \Omega^4 \left( J_n'(ne)^2 + \frac{1-e^2}{e^2} J_n(ne)^2 \right) \int_{n_\psi}^{n-n_\psi} \mathrm{d}x F^A(x), \tag{C.23}$$

which gives us Eq. (4.19) for the case $M = A$, where we define for mediator $M$

$$B_n^M(n_M, n_\nu, n_\Gamma) \equiv \left( J_n'(ne)^2 + \frac{1-e^2}{e^2} J_n(ne)^2 \right) \int^{n-} \mathrm{d}x \; F^M(x, n, n_M, n_\nu, n_\Gamma), \tag{C.24}$$

where $J_n(z)$ is a Bessel function of order $n$ in the variable $z$.

## C.2 The case of the scalar mediator

The derivation for the power loss in the scalar mediator is similar to the vector case, but the matrix element is different, as shown in Eq. (4.15). This matrix element contains the number density $\rho_{\rm cl}(x)$ of source particles, instead of a current. As such, the difference in the calculation in this case comes from the calculation of the squared matrix element, which in this case, is given by:

$$\begin{aligned} \sum_{s_1,s_2} |\mathcal{M}_n(s_1, s_2)|^2 &= \frac{g^2 g'^2}{((k_1+k_2)^2 - m_\phi^2)^2 + m_\phi^2 \Gamma_\phi^2} \mathrm{Tr}((\not{k}_1 + m_\psi)(\not{k}_2 - m_\psi)) |\rho_{\rm cl}(\Omega_n)|^2 \\ &= \frac{4g^2 g'^2}{((k_1+k_2)^2 - m_\phi^2)^2 + m_\phi^2 \Gamma_\phi^2} (k_1 \cdot k_2 - m_\psi^2) |\rho_{\rm cl}(\Omega_n)|^2 \,]. \end{aligned} \tag{C.25}$$

The power loss is again given by Eq. (C.4).

Using Eqs. (4.3) and (4.5), we find the Fourier Transform $\rho_{\rm cl}^\mu(\Omega_n)$ as:

$$\rho_{\rm cl}^0(\Omega_n) = a\Omega N \left( \frac{\boldsymbol{j}_n \cdot \boldsymbol{p}}{n\Omega} \right), \tag{C.26}$$

where, like in the vector case, we define the 3-vector $j_n^i$ as follows:

$$\boldsymbol{j}_n = \left(-iJ_n'(ne), \frac{\sqrt{1-e^2}}{e} J_n(ne), 0\right), \tag{C.27}$$

with $J_n(z)$ denoting a Bessel function, amd $\boldsymbol{p} = \boldsymbol{k}_1 + \boldsymbol{k}_2$.

After performing all the steps analogous to Eqns. (C.4)–(C.20) in the previous section, i.e, after performing the angular integration, we get:

$$P_n = \frac{g^2 g'^2}{12\pi^3} a^2 \Omega^4 N^2 |\boldsymbol{j}_n|^2 \int_{n_\psi}^{n-n_\psi} \mathrm{d}x \int_{-1}^{1} \mathrm{d}\cos\gamma \, \mathcal{F}(\cos\gamma, x)\,, \tag{C.28}$$

where function $\mathcal{F}(\cos\gamma, x)$ is given by

$$\mathcal{F}(\cos\gamma, x) = -\frac{b(x)}{2n} \frac{\frac{1}{2}b^2(x)\cos^2\gamma + b(x)c(x)\cos\gamma + d(x)}{(a(x) - b(x)\cos\gamma)^2 + g^2}\,, \tag{C.29}$$

with

$$\begin{aligned}
a(x) &= 2n_\psi^2 + 2x(n-x) - n_\phi^2\,, \\
b(x) &= 2\sqrt{x^2 - n_\psi^2}\,\sqrt{(n-x)^2 - n_\psi^2}\,, \\
c(x) &= \frac{(n-2x)^2}{2}, \\
d(x) &= ({}^2{-nx} + x^2)(n^2 - 2^2 - 2nx + 2x^2), \\
g^2 &= n_\phi^2 n_\Gamma^2\,.
\end{aligned} \tag{C.30}$$

Like before, we define

$$F^\phi(x) \equiv F^\phi(n, x, , , ) = \int_{-1}^{1} \mathrm{d}\,(\cos\gamma)\,\mathcal{F}\,(\cos\gamma, x, n)\,, \tag{C.31}$$

where the superscript $\phi$ denotes the scalar mediator.

The integral over $\cos\gamma$ can be taken analytically to find a form for $F^\phi$:

$$\begin{aligned} F^\phi(x) = F_0^\phi(x) &+ \frac{F_1^\phi(x)}{n_M}\left[\tan^{-1}\left(\frac{a(x)+b(x)}{n_M}\right) - \tan^{-1}\left(\frac{a(x)-b(x)}{n_M}\right)\right] \\ &+ F_2^\phi(x)\tanh^{-1}\left(\frac{2a(x)b(x)}{a(x)^2+b(x)^2+n_M^2{}^2}\right), \end{aligned} \tag{C.32}$$

with:

$$\begin{aligned} F_0^\phi(x) &= -b(x)/2n\,, \\ F_1^\phi(x) &= \frac{1}{4n}\left(^{22} + (n^2-^2)(^2-4^2)\right), \\ F_2^\phi(x) &= \frac{1}{4n}\left(n^2+4^2-2^2\right). \end{aligned} \tag{C.33}$$

Consequently, the power loss formula of each mode with $n > 2n_\psi$ becomes

$$P_n = \frac{2g^2g'^2}{3(2\pi)^3}a^2\Omega^4N^2\left(J_n'(ne)^2 + \frac{1-e^2}{e^2}J_n(ne)^2\right)\int_{n_\psi}^{n-n_\psi}\mathrm{d}xF^\phi(x), \tag{C.34}$$

which gives us Eq. (4.20) for the case $M = \phi$

$$P_n^\phi = \frac{g^2g'^2}{12\pi^3}a^2\Omega^4\left(\frac{N_1}{m_1}-\frac{N_2}{m_2}\right)^2 B_n^\phi(n_A, n_\nu, n_\Gamma). \tag{C.35}$$

We find that the form of the function $F^M$ is general for the two types of mediators, the difference lying in the explicit forms of the functions $F_0^M, F_1^M$ and $F_2^M$. This is due to the fact that the $\cos\gamma$ dependence of the function $\mathcal{F}$ is the same in both cases, as in both cases, the theory considered is a renormalizable one. As we explained in the previous sub-section, this general form of $F^M$ is not what we will have when we consider non-renormalizable theories that give us higher powers of momenta in the numerator of $\mathcal{F}$.

APPENDIX D

# $K \to \mu\mu$ - SOME DETAILS

## D.1 Extracting $\mathcal{B}(K_S \to \mu^+\mu^-)_{\ell=0}$ without a pure kaon beam

In the main text, we demonstrated how we can determine $\mathcal{B}(K_S \to \mu^+\mu^-)_{\ell=0}$ for the case of a pure $K^0$ beam in empty space. Here we present a discussion on two other cases which are more related to realistic experimental situations. The first case is when we have a beam with unequal initial number of $K^0$ and $\overline{K}^0$. The second case is when we have a pure $K_L$ beam going via a regenerator before the kaons decay. In both cases, it is possible to extract the branching ratio $\mathcal{B}(K_S \to \mu^+\mu^-)_{\ell=0}$ cleanly as in Eq. (5.31), with the addition of a dilution factor as in Eq. (5.32).

### D.1.1 A mixed beam of $K^0$ and $\overline{K}^0$

Consider a beam which initially consists of an incoherent mixture of kaons and anti-kaons. We define the production asymmetry,

$$D = \frac{N_{K^0} - N_{\overline{K}^0}}{N_{K^0} + N_{\overline{K}^0}}. \tag{D.1}$$

such that the fractions of $K^0$ and $\overline{K}^0$ particles are given respectively by

$$\frac{N_{K^0}}{N_{K^0} + N_{\overline{K}^0}} = \frac{1+D}{2}, \qquad \frac{N_{\overline{K}^0}}{N_{K^0} + N_{\overline{K}^0}} = \frac{1-D}{2}. \tag{D.2}$$

Note that $D = 1$ corresponds to a pure $K^0$ beam, while $D = -1$ corresponds to a pure $\overline{K}^0$ beam.

The decay rate to a final state $f$ is given by the incoherent sum

$$\frac{\mathrm{d}\Gamma}{\mathrm{d}t} = \frac{1+D}{2}\left(\frac{\mathrm{d}\Gamma_{K^0}}{\mathrm{d}t}\right) + \frac{1-D}{2}\left(\frac{\mathrm{d}\Gamma_{\overline{K}^0}}{\mathrm{d}t}\right), \tag{D.3}$$

such that its form is given by Eq. (7.13) with the following coefficients:

$$\begin{aligned} C_L &= |A_0^{\text{CP-even}}|^2, \\ C_S &= |A_0^{\text{CP-odd}}|^2 + \beta_\mu^2 |A_1^{\text{CP-even}}|^2, \\ C_{cos} &= D\,|A_0^{\text{CP-odd}^*} A_0^{\text{CP-even}}| \cos\varphi_0, \\ C_{sin} &= D\,|A_0^{\text{CP-odd}^*} A_0^{\text{CP-even}}| \sin\varphi_0. \end{aligned} \tag{D.4}$$

It is then straightforward to extract our parameter of interest. For $D \neq 0$ we obtain

$$|A_0^{\text{CP-odd}}|^2 = \mathcal{D}_F \frac{{C_{cos}}^2 + {C_{sin}}^2}{C_L}, \qquad \mathcal{D}_F = \frac{1}{D^2}\,. \tag{D.5}$$

In terms of the branching ratios we have

$$\mathcal{B}(K_S \to \mu^+\mu^-)_{\ell=0} = \mathcal{D}_F \times \mathcal{B}(K_L \to \mu^+\mu^-) \times \frac{\tau_S}{\tau_L} \times \left(\frac{C_{int}}{C_L}\right)^2, \tag{D.6}$$

We learn that the beam asymmetry serves as a dilution factor compared to the case of a pure $K^0$ or $\overline{K}^0$ beam. Note that if $D = 0$ (which means that the beam is an equal admixture of $K^0$ and $\overline{K}^0$), one cannot use the beam to measure $\mathcal{B}(K_S \to \mu^+\mu^-)_{\ell=0}$.

We close with a remark regarding the LHCb search for the $K_S$ rate [179]. To a very good approximation at LHCb we have $D = 0$. In that case the interference

terms cancel and we are left with just $C_L$ and $C_S$. Thus, without any further analysis to tag the flavor of the kaon, LHCb is working on extracting the $C_S$ term that includes the decay to both the $\ell = 0$ and $\ell = 1$ states.

### D.1.2 $K_L$ propagating through a slab of matter

When kaons travel through matter, the time dependence of the kaon wave function is modified via the inclusion of the momentum dependent regeneration parameter [206, 207, 208, 367, 209, 368].

We define

$$re^{i\alpha} = -\frac{\pi N}{m}\left(\frac{\Delta f}{\Delta \lambda}\right), \tag{D.7}$$

where $r$ and $\alpha$ are real, and

$$\Delta f \equiv f - \bar{f}, \qquad \Delta\lambda \equiv \Delta m - \frac{i}{2}\Delta\Gamma. \tag{D.8}$$

Here, $f$ ($\bar{f}$) is the difference of forward scattering amplitudes for kaons (anti-kaons), and $N$ is the density of scattering centers in the regenerator. Note that $r$ and $\alpha$ are physical and can be determined from experiment.

Let us consider a pure $K_L$ beam, which is produced by letting the $K_S$ (and interferences) terms decay away. Then we put a regenerator of length $L$ in the path of the beam. Let $t_L$ be the time taken by the kaon to travel through the regenerator. We define $t = 0$ to be the time the kaon emerges from the regenerator. We

then study the time dependence of the kaon wave function at later times. For simplicity, in the following we present the result to leading order in $r$.

The normalized decay rate is given by Eq. (7.13), with the coefficients:

$$\begin{aligned} C_L &= |A_0^{\text{CP-even}}|^2, \\ C_S &= 0, \\ C_{sin} &= -r\,|A_0^{\text{CP-even}} A_0^{\text{CP-odd}}|\left(\sin(\alpha-\varphi_0) - e^{t_L\Delta\Gamma/2}\sin(\alpha-\varphi_0+\Delta m t_L)\right), \\ C_{cos} &= r\,|A_0^{\text{CP-even}} A_0^{\text{CP-odd}}|\left(\cos(\alpha-\varphi_0) - e^{t_L\Delta\Gamma/2}\cos(\alpha-\varphi_0+\Delta m t_L)\right). \end{aligned} \tag{D.9}$$

We can check that for $t_L = 0$ (which means that the regenerator thickness is negligible) or $r = 0$ (the regenerator material is just vacuum), the interference terms vanish as it should.

Using the above, we find the dilution factor $\mathcal{D}_F$, for $t_L \neq 0$ and $r \neq 0$ to be

$$\mathcal{D}_F = \frac{1}{2r^2}\left(\frac{\cosh(\Delta\Gamma t_L/2) - \sinh(\Delta\Gamma t_L/2)}{\cosh(\Delta\Gamma t_L/2) - \cos(\Delta m t_L)}\right). \tag{D.10}$$

We learn that the dilution parameter depends on both $r$ and $t_L$. The extraction of the rate is given by Eq. (D.6).

We close with two remarks

1. As we already emphasized, the interference terms are the key to the extraction of $\mathcal{B}(K_S \to \mu^+\mu^-)_{\ell=0}$. Having $D \neq 0$ or $r \neq 0$ are some of the ways of obtaining interference terms in the time dependence of the kaon beam.
2. More generally one may also have combinations with both non-zero $D$ and $r$, as well as a general initial state. The calculation is straightforward, though

tedious and does not provide much further insight, and so we do not show it here.

## D.2 SM Calculations

In the following we first derive the SM prediction for $\mathcal{B}(K_S \to \mu^+\mu^-)_{\ell=0}$, and then derive approximate numerical estimates for the experimental parameters within the SM.

### D.2.1 SM calculation

Using the standard formula for two body decays [195], as well as the results of Eqs. (5.45) and (5.36), we write

$$\mathcal{B}(K_S \to (\mu^+\mu^-)_{\ell=0}) = \frac{\beta_\mu \tau_S}{16\pi m_K} \times 2 \sum |\mathcal{M}^{SD}(K_S \to (\mu^+\mu^-)_{\ell=0})|^2 \times \sin^2\theta_{ct}, \qquad \text{(D.11)}$$

where the sum is over the outgoing spin, as usual. Note that $\mathcal{M}$ is proportional to $A$, defined in Eq. (5.5) but it uses the standard normalization that is used when making calculations.

We write the matrix element for the short-distance contribution as

$$\mathcal{M}^{SD} = g_{\rm SM} \langle \mu\bar{\mu}|\mathcal{O}_\ell|0\rangle \times \langle 0|\mathcal{O}_H|K\rangle, \qquad \text{(D.12)}$$

where

$$O_\ell = (\bar{\mu}_L \gamma^\rho \mu_L), \qquad \langle 0|O_H|K\rangle \equiv -i\, p_K^\rho\, f_K. \tag{D.13}$$

For the kaon decay constant we employ here the convention

$$\langle 0|\bar{s}\gamma_\mu\gamma_5 d|K^0(p)\rangle = i p_\mu f_{K^0}\,. \tag{D.14}$$

The coupling, $g_{\rm SM}$, can be read from Eq. (6.59) (note that $(\bar{\mu}\mu)_{V-A} = 2(\bar{\mu}_L\gamma^\rho\mu_L)$)

$$g_{\rm SM} = -\frac{G_F}{\sqrt{2}}\frac{\alpha_{em}}{\pi \sin^2\theta_W}\left[V_{cs}^* V_{cd} Y_{NL} + V_{ts}^* V_{td} Y(x_t)\right]. \tag{D.15}$$

Since under our assumption of $\theta_{uc} = 0$ the part proportional to $V_{cs}^* V_{cd}$ is relatively real, we can further define

$$\tilde{g}_{\rm SM} = -\frac{G_F}{\sqrt{2}}\frac{\alpha_{em}}{\pi \sin^2\theta_W} V_{ts}^* V_{td} Y(x_t). \tag{D.16}$$

As long as what we are after is the CP violating decay rate, we can use $\tilde{g}_{\rm SM}$.

Squaring the amplitude and summing over spins, we find

$$\begin{aligned}
\sum |\mathcal{M}^{SD}_{K\to\mu\mu}|^2 &= \Big[ - p_K^\rho p_K^\sigma f_K^2\Big] |g_{\rm SM}|^2 \,{\rm Tr}\Big[\bar{u}(k_1)\gamma_\rho P_L v(k_2)\bar{v}(k_2) P_L \gamma_\sigma u(k_1)\Big] \\
&= -|g_{\rm SM}|^2 f_K^2 p_K^\rho p_K^\sigma {\rm Tr}\Big[\gamma_\rho P_L (\not{k}_2 - m_\mu) P_L \gamma_\sigma (\not{k}_1 + m_\mu)\Big] \\
&= |g_{\rm SM}|^2 f_K^2 m_\mu^2 p_K^\rho p_K^\sigma {\rm Tr}\Big[\gamma_\rho \frac{1}{2}(1-\gamma_5)\gamma_\sigma\Big] \\
&= 2|g_{\rm SM}|^2 f_K^2 m_\mu^2 m_K^2.
\end{aligned} \tag{D.17}$$

Using Eq. (D.11) we find

$$\begin{aligned}
\mathcal{B}(K_S \to (\mu^+\mu^-)_{\ell=0}) &= \frac{\beta_\mu \tau_S}{16\pi m_K} 4|\tilde{g}_{\rm SM}|^2 f_K^2 m_\mu^2 m_K^2 \sin^2\theta_{ct} \\
&= \frac{\beta_\mu\, \tau_S}{16\pi m_K}\left|\frac{G_F}{\sqrt{2}}\frac{2\alpha_{em}}{\pi\sin^2\theta_W} m_K m_\mu \times Y(x_t) \times f_K \times V_{ts}V_{td}\sin\theta_{ct}\right|^2,
\end{aligned} \tag{D.18}$$

in agreement with Eqs. (37) and (39) of Ref. [187].

We next get numerical estimates. We use the lattice QCD result [202] for the hadronic parameter, assuming isospin symmetry:

$$f_K = 155.7 \pm 0.3\,\text{MeV}\,. \tag{D.19}$$

We use the following values for the measured parameters [195],

$$\begin{aligned} &m_K = 497.61\,\text{MeV}, && m_\mu = 105.658\,\text{MeV}, \\ &G_F = 1.166378 \times 10^{-5}\,\text{GeV}^{-2}, && \alpha_{em} = 1/129, \\ &\sin^2\theta_W = 0.23, && Y(x_t) = 0.95, \\ &\tau_L = 5.116 \times 10^{-8}\,\text{s}, && \tau_S = 8.95 \times 10^{-11}\,\text{s}, \end{aligned} \tag{D.20}$$

and for the CKM values we use

$$|V_{ts}V_{td}\,\sin\theta_{ct}| = A^2\lambda^5\bar{\eta}, \qquad \text{with} \quad A = 0.79,\ \lambda = 0.2265,\ \bar{\eta} = 0.357, \tag{D.21}$$

to arrive at the prediction

$$\mathcal{B}(K_S \to (\mu^+\mu^-)_{\ell=0}) \approx 1.64 \cdot 10^{-13} \times \left|\frac{V_{ts}V_{td}\sin\theta_{ct}}{(A^2\lambda^5\bar{\eta})_{\text{best fit}}}\right|^2 , \tag{D.22}$$

with

$$(A^2\lambda^5\bar{\eta})_{\text{best fit}} = 1.33 \cdot 10^{-4}. \tag{D.23}$$

### D.2.2 SM approximate values for the experimental parameters

In order to estimate the magnitude of the effect we are after and to illustrate the expected time dependence, we require approximate values for the remaining two

branching ratios within the SM. First, we use the measured branching ratio,

$$\mathcal{B}(K_L \to \mu^+\mu^-)_{\text{exp.}} = \mathcal{B}(K_L \to (\mu^+\mu^-)_{\ell=0})_{\text{exp.}} = (6.84 \pm 0.11) \cdot 10^{-9}, \tag{D.24}$$

which sets the value of the parameter $C_L$.

The remaining branching ratio, $\mathcal{B}(K_S \to \mu^+\mu^-)_{\ell=1}$, can only be estimated a priori by relying on non-perturbative calculations from the literature that suffer from large hadronic uncertainties. Nonetheless, we use these results to get an estimate for its magnitude. Below we use the prediction for the long-distance contribution, [142]

$$\mathcal{B}(K_S \to \mu^+\mu^-)^{LD}_{\text{SM}} = \mathcal{B}(K_S \to \mu^+\mu^-)_{\ell=1} \approx 4.99 \cdot 10^{-12}. \tag{D.25}$$

Note that while we quote results to three significant digits, the theoretical uncertainties are much larger. Altogether we have

$$\begin{aligned} \mathcal{B}(K_S \to \mu^+\mu^-)_{\ell=0} &\approx 1.64 \cdot 10^{-13}, \\ \mathcal{B}(K_L \to \mu^+\mu^-)_{\ell=0} &\approx 6.84 \cdot 10^{-9}, \\ \mathcal{B}(K_S \to \mu^+\mu^-)_{\ell=1} &\approx 4.99 \cdot 10^{-12}. \end{aligned} \tag{D.26}$$

The first is the result of the calculation from the SM effective Hamiltonian, the second is the experimental measured value, and the third uses the non-perturbative estimation together with the calculated SM short-distance contribution.

For illustration of the time dependence, we choose to normalize the $C$ coefficients such that $C_L = 1$. The numerical values for the coefficients, as defined in

Eqs. (7.13) and (5.9), for the case of a pure $K^0$ or $\overline{K}^0$ beam, are then given by:

$$\begin{aligned}(C_L)_{\rm SM} &\equiv 1, \\ (C_S)_{\rm SM} &= \frac{\tau_L}{\tau_S}\frac{\mathcal{B}(K_S\to\mu^+\mu^-)_{\ell=0}+\mathcal{B}(K_S\to\mu^+\mu^-)_{\ell=1}}{\mathcal{B}(K_L\to\mu^+\mu^-)_{\ell=0}} \approx 0.43, \\ (C_{Int.})_{\rm SM} &= \sqrt{\frac{\tau_L}{\tau_S}\frac{\mathcal{B}(K_S\to\mu^+\mu^-)_{\ell=0}}{\mathcal{B}(K_L\to\mu^+\mu^-)_{\ell=0}}} \approx 0.12\,.\end{aligned} \tag{D.27}$$

There is one more experimental parameter, the phase $\varphi_0$. It is related to the strong phase and we do not provide any estimate for it.

## D.3 The short-distance operator

For completeness, we explain below the well-known results that the short-distance SM amplitude cannot generate an $\ell = 1$ state, and that only the axial parts of both the hadronic and leptonic currents contribute in two-body pseudoscalar decays.

Our starting point is the factorization of the matrix element

$$\mathcal{M} = \langle\mu^+\mu^-|O_L^\mu O_{H\mu}|K\rangle = \langle\mu^+\mu^-|O_L^\mu|0\rangle\times\langle 0|O_{H\mu}|K\rangle, \tag{D.28}$$

where

$$O_H^\mu = (\bar{s}d)_{V-A}, \qquad O_L^\mu = (\bar{\mu}\mu)_{V-A}. \tag{D.29}$$

The leading breaking of this factorization is from the photon loop, and thus it is suppressed by roughly $O(\alpha_{EM}/4\pi)\sim 10^{-3}$.

Considering the leptonic part is sufficient to explain why short-distance physics does not contribute to the $K \to (\mu^+\mu^-)_{\ell=1}$ amplitude. For two spinors $\psi$ and $\chi$, we recall the transformation of the $V-A$ operator under CPT [369]:

$$\Theta\bar{\psi}\gamma^\mu(1-\gamma^5)\chi\Theta^\dagger = -\bar{\chi}\gamma^\mu(1-\gamma^5)\psi\,, \tag{D.30}$$

where $\Theta = \mathcal{CPT}$ is the CPT operator. This implies

$$\Theta O_L^\mu \Theta^\dagger = -O_L^\mu. \tag{D.31}$$

Using

$$\Theta|\mu^+\mu^-\rangle_\ell = (-1)^{\ell+1}|\mu^+\mu^-\rangle_\ell, \qquad \Theta|0\rangle = |0\rangle, \tag{D.32}$$

we conclude

$$\langle(\mu^+\mu^-)_\ell|O_L^\mu|0\rangle = \langle(\mu^+\mu^-)_\ell|\Theta\Theta^\dagger O_L^\mu \Theta\Theta^\dagger|0\rangle = (-1)^\ell\langle(\mu^+\mu^-)_\ell|O_L^\mu|0\rangle. \tag{D.33}$$

From the above we see that $\mathcal{M}$, defined in Eq. (D.28), vanishes when $\ell$ is odd.

As for the axial part of the hadronic current, the argument is the same as the well-known one for charged pion decay, that we recall below. Consider

$$\langle 0|V^\mu - A^\mu|K(p_K)\rangle. \tag{D.34}$$

The kaon is a pseudo-scalar and the vacuum is parity-even. Thus, the matrix element of $V^\mu$ must transform as a pseudovector, and the matrix element of $A^\mu$ must transform as a vector. The only available physical observable is the kaon momentum, $p_K$, which is a vector. It is impossible to construct a product of any number of $p_K^\mu$ that transforms like as a pseudovector. We conclude that

$$\langle 0|V^\mu|K\rangle = 0. \tag{D.35}$$

In order to see that also for the leptonic current only the axial part is relevant, we write the matrix element in the following form, leaving the vector and axial-vector components of the leptonic operator general:

$$\mathcal{M} \sim p_K^\alpha \; \bar{u}(k_2)\gamma_\alpha(B + A\gamma^5)v(k_1) \tag{D.36}$$

Then,

$$\begin{aligned} \sum |\mathcal{M}|^2 &\propto \mathrm{Tr}\Big[(\not{k}_2 + m_\mu)\not{p}_K(B + A\gamma^5)(\not{k}_1 - m_\mu)(B^* + A^*\gamma^5)\not{p}_K\Big] \\ &= 4(|B|^2 - |A|^2)\Big[2(k_1 \cdot p_K)(k_2 \cdot p_K) - m_K^2(k_1 \cdot k_2)\Big] \; - \; 4(|B|^2 + |A|^2)m_\mu^2 m_K^2 \end{aligned} \tag{D.37}$$

Using two-body kinematics, we have

$$\begin{aligned} (k_1 \cdot p_K) &= (k_2 \cdot p_K) = \frac{1}{2}m_K^2, \\ (k_1 \cdot k_2) &= \frac{1}{2}m_K^2 - m_\mu^2. \end{aligned} \tag{D.38}$$

Plugging this in to Eq. (D.37), the $|B|^2$ terms drop out and we are left only with the terms proportional to $|A|^2$,

$$\sum |\mathcal{M}|^2 \propto |A|^2 m_\mu^2 m_K^2, \tag{D.39}$$

i.e., only the axial-vector part of the operator is relevant.

APPENDIX E

## UPDATE OF THE THEORY ESTIMATE FOR $\chi_{\gamma\gamma}(\mu)$

In this section we update the theory estimate of Ref. [187]. The experimental input that goes into this estimate comes from analyses of the form factor in $K_L \to \gamma e^+ e^-$, $K_L \to \gamma \mu^+ \mu^-$ and $K_L \to e^+ e^- \mu^+ \mu^-$, and can be summarized by the parameter $\alpha_{\text{exp.}}$, defined by

$$\alpha_{\text{exp.}} = -m_\rho^2 \frac{d}{dq^2} f(q^2, 0)\Big|_{q^2=0}, \tag{E.1}$$

where $f(q_1^2, q_2^2)$ is the $K_L \to \gamma\gamma$ form factor. The experimental value derived from $K_L \to \gamma e^+ e^-$ has been updated by the KTeV collaboration after Ref. [187] was published. We take [370]

$$\alpha_{\text{exp.}}|_{ee} = -1.73 \pm 0.05\,, \tag{E.2}$$

combined with [371, 372]

$$\begin{aligned} \alpha_{\text{exp.}}|_{\mu\mu} &= -1.54 \pm 0.10\,, \\ \alpha_{\text{exp.}}|_{ee\mu\mu} &= -1.59 \pm 0.37\,, \end{aligned} \tag{E.3}$$

and arrive at the weighted average

$$\alpha_{\text{exp.}} = -1.691 \pm 0.044\,. \tag{E.4}$$

Comparing with Ref. [187] (who quote $\alpha_{\text{exp.}} = -1.611 \pm 0.044$), the central value has gone up by $\sim 5\%$ while the relative error remains the same.

Inserting this into Eq. (22) of Ref. [187], we have

$$\chi_{\gamma\gamma}(m_\rho) = (6.10 \pm 0.16_{\text{exp.}}) - \Delta_\Lambda\,, \tag{E.5}$$

(updated from $(5.83 \pm 0.15_{\text{exp.}}) - \Delta_\Lambda$). Following Ref. [187] we take

$$|\Delta_\Lambda| \leq 1.0\,, \tag{E.6}$$

and reach the result

$$\left[\chi_{\gamma\gamma}(m_\rho)\right]_{\text{IU}} = 6.10 \pm 0.16_{\text{exp.}} \pm 1.0_{\text{th.}}\,. \tag{E.7}$$

## BIBLIOGRAPHY


[1] Margarita Gavrilova, Mitrajyoti Ghosh, Yuval Grossman, Walter Tangarife, and Tien-Hsueh Tsai. Fermion pair radiation from accelerating classical systems. 2023. arXiv 2301.01303.

[2] Avital Dery, Mitrajyoti Ghosh, Yuval Grossman, and Stefan Schacht. $K \to \mu^+\mu$ as a clean probe of short-distance physics. *JHEP*, 07:103, 2021. arXiv 2104.06427.

[3] Avital Dery and Mitrajyoti Ghosh. $K \to \mu^+\mu$ beyond the standard model. *JHEP*, 03:048, 2022. arXiv 2112.05801.

[4] Avital Dery, Mitrajyoti Ghosh, Yuval Grossman, Teppei Kitahara, and Stefan Schacht. A Precision Relation between $\Gamma(K \to \mu^+\mu^-)(t)$ and $\mathcal{B}(K_L \to \mu^+\mu^-)/\mathcal{B}(K_L \to \gamma\gamma)$. 2022. arXiv 2211.03804.

[5] Avital Dery, Mitrajyoti Ghosh, Yuval Grossman, and Stefan Schacht. $SU(3)_F$ analysis for beauty baryon decays. *JHEP*, 03:165, 2020. arXiv 2001.05397.

[6] G. Feinberg and J. Sucher. Long-Range Forces from Neutrino-Pair Exchange. *Phys. Rev.*, 166:1638–1644, 1968.

[7] G. Feinberg, J. Sucher, and C. K. Au. The Dispersion Theory of Dispersion Forces. *Phys. Rept.*, 180:83, 1989.

[8] Stephen D. H. Hsu and Pierre Sikivie. Long range forces from two neutrino exchange revisited. *Phys. Rev. D*, 49:4951–4953, 1994.

[9] Ephraim Fischbach. Long range forces and neutrino mass. *Annals Phys.*, 247:213–291, 1996.

[10] Sylvain Fichet. Quantum forces from dark matter and where to find them. *Phys. Rev. Lett.*, 120(13):131801, 2018.

[11] Yevgeny V. Stadnik. Probing Long-Range Neutrino-Mediated Forces with Atomic and Nuclear Spectroscopy. *Phys. Rev. Lett.*, 120(22):223202, 2018.

[12] Giorgio Arcadi, Manfred Lindner, Jessica Martins, and Farinaldo S. Queiroz. New physics probes: Atomic parity violation, polarized electron scattering and neutrino-nucleus coherent scattering. *Nucl. Phys. B*, 959:115158, 2020.

[13] R.P. Feynman. *Feynman lectures on gravitation*. 12 1996.

[14] Alexei Yu. Smirnov and Francesco Vissani. Long range neutrino forces and the lower bound on neutrino mass. 4 1996.

[15] P. F. Smith. Coherent Neutrino Scattering - Relativistic and Non-relativistic. *Nuovo Cim.*, A83:263–274, 1984.

[16] E. Fischbach. A Lower bound on neutrino mass. In *Dark matter in cosmology, quantum measurements, experimental gravitation. Proceedings, 31st Rencontres de Moriond, 16th Moriond Workshop, Les Arcs, France, January 2-27, 1996*, pages 405–408, 1996.

[17] Ken Kiers and Michel H. G. Tytgat. Neutrino ground state in a dense star. *Phys. Rev. D*, 57:5970–5981, 1998.

[18] E. Fischbach. Many-Body Neutrino-Exchange Interactions and Neutrino Mass: Comment on Phys. Rev. Lett. 120, 223202 (2018). 2018.

[19] J. A. Grifols, E. Masso, and R. Toldra. Majorana neutrinos and long range forces. *Phys. Lett. B*, 389:563–565, 1996.

[20] A. Strumia and F. Vissani. Neutrino masses and mixings and... 2006.

[21] Maurizio Lusignoli and Silvano Petrarca. Remarks on the forces generated by two-neutrino exchange. *Eur. Phys. J. C*, 71:1568, 2011.

[22] Quan Le Thien and Dennis E. Krause. Spin-Independent Two-Neutrino Exchange Potential with Mixing and $CP$-Violation. *Phys. Rev.*, D99(11):116006, 2019.

[23] F. Ferrer, J. A. Grifols, and M. Nowakowski. Long range forces induced by neutrinos at finite temperature. *Phys. Lett. B*, 446:111–116, 1999.

[24] M. A. Bouchiat and C. Bouchiat. Parity violation in atoms. *Rept. Prog. Phys.*, 60:1351–1396, 1997.

[25] J. Guena, M. Lintz, and M. A. Bouchiat. Atomic parity violation: Principles, recent results, present motivations. *Mod. Phys. Lett.*, A20:375–390, 2005.

[26] I. B. Khriplovich. *Parity Nonconservation in Atomic Phenomenon*. Gordon and Breach Science Publishers, 1991.

[27] J. Bernabeu, T. E. O. Ericson, and C. Jarlskog. Parity Violations by Neutral Currents in Muonic Atoms. *Phys. Lett.*, 50B:467, 1974.

[28] John David Jackson. *Classical Electrodynamics*. Wiley, 1998.

[29] T. Peter Emmons and E. Norval Fortson. *Parity Nonconservation in Atoms*, pages 237–269. Springer US, Boston, MA, 1987.

[30] J. S. Toll. Causality and the Dispersion Relation: Logical Foundations. *Phys. Rev.*, 104:1760–1770, 1956.

[31] E. Hecht. *Optics, 5th edition*. Pearson, 2015.

[32] B. A. Dobrescu and I. Mocioiu. Spin-dependent macroscopic forces from new particle exchange. *JHEP*, 11:005, 2006.

[33] D. Mund, B. Maerkisch, M. Deissenroth, J. Krempel, M. Schumann, H. Abele, A. Petoukhov, and T. Soldner. Determination of the Weak Axial Vector Coupling from a Measurement of the Beta-Asymmetry Parameter A in Neutron Beta Decay. *Phys. Rev. Lett.*, 110:172502, 2013.

[34] M. A. Bouchiat and C. Bouchiat. 1. Parity Violation Induced by Weak Neutral Currents in Atomic Physics. *J. Phys.(France)*, 35:899–927, 1974.

[35] R. Shankar. *Principles of quantum mechanics*. Springer Science & Business Media, 2012.

[36] Mitchel Weissbluth. Chapter 18 - hyperfine interactions. In Mitchel Weissbluth, editor, *Atoms and Molecules*, pages 358 – 384. Academic Press, 1978.

[37] A. Mooser, S. Ulmer, K. Blaum, K. Franke, H. Kracke, C. Leiteritz, W Quint, C. C. Rodegheri, C. Smorra, and J. Walz. Direct high-precision measurement of the magnetic moment of the proton. *Nature*, 509:596–599, 2014.

[38] G. P. Lepage. How to renormalize the Schrodinger equation. In *Nuclear physics. Proceedings, 8th Jorge Andre Swieca Summer School, Sao Jose dos Campos, Campos do Jordao, Brazil, January 26-February 7, 1997*, pages 135–180, 1997.

[39] W. Frank, D. J. Land, and R. M. Spector. Singular potentials. *Rev. Mod. Phys.*, 43:36–98, 1971.

[40] T. Asaka, M. Tanaka, K. Tsumura, and M. Yoshimura. Precision electroweak shift of muonium hyperfine splitting. 10 2018.

[41] Philippe Brax, Sylvain Fichet, and Guillaume Pignol. Bounding quantum dark forces. *Phys. Rev. D*, 97(11):115034, 2018.

[42] Alexandria Costantino, Sylvain Fichet, and Philip Tanedo. Exotic spin-dependent forces from a hidden sector. *JHEP*, 03:148, 2020.

[43] R. P. Feynman. *Feynman Lectures on Gravitation, section 2.3*. Addison-Wesley, Reading, MA, 1995.

[44] Quan Le Thien and Dennis E. Krause. Spin-Independent Two-Neutrino Exchange Potential with Mixing and $CP$-Violation. *Phys. Rev. D*, 99(11):116006, 2019.

[45] Alexandria Costantino and Sylvain Fichet. The Neutrino Casimir Force. *JHEP*, 09:122, 2020.

[46] Alejandro Segarra and José Bernabéu. Absolute neutrino mass and the Dirac/Majorana distinction from the weak interaction of aggregate matter. *Phys. Rev. D*, 101(9):093004, 2020.

[47] Patrick D. Bolton, Frank F. Deppisch, and Chandan Hati. Probing new physics with long-range neutrino interactions: an effective field theory approach. *JHEP*, 07:013, 2020.

[48] A. Abada, M. B. Gavela, and O. Pene. To rescue a star. *Phys. Lett. B*, 387:315–319, 1996.

[49] M. Kachelriess. Neutrino selfenergy and pair creation in neutron stars. *Phys. Lett. B*, 426:89–94, 1998.

[50] A. Abada, O. Pene, and J. Rodriguez-Quintero. Finite size effects on multibody neutrino exchange. *Phys. Rev. D*, 58:073001, 1998.

[51] Jiro Arafune and Yukihiro Mimura. Finiteness of multibody neutrino exchange potential energy in neutron stars. *Prog. Theor. Phys.*, 100:1083–1088, 1998.

[52] Nicholas Orlofsky and Yue Zhang. Neutrino as the dark force. *Phys. Rev. D*, 104(7):075010, 2021.

[53] Rupert Coy, Xun-Jie Xu, and Bingrong Yu. Neutrino forces and the Sommerfeld enhancement. *JHEP*, 06:093, 2022.

[54] Xun-jie Xu and Bingrong Yu. On the short-range behavior of neutrino forces beyond the Standard Model: from $1/r^5$ to $1/r^4$, $1/r^2$, and $1/r$. *JHEP*, 02:008, 2022.

[55] J. A. Grifols and S. Tortosa. Residual long range pseudoscalar forces between unpolarized macroscopic bodies. *Phys. Lett. B*, 328:98–102, 1994.

[56] F. Ferrer and J. A. Grifols. Long range forces from pseudoscalar exchange. *Phys. Rev. D*, 58:096006, 1998.

[57] Hannah Banks and Matthew Mccullough. Charting the fifth force landscape. *Phys. Rev. D*, 103(7):075018, 2021.

[58] Mitrajyoti Ghosh, Yuval Grossman, and Walter Tangarife. Probing the two-neutrino exchange force using atomic parity violation. *Phys. Rev. D*, 101(11):116006, 2020.

[59] C. J. Horowitz and James T. Pantaleone. Long range forces from the cosmological neutrinos background. *Phys. Lett. B*, 319:186–190, 1993.

[60] F. Ferrer, J. A. Grifols, and M. Nowakowski. Long range neutrino forces in the cosmic relic neutrino background. *Phys. Rev. D*, 61:057304, 2000.

[61] Carlo Giunti and Chung W. Kim. *Fundamentals of Neutrino Physics and Astrophysics*. 2007.

[62] N. P. Landsman and C. G. van Weert. Real and Imaginary Time Field Theory at Finite Temperature and Density. *Phys. Rept.*, 145:141, 1987.

[63] Dirk Notzold and Georg Raffelt. Neutrino Dispersion at Finite Temperature and Density. *Nucl. Phys. B*, 307:924–936, 1988.

[64] Mariano Quiros. Finite temperature field theory and phase transitions. In *ICTP Summer School in High-Energy Physics and Cosmology*, pages 187–259, 1 1999.

[65] J. I. Kapusta and Charles Gale. *Finite-temperature field theory: Principles and applications*. Cambridge Monographs on Mathematical Physics. Cambridge University Press, 2011.

[66] Mikko Laine and Aleksi Vuorinen. *Basics of Thermal Field Theory*, volume 925. Springer, 2016.

[67] Steven Weinberg. *Cosmology*. OUP Oxford, 2008.

[68] Ivan Esteban, M. C. Gonzalez-Garcia, Michele Maltoni, Thomas Schwetz, and Albert Zhou. The fate of hints: updated global analysis of three-flavor neutrino oscillations. *JHEP*, 09:178, 2020.

[69] Pasquale D. Serpico and Georg G. Raffelt. Lepton asymmetry and primordial nucleosynthesis in the era of precision cosmology. *Phys. Rev. D*, 71:127301, 2005.

[70] Julien Lesgourgues and Sergio Pastor. Massive neutrinos and cosmology. *Phys. Rept.*, 429:307–379, 2006.

[71] Ken Van Tilburg. Wake Forces. *to appear*.

[72] T. A. Wagner, S. Schlamminger, J. H. Gundlach, and E. G. Adelberger. Torsion-balance tests of the weak equivalence principle. *Class. Quant. Grav.*, 29:184002, 2012.

[73] E. G. Adelberger, J. H. Gundlach, B. R. Heckel, S. Hoedl, and S. Schlamminger. Torsion balance experiments: A low-energy frontier of particle physics. *Prog. Part. Nucl. Phys.*, 62:102–134, 2009.

[74] Allan Franklin and Ephraim Fischbach. *The Rise and Fall of the Fifth Force*. Springer, 2016.

[75] J. K. Hoskins, R. D. Newman, R. Spero, and J. Schultz. Experimental tests of the gravitational inverse square law for mass separations from 2-cm to 105-cm. *Phys. Rev. D*, 32:3084–3095, 1985.

[76] J. G. Lee, E. G. Adelberger, T. S. Cook, S. M. Fleischer, and B. R. Heckel. New Test of the Gravitational $1/r^2$ Law at Separations down to 52 $\mu$m. *Phys. Rev. Lett.*, 124(10):101101, 2020.

[77] Wen-Hai Tan et al. Improvement for Testing the Gravitational Inverse-Square Law at the Submillimeter Range. *Phys. Rev. Lett.*, 124(5):051301, 2020.

[78] Stephan Schlamminger, K. Y. Choi, T. A. Wagner, J. H. Gundlach, and E. G. Adelberger. Test of the equivalence principle using a rotating torsion balance. *Phys. Rev. Lett.*, 100:041101, 2008.

[79] G. L. Smith, C. D. Hoyle, J. H. Gundlach, E. G. Adelberger, Blayne R. Heckel,

and H. E. Swanson. Short range tests of the equivalence principle. *Phys. Rev. D*, 61:022001, 2000.

[80] Shan-Qing Yang, Bi-Fu Zhan, Qing-Lan Wang, Cheng-Gang Shao, Liang-Cheng Tu, Wen-Hai Tan, and Jun Luo. Test of the Gravitational Inverse Square Law at Millimeter Ranges. *Phys. Rev. Lett.*, 108:081101, 2012.

[81] David C. Moore and Andrew A. Geraci. Searching for new physics using optically levitated sensors. *Quantum Sci. Technol.*, 6:014008, 2021.

[82] Daniel R Long. Experimental examination of the gravitational inverse square law. *Nature*, 260(5550):417–418, 1976.

[83] V. I. Kopeikin. Flux and spectrum of reactor antineutrinos. *Phys. Atom. Nucl.*, 75:143–152, 2012.

[84] Núria Vinyoles, Aldo M. Serenelli, Francesco L. Villante, Sarbani Basu, Johannes Bergström, M. C. Gonzalez-Garcia, Michele Maltoni, Carlos Peña Garay, and Ningqiang Song. A new Generation of Standard Solar Models. *Astrophys. J.*, 835(2):202, 2017.

[85] M. Kachelriess, Ricard Tomas, R. Buras, H. Th. Janka, A. Marek, and M. Rampp. Exploiting the neutronization burst of a galactic supernova. *Phys. Rev. D*, 71:063003, 2005.

[86] Edoardo Vitagliano, Irene Tamborra, and Georg Raffelt. Grand Unified Neutrino Spectrum at Earth: Sources and Spectral Components. *Rev. Mod. Phys.*, 92:45006, 2020.

[87] Babak Abi et al. Deep Underground Neutrino Experiment (DUNE), Far Detector Technical Design Report, Volume I Introduction to DUNE. *JINST*, 15(08):T08008, 2020.

[88] Diego Blas, Ivan Esteban, M. C. Gonzalez-Garcia, and Jordi Salvado. On neutrino-mediated potentials in a neutrino background. 12 2022.

[89] Joseph Sir b. Larmor. Lxiii. on the theory of the magnetic influence on spectra; and on the radiation from moving ions. *Philosophical Magazine Series 1*, 44:503–512, 1897.

[90] Dennis Krause, Harry T. Kloor, and Ephraim Fischbach. Multipole radiation from massive fields: Application to binary pulsar systems. *Phys. Rev. D*, 49:6892–6906, 1994.

[91] Subhendra Mohanty and Prafulla Kumar Panda. Particle physics bounds from the Hulse-Taylor binary. *Phys. Rev. D*, 53:5723–5726, 1996.

[92] Jeff A. Dror, Ranjan Laha, and Toby Opferkuch. Probing muonic forces with neutron star binaries. *Phys. Rev. D*, 102(2):023005, 2020.

[93] Tanmay Kumar Poddar, Subhendra Mohanty, and Soumya Jana. Vector gauge boson radiation from compact binary systems in a gauged $L_\mu - L_\tau$ scenario. *Phys. Rev. D*, 100(12):123023, 2019.

[94] Junwu Huang, Matthew C. Johnson, Laura Sagunski, Mairi Sakellariadou, and Jun Zhang. Prospects for axion searches with Advanced LIGO through binary mergers. *Phys. Rev. D*, 99(6):063013, 2019.

[95] Tanmay Kumar Poddar, Subhendra Mohanty, and Soumya Jana. Constraints on ultralight axions from compact binary systems. *Phys. Rev. D*, 101(8):083007, 2020.

[96] Anson Hook and Junwu Huang. Probing axions with neutron star inspirals and other stellar processes. *JHEP*, 06:036, 2018.

[97] Robert Foot. New Physics From Electric Charge Quantization? *Mod. Phys. Lett. A*, 6:527–530, 1991.

[98] Xiao-Gang He, Girish C. Joshi, H. Lew, and R. R. Volkas. Simplest Z-prime model. *Phys. Rev. D*, 44:2118–2132, 1991.

[99] Robert Foot, X. G. He, H. Lew, and R. R. Volkas. Model for a light Z-prime boson. *Phys. Rev. D*, 50:4571–4580, 1994.

[100] Julian Heeck and Werner Rodejohann. Gauged $L_\mu - L_\tau$ Symmetry at the Electroweak Scale. *Phys. Rev. D*, 84:075007, 2011.

[101] Joachim Kopp, Ranjan Laha, Toby Opferkuch, and William Shepherd. Cuckoo's eggs in neutron stars: can LIGO hear chirps from the dark sector? *JHEP*, 11:096, 2018.

[102] Stephon Alexander, Evan McDonough, Robert Sims, and Nicolas Yunes. Hidden-Sector Modifications to Gravitational Waves From Binary Inspirals. *Class. Quant. Grav.*, 35(23):235012, 2018.

[103] Han Gil Choi and Sunghoon Jung. New probe of dark matter-induced fifth force with neutron star inspirals. *Phys. Rev. D*, 99(1):015013, 2019.

[104] Marco Fabbrichesi and Alfredo Urbano. Charged neutron stars and observational tests of a dark force weaker than gravity. *JCAP*, 06:007, 2020.

[105] Brian C. Seymour and Kent Yagi. Probing Massive Scalar Fields from a Pulsar in a Stellar Triple System. *Class. Quant. Grav.*, 37(14):145008, 2020.

[106] Mitrajyoti Ghosh, Yuval Grossman, Walter Tangarife, Xun-Jie Xu, and Bingrong Yu. Neutrino forces in neutrino backgrounds. 9 2022.

[107] Willem van Straten, M. Bailes, M. C. Britton, S. R. Kulkarni, S. B. Anderson, R. N. Manchester, and J. Sarkissian. A Test of General Relativity from the three-dimensional orbital geometry of a binary pulsar. *Nature*, 412:158–160, 2001.

[108] M. Kramer et al. Tests of general relativity from timing the double pulsar. *Science*, 314:97–102, 2006.

[109] I. H. Stairs, S. E. Thorsett, J. H. Taylor, and A. Wolszczan. Studies of the relativistic binary pulsar psr b1534+12: I. timing analysis. *Astrophys. J.*, 581:501–508, 2002.

[110] R. M. Shannon, S. Johnston, and R. N. Manchester. The kinematics and

orbital dynamics of the PSR B1259−63/LS 2883 system from 23 yr of pulsar timing. *Mon. Not. Roy. Astron. Soc.*, 437(4):3255–3264, 2014.

[111] John Antoniadis et al. A Massive Pulsar in a Compact Relativistic Binary. *Science*, 340:6131, 2013.

[112] N. D. Ramesh Bhat, Matthew Bailes, and Joris P. W. Verbiest. Gravitational-radiation losses from the pulsar-white-dwarf binary PSR J1141-6545. *Phys. Rev. D*, 77:124017, 2008.

[113] Paulo C. C. Freire, Norbert Wex, Gilles Esposito-Farese, Joris P. W. Verbiest, Matthew Bailes, Bryan A. Jacoby, Michael Kramer, Ingrid H. Stairs, John Antoniadis, and Gemma H. Janssen. The relativistic pulsar-white dwarf binary PSR J1738+0333 II. The most stringent test of scalar-tensor gravity. *Mon. Not. Roy. Astron. Soc.*, 423:3328, 2012.

[114] Robert D. Ferdman et al. PSR J1756−2251: a pulsar with a low-mass neutron star companion. *Mon. Not. Roy. Astron. Soc.*, 443(3):2183–2196, 2014.

[115] Joeri van Leeuwen et al. The Binary Companion of Young, Relativistic Pulsar J1906+0746. *Astrophys. J.*, 798(2):118, 2015.

[116] Bryan A. Jacoby, P. B. Cameron, F. A. Jenet, S. B. Anderson, R. N. Murty, and S. R. Kulkarni. Measurement of Orbital Decay in the Double Neutron Star Binary PSR B2127+11C. *Astrophys. J. Lett.*, 644:L113–L116, 2006.

[117] Hooman Davoudiasl and Peter B Denton. Ultralight Boson Dark Matter and Event Horizon Telescope Observations of M87*. *Phys. Rev. Lett.*, 123(2):021102, 2019.

[118] R. A. Hulse and J. H. Taylor. Discovery of a pulsar in a binary system. *Astrophys. J. Lett.*, 195:L51–L53, 1975.

[119] J. H. Taylor and J. M. Weisberg. A new test of general relativity: Gravitational radiation and the binary pulsar PS R 1913+16. *Astrophys. J.*, 253:908–920, 1982.

[120] Joel M Weisberg and Yuping Huang. Relativistic measurements from timing the binary pulsar psr b1913+ 16. *The Astrophysical Journal*, 829(1):55, 2016.

[121] Mukremin Kilic, JJ Hermes, A Gianninas, and Warren R Brown. Psr j1738+ 0333: the first millisecond pulsar+ pulsating white dwarf binary. *Monthly Notices of the Royal Astronomical Society: Letters*, 446(1):L26–L30, 2015.

[122] P. C. Peters and J. Mathews. Gravitational radiation from point masses in a Keplerian orbit. *Phys. Rev.*, 131:435–439, 1963.

[123] D. G. Yakovlev, A. D. Kaminker, Oleg Y. Gnedin, and P. Haensel. Neutrino emission from neutron stars. *Phys. Rept.*, 354:1, 2001.

[124] Raghuveer Garani and Julian Heeck. Dark matter interactions with muons in neutron stars. *Phys. Rev. D*, 100(3):035039, 2019.

[125] J. M. Pearson, N. Chamel, A. Y. Potekhin, A. F. Fantina, C. Ducoin, A. K. Dutta, and S. Goriely. Unified equations of state for cold non-accreting neutron stars with Brussels–Montreal functionals – I. Role of symmetry energy. *Mon. Not. Roy. Astron. Soc.*, 481(3):2994–3026, 2018. [Erratum: Mon.Not.Roy.Astron.Soc. 486, 768 (2019)].

[126] Ian Harry and Tanja Hinderer. Observing and measuring the neutron-star equation-of-state in spinning binary neutron star systems. *Class. Quant. Grav.*, 35(14):145010, 2018.

[127] FengShou Zhang and LieWen Chen. Proton fraction in neutron stars. *Chin. Phys. Lett.*, 18:142, 2001.

[128] Ziro Maki, Masami Nakagawa, and Shoichi Sakata. Remarks on the unified model of elementary particles. *Prog. Theor. Phys.*, 28:870–880, 1962.

[129] T. Inami and C. S. Lim. Effects of Superheavy Quarks and Leptons in Low-Energy Weak Processes k(L) —> mu anti-mu, K+ —> pi+ Neutrino anti-neutrino and K0 <—> anti-K0. *Prog. Theor. Phys.*, 65:297, 1981. [Erratum: Prog.Theor.Phys. 65, 1772 (1981)].

[130] John S. Hagelin and Laurence S. Littenberg. Rare Kaon Decays. *Prog. Part. Nucl. Phys.*, 23:1, 1989.

[131] Claudio O. Dib. Bound on V(td) from K+- —> pi+- neutrino anti-neutrino and B factories. *Phys. Lett. B*, 282:201–206, 1992.

[132] Gerhard Buchalla and Andrzej J. Buras. The rare decays $K^+ \to \pi^+ \nu\bar{\nu}$ and $K_L \to \mu^+\mu^-$ beyond leading logarithms. *Nucl. Phys. B*, 412:106–142, 1994.

[133] Giancarlo D'Ambrosio and Gino Isidori. CP violation in kaon decays. *Int. J. Mod. Phys. A*, 13:1–94, 1998.

[134] A. Pich. Rare kaon decays. In *Workshop on K Physics*, 10 1996.

[135] Andrzej J. Buras and Robert Fleischer. Quark mixing, CP violation and rare decays after the top quark discovery. *Adv. Ser. Direct. High Energy Phys.*, 15:65–238, 1998.

[136] Eduardo Cortina Gil et al. An investigation of the very rare $K^+ \to \pi^+ \nu\bar{\nu}$ decay. *JHEP*, 11:042, 2020.

[137] J. K. Ahn et al. Study of the $K_L \to \pi^0 \nu\bar{\nu}$ decay at the J-PARC KOTO experiment. 12 2020.

[138] Andrzej J. Buras, Dario Buttazzo, Jennifer Girrbach-Noe, and Robert Knegjens. $K^+ \to \pi^+ \nu\bar{\nu}$ and $K_L \to \pi^0 \nu\bar{\nu}$ in the Standard Model: status and perspectives. *JHEP*, 11:033, 2015.

[139] Gerhard Buchalla and Andrzej J. Buras. The rare decays $K \to \pi\nu\bar{\nu}$, $B \to X\nu\bar{\nu}$ and $B \to l^+l^-$: An Update. *Nucl. Phys. B*, 548:309–327, 1999.

[140] Federico Mescia and Christopher Smith. Improved estimates of rare K decay matrix-elements from Kl3 decays. *Phys. Rev. D*, 76:034017, 2007.

[141] Richard F. Lebed. Relating CKM parametrizations and unitarity triangles. *Phys. Rev. D*, 55:348–352, 1997.

[142] Giancarlo D'Ambrosio and Teppei Kitahara. Direct $CP$ Violation in $K \to \mu^+\mu^-$. *Phys. Rev. Lett.*, 119(20):201802, 2017.

[143] B. R. Martin, E. De Rafael, and J. Smith. Neutral kaon decays into lepton pairs. *Phys. Rev. D*, 2:179–200, 1970.

[144] A. Pais and S. B. Treiman. Study of the decays k —¿ l + anti-l and k —¿ pi + l + anti-l. *Phys. Rev.*, 176:1974–1978, 1968.

[145] L. M. Sehgal. Tests of cp and cpt invariance in the decay k(l) —¿ l + anti-l. *Phys. Rev.*, 181:2151, 1969.

[146] Norman H. Christ and T. D. Lee. CP Nonconservation and Inequalities Between $\mu^+\mu^-$ and $2\gamma$ Decay Rates of $K_S^0$ and $K_L^0$. *Phys. Rev. D*, 4:209–212, 1971.

[147] L. M. Sehgal. Electromagnetic contribution to the decays K(S) —> lepton anti-lepton and K(L) —> lepton anti-lepton. *Phys. Rev.*, 183:1511, 1969. [Erratum: Phys.Rev.D 4, 1582 (1971)].

[148] G. V. Dass and L. Wolfenstein. Cp non-invariance and the k(s) —> mu+ mu- decay rate. *Phys. Lett. B*, 38:435–438, 1972.

[149] M. K. Gaillard and Benjamin W. Lee. Rare Decay Modes of the K-Mesons in Gauge Theories. *Phys. Rev. D*, 10:897, 1974.

[150] M. K. Gaillard, Benjamin W. Lee, and R. E. Shrock. Comment on calculations of the $K_L \to \mu^+\mu^-$ decay rate in gauge theories. *Phys. Rev.*, D13:2674, 1976.

[151] Andrzej J. Buras. An Upper Bound on the Top Quark Mass from Rare Processes. *Phys. Rev. Lett.*, 46:1354, 1981.

[152] L. Bergstrom, E. Masso, P. Singer, and D. Wyler. $K_L \to \mu^+\mu^-$, Top Mass and Bottom Lifetime. *Phys. Lett.*, 134B:373, 1984.

[153] C. Q. Geng and John N. Ng. Constraints on T Quark Mass, Quark Mixings From $K_L \to \mu\bar{\mu}$ and Relations to Other Rare Decays. *Phys. Rev.*, D41:2351, 1990.

[154] E. B. Bogomolny, V. A. Novikov, and Mikhail A. Shifman. K(L) –¿ 2 mu Decay in the Weinberg-Salam Model. *Sov. J. Nucl. Phys.*, 23:435, 1976. [Yad. Fiz.23,825(1976)].

[155] Benjamin W. Lee, J. R. Primack, and S. B. Treiman. Some Physical Constraints on Gauge Models of Weak Interactions. *Phys. Rev.*, D7:510–516, 1973.

[156] M. B. Voloshin and E. P. Shabalin. Contribution of Two Photon Mechanism to Real Part of the K(L) –¿ mu+ mu- Decay Amplitude and Calculations of Charmed Particle Mass. *JETP Lett.*, 23:107–110, 1976. [Pisma Zh. Eksp. Teor. Fiz.23,123(1976)].

[157] R. E. Shrock and M. B. Voloshin. Bounds on Quark Mixing Angles From the Decay $K(\mathrm{l}) \to \mu\bar{\mu}$. *Phys. Lett.*, 87B:375–378, 1979.

[158] Peter Herczeg. Muon Polarization in $K_L \to \mu^+\mu^-$. *Phys. Rev. D*, 27:1512, 1983.

[159] H. Stern and M. K. Gaillard. Review of the $K_L \to \mu^+\mu^-$ puzzle. *Annals Phys.*, 76:580–606, 1973.

[160] Yuval Grossman and Yosef Nir. K(L) —> pi0 neutrino anti-neutrino beyond the standard model. *Phys. Lett. B*, 398:163–168, 1997.

[161] Jason Aebischer, Andrzej J. Buras, and Jacky Kumar. Another SMEFT Story: $Z'$ Facing New Results on $\varepsilon'/\varepsilon$, $\Delta M_K$ and $K \to \pi\nu\bar{\nu}$. *JHEP*, 12:097, 2020.

[162] Rusa Mandal and Antonio Pich. Constraints on scalar leptoquarks from lepton and kaon physics. *JHEP*, 12:089, 2019.

[163] Motoi Endo, Toru Goto, Teppei Kitahara, Satoshi Mishima, Daiki Ueda, and Kei Yamamoto. Gluino-mediated electroweak penguin with flavor-violating trilinear couplings. *JHEP*, 04:019, 2018.

[164] Christoph Bobeth and Andrzej J. Buras. Leptoquarks meet $\varepsilon'/\varepsilon$ and rare Kaon processes. *JHEP*, 02:101, 2018.

[165] Veronika Chobanova, Giancarlo D'Ambrosio, Teppei Kitahara, Miriam Lucio Martinez, Diego Martinez Santos, Isabel Suarez Fernandez, and Kei Yamamoto. Probing SUSY effects in $K_S^0 \to \mu^+\mu^-$. *JHEP*, 05:024, 2018.

[166] Christoph Bobeth, Andrzej J. Buras, Alejandro Celis, and Martin Jung. Yukawa enhancement of $Z$-mediated new physics in $\Delta S = 2$ and $\Delta B = 2$ processes. *JHEP*, 07:124, 2017.

[167] Motoi Endo, Teppei Kitahara, Satoshi Mishima, and Kei Yamamoto. Revisiting Kaon Physics in General $Z$ Scenario. *Phys. Lett. B*, 771:37–44, 2017.

[168] Morimitsu Tanimoto and Kei Yamamoto. Probing SUSY with 10 TeV stop mass in rare decays and CP violation of kaon. *PTEP*, 2016(12):123B02, 2016.

[169] Andrzej J. Buras. New physics patterns in $\varepsilon'/\varepsilon$ and $\varepsilon_K$ with implications for rare kaon decays and $\Delta M_K$. *JHEP*, 04:071, 2016.

[170] Andrzej J. Buras, Dario Buttazzo, and Robert Knegjens. $K \to \pi\nu\bar{\nu}$ and $\varepsilon'/\varepsilon$ in simplified new physics models. *JHEP*, 11:166, 2015.

[171] Monika Blanke, Andrzej J. Buras, Bjorn Duling, Katrin Gemmler, and Stefania Gori. Rare K and B Decays in a Warped Extra Dimension with Custodial Protection. *JHEP*, 03:108, 2009.

[172] Federico Mescia, Christopher Smith, and Stephanie Trine. K(L) —> pi0 e+ e- and K(L) —> pi0 mu+ mu-: A Binary star on the stage of flavor physics. *JHEP*, 08:088, 2006.

[173] N. G. Deshpande, Dilip Kumar Ghosh, and Xiao-Gang He. Constraints on new physics from K —> pi nu anti-nu. *Phys. Rev. D*, 70:093003, 2004.

[174] Andreas Crivellin, Giancarlo D'Ambrosio, Martin Hoferichter, and Lewis C. Tunstall. Violation of lepton flavor and lepton flavor universality in rare kaon decays. *Phys. Rev. D*, 93(7):074038, 2016.

[175] Teppei Kitahara, Takemichi Okui, Gilad Perez, Yotam Soreq, and Kohsaku

Tobioka. New physics implications of recent search for $K_L \to \pi^0 \nu\bar{\nu}$ at KOTO. *Phys. Rev. Lett.*, 124(7):071801, 2020.

[176] Robert Ziegler, Jure Zupan, and Roman Zwicky. Three Exceptions to the Grossman-Nir Bound. *JHEP*, 07:229, 2020.

[177] Xiao-Gang He, Xiao-Dong Ma, Jusak Tandean, and German Valencia. Evading the Grossman-Nir bound with $\Delta I = 3/2$ new physics. *JHEP*, 08(08):034, 2020.

[178] Stefania Gori, Gilad Perez, and Kohsaku Tobioka. KOTO vs. NA62 Dark Scalar Searches. *JHEP*, 08:110, 2020.

[179] Roel Aaij et al. Constraints on the $K_0^S \to \mu^+\mu^-$ Branching Fraction. *Phys. Rev. Lett.*, 125(23):231801, 2020.

[180] F. Ambrosino et al. KLEVER: An experiment to measure BR($K_L \to \pi^0 \nu\bar{\nu}$) at the CERN SPS. 1 2019.

[181] Roel Aaij et al. Improved limit on the branching fraction of the rare decay $K_S^0 \to \mu^+\mu^-$. *Eur. Phys. J. C*, 77(10):678, 2017.

[182] G. Amelino-Camelia et al. Physics with the KLOE-2 experiment at the upgraded DA$\phi$NE. *Eur. Phys. J. C*, 68:619–681, 2010.

[183] E. Abouzaid et al. Measurements of the Decay $K_L \to e^+e^-\gamma$. *Phys. Rev. Lett.*, 99:051804, 2007.

[184] Riccardo Lollini. The $K^+ \to \pi^+ \nu\bar{\nu}$ Decay and New Physics Searches at NA62. *Acta Phys. Polon. Supp.*, 14:41, 2021.

[185] A. Cerri et al. Opportunities in Flavour Physics at the HL-LHC and HE-LHC. 2018.

[186] G. Ecker and A. Pich. The Longitudinal muon polarization in K(L) —> mu+ mu-. *Nucl. Phys. B*, 366:189–205, 1991.

[187] Gino Isidori and Rene Unterdorfer. On the short distance constraints from $K_{L,S} \to \mu^+\mu^-$. *JHEP*, 01:009, 2004.

[188] Martin Gorbahn and Ulrich Haisch. Charm Quark Contribution to $K_L \to \mu^+\mu^-$ at Next-to-Next-to-Leading. *Phys. Rev. Lett.*, 97:122002, 2006.

[189] Gilberto Colangelo, Ramon Stucki, and Lewis C. Tunstall. Dispersive treatment of $K_S \to \gamma\gamma$ and $K_S \to \gamma\ell^+\ell^-$. *Eur. Phys. J. C*, 76(11):604, 2016.

[190] D. Gomez Dumm and A. Pich. Long distance contributions to the $K_L \to \mu^+\mu^-$ decay width. *Phys. Rev. Lett.*, 80:4633–4636, 1998.

[191] M. Knecht, S. Peris, M. Perrottet, and E. de Rafael. Decay of pseudoscalars into lepton pairs and large-$N_c$ QCD. *Phys. Rev. Lett.*, 83:5230–5233, 1999.

[192] Giancarlo D'Ambrosio, David Greynat, and Grégory Vulvert. Standard Model and New Physics contributions to $K_L$ and $K_S$ into four leptons. *Eur. Phys. J. C*, 73(12):2678, 2013.

[193] Vincenzo Cirigliano, Gerhard Ecker, Helmut Neufeld, Antonio Pich, and Jorge Portoles. Kaon Decays in the Standard Model. *Rev. Mod. Phys.*, 84:399, 2012.

[194] Andrzej J. Buras, Felix Schwab, and Selma Uhlig. Waiting for precise measurements of $K^+ \to \pi^+\nu\bar{\nu}$ and $K_L \to \pi^0\nu\bar{\nu}$. *Rev. Mod. Phys.*, 80:965–1007, 2008.

[195] P. A. Zyla et al. Review of Particle Physics. *PTEP*, 2020(8):083C01, 2020.

[196] Laurence Littenberg. Rare kaon and pion decays. In *PSI Zuoz Summer School on Exploring the Limits of the Standard Model Zuoz, Engadin, Switzerland, August 18-24, 2002*, 2002.

[197] David Greynat and Eduardo de Rafael. Theoretical aspects of rare kaon decays. In *14th Rencontres de Blois on Matter - Anti-matter Asymmetry Chateau de Blois, France, June 17-22, 2002*, 2003.

[198] G. D'Ambrosio, G. Isidori, and J. Portoles. Can we extract short distance information from B($K_L \to \mu^+\mu^-$)? *Phys. Lett. B*, 423:385–394, 1998.

[199] R. Aleksan, Boris Kayser, and David London. Determining the quark mixing matrix from CP violating asymmetries. *Phys. Rev. Lett.*, 73:18–20, 1994.

[200] Gerhard Buchalla, Andrzej J. Buras, and Markus E. Lautenbacher. Weak decays beyond leading logarithms. *Rev. Mod. Phys.*, 68:1125–1144, 1996.

[201] Thomas Hermann, Mikolaj Misiak, and Matthias Steinhauser. Three-loop QCD corrections to $B_s \to \mu^+\mu^-$. *JHEP*, 12:097, 2013.

[202] S. Aoki et al. FLAG Review 2019. 2019.

[203] Alina Kleimenova. Latest results from NA62. *PoS*, DIS2019:122, 2019.

[204] A. A. Alves Junior et al. Prospects for Measurements with Strange Hadrons at LHCb. *JHEP*, 05:048, 2019.

[205] E. Mazzucato. NA48: Results on rare decays and future prospects. *Nucl. Phys. B Proc. Suppl.*, 99:81–92, 2001.

[206] R. H. Good, R. P. Matsen, F. Muller, O. Piccioni, W. M. Powell, H. S. White, W. B. Fowler, and R. W. Birge. Regeneration of Neutral $K$ Mesons and Their Mass Difference. *Phys. Rev.*, 124:1223–1239, 1961.

[207] A. Bohm, P. Darriulat, C. Grosso, V. Kaftanov, K. Kleinknecht, H. L. Lynch, C. Rubbia, H. Ticho, and K. Tittel. On $K_L$ - $K_S$ Regeneration in Copper. *Phys. Lett. B*, 27:594–598, 1968.

[208] K. Kleinknecht. K(l)-k(s) regeneration. *Fortsch. Phys.*, 21:57–84, 1973.

[209] A. Angelopoulos et al. Measurement of the neutral kaon regeneration amplitude in carbon at momenta below 1-GeV/c. *Phys. Lett. B*, 413:422–430, 1997.

[210] P. B. Siegel, W. B. Kaufmann, and W. R. Gibbs. K+ NUCLEUS ELASTIC SCATTERING AND CHARGE EXCHANGE. *Phys. Rev. C*, 30:1256–1266, 1984.

[211] W. A. Mehlhop, S. S. Murty, P. Bowles, T. H. Burnett, R. H. Good, C. H. Holland, O. Piccioni, and R. A. Swanson. Interference between Neutral Kaons and Their Mass Difference. *Phys. Rev.*, 172:1613–1625, 1968.

[212] Joachim Brod and Emmanuel Stamou. Impact of indirect CP violation on $\mathrm{Br}(K_S \to \mu^+\mu^-)_{\ell=0}$. 9 2022.

[213] L. M. Sehgal. $K_2^0 \to \mu^+ + \mu^-$ as a test of neutral lepton currents. *Nuovo Cim. A*, 45:785–788, 1966.

[214] L. M. Sehgal. Electromagnetic contribution to the decays $K_S \to l\bar{l}$ and $K_L \to l\bar{l}$. *Phys. Rev.*, 183:1511, 1969. [Erratum: Phys.Rev.D 4, 1582 (1971)].

[215] A. R. Clark, T. Elioff, R. C. Field, Henry J. Frisch, R. P. Johnson, L. T. Kerth, and W. A. Wenzel. Experimental Limits on the Decays $K_L^0 \to \mu^+\mu^-$, $e^+e^-$, and $\mu^\pm e^\mp$. *Phys. Rev. Lett.*, 26:1667–1671, 1971.

[216] R. G. Arnold et al. A Measurement of the Ratio of the Decay Rates $K_L^0 \to 2\gamma / K_L^0 \to 3\pi^0$. *Phys. Lett. B*, 28:56–57, 1968.

[217] H. H. Chen, K. Kawarabayashi, and Gordon L. Shaw. Comments on the unitarity bound in $K_L^0 \to \mu^+\mu^-$. *Phys. Rev. D*, 4:3514–3518, 1971.

[218] R. L. Workman. Review of Particle Physics. *PTEP*, 2022:083C01, 2022.

[219] Andrzej J. Buras and Elena Venturini. Searching for New Physics in Rare $K$ and $B$ Decays without $|V_{cb}|$ and $|V_{ub}|$ Uncertainties. *Acta Phys. Polon. B*, 53(6):A1, 9 2021.

[220] Norman H. Christ, Xu Feng, Luchang Jin, Cheng Tu, and Yidi Zhao. Lattice QCD calculation of the two-photon contributions to $K_L \to \mu^+\mu^-$ and $\pi^0 \to e^+e^-$ decays. *PoS*, LATTICE2019:128, 2020.

[221] Yidi Zhao and Norman H. Christ. Calculating $K \to \gamma\gamma$ using lattice QCD. *PoS*, LATTICE2021:451, 2022.

[222] Norman Christ, Xu Feng, Luchang Jin, Cheng Tu, and Yidi Zhao. Lattice QCD calculation of $\pi^0 \to e^+e^-$ decay. 8 2022.

[223] Roel Aaij et al. Constraints on the $K_S^0 \to \mu^+\mu^-$ Branching Fraction. *Phys. Rev. Lett.*, 125(23):231801, 2020.

[224] Miguel Fernandez Gomez on behalf of the LHCb Collaboration. Search for $k^0 \to \mu^+\mu^-\mu^+\mu^-$. Talk at the "International Conference on Kaon Physics" (KAON 2022), 13–16 September 2022, Osaka, Japan, `https://conference-indico.kek.jp/event/169/contributions/3464/`.

[225] Y. Aoki et al. FLAG Review 2021. *Eur. Phys. J. C*, 82(10):869, 2022.

[226] Rafel Escribano, Sergi Gonzàlez-Solís, Pere Masjuan, and Pablo Sanchez-Puertas. $\eta'$ transition form factor from space- and timelike experimental data. *Phys. Rev. D*, 94(5):054033, 2016.

[227] Liping Gan, Bastian Kubis, Emilie Passemar, and Sean Tulin. Precision tests of fundamental physics with $\eta$ and $\eta'$ mesons. *Phys. Rept.*, 945:1–105, 2022.

[228] John F. Donoghue, Barry R. Holstein, and Y. C. R. Lin. Chiral perturbation theory corrections to $K_L \to \gamma\gamma$. *Nucl. Phys. B*, 277:651–660, 1986.

[229] X. G. He, C. S. Huang, and X. Q. Li. SU(3) and nonet breaking effects in $K_L \to \gamma\gamma$ induced by $s \to d2$gluon due to anomaly. *Phys. Rev. D*, 67:096005, 2003.

[230] John F. Donoghue, Eugene Golowich, and Barry R. Holstein. Long Distance Chiral Contributions to the $K_L K_S$ Mass Difference. *Phys. Lett. B*, 135:481–486, 1984.

[231] Hai-Yang Cheng. How Good Is Nonet Symmetry for Pseudoscalar Mesons? *Phys. Lett. B*, 245:122–128, 1990.

[232] Giancarlo D'Ambrosio and Jorge Portoles. Analysis of $K_L \to \pi^+\pi^-\gamma$ in chiral perturbation theory. *Nucl. Phys. B*, 533:523–554, 1998.

[233] Antonio Pich and Eduardo de Rafael. Weak $K$-amplitudes in the chiral and $1/N_c$-expansions. *Phys. Lett. B*, 374:186–192, 1996.

[234] Jean-Marc Gerard, Christopher Smith, and Stephanie Trine. Radiative kaon decays and the penguin contribution to the $\Delta I = 1/2$ rule. *Nucl. Phys. B*, 730:1–36, 2005.

[235] R. Abbott et al. Direct CP violation and the $\Delta I = 1/2$ rule in $K \to \pi\pi$ decay from the standard model. *Phys. Rev. D*, 102(5):054509, 2020.

[236] Z. Bai et al. Standard Model Prediction for Direct CP Violation in K$\to\pi\pi$ Decay. *Phys. Rev. Lett.*, 115(21):212001, 2015.

[237] T. Blum et al. $K \to \pi\pi$ $\Delta I = 3/2$ decay amplitude in the continuum limit. *Phys. Rev. D*, 91(7):074502, 2015.

[238] T. Blum et al. The $K \to (\pi\pi)_{I=2}$ Decay Amplitude from Lattice QCD. *Phys. Rev. Lett.*, 108:141601, 2012.

[239] Antonio Pich and Antonio Rodríguez-Sánchez. SU(3) analysis of four-quark operators: $K \to \pi\pi$ and vacuum matrix elements. *JHEP*, 06:005, 2021.

[240] R Aaij et al. Measurements of the $\Lambda_b^0 \to J/\psi\Lambda$ decay amplitudes and the $\Lambda_b^0$ polarisation in $pp$ collisions at $\sqrt{s} = 7$ TeV. *Phys. Lett.*, B724:27–35, 2013.

[241] Georges Aad et al. Measurement of the parity-violating asymmetry parameter $\alpha_b$ and the helicity amplitudes for the decay $\Lambda_b^0 \to J/\psi + \Lambda^0$ with the ATLAS detector. *Phys. Rev.*, D89(9):092009, 2014.

[242] Roel Aaij et al. Measurement of matter-antimatter differences in beauty baryon decays. *Nature Phys.*, 13:391–396, 2017.

[243] Roel Aaij et al. First Observation of the Radiative Decay $\Lambda_b^0 \to \Lambda\gamma$. *Phys. Rev. Lett.*, 123(3):031801, 2019.

[244] Roel Aaij et al. Isospin amplitudes in $\Lambda_b^0 \to J/\psi\Lambda(\Sigma^0)$ and $\Xi_b^0 \to J/\psi\Xi^0(\Lambda)$ decays. 2019.

[245] M. B. Voloshin. Remarks on measurement of the decay $\Xi_b^- \to \Lambda_b\pi^-$. 2015.

[246] Fayyazuddin and M. Jamil Aslam. Hadronic weak decay $\mathcal{B}_b(\frac{1}{2}^+) \to \mathcal{B}(\frac{1}{2}^+, \frac{3}{2}^+) + V$. *Phys. Rev.*, D95(11):113002, 2017.

[247] Thomas Gutsche, Mikhail A. Ivanov, Jürgen G. Körner, and Valery E. Lyubovitskij. Nonleptonic two-body decays of single heavy baryons $\Lambda_Q$, $\Xi_Q$, and $\Omega_Q$ ($Q = b, c$) induced by $W$ emission in the covariant confined quark model. *Phys. Rev.*, D98(7):074011, 2018.

[248] Y. K. Hsiao, P. Y. Lin, C. C. Lih, and C. Q. Geng. Charmful two-body anti-triplet $b$-baryon decays. *Phys. Rev.*, D92:114013, 2015.

[249] Y. K. Hsiao, P. Y. Lin, L. W. Luo, and C. Q. Geng. Fragmentation fractions of two-body b-baryon decays. *Phys. Lett.*, B751:127–130, 2015.

[250] Jie Zhu, Zheng-Tao Wei, and Hong-Wei Ke. Semileptonic and nonleptonic weak decays of b0. *Phys. Rev.*, D99(5):054020, 2019.

[251] Thomas Gutsche, Mikhail A. Ivanov, Jürgen G. Körner, Valery E. Lyubovitskij, Vladimir V. Lyubushkin, and Pietro Santorelli. Theoretical description of the decays $\Lambda_b \to \Lambda^{(*)}(\frac{1}{2}^\pm, \frac{3}{2}^\pm) + J/\psi$. *Phys. Rev.*, D96(1):013003, 2017.

[252] Shibasis Roy, Rahul Sinha, and N. G. Deshpande. Non-leptonic beauty baryon decays and $CP$-asymmetries based on $SU(3)$-Flavor analysis. 2019.

[253] Michael Gronau and Jonathan L. Rosner. Flavor SU(3) and $\Lambda_b$ decays. *Phys. Rev.*, D89(3):037501, 2014. [Erratum: Phys. Rev.D91,no.11,119902(2015)].

[254] Min He, Xiao-Gang He, and Guan-Nan Li. CP-Violating Polarization Asymmetry in Charmless Two-Body Decays of Beauty Baryons. *Phys. Rev.*, D92(3):036010, 2015.

[255] Xiao-Gang He and Guan-Nan Li. Predictive $CP$ violating relations for charmless two-body decays of beauty baryons $\Xi_b^{-,0}$ and $\Lambda_b^0$ with flavor $SU(3)$ symmetry. *Phys. Lett.*, B750:82–88, 2015.

[256] R. Arora, G. K. Sidana, and M. P. Khanna. SU(3) predictions for nonleptonic weak decays of bottom baryons. *Phys. Rev.*, D45:4121–4127, 1992.

[257] Dong-Sheng Du and Da-Xin Zhang. SU(3) breaking effects in nonleptonic decays of the bottom baryons. *Phys. Rev.*, D50:2058–2066, 1994.

[258] J. G. Korner, M. Kramer, and D. Pirjol. Heavy baryons. *Prog. Part. Nucl. Phys.*, 33:787–868, 1994.

[259] Y. K. Hsiao and C. Q. Geng. Direct CP violation in $\Lambda_b$ decays. *Phys. Rev.*, D91(11):116007, 2015.

[260] Michael Gronau and Jonathan L. Rosner. $S$-wave nonleptonic hyperon decays and $\Xi_b^- \to \pi^-\Lambda_b$. *Phys. Rev.*, D93(3):034020, 2016.

[261] Michael Gronau and Jonathan L. Rosner. From $\Xi_b \to \Lambda_b\pi$ to $\Xi_c \to \Lambda_c\pi$. *Phys. Lett.*, B757:330–333, 2016.

[262] David A. Egolf, Roxanne P. Springer, and Joerg Urban. SU(3) predictions for weak decays of doubly heavy baryons including SU(3) breaking terms. *Phys. Rev.*, D68:013003, 2003.

[263] Adam K. Leibovich, Zoltan Ligeti, Iain W. Stewart, and Mark B. Wise. Predictions for nonleptonic Lambda(b) and Theta(b) decays. *Phys. Lett.*, B586:337–344, 2004.

[264] Yuval Grossman and Stefan Schacht. U-Spin Sum Rules for CP Asymmetries of Three-Body Charmed Baryon Decays. *Phys. Rev.*, D99(3):033005, 2019.

[265] Cai-Dian Lü, Wei Wang, and Fu-Sheng Yu. Test flavor SU(3) symmetry in exclusive $\Lambda_c$ decays. *Phys. Rev.*, D93(5):056008, 2016.

[266] C. Q. Geng, Y. K. Hsiao, Chia-Wei Liu, and Tien-Hsueh Tsai. Three-body charmed baryon Decays with SU(3) flavor symmetry. *Phys. Rev.*, D99(7):073003, 2019.

[267] Cai-Ping Jia, Di Wang, and Fu-Sheng Yu. Charmed baryon decays in $SU(3)_F$ symmetry. 2019.

[268] Martin J. Savage and Roxanne P. Springer. SU(3) Predictions for Charmed Baryon Decays. *Phys. Rev.*, D42:1527–1543, 1990.

[269] Martin J. Savage and Roxanne P. Springer. Very charming baryons. *Int. J. Mod. Phys.*, A6:1701–1712, 1991.

[270] Ru-Min Wang, Mao-Zhi Yang, Hai-Bo Li, and Xiao-Dong Cheng. Testing SU(3) Flavor Symmetry in Semileptonic and Two-body Nonleptonic Decays of Hyperons. *Phys. Rev.*, D100(7):076008, 2019.

[271] C. Q. Geng, Y. K. Hsiao, Chia-Wei Liu, and Tien-Hsueh Tsai. SU(3) symmetry breaking in charmed baryon decays. *Eur. Phys. J.*, C78(7):593, 2018.

[272] C. Q. Geng, Y. K. Hsiao, Chia-Wei Liu, and Tien-Hsueh Tsai. Antitriplet charmed baryon decays with SU(3) flavor symmetry. *Phys. Rev.*, D97(7):073006, 2018.

[273] C. Q. Geng, Y. K. Hsiao, Chia-Wei Liu, and Tien-Hsueh Tsai. Charmed Baryon Weak Decays with SU(3) Flavor Symmetry. *JHEP*, 11:147, 2017.

[274] H. J. Zhao, Yan-Li Wang, Y. K. Hsiao, and Yao Yu. A diagrammatic analysis of two-body charmed baryon decays with flavor symmetry. 2018.

[275] Michael Gronau, Jonathan L. Rosner, and Charles G. Wohl. Overview of $\Lambda_c$ decays. *Phys. Rev.*, D97(11):116015, 2018. [Addendum: Phys. Rev.D98,no.7,073003(2018)].

[276] D. Ebert and W. Kallies. Nonleptonic Decays of Charmed Baryons in the MIT Bag Model. *Phys. Lett.*, 131B:183, 1983. [Erratum: Phys. Lett.148B,502(1984)].

[277] Ikaros I. Y. Bigi. Weak Annihilation in Charm Baryon Decays: A Reevaluation. *Z. Phys.*, C9:197, 1981.

[278] I. I. Bigi. Probing CP Asymmetries in Charm Baryons Decays. 2012.

[279] Nathan Isgur and Mark B. Wise. Heavy baryon weak form-factors. *Nucl. Phys.*, B348:276–292, 1991.

[280] A. Khodjamirian, Ch. Klein, Th. Mannel, and Y. M. Wang. Form Factors and Strong Couplings of Heavy Baryons from QCD Light-Cone Sum Rules. *JHEP*, 09:106, 2011.

[281] Yu-Ming Wang and Yue-Long Shen. Perturbative Corrections to $\Lambda_b \to \Lambda$ Form Factors from QCD Light-Cone Sum Rules. *JHEP*, 02:179, 2016.

[282] Tomáš Husek and Stefan Leupold. Radiative corrections for the decay $\Sigma^0 \to \Lambda e^+ e^-$. 2019.

[283] Carlos Granados, Stefan Leupold, and Elisabetta Perotti. The electromagnetic Sigma-to-Lambda hyperon transition form factors at low energies. *Eur. Phys. J.*, A53(6):117, 2017.

[284] Bastian Kubis and Ulf G. Meissner. Baryon form-factors in chiral perturbation theory. *Eur. Phys. J.*, C18:747–756, 2001.

[285] Thomas Mannel and Yu-Ming Wang. Heavy-to-light baryonic form factors at large recoil. *JHEP*, 12:067, 2011.

[286] William Detmold, C. J. David Lin, Stefan Meinel, and Matthew Wingate. b→+- form factors and differential branching fraction from lattice QCD. *Phys. Rev.*, D87(7):074502, 2013.

[287] William Detmold and Stefan Meinel. $\Lambda_b \to \Lambda \ell^+ \ell^-$ form factors, differential branching fraction, and angular observables from lattice QCD with relativistic $b$ quarks. *Phys. Rev.*, D93(7):074501, 2016.

[288] Florian U. Bernlochner, Zoltan Ligeti, Dean J. Robinson, and William L. Sutcliffe. Precise predictions for $\Lambda_b \to \Lambda_c$ semileptonic decays. *Phys. Rev.*, D99(5):055008, 2019.

[289] D. Zeppenfeld. SU(3) Relations for B Meson Decays. *Z. Phys.*, C8:77, 1981.

[290] Martin Jung. Determining weak phases from $B \to J/\psi P$ decays. *Phys. Rev.*, D86:053008, 2012.

[291] Martin Jung and Stefan Schacht. Standard model predictions and new physics sensitivity in $B \to DD$ decays. *Phys. Rev.*, D91(3):034027, 2015.

[292] J. J. de Swart. The Octet model and its Clebsch-Gordan coefficients. *Rev. Mod. Phys.*, 35:916–939, 1963. [Erratum: Rev. Mod. Phys.37,326(1965)].

[293] Thomas A. Kaeding. Tables of SU(3) isoscalar factors. *Atom. Data Nucl. Data Tabl.*, 61:233–288, 1995.

[294] Thomas A. Kaeding and H. Thomas Williams. Program for generating tables of SU(3) coupling coefficients. *Comput. Phys. Commun.*, 98:398–414, 1996.

[295] Thomas Gutsche, Mikhail A. Ivanov, Jürgen G. Körner, Valery E. Lyubovitskij, and Pietro Santorelli. Polarization effects in the cascade decay ${}_b\ß(\ß p^-) + J/(\ß^{+-})$ in the covariant confined quark model. *Phys. Rev. D*, 88(11):114018, 2013.

[296] M. Tanabashi et al. Review of Particle Physics. *Phys. Rev.*, D98(3):030001, 2018.

[297] Oscar F. Hernandez, David London, Michael Gronau, and Jonathan L. Rosner. Measuring strong and weak phases in time independent B decays. *Phys. Lett.*, B333:500–506, 1994.

[298] Michael Gronau, Jonathan L. Rosner, and David London. Weak coupling phase from decays of charged B mesons to pi K and pi pi. *Phys. Rev. Lett.*, 73:21–24, 1994.

[299] Michael Gronau, Oscar F. Hernandez, David London, and Jonathan L. Rosner. Decays of B mesons to two light pseudoscalars. *Phys. Rev.*, D50:4529–4543, 1994.

[300] Michael Gronau, Oscar F. Hernandez, David London, and Jonathan L. Rosner. Broken SU(3) symmetry in two-body B decays. *Phys. Rev.*, D52:6356–6373, 1995.

[301] Matthias Neubert and Jonathan L. Rosner. Determination of the weak phase gamma from rate measurements in B+- —¿ pi K, pi pi decays. *Phys. Rev. Lett.*, 81:5076–5079, 1998.

[302] Michael Gronau. U spin symmetry in charmless B decays. *Phys. Lett.*, B492:297–302, 2000.

[303] Robert Fleischer. New strategies to extract Beta and gamma from B(d) —¿ pi+ pi- and B(S) —¿ K+ K-. *Phys. Lett.*, B459:306–320, 1999.

[304] Michael Gronau and Jonathan L. Rosner. The Role of $B_s \to K\pi$ in determining the weak phase $\gamma$. *Phys. Lett.*, B482:71–76, 2000.

[305] Xiao-Gang He. SU(3) analysis of annihilation contributions and CP violating relations in B —¿ P P decays. *Eur. Phys. J.*, C9:443–448, 1999.

[306] Bhubanjyoti Bhattacharya, Michael Gronau, and Jonathan L. Rosner. CP asymmetries in three-body $B^{\pm}$ decays to charged pions and kaons. *Phys. Lett.*, B726:337–343, 2013.

[307] Nathan Isgur. Isospin violating mass differences and mixing angles: the role of quark masses. *Phys. Rev.*, D21:779, 1980. [Erratum: Phys. Rev.D23,817(1981)].

[308] Di Wang. Sum rules for $CP$ asymmetries of charmed baryon decays in the $SU(3)_F$ limit. *Eur. Phys. J.*, C79(5):429, 2019.

[309] Bhubanjyoti Bhattacharya and Jonathan L. Rosner. Charmed meson decays to two pseudoscalars. *Phys. Rev.*, D81:014026, 2010.

[310] Gudrun Hiller, Martin Jung, and Stefan Schacht. SU(3)-flavor anatomy of nonleptonic charm decays. *Phys. Rev.*, D87(1):014024, 2013.

[311] Yuval Grossman and Stefan Schacht. The emergence of the $\Delta U = 0$ rule in charm physics. *JHEP*, 07:020, 2019.

[312] Sarah Müller, Ulrich Nierste, and Stefan Schacht. Sum Rules of Charm CP Asymmetries beyond the $SU(3)_F$ Limit. *Phys. Rev. Lett.*, 115(25):251802, 2015.

[313] Sarah Müller, Ulrich Nierste, and Stefan Schacht. Topological amplitudes in $D$ decays to two pseudoscalars: A global analysis with linear $SU(3)_F$ breaking. *Phys. Rev.*, D92(1):014004, 2015.

[314] Joachim Brod, Yuval Grossman, Alexander L. Kagan, and Jure Zupan. A Consistent Picture for Large Penguins in D -¿ pi+ pi-, K+ K-. *JHEP*, 10:161, 2012.

[315] Yuval Grossman, Alexander L. Kagan, and Jure Zupan. Testing for new physics in singly Cabibbo suppressed D decays. *Phys. Rev.*, D85:114036, 2012.

[316] Yuval Grossman, Alexander L. Kagan, and Yosef Nir. New physics and CP violation in singly Cabibbo suppressed D decays. *Phys. Rev.*, D75:036008, 2007.

[317] Adam F. Falk, Yuval Grossman, Zoltan Ligeti, and Alexey A. Petrov. SU(3) breaking and D0 - anti-D0 mixing. *Phys. Rev.*, D65:054034, 2002.

[318] Martin J. Savage. SU(3) violations in the nonleptonic decay of charmed hadrons. *Phys. Lett.*, B257:414–418, 1991.

[319] Ian Hinchliffe and Thomas A. Kaeding. Nonleptonic two-body decays of D mesons in broken SU(3). *Phys. Rev.*, D54:914–928, 1996.

[320] Martin Jung and Thomas Mannel. General Analysis of U-Spin Breaking in B Decays. *Phys. Rev.*, D80:116002, 2009.

[321] Michael Gronau, Yuval Grossman, Guy Raz, and Jonathan L. Rosner. Suppression of flavor symmetry breaking in B decay sum rules. *Phys. Lett.*, B635:207–212, 2006.

[322] David Pirtskhalava and Patipan Uttayarat. CP Violation and Flavor SU(3) Breaking in D-meson Decays. *Phys. Lett.*, B712:81–86, 2012.

[323] Franco Buccella, Ayan Paul, and Pietro Santorelli. $SU(3)_F$ breaking through final state interactions and $CP$ asymmetries in $D \to PP$ decays. *Phys. Rev.*, D99(11):113001, 2019.

[324] Yuval Grossman and Dean J. Robinson. SU(3) Sum Rules for Charm Decay. *JHEP*, 04:067, 2013.

[325] L. A. Copley, Nathan Isgur, and Gabriel Karl. Charmed Baryons in a Quark Model with Hyperfine Interactions. *Phys. Rev.*, D20:768, 1979. [Erratum: Phys. Rev.D23,817(1981)].

[326] Kim Maltman and Nathan Isgur. Baryons With Strangeness and Charm in a Quark Model With Chromodynamics. *Phys. Rev.*, D22:1701, 1980.

[327] J. Franklin, D. B. Lichtenberg, W. Namgung, and D. Carydas. Wave Function Mixing of Flavor Degenerate Baryons. *Phys. Rev.*, D24:2910, 1981.

[328] Martin J. Savage and Mark B. Wise. SU(3) Predictions for Nonleptonic $B$ Meson Decays to Charmed Baryons. *Nucl. Phys.*, B326:15–30, 1989.

[329] C. Glenn Boyd, Ming Lu, and Martin J. Savage. Heavy baryon mixing in chiral perturbation theory. *Phys. Rev.*, D55:5474–5478, 1997.

[330] Marek Karliner, Boaz Keren-Zur, Harry J. Lipkin, and Jonathan L. Rosner. The Quark Model and $b$ Baryons. *Annals Phys.*, 324:2–15, 2009.

[331] Sidney R. Coleman and Sheldon Lee Glashow. Electrodynamic properties of baryons in the unitary symmetry scheme. *Phys. Rev. Lett.*, 6:423, 1961.

[332] R. H. Dalitz and F. Von Hippel. Electromagnetic $\Lambda - \sigma^0$ mixing and charge symmetry for the $\Lambda$-hyperon. *Phys. Lett.*, 10:153–157, 1964.

[333] R. Horsley, J. Najjar, Y. Nakamura, H. Perlt, D. Pleiter, P. E. L. Rakow, G. Schierholz, A. Schiller, H. Stüben, and J. M. Zanotti. Lattice determination of Sigma-Lambda mixing. *Phys. Rev.*, D91(7):074512, 2015.

[334] Avraham Gal. Comment on "Lattice determination of $\Sigma$-$\Lambda$ mixing". *Phys. Rev.*, D92(1):018501, 2015.

[335] R. Horsley, J. Najjar, Y. Nakamura, H. Perlt, D. Pleiter, P. E. L. Rakow, G. Schierholz, A. Schiller, H. Stüben, and J. M. Zanotti. Reply to "Comment on 'Lattice determination of $\Sigma$-$\Lambda$ mixing'". *Phys. Rev.*, D92:018502, 2015.

[336] Z. R. Kordov, R. Horsley, Y. Nakamura, H. Perlt, P. E. L. Rakow, G. Schierholz, H. Stüben, R. D. Young, and J. M. Zanotti. Electromagnetic contribution to $\Sigma$-$\Lambda$ mixing using lattice QCD+QED. 2019.

[337] T. Feldmann and P. Kroll. Mixing of pseudoscalar mesons. *Phys. Scripta*, T99:13–22, 2002.

[338] T. Feldmann, P. Kroll, and B. Stech. Mixing and decay constants of pseudoscalar mesons: The Sequel. *Phys. Lett.*, B449:339–346, 1999.

[339] T. Feldmann, P. Kroll, and B. Stech. Mixing and decay constants of pseudoscalar mesons. *Phys. Rev.*, D58:114006, 1998.

[340] Thorsten Feldmann and Peter Kroll. Flavor symmetry breaking and mixing effects in the eta gamma and eta-prime gamma transition form-factors. *Eur. Phys. J.*, C5:327–335, 1998.

[341] Jozef J. Dudek, Robert G. Edwards, Balint Joo, Michael J. Peardon, David G. Richards, and Christopher E. Thomas. Isoscalar meson spectroscopy from lattice QCD. *Phys. Rev.*, D83:111502, 2011.

[342] Konstantin Ottnad. Pseudoscalar flavor-singlet mesons from lattice QCD.

In *9th International Workshop on Chiral Dynamics (CD18) Durham, NC, USA, September 17-21, 2018*, 2019.

[343] A. De Rujula, Howard Georgi, and S. L. Glashow. Hadron Masses in a Gauge Theory. *Phys. Rev.*, D12:147–162, 1975.

[344] J. Gasser and H. Leutwyler. Quark Masses. *Phys. Rept.*, 87:77–169, 1982.

[345] John F. Donoghue, Eugene Golowich, and Barry R. Holstein. Low-Energy Weak Interactions of Quarks. *Phys. Rept.*, 131:319–428, 1986.

[346] John F. Donoghue. Light Quark Masses and Chiral Symmetry. *Ann. Rev. Nucl. Part. Sci.*, 39:1–17, 1989.

[347] Gabriel Karl. Isospin violation and hyperon semileptonic decays. *Phys. Lett.*, B328:149–152, 1994. [Erratum: Phys. Lett.B341,449(1995)].

[348] J. Gasser and H. Leutwyler. Chiral Perturbation Theory: Expansions in the Mass of the Strange Quark. *Nucl. Phys.*, B250:465–516, 1985.

[349] Abraham Gal and Florian Scheck. Electromagnetic mass splittings of mesons and baryons in the quark model. *Nucl. Phys.*, B2:110–120, 1967.

[350] E. M. Henley and G. A. Miller. A Proposed test of charge symmetry in Sigma decay. *Phys. Rev.*, D50:7077–7078, 1994.

[351] Kim Maltman. Strong isospin mixing effects on the extraction of Delta I = 3/2 nonleptonic hyperon decay amplitudes. *Phys. Lett.*, B345:541–546, 1995.

[352] Gabriel Karl. Isospin violation in hyperon semileptonic decays. In *Hyperon physics symposium : Hyperon 99, September 27-29, 1999, Fermi National Accelerator Laboratory, Batavia, Illinois*, pages 41–42, 1999.

[353] Euy Soo Na and Barry R. Holstein. Isospin mixing and model dependence. *Phys. Rev.*, D56:4404–4407, 1997.

[354] David J. Gross, S. B. Treiman, and Frank Wilczek. Light Quark Masses and Isospin Violation. *Phys. Rev.*, D19:2188, 1979.

[355] P. Kroll. Isospin symmetry breaking through pi0 - eta - eta-prime mixing. *Mod. Phys. Lett.*, A20:2667–2684, 2005.

[356] Stephen L. Adler. Axial vector vertex in spinor electrodynamics. *Phys. Rev.*, 177:2426–2438, 1969. [,241(1969)].

[357] J. S. Bell and R. Jackiw. A PCAC puzzle: $\pi^0 \to \gamma\gamma$ in the $\sigma$ model. *Nuovo Cim.*, A60:47–61, 1969.

[358] Kim Maltman. q**2 dependence of meson mixing in few body charge symmetry breaking: pi0 - eta mixing to one loop in chiral perturbation theory. *Phys. Lett.*, B313:203–208, 1993.

[359] G. Berlad, A. Dar, G. Eilam, and J. Franklin. Dominance of electromagnetic effects in high energy hadron and photon induced reactions. *Annals Phys.*, 75:461–478, 1973.

[360] A. Ali, C. Hambrock, A. Ya. Parkhomenko, and Wei Wang. Light-Cone Distribution Amplitudes of the Ground State Bottom Baryons in HQET. *Eur. Phys. J.*, C73(2):2302, 2013.

[361] W. Roberts and Muslema Pervin. Heavy baryons in a quark model. *Int. J. Mod. Phys.*, A23:2817–2860, 2008.

[362] W. Greiner and Berndt Muller. *Theoretical physics. Vol. 2: Quantum mechanics. Symmetries*. 1989.

[363] Jonathan L. Rosner. Magnetic Moments of Composite Baryons, Quarks and Leptons. *Prog. Theor. Phys.*, 66:1422, 1981.

[364] Yu. V. Novozhilov. *Introduction to Elementary Particle Theory*. 1975.

[365] M. Peskin and D. Schroeder, *An Introduction to quantum field theory*, Addison-Wesley, 1995, USA.

[366] Alexei Yu. Smirnov and Xun-Jie Xu. Neutrino bound states and bound systems. *JHEP*, 08:170, 2022.

[367] W. Fetscher, P. Kokkas, P. Pavlopoulos, T. Schietinger, and T. Ruf. Regeneration of arbitrary coherent neutral kaon states: A new method for measuring the K0 anti-K0 forward scattering amplitude. *Z. Phys.*, C72:543–547, 1996.

[368] Helen R. Quinn, Thomas Schietinger, Joao P. Silva, and Arthur E. Snyder. Using kaon regeneration to probe the quark mixing parameter cos 2 beta in $B \to \psi K$ decays. *Phys. Rev. Lett.*, 85:5284–5287, 2000.

[369] Gustavo C. Branco, Luis Lavoura, and Joao P. Silva. CP Violation. *Int. Ser. Monogr. Phys.*, 103:1–536, 1999.

[370] E. Abouzaid et al. Measurements of the Decay $K_L \to e^+e^-\gamma$. *Phys. Rev. Lett.*, 99:051804, 2007.

[371] A. Alavi-Harati et al. Measurement of the branching ratio and form-factor of $K_L \to \mu^+\mu^-\gamma$. *Phys. Rev. Lett.*, 87:071801, 2001.

[372] A. Alavi-Harati et al. Measurements of the Decay $K_L \to e^+e^-\mu^+\mu^-$. *Phys. Rev. Lett.*, 90:141801, 2003.